frontiers | Research Topics

Updates in ocular therapeutics and surgery, volume III

Edited by
Georgios D. Panos and Horace Massa

Published in
Frontiers in Medicine

ISSN 1664-8714
ISBN 978-2-8325-5935-2
DOI 10.3389/978-2-8325-5935-2

About Frontiers

Frontiers is more than just an open access publisher of scholarly articles: it is a pioneering approach to the world of academia, radically improving the way scholarly research is managed. The grand vision of Frontiers is a world where all people have an equal opportunity to seek, share and generate knowledge. Frontiers provides immediate and permanent online open access to all its publications, but this alone is not enough to realize our grand goals.

Frontiers journal series

The Frontiers journal series is a multi-tier and interdisciplinary set of open-access, online journals, promising a paradigm shift from the current review, selection and dissemination processes in academic publishing. All Frontiers journals are driven by researchers for researchers; therefore, they constitute a service to the scholarly community. At the same time, the *Frontiers journal series* operates on a revolutionary invention, the tiered publishing system, initially addressing specific communities of scholars, and gradually climbing up to broader public understanding, thus serving the interests of the lay society, too.

Dedication to quality

Each Frontiers article is a landmark of the highest quality, thanks to genuinely collaborative interactions between authors and review editors, who include some of the world's best academicians. Research must be certified by peers before entering a stream of knowledge that may eventually reach the public - and shape society; therefore, Frontiers only applies the most rigorous and unbiased reviews. Frontiers revolutionizes research publishing by freely delivering the most outstanding research, evaluated with no bias from both the academic and social point of view. By applying the most advanced information technologies, Frontiers is catapulting scholarly publishing into a new generation.

What are Frontiers Research Topics?

Frontiers Research Topics are very popular trademarks of the *Frontiers journals series*: they are collections of at least ten articles, all centered on a particular subject. With their unique mix of varied contributions from Original Research to Review Articles, Frontiers Research Topics unify the most influential researchers, the latest key findings and historical advances in a hot research area.

Find out more on how to host your own Frontiers Research Topic or contribute to one as an author by contacting the Frontiers editorial office: frontiersin.org/about/contact

Updates in ocular therapeutics and surgery, volume III

Topic editors

Georgios D. Panos — Aristotle University of Thessaloniki, Greece

Horace Massa — Hôpitaux universitaires de Genève (HUG), Switzerland

Citation

Panos, G. D., Massa, H., eds. (2025). *Updates in ocular therapeutics and surgery, volume III*. Lausanne: Frontiers Media SA. doi: 10.3389/978-2-8325-5935-2

Table of contents

frontiers | Frontiers in Medicine

TYPE Editorial
PUBLISHED 13 January 2025
DOI 10.3389/fmed.2024.1536632

OPEN ACCESS

EDITED AND REVIEWED BY
Jodhbir Mehta,
Singapore National Eye Center, Singapore

*CORRESPONDENCE
Georgios D. Panos
✉ gdpanos@gmail.com

RECEIVED 29 November 2024
ACCEPTED 09 December 2024
PUBLISHED 13 January 2025

CITATION
Panos GD and Massa H (2025) Editorial: Updates in ocular therapeutics and surgery, volume III. *Front. Med.* 11:1536632. doi: 10.3389/fmed.2024.1536632

Editorial: Updates in ocular therapeutics and surgery, volume III

Georgios D. Panos[1,2]* and Horace Massa[3]

[1]First Department of Ophthalmology, AHEPA University Hospital, School of Medicine, Aristotle University of Thessaloniki, Thessaloniki, Greece, [2]Division of Ophthalmology and Visual Sciences, School of Medicine, University of Nottingham, Nottingham, United Kingdom, [3]Department of Ophthalmology, Geneva University Hospitals, Geneva, Switzerland

KEYWORDS

cornea, macular oedema, uveitis, glaucoma, vitreoretinal surgery, machine learning, eyelid surgery, paediatric ophthalmology

Editorial on the Research Topic
Updates in ocular therapeutics and surgery, volume III

Ophthalmology stands as one of the most rapidly evolving fields in medicine, characterised by groundbreaking advancements in therapeutics and surgery over the last few decades. The introduction of transformative treatments for ocular conditions, such as age-related macular degeneration, glaucoma, retinal vein occlusions, diabetic macular oedema, genetic disorders, and uveitis, has significantly enhanced patient outcomes and reshaped clinical paradigms. Simultaneously, technological innovations and refined surgical techniques have ushered in a new era for eye surgeons, enabling procedures that are safer, faster, and more precise than ever before.

This Research Topic, *Updates in ocular therapeutics and surgery, volume III*, builds upon the foundation of its successful predecessors, continuing the journey of exploring the latest therapeutic and surgical advances. It aims to consolidate contemporary knowledge, highlight cutting-edge research, and chart the trajectory of future developments in the field.

The contributions in this Research Topic underscore the dynamic interplay between clinical innovation and translational research. They reflect the commitment of ophthalmologists, researchers, and industry pioneers to address complex ocular diseases with novel solutions while enhancing the efficacy and safety of surgical interventions.

By bringing together a diverse array of studies and reviews, this Research Topic aspires to serve as a valuable resource for clinicians, researchers, and trainees. It not only encapsulates the current state-of-the-art in ocular therapeutics and surgery but also seeks to inspire future inquiries that will further refine the practice of ophthalmology.

Guo et al. investigated the therapeutic potential of Urolithin A in addressing delayed corneal epithelial wound healing. By inhibiting ferroptosis, a form of oxidative stress-induced cell death, Urolithin A demonstrated significant promise in mitigating hyperosmotic stress and promoting healing.

Li et al. evaluated the efficacy and safety of CO_2 laser-assisted sclerectomy for secondary glaucoma following vitrectomy. Their findings underscored the advantages of this novel approach in achieving substantial intraocular pressure reduction with a lower risk of complications. Similarly, He et al. performed a systematic review and meta-analysis exploring the synergistic effect of anti-VEGF therapy combined with Ahmed valve implantation in neovascular glaucoma, revealing enhanced surgical success rates and improved long-term outcomes compared to valve implantation alone.

Liu et al. presented an innovative approach to managing Descemet's membrane detachment post-cataract surgery. Their technique of using air tamponade offered a minimally invasive and highly effective solution to this challenging complication. Ning et al. contributed a bibliometric analysis of 20 years of research on posterior chamber phakic intraocular lenses (pIOLs), identifying key research areas including clinical outcomes, complications, and postoperative visual quality. This comprehensive analysis provides valuable insights for advancing the field.

Wang and Zheng introduced the Prism and Maddox Rod Test as a reliable and cost-effective tool for determining surgical measurements in type III acute acquired comitant esotropia. Their work demonstrated its precision and applicability in improving alignment outcomes post-surgery.

In a review of corneal epithelial repair mechanisms, Gong et al. detailed the critical roles of growth factors such as epidermal growth factor and transforming growth factor-α, highlighting their therapeutic potential in ocular surface disease management.

Ye et al. proposed a modified technique for the intrascleral fixation of three-piece foldable intraocular lenses using Hoffman pockets. This approach minimised complications and improved lens stability, offering a refined method for secondary IOL implantation.

In the domain of ocular trauma, Sather et al. examined the outcomes of secondary surgeries following open globe injury repair. Their findings emphasised the importance of a structured surgical rehabilitative process, with ∼50% of patients achieving ambulatory vision and 30% attaining reading vision.

Körber et al. explored the use of picosecond ultrashort laser pulses in ophthalmic surgeries, showcasing their superior precision and reduced collateral damage compared to traditional nanosecond lasers. Their research paves the way for safer and more efficient laser-based procedures.

Finally, Jin et al. investigated the efficacy and safety of platelet-rich plasma (PRP) in acute non-arteritic anterior ischaemic optic neuropathy (NAION). PRP treatment significantly improved capillary perfusion of the optic nerve head and short-term visual acuity, demonstrating its potential as a novel therapeutic option for this challenging condition.

This Research Topic of studies reflects the vibrancy and innovation in ocular therapeutics and surgery. We hope that readers will find this volume as engaging and enlightening as we did in editing and presenting it, and that it inspires future endeavours aimed at further refining the care of patients with ocular diseases.

Author contributions

GP: Conceptualization, Supervision, Validation, Writing – original draft, Writing – review & editing. HM: Validation, Writing – review & editing.

Conflict of interest

The authors declare that the research was conducted in the absence of any commercial or financial relationships that could be construed as a potential conflict of interest.

The author(s) declared that they were an editorial board member of Frontiers, at the time of submission. This had no impact on the peer review process and the final decision.

Publisher's note

frontiers | Frontiers in Medicine

TYPE Original Research
PUBLISHED 08 February 2024
DOI 10.3389/fmed.2024.1345976

OPEN ACCESS

EDITED BY
Horace Massa,
Hôpitaux universitaires de Genève (HUG), Switzerland

REVIEWED BY
Bojan Pajic,
University of Novi Sad, Serbia
Azhar Zam,
New York University Abu Dhabi, United Arab Emirates

*CORRESPONDENCE
Michael Körber
✉ michael.koerber@th-nuernberg.de

RECEIVED 28 November 2023
ACCEPTED 30 January 2024
PUBLISHED 08 February 2024

CITATION
Körber M, Fellinger J, Fritsche M, Giese A, Kostourou K, Kopf D, Kottcke M, Luciani F, Schmidbauer JM, Wenk J and Braun B (2024) Ophthalmic surgeries on *post mortem* porcine eyes with picosecond ultrashort laser pulses.
Front. Med. 11:1345976.
doi: 10.3389/fmed.2024.1345976

Ophthalmic surgeries on *post mortem* porcine eyes with picosecond ultrashort laser pulses

Michael Körber[1,2]*, Jakob Fellinger[3], Milan Fritsche[1], Andreas Giese[1], Konstantina Kostourou[4], Daniel Kopf[3], Manfred Kottcke[1], Francesco Luciani[5], Josef M. Schmidbauer[2,5], Jonathan Wenk[1] and Bernd Braun[1]

[1]Applied Mathematics, Physics and Humanities, Nuremberg Institute of Technology, Nuremberg, Germany, [2]Paracelsus Medical University, Nuremberg, Germany, [3]MONTFORT Laser GmbH, Götzis, Austria, [4]NANEO Precision IBS Coatings GmbH, Lindau, Germany, [5]Clinic of Ophthalmology, Klinikum Nürnberg Nord, Nuremberg, Germany

Purpose: This work demonstrates significant advantages in ophthalmic surgeries through the use of picosecond ultrashort laser pulses instead of state-of-the-art nanosecond laser pulses. These ultrashort lasers shall serve as universal tools more effectively combining advantages of high precision, low impact and economic advantages compared to existing instruments.

Methods: As samples, we used post-mortem porcine eyes on which we performed the experiments with both picosecond and nanosecond lasers. Performed surgeries were laser iridotomy, (post-) cataract treatment/capsulotomy and selective laser-trabeculoplasty. Pulse widths were between 12 ps and 220 ns with pulse energies between 30 µJ and 10 mJ at 532 nm and 1,064 nm. Additionally, we investigated accompanying shock waves, cavitation bubbles, and heat effects during the ablation processes.

Results: For all surgeries, significant differences were observed between picosecond and nanosecond pulses: It was possible to scale the pulse energy down to 10 of microjoules rather than requiring millijoules, and resulting tissue ablations are much more precise, more deterministic and less frayed. The shock wave and cavitation bubble investigation revealed major differences in pressure between picosecond pulses (0.25 MPa, 50 µJ) and nanosecond pulses (37 MPa, 5 mJ). The heat input during ablation could be lowered by two orders of magnitude.

Conclusion: Picosecond ultrashort laser pulses show substantial benefits for several ophthalmic surgeries, with regard to ablation precision, shock wave generation and heat input. They are better than state-of-the-art ophthalmic nanosecond lasers in all aspects tested.

KEYWORDS

iridotomy, capsulotomy, SLT, picosecond laser, shock waves, glaucoma, cataract

1 Introduction

In ophthalmology, laser sources are commonly used for non-invasive/incisionless or minimally invasive surgeries. These lasers are mainly neodymium doped yttrium-aluminum-garnet (Nd:YAG) lasers. They emit comparatively long pulse widths in the nanosecond (ns) range that lead to a non-negligible heat input during surgical tissue ablation.

The energy input then causes immediate boiling, expansion and evaporation of the tissue. This results in acoustic shock waves and non-deterministic tissue ablation with collateral damage of surrounding tissue. Consequently, the ablation achieved is much larger than the actual laser spot, which can lead to side effects and additional clinical patterns such as ghost images, iris bleeding, corneal endothelial damage or retinal detachment. Furthermore, the tissue ablation with ns laser sources depends on the linear absorption properties of the tissue and therefore on the color of the eye (1–7). However, such unintended results can be counteracted by using ultrashort pulses (USP) (8–13). The main advantage of these pulses—which have a pulse width of a few picoseconds or less—is to be near the regime of cold material ablation. This physical effect results from the very short pulse width and the associated high peak intensity. Due to the high peak intensities, ionization and plasma formation occur through multi-photon processes when a single laser pulse interacts with the tissue. This interaction time is too short to transfer energy to the atomic lattice of the material, as the heat diffusion time in the lattice is much longer than the duration of the laser pulse. This results in material removal with very little heat input. Another advantage of cold material ablation is that the non-linear absorption properties of the material is predominant, which is why the ablation is almost independent of the material properties in terms of linear absorption, reflection and transmission (14–17). Consequently, USP lasers should ablate tissue very precisely and deterministically independent of eye color (10, 18–23). However, currently available ultrashort pulse lasers, such as those used for LASIK (laser *in situ* keratomileusis), are very expensive and therefore economically not appropriate for small surgeries such as laser iridotomy and post-cataract treatment. For this reason, ns laser sources are state-of-the-art in ophthalmology.

This paper discusses the use of an ultrashort pulse laser source emitting in the picosecond regime for ophthalmic surgeries and evaluates the potential benefits of these lasers, particularly for iridotomy, capsulotomy/post-cataract treatment and selective laser-trabeculoplasty (SLT). This research was motivated by ultra-compact Q-switched picosecond lasers recently becoming available, combining the advantages of the low price of currently used ns laser sources with cold material ablation capabilities of high-end femtosecond lasers (24, 25).

Laser iridotomy as treatment of narrow angle glaucoma involves piercing the iris next to the Schlemm's canal to create a new floating path for the eye fluid. This piercing is done with a series of laser pulses that are applied to the tissue via an ophthalmic slit lamp laser system. The energy ranges from 1 to 10 mJ per pulse for the ns laser sources currently in use. The same laser source is used for post-cataract treatment, where the posterior lens capsule is opened with laser pulses applied in a cross-shaped pattern. Both treatments may lead to adverse effects and additional clinical patterns such as frayed edges, collateral damage and strong shock wave generation. The latter takes place, because tissue ablation with laser sources is accompanied by a laser-induced optical breakdown in the laser focus (8). Such breakdown leads to plasma formation and the generation of shock waves caused by cavitation formation inside the material (tissue). The cavitation bubble then oscillates as long as enough energy is available in the breakdown region. Here, the initial breakdown and every cavitation bubble collapse lead to a separate shock wave. Therefore, several shock waves are generated per laser pulse and alter the mechanisms of laser ablation by affecting tissue adjacent to the target. This leads to bigger ablation areas and—if the shock waves are strong enough—to additional undesired side effects such as retinal detachment after iridotomy or (post-) cataract surgery (2, 5, 26–28). Therefore, it is necessary to ablate tissue with as low pulse energy as possible. With ultrashort pulse ps laser sources, the same treatment can be performed with much lower energy input. Furthermore, it can be shown that USP lasers lead to much less intense shock wave formation than ns lasers due to the aforementioned cold material ablation (8, 9, 29–33). The same principle can be applied to SLT, whereby the trabecular meshwork (TM) is irradiated with a 532 nm laser source. Here, the laser pulses ablate some TM tissue and also stimulate the remaining TM tissue so that previously restricted immune reactions are made viable again. Furthermore, the lasers can also be used to penetrate the TM completely down to the Schlemm's canal to create a drainage (34–36). Both surgical methods can be performed with lower pulse energy and higher precision by using ultrashort pulse laser sources.

To investigate and prove our hypotheses, the research was executed as follows: First, the method and its application in laser iridotomy, post-cataract treatment/capsulotomy and SLT are described. Then, a quantitative analysis of shock waves associated with the treatment is presented. Finally, this paper investigates heat input of ultrashort laser pulses on biological tissue (porcine iris) and on aluminum plates, to gain a better understanding of the ablation processes and heat effects inside the tissue.

2 Materials and methods

This section describes the laser sources and methods used for the different experiments, namely ophthalmic surgeries, shock wave and cavitation bubble examination, and heat investigation.

2.1 Laser sources

Different laser beam sources are used for the experiments, emitting $sech^2$ (picosecond laser) and gaussian (nanosecond lasers) shaped pulses with pulse widths between 12 ps and 220 ns and pulse energies between 30 µJ and 10 mJ, optionally at 1064 nm and 532 nm wavelength. Here, the nanosecond lasers are used as reference laser sources for state-of-the-art results. For all beam sources, the pulse energy can be adjusted manually with a polarizing beam splitter and a wave-plate up to the specific maximum. The following list describes the laser sources in more detail:

Laser 1: USP laser source with 12 ps pulse width: USP laser system consisting of a passively mode-locked Nd:YVO_4 (neodymium-doped yttrium orthovanadate) oscillator and an Nd:YVO_4 regenerative amplifier (37). The laser system emits a 1,064 nm pulse train with an adjustable pulse repetition rate between 1 Hz and 300 kHz, a pulse energy of up to 164 µJ, and a pulse width of 12 ps. The laser output can additionally be frequency doubled with a KTP (potassium titanyl phosphate—$KTiOPO_4$) nonlinear crystal, leading to a wavelength of 532 nm with a pulse energy conversion efficiency of up to 70%.

Laser 2: ns laser source with 1.6 ns pulse width: 1.6 ns, 20 Hz quasi-continuous-wave (QCW) passively Q-switched (PQS) Nd:YAG (neodymium-doped yttrium aluminum garnet) laser source with pulse energies up to 7 mJ at 1064 nm from *MONTFORT Laser GmbH, Götzis, Austria*.

Laser 3: ns laser source with 8 ns pulse width: 8 ns, 10 Hz actively Q-switched laser source with pulse energies up to 50 mJ at 1064 nm from *MONTFORT Laser GmbH, Götzis, Austria*. The laser output can additionally be frequency doubled with a KTP nonlinear crystal, leading to a wavelength of 532 nm.

Laser 4: ns laser source with adjustable pulse width: 20 W, 1062 nm pulsed fiber master oscillator power amplifier (MOPA) laser from *JENOPTIK Laser GmbH, Jena, Germany ('JenLas®fiber ns 20 advanced single mode')*. It emits in continuous wave (cw) operation or pulsed operation with pulse widths between 15 ns and 220 ns with maximum pulse energies between 68 and 570 µJ, respectively.

2.2 Method for ophthalmic surgeries

In contrast to ophthalmic surgical methods with special eye attachment optics/system, the different laser beams are focused on the samples via the following beam delivery system: This system consists of a 60 mm plano convex focusing lens, an x-y-z-translation stage for sample positioning, two laser diodes for laser focus alignment (*FP-D-532-1-C-F* from *Laser Components GmbH, Olching, Germany*), and a stereo microscope as visualization device for real-time observation and magnification (*Stemi 508 trino* from *Carl Zeiss Microscopy GmbH, Oberkochen, Germany*). This set-up is based on slit-lamp laser beam delivery systems such as used in clinics and is similar in function. For part of the capsulotomies and SLT, a laser scanner set-up is used, consisting of a two-axis laser scanner head (*SS-II-15 [Y] D2* from *Raylase GmbH, Wessling, Germany*) with the F-Theta flat field objective *S4LFT3046/328* (*Sill Optics GmbH & Co. KG, Wendelstein, Germany*) with a focal length of 50 mm. Since these components of the set-ups are designed for the near infrared (NIR), a second set-up for 532 nm was built, using another 60 mm plano convex focusing lens and the scanner head *SS-IIE-15 [DY] D2* (*Raylase GmbH, Wessling, Germany*) with the F-Theta flat field objective *S4LFT4066/292* (*Sill Optics GmbH & Co. KG, Wendelstein, Germany*) with a focal length of 67.2 mm. Focusing results in a focal spot diameter of about 25 µm for all focusing set-ups. This leads to fluences of 8 J/cm² (12 ps, 50 µJ) and 800 J/cm² (8 ns, 5 mJ), and peak intensities of 587 GW/cm² and 94 GW/cm², respectively.

The tissue samples used are *post mortem* porcine eyes, which are processed about 4 h after excision. The eyes are moistened with water before, during and after all surgeries. The iridotomy and capsulotomy surgeries were performed as open sky surgeries (with prior cornea removal) for better comparability without the influence of the cornea. SLT surgeries were performed in two ways: First, on a bisected porcine eye (removed lens) with the slit-lamp set-up to focus the laser beams directly on the trabecular meshwork (TM) without the necessity of a clinically used gonioscope. Second, on an exposed trabecular meshwork with the scanner set-up. For this, the eyes were prepared in such a way that the cornea, about 2 mm of the sclera around the cornea, and the TM were preserved. This is comparable to pieces of human donor corneas, where a part of the sclera and the TM are also still attached. The lasers can then be focused directly on the TM from the posterior side. Visualization, examination and measurement of the results are carried out using high-resolution light microscopy and scanning electron microscopy (SEM). For the latter, a special sample preparation and drying method is applied to the tissue samples that avoid water inside the tissue to boil and expand under vacuum in the plasma coating machine and the SEM. This would lead to warpage/deformation/distortion and destruction of the tissue. The preparation method starts with 1,5-pentanedial (glutaraldehyde solution 50% in water (5.6 mol); *Sigma-Aldrich, St. Louis, United States*) for protein linkage and tissue fixation. The tissue is then buffered with a phosphate buffer of pH = 7.0 (*Bernd Kraft, Duisburg, Germany*) and subsequently placed in an alcoholic solution in ascending concentration (start: 20%/80% ethanol/water; end: 100% ethanol; gradation: 10% ethanol—water: purified water; ethanol: Ethanol absolute ≥99.5% from *VWR International, Radnor, United States*). The last step before air drying is soaking the tissue in 1,1,1-Trimethyl-N-(trimethylsilyl)silanamine (hexamethyldisilazane, HMDS; *Sigma-Aldrich, St. Louis, United States*). The samples of the exposed TM for SLT are soaked in pure ethanol only and subsequently air dried, because the cornea and sclera lead to a high stiffness even without fixation. Some of the capsule samples are strictly air dried during compression to avoid warpage/deformation/distortion.

All samples can then be metal-coated (metal: gold/palladium—*SC502-314B* from *Quorum Technologies, Laughton, United Kingdom*) and visualized by SEM. For this, the plasma coating machine *Q150R ES* (*Quorum Technologies, Laughton, United Kingdom*) and the *SEM JSM 6510* (*Jeol Ltd., Tokyo, Japan*) are used. Light microscope images were taken using the incident light microscope *Axio Lab.A1*, the transmitted light microscope *Primo Star* and the stereo microscope *Stemi 508 trino*, all from *Carl Zeiss AG, Oberkochen, Germany*.

In total, the research was performed on about 400 porcine eyes with over 1,000 surgeries (approx. 800 iridotomies, 25 capsulotomies, 200 SLTs).

2.3 Method for shock wave and cavitation bubble investigation

Shock waves generated by laser pulses were investigated using the following method and set-up (see Figure 1): The different laser sources are focused via a laser mirror and an $f = 40$ mm aspherical plano-convex lens in a basin (74 mm × 74 mm × 33 mm; l × w × h) filled with distilled water. Focusing results in a diameter of about 10 µm, leading to fluences of 50 J/cm² (12 ps, 50 µJ) and 5 kJ/cm² (8 ns, 5 mJ), and peak intensities of 5.5 TW/cm² and 587 GW/cm², respectively. The laser input results in an optical breakdown and shock waves, which are visualized using a streak camera system. The field of observation has a diameter of approximately 20 mm, roughly corresponding to the distance between laser focus and retina.

The light source of the system, a collimated pulsed green laser diode *PLT5 510 B1-3* (*OSRAM GmbH, München, Germany*), is synchronized to the pulse repetition rate of the breakdown laser. The phase delay between the laser pulse and the illumination pulse can be adjusted manually with a ns-increment to illuminate different shock wave propagation points. Both synchronization and delay adjustment are performed with a waveform generator (*33500B* from *Agilent Technologies, Inc., Santa Clara, United States*). Recording is done with a digital camera (*RX100* from *Sony, Tokyo, Japan*). In addition to the photographs, a 2 mm diameter needle hydrophone with attenuator, pre-amplifier and DC-coupler (*Precision Acoustics Ltd., Dorchester, United Kingdom*) is placed next to the breakdown below the water surface. It serves as a receiver of the shock wave fronts. For visualization and measurement, it is connected to an oscilloscope (*MSO64 from Tektronix, Inc., Beaverton, United States*,

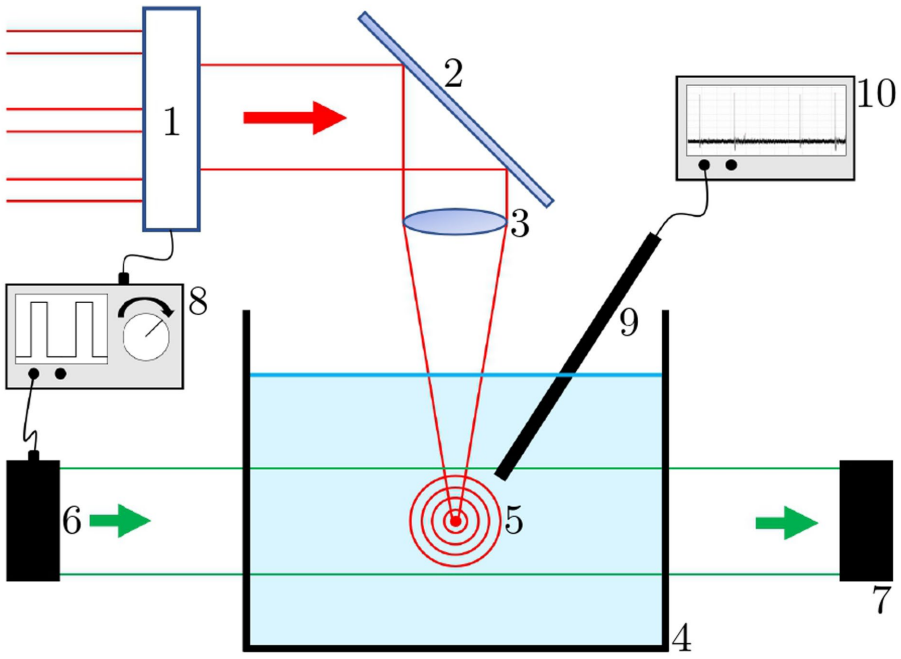

FIGURE 1
Shock wave measurement set-up. 1: switch for different laser sources; 2: laser mirror; 3: focusing lens; 4: water bath; 5: laser induced breakdown with shock waves; 6: illumination source; 7: camera; 8: function generator; 9: needle hydrophone; 10: oscilloscope.

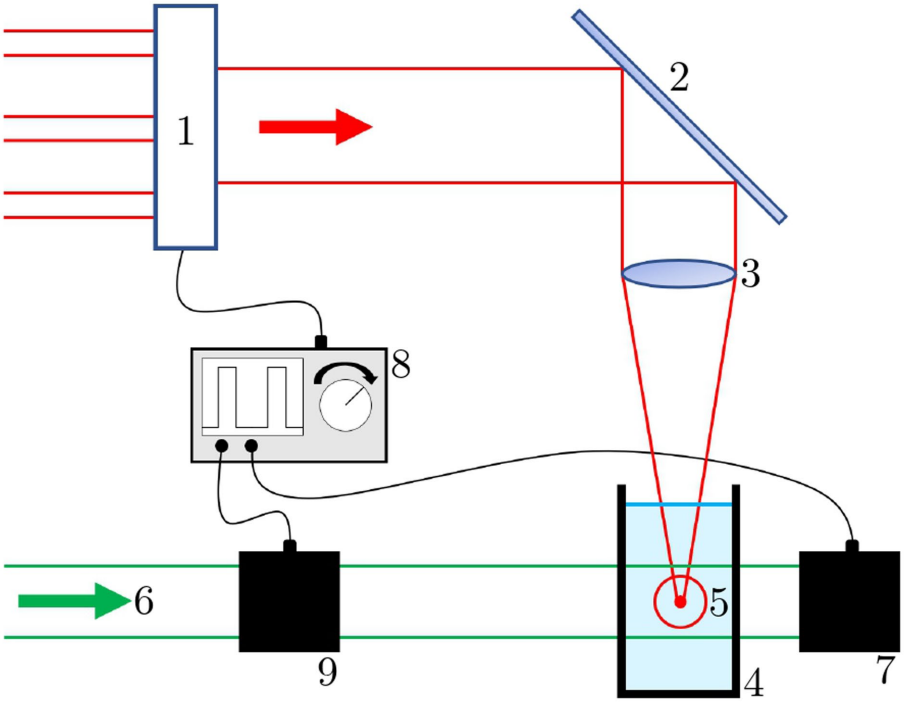

FIGURE 2
Cavitation bubble measurement set-up. 1: switch for different laser sources; 2: laser mirror; 3: focusing lens; 4: water cuvette; 5: laser breakdown with cavitation bubble; 6: illumination source; 7: camera; 8: function generator; 9: Pockels cell.

6 GHz bandwidth). The result of this measurement is a quantitative intensity profile of the shock waves as a function of the laser parameters.

For cavitation bubble investigation, the streak camera set-up was modified (see Figure 2): The water bath was replaced by a 2.5 mL polystyrene macro cuvette and the illumination source was replaced

by a 1,062 nm cw laser source (Laser 4, see Sec. 2.1), triggered and modulated with a Pockels cell. The camera was changed to the system camera *VEXU-24 M* (*Baumer Electric AG, Frauenfeld, Switzerland*). Both the Pockels cell and the camera are triggered by the waveform generator to the pulse repetition rate of the breakdown laser. This set-up provides a minimum illumination time of 5 ns, which is limited by the switching time of the Pockels cell.

2.4 Method for heat investigation

The heat input of the different laser sources was investigated using the thermal imaging camera optris *Xi 400* (*Optris GmbH, Berlin, Germany*). The different lasers were focused via the laser scanner set-up either on black anodized aluminum plates or on porcine eye irises. The scanner scribed a 5 mm long line with 10 mm/s. The emissivity was set to to $\varepsilon_{eye} = 0.98$ for the iris tissue (equal to water and skin) and $\varepsilon_{alu} = 0.67$ for anodized aluminum (38). The measurements are then compared to simulations computed with *MATLAB* (*The MathWorks, Inc., Natick, United States*) following the approach of Ansari et al. (39).

3 Results

This section includes results of the different ophthalmic surgeries, shock wave and cavitation bubble examination, and heat investigation.

3.1 Laser Iridotomy

The study revealed a major variation in size, shape, quality and reproducibility of iridotomies with different pulse widths. A comparison of four different pulse widths (12 ps, 8 ns, 15 ns, 220 ns) is shown in Figure 3. The images show typical results for each pulse width. In each case, the SEM magnification factor is 500 and the scale bars are 50 µm. While results (**A**) and (**B**) for 12 ps, 1 kHz at 1064 nm and 532 nm are very good, showing small and well-defined holes, the nanosecond results (**C**)–(**F**) with different pulse lengths, pulse energies, repetition rates, and wavelengths show frayed edges, ejection of ablated material, and large areas of altered surrounding tissue. The latter is attributed to the higher temperatures incurred through these pulse widths. Furthermore, Figure 4G shows an ideal result, which was achieved with the 12 ps USP laser source, with 40 µJ pulse energy, 1 kHz repetition rate, and 1 s irradiation time. Here, the quality is almost perfect: The ablated hole has very sharp edges and appears almost as if punched. The scale bar is also 50 µm but the SEM magnification factor is 230.

In addition to the far better defined laser processing, the pulse energy necessary for piercing the iris could be reduced to several 10 of microjoules (between 30 µJ and 70 µJ) when using USP laser pulses compared to several millijoules (1 mJ to 10 mJ) when using ns laser sources. To achieve complete penetration of the iris, approximately 1,000 USP pulses, dependent on the pulse energy, are required (and thus an exposure time of 1 s at 1 kHz repetition rate). The ablation per pulse is considerably lower than with nanosecond pulses, where a few pulses (with 5 mJ pulse energy) are sufficient to achieve complete penetration of the iris.

3.2 Capsulotomy

With ps pulses, well-defined capsulotomies can be performed in addition to iridotomies. As seen in Figure 4, precise cutting (left) and piercing (right) of the anterior lens capsule of porcine eyes is possible with 12 ps laser pulses—without tearing the remaining capsule. Similar to iridotomy, pulse energies between 30 µJ and 70 µJ prove to be suitable.

Figure 5 shows a comparison of capsulotomies with (**A**) 8 ns, 3 mJ and (**B**) 12 ps, 50 µJ. Both capsulotomies are performed on dissected anterior lens capsules. The lasers were focused on the capsules via the laser scanner head set-up. The capsulotomy diameter was set to 4 mm and the laser processing speed was set to 2.5 mm/s, resulting in a spot spacing of 5 µm for the 1 kHz ultrashort pulse train and 250 µm for the 10 Hz, 8 ns pulse train. Due to high energy input with accompanying high shock impact of the ns laser pulses, the processing speed could not be reduced to achieve the same spot spacing as for the USP pulses, since the capsule would have been torn right away. A comparison of the images reveals a big difference in capsules shape and cut quality. While the ns capsulotomy is torn and has frayed edges due to the high pulse energy required for these pulse widths, the USP capsulotomy is almost perfectly round with sharp and smooth cutting edges. The lower images (**C**) and (**D**) show higher magnifications of the respective capsulotomies cutting edges, visualized by light microscopy. In (**C**) the cutting edge is marked with a black arrow, since the capsule is folded over due to the high shock input. Additionally, Figure 5E shows an SEM visualization of the cutting edge of (**B**) with a magnification factor of 1,500. Here, the edge is very sharp and flat, which is comparable to state-of-the-art femtosecond and manual capsulotomies (19, 23).

3.3 SLT—selective laser-trabeculoplasty

Similar to the results of the iridotomy and the capsulotomy, SLT is possible with the 12 ps USP laser pulses at much lower pulse energies compared to ns pulses, namely 30 µJ to 70 µJ instead of 1 mJ (40). A result with 12 ps, 50 µJ at 1064 nm is shown in Figure 6, where "champagne bubbles" can be seen to the left of the green target laser (marked with black arrow). These bubbles appeared during the surgery and are considered an indicator of successful treatment. All tested pulse energies between 30 µJ and 70 µJ led to comparable results.

Figure 7 shows four typical results of SLTs in exposed trabecular meshwork with (**A**) picosecond ultrashort laser pulses and (**B**)–(**D**) nanosecond laser pulses. All SEM visualizations were taken with a magnification factor of 200. As with the other surgeries, the differences between USP and ns pulses are significant.Regardless of wavelength and pulse energy, 12 ps produce a small hole with sharp edges and clear boundaries. In contrast, all results with nanosecond pulses show large holes with poor quality. Furthermore, the heat affected zones are strongly pronounced around the holes.

3.4 Shock wave and cavitation bubble investigations

Figure 8 shows the visualization of a laser induced shock wave in water—real image on the left and false color image on the right. The

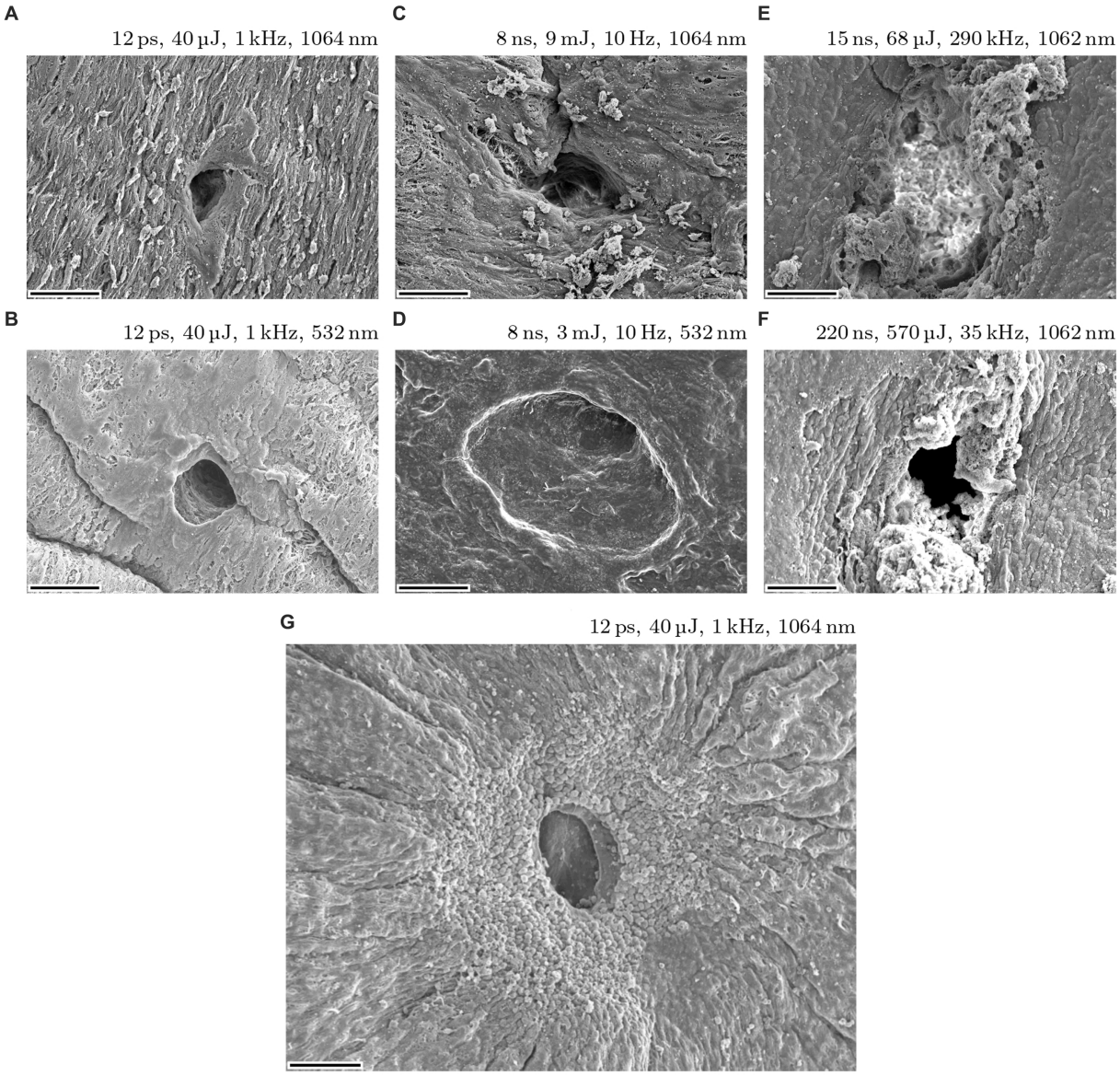

FIGURE 3
Iridotomies on *post mortem* porcine eye irises with pulse widths of 12 ps, 8 ns, 15 ns and 220 ns. Images **(A–F)** show typical results for each pulse width. Magnification factor is 500 and scale bars are 50 µm. Image **(G)** shows an ideal result for an iridotomy (SEM mag. Factor is 230).

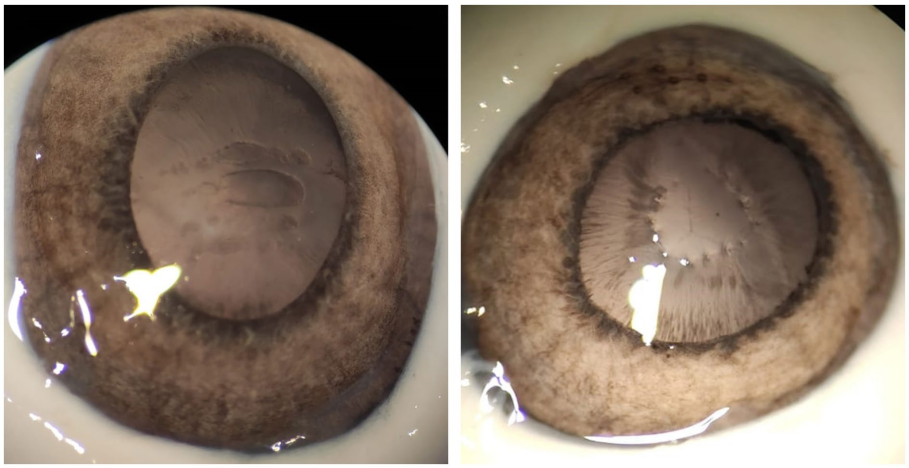

FIGURE 4
Cuts (left) and piercings (right) in anterior lens capsules of porcine eyes with low-energy 12 ps USP laser pulses.

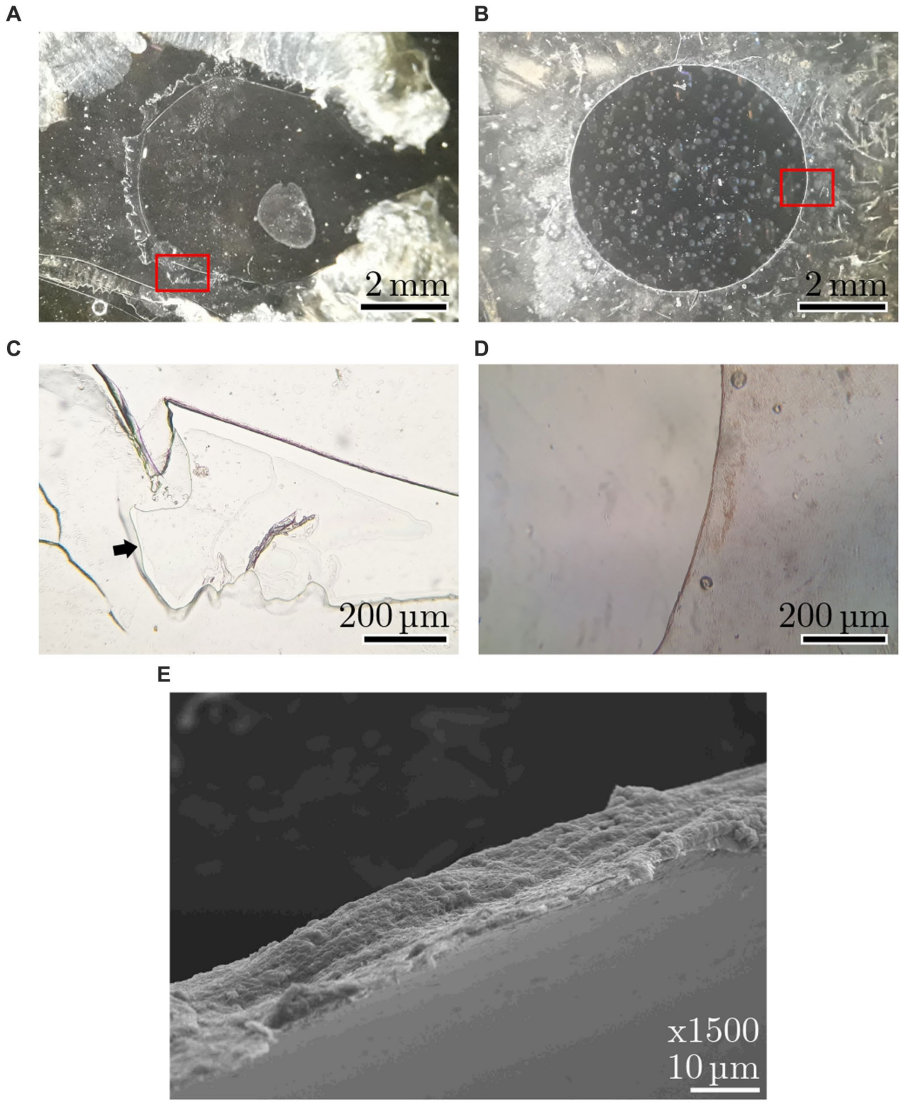

FIGURE 5
Anterior capsules with 4 mm capsulotomies with **(A)** 8 ns, 3 mJ and **(B)** 12 ps, 50 µJ. Images **(C,D)** show light microscopy magnifications of respective cutting edges [magnified areas are marked in red in **(A,B)**]. The black arrow in **(C)** marks the edge, since it is folded over. Image **(E)** shows an SEM visualization of the cutting edge of the 12 ps, 50 µJ capsulotomy.

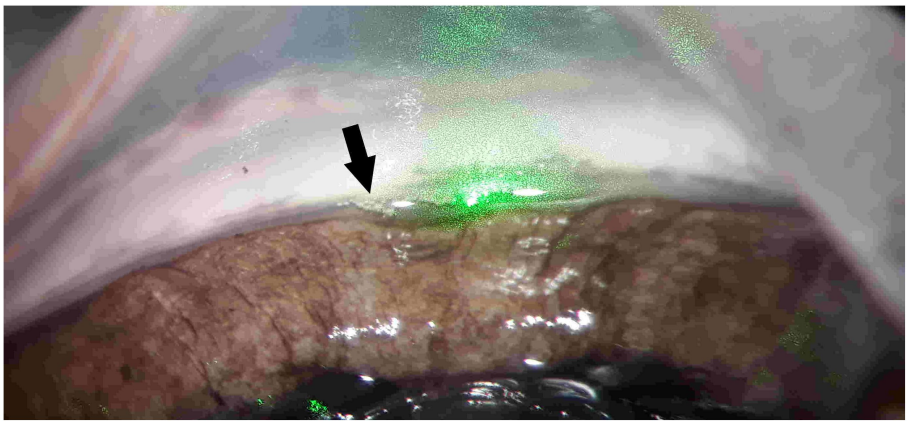

FIGURE 6
SLT with 1,064 nm, 12 ps and 50 µJ on a bisected porcine eye. "Champagne bubbles" (marked with black arrow) to the left of the green target lasers are considered an indicator of successful treatment.

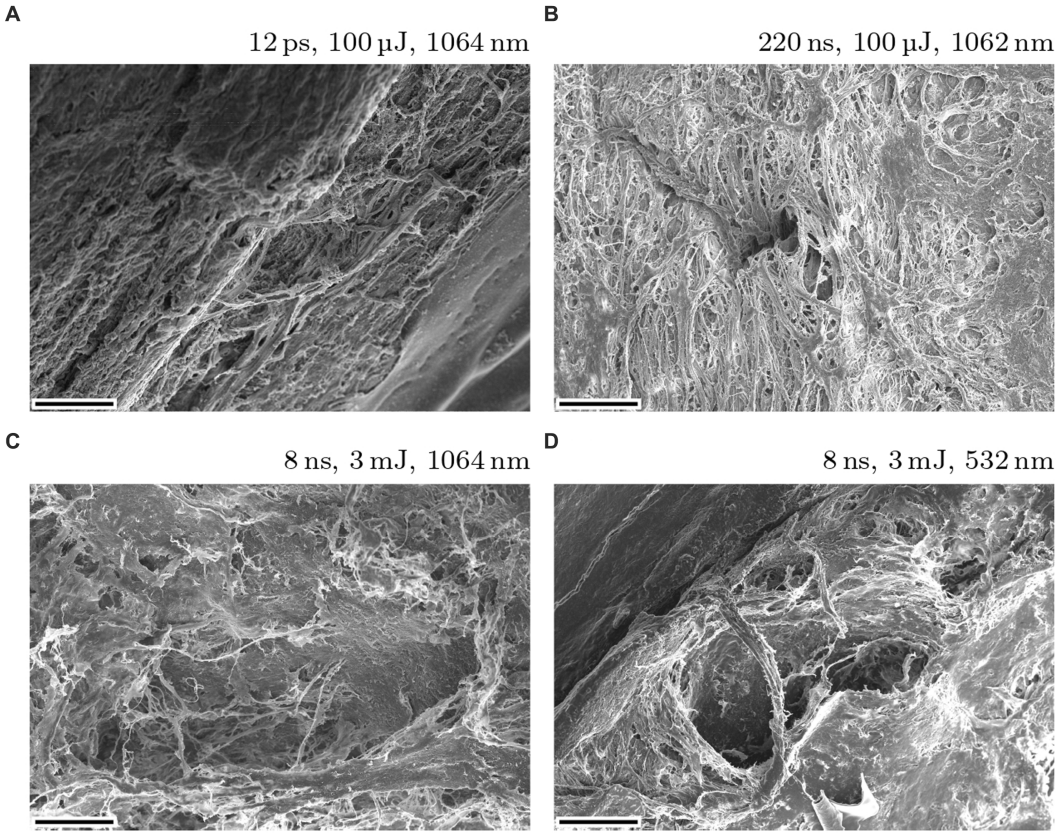

FIGURE 7
Typical SLT results on exposed porcine eye's trabecular meshwork using 12 ps USP **(A)** and nanosecond **(B–D)** laser sources. The magnification factor is 200 and the scale bars are 100 µm.

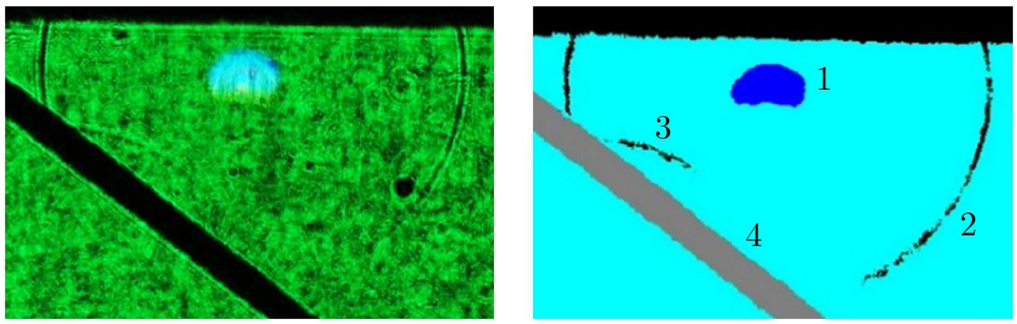

FIGURE 8
Visualization of a shock wave in water induced with a 147 µJ, 12 ps, 1,064 nm pulse train; left: real image; right: false color representation. 1: Laser induced breakdown; 2: Shock wave; 3: Shock wave reflection; 4: Steel target for reflection. The laser was irradiated from the top (41).

laser induced breakdown leads to a shock wave, which is reflected on a steel target. Here, the breakdown was induced with 147 µJ, 12 ps at 1064 nm from the top. Figure 9 shows a color-inverted photograph of a laser induced breakdown (dark spot) with 161 µJ, 12 ps at 1064 nm together with a cavitation bubble (brighter cycle) and a typical jet formation to the left of the bubble.

The shock wave pressure was measured with a hydrophone. Figure 10 shows a typical hydrophone measurement visualized with an oscilloscope. Peak 1 is the initial breakdown with expansion of the cavitation bubble—this is the shock wave of the laser induced breakdown (LIB). Peak 2 is the signal from the first bubble collapse and peak 3 from the second bubble collapse. Dependent on the breakdown energy, and therefore on the pulse energy, the cavitation bubble oscillation of expansion and collapse repeats more often. Here, the pulse energy of 5 mJ at a pulse width of 1.6 ns led to three (detectable) shock waves.

The needle hydrophone measurements are shown in Figure 11 (logarithmic scale due to major differences in amplitude). Here, the

normalized hydrophone signal (voltage) U_{hyd} is plotted for 12 ps and 1.6 ns pulse width as a function of the pulse energy E_{pulse} and the hydrophone distance d_{hyd} to the focal spot. The pulse energies were chosen accordingly to the results from the ophthalmic surgeries, as 50 µJ are typical for USP and 3 mJ and 6 mJ are typical for ns laser sources. 100 µJ at 12 ps are measured to gain information about energy dependency at a fixed pulse width. As can be seen, there are large differences of a factor of 25 in average for ns/USP lasers between the different parameters.

To determine the actual pressure of the shock waves, the hydrophone voltages are converted to pressure values via spectrum analysis. In Figure 12, the LIB shock wave and the first collapse shock wave pressure are plotted for different pulse energies. The pulse width is 12 ps and the distance between the hydrophone and the breakdown area is 6 mm. This measurement results in higher pressures for higher pulse energies with a maximum pressure of 0.6 MPa at 161 µJ pulse energy.

A similar measurement is made for pulse energies between 0.2 mJ and 5 mJ at 1.6 ns pulse width (Figure 13). The distance between the needle hydrophone and the laser induced breakdown is 17 mm. The measurement was done for the LIB, the 1st and the 2nd collapse shock wave. It results in much stronger shock wave pressures compared to 12 ps pulses—even for longer distance. For example, a 50 µJ, 12 ps laser pulse leads to a maximum pressure of 0.25 MPa while a 5 mJ, 1.6 ns laser pulse generates 37 MPa.

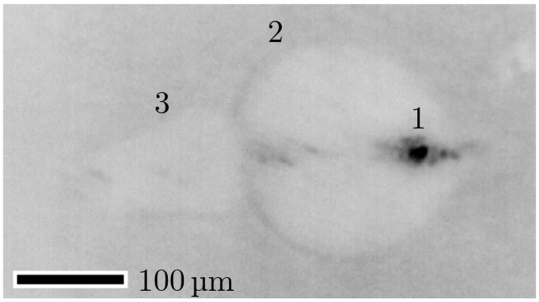

FIGURE 9
Photograph (inverted colors) of a cavitation bubble with 161 µJ, 12 ps at 1064 nm. The dark spot (1) results from the laser induced plasma and the brighter circle from the cavitation bubble (2). The maximum bubble radius is 198 µm. Moreover, a typical jet formation (3) can be seen left of the bubble. The laser was irradiated from the left (42, 43).

3.5 Heat investigation

Large differences between treatment with picosecond and nanosecond pulses also exist with respect to heat input and transfer around the laser focus (see Figure 14). On the left, the test is shown on porcine eyes for pulse widths of 12 ps, 8 ns, 15 ns and 220 ns as used for ophthalmic surgeries (Figures 14A,C,E,G), on the right, for comparison on black anodized aluminum (Figures 14B,D,F,H). As mentioned in the methods (see Sec. 2.4), the lasers scribed a 5 mm long line with 10 mm/s. The respective temperature before irradiation P, maximum temperature during irradiation M, and heating difference H in °C are indicated. Results (**A**) and (**C**), as well as (**B**) and (**D**) are the same, with different temperature scales for both better visibility and comparability to the nanosecond results. While 12 ps only lead to a marginal heating of a few degrees which is not even recognizable in the images (**C**) and (**D**), both 15 ns and 220 ns lead to a heating of more than 150°C. Again, the pulse energies for the various pulse widths were selected as required for the treatment.

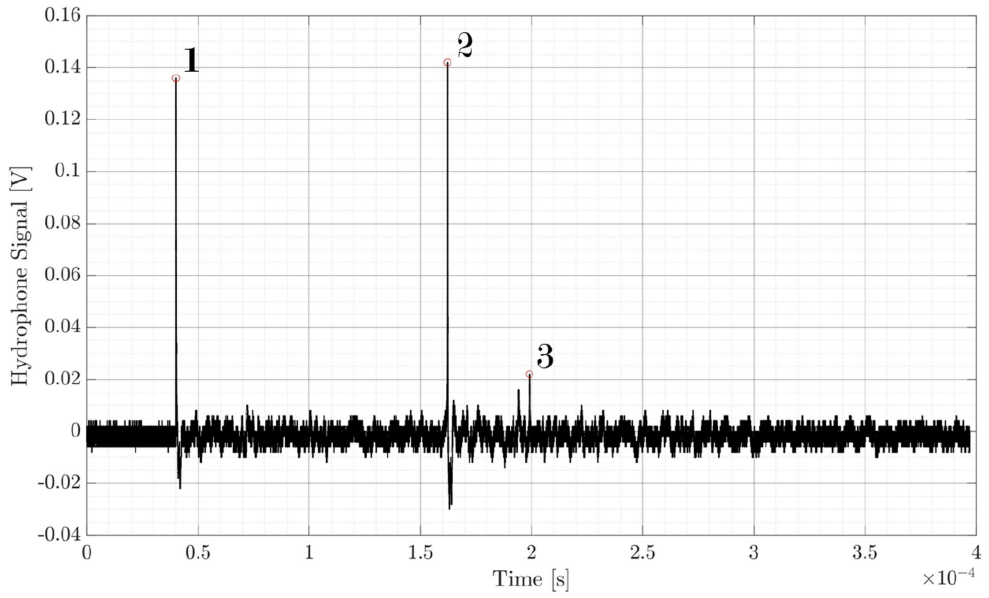

FIGURE 10
Shock wave pressure measurement with a needle hydrophone. Peak 1: initial breakdown with expansion of the cavitation bubble; Peak 2: first bubble collapse; Peak 3: second bubble collapse. The laser induced breakdown is initiated with 5 mJ pulse energy and 1.6 ns pulse width.

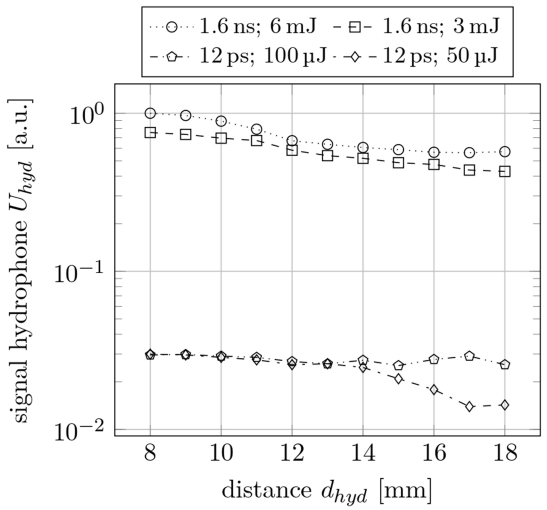

FIGURE 11
Normalized shock wave signal U_{hyd} as a function of the hydrophone distance d_{hyd} for different pulse widths τ_{pulse} and pulse energies E_{pulse}.

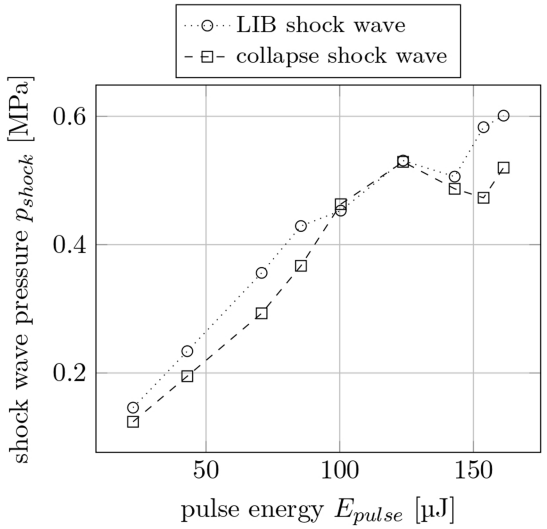

FIGURE 12
Shock wave pressure p_{shock} for LIB and collapse shock waves for different pulse energies E_{pulse} at 6 mm distance to the breakdown. The pulse width is 12 ps.

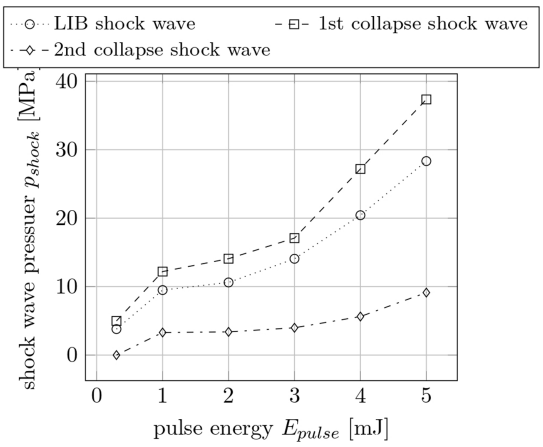

FIGURE 13
Shock wave pressures p_{shock} for the first, second and third shock wave per pulse for different pulse energies E_{pulse} at 17 mm distance to the breakdown. The pulse width is 1.6 ns.

Figure 15 presents simulations of the temperature change on a water surface for different pulse widths. The simulations are calculated for one single pulse each, so that the heat accumulation for several pulses has no effect. As displayed in Figure 15 left (temperature change as function of pulse energy), there is a large difference for pulse widths of 12 ps, 100 ps, 1 ns, 15 ns and 220 ns: The longer the pulse width and the higher the pulse energy, the higher the temperature change. As expected, utilization of low energy ultrashort pulses results in much lower heat inputs than high energy nanosecond pulses (2.5 K change for 12 ps, 50 µJ and 250 K change for 1 ns, 570 µJ). This simulation in general agrees with the experimental results. It should be noted that the simulation reflects the maximum temperature at the center of the laser focus, while the measurement averages over a larger area of space (about 0.15 mm^2). On the right in Figure 15, the temperature change is plotted as a function of distance to the laser spot. Here, 12 ps, 50 µJ pulses lead to a heat-affected zone of about 300 µm, while it is about 900 µm for 220 ns, 50 µJ and even larger for 220 ns, 570 µJ. Pulses with 8 ns, 3 mJ show a similar heat-affected zone than 12 ps. However, the much higher temperature change of 1800 K (8 ns) compared to 2.5 K (12 ps) would affect the surrounding tissue, e.g., due to the aforementioned stronger shock waves and instant evaporation.

Whereas the impact of a single ps laser pulse is significantly lower compared to nanosecond pulses, the question remains whether or not this holds true for the required pulse train of some hundreds to thousand pulses. The thermo mechanical response of tissue to pulsed irradiation was investigated by, e.g., Vogel et al. (44) and Yakovlev et al. (45). According to these studies typical thermal relaxation times are in the range of a few microseconds. In comparison to the temporal distance of consequent pulses, which is in the millisecond range for ps lasers, this relaxation time ensures temperature and stress confinement in any case.

4 Discussion and conclusion

As expected, the use of ultrashort pulses in ophthalmic surgeries led to significant improvements with regard to ablation precision, surgery quality, and impact on surrounding tissue. By using picosecond pulses instead of nanosecond pulses, the pulse energy could be reduced from a few millijoules to 10 of microjoules (an on-average reduction factor of 100). As with femtosecond lasers, this regime is referred to as cold material processing. At a pulse width of 12 ps, all of the aforementioned ocular procedures, i.e., laser-iridotomy, (post-) cataract treatment/capsulotomy, and selective laser-trabeculoplasty, could be successfully performed in an energy range of 30 µJ to 70 µJ at

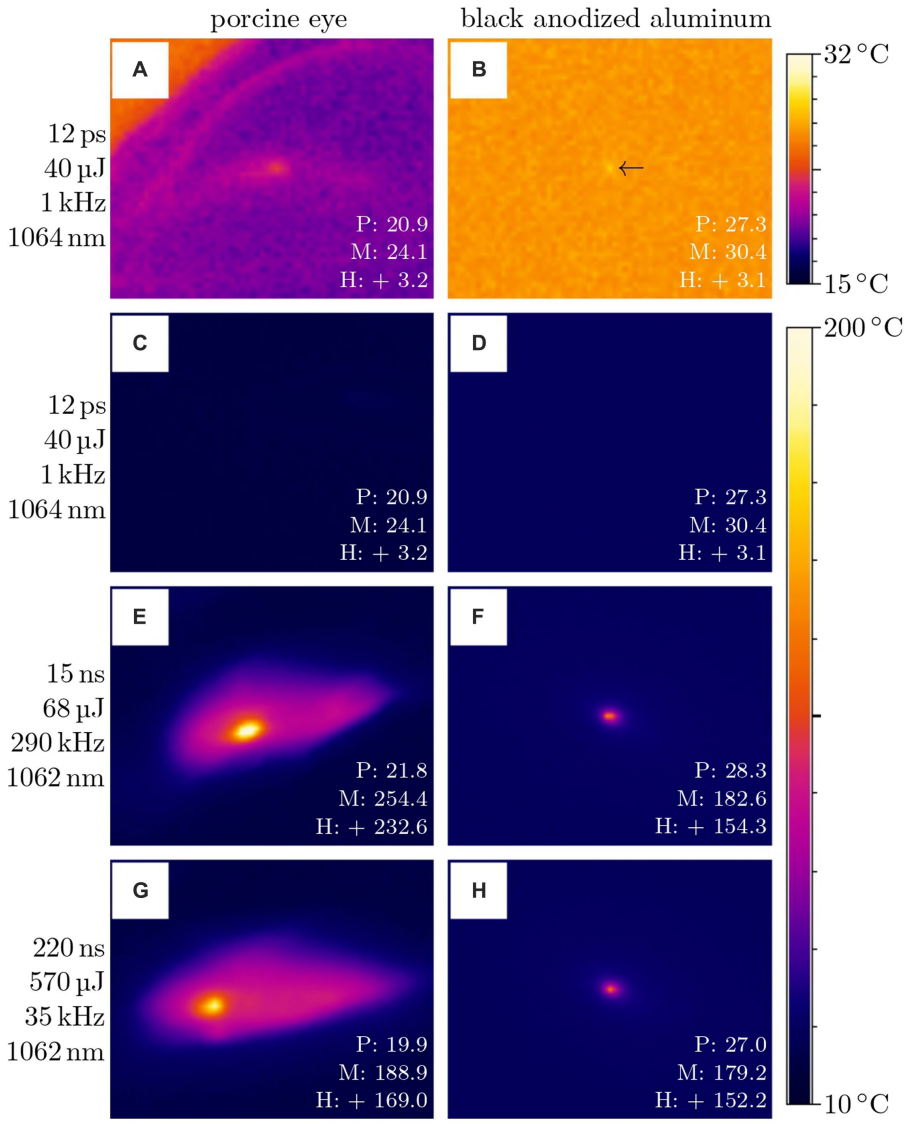

FIGURE 14
Temperature measurement on porcine eyes **(A,C,E,G)** and black anodized aluminum **(B,D,F,H)** with different laser parameters. The values given are the temperature before irradiation *P*, the maximum temperature during irradiation *M*, and the heating difference *H* in °C. Measurement **(A)** and **(C)** as well as **(B)** and **(D)** are the same, with different temperature scales. The lasers scribed a 5 mm long line with 10 mm/s.

both 532 nm and 1,064 nm. Furthermore, the shock wave and cavitation bubble formation during the surgeries could be reduced by a factor of x25 on average due to the shorter pulse widths and lower pulse energies. Finally, the thermal studies (experimental and simulative) revealed a significant reduction in both the temperature change and the temperature spreading (spatially and temporally) between picosecond and nanosecond laser pulses.

The recent availability of ultra-compact picosecond lasers—due to new physical approaches in laser physics—could lead to smaller and simpler laser sources. Therefore, the size- and cost-related disadvantages of former picosecond lasers are counteracted, as these systems consist of a two-stage set-up with two different laser resonators. The new approach is just one single micro-chip resonator with (if needed) subsequent pulse compression and/or pulse amplification (24, 25). Thus, the new technology is much simpler than existing systems, leading to a cost reduction and prices comparable to that of state-of-the-art ophthalmic nanosecond lasers.

Compared to former results with picosecond laser sources, we achieved at least comparable, mostly better results. Now it must be confirmed whether these results are also possible with the novel picosecond laser sources, which will be the next step in our project-plan. Furthermore, all results must then be transferred to human tissue *ex vivo*, in order to test the ablation possibilities as closely as possible to *in vivo* samples.

In conclusion, the use of picosecond ultrashort pulse laser sources in ophthalmology leads to substantial improvements and could be the stable basis for a very precise, universal tool for current ophthalmic surgeries and new surgical methods. Therefore, the next step will be to

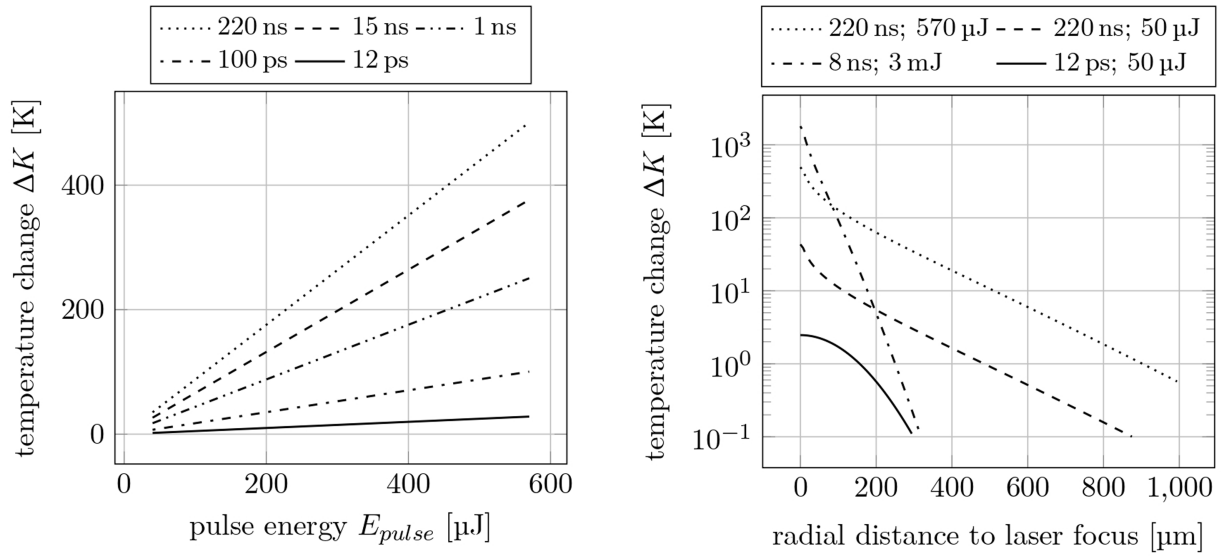

FIGURE 15
Simulated temperature changes on a water surface. Left: for different pulse widths τ_{pulse} and pulse energies E_{pulse}; Right: radial to the laser spot for 220 ns, 8 ns and 12 ps pulse width.

investigate the transferability of results from animal to pathological human tissue, and eventually a clinical study.

Data availability statement

The original contributions presented in the study are included in the article/supplementary material, further inquiries can be directed to the corresponding author.

Ethics statement

Ethical approval was not required for the study involving animals in accordance with the local legislation and institutional requirements because the used porcine eyes were exclusively from slaughterhouse waste.

Author contributions

MiK: Conceptualization, Formal analysis, Investigation, Methodology, Visualization, Writing – original draft. JF: Resources, Writing – review & editing. MF: Investigation, Resources, Writing – review & editing. AG: Investigation, Resources, Writing – review & editing. KK: Funding acquisition, Resources, Writing – review & editing. DK: Funding acquisition, Resources, Writing – review & editing. MaK: Conceptualization, Funding acquisition, Methodology, Supervision, Validation, Writing – review & editing. FL: Formal analysis, Investigation, Methodology, Resources, Validation, Writing – review & editing. JS: Funding acquisition, Methodology, Supervision, Validation, Writing – review & editing. JW: Investigation, Writing – review & editing. BB: Conceptualization, Funding acquisition, Methodology, Project administration, Supervision, Validation, Writing – review & editing.

Funding

The author(s) declare financial support was received for the research, authorship, and/or publication of this article. This project has received funding from the Eurostars-2 joint program with co-funding from the European Union Horizon 2020 research and innovation program - grant number E! 113846. The funder was not involved in the study design, collection, analysis, interpretation of data, the writing of this article or the decision to submit it for publication.

Conflict of interest

DK and JF are employed by MONTFORT Laser GmbH. KK is employed by NANEO Precision IBS Coatings GmbH.

The remaining authors declare that the research was conducted in the absence of any commercial or financial relationships that could be construed as a potential conflict of interest.

Publisher's note

References

1. Bazard MC, Guldenfls Y, Raspiller A. Early endothelial complications after treatment using a neodymium-Yag laser. *J Fr Ophthalmol*. (1989) 12:17–23.

2. Wu SC, Jeng S, Huang SC, Lin SM. Corneal endothelial damage after neodymium:YAG laser iridotomy. *Ophthalmic Surg Lasers*. (2000) 31:411–6. doi: 10.3928/1542-8877-20000901-09

3. Hsiao CH, Hsu CT, Shen SC, Chen HS. Midterm follow-up of Nd:YAG laser iridotomy in Asian eyes. *Ophthalmic Surg Lasers Imaging*. (2003) 34:291–8. doi: 10.3928/1542-8877-20030701-04

4. Kumar H, Mansoori T, Warjri GB, Somarajan BI, Bandil S, Gupta V. Lasers in glaucoma. *Indian J Ophthalmol*. (2018) 66:1539–53. doi: 10.4103/ijo.IJO_555_18

5. Ono T, Iida M, Sakisaka T, Minami K, Miyata K. Effect of laser peripheral iridotomy using argon and neodymium-YAG lasers on corneal endothelial cell density: 7-year longitudinal evaluation. *Jpn J Ophthalmol*. (2018) 62:216–20. doi: 10.1007/s10384-018-0569-6

6. Agarwal G, Kumar S, Malik VK. Effect of Nd:YAG laser posterior capsulotomy on corneal endothelial cell count in relation to the power of laser used. *Int J Sci Res*. (2019) 8:1178–83.

7. Saha BC, Kumari R, Sinha BP, Ambasta A, Kumar S. Lasers in Glaucoma: an overview. *Int Ophthalmol*. (2021) 41:1111–28. doi: 10.1007/s10792-020-01654-4

8. Vogel A, Busch S, Jungnickel K, Birngruber R. Mechanisms of intraocular photodisruption with picosecond and nanosecond laser pulses. *Lasers Surg Med*. (1994) 15:32–43. doi: 10.1002/lsm.1900150106

9. Vogel A, Capon MR, Asiyo-Vogel MN, Birngruber R. Intraocular photodisruption with picosecond and nanosecond laser pulses: tissue effects in cornea, lens, and retina. *Invest Ophthalmol Vis Sci*. (1994) 35:3032–44.

10. Momma C, Nolte S, Chichkov B, Tuennermann A, von Alvensleben F. Precise laser ablation with ultrashort pulses. *Appl Surf Sci*. (1997) 109-110:15–9. doi: 10.1016/S0169-4332(96)00613-7

11. Kim BM, Feit MD, Rubenchik AM, Joslin EJ, Celliers PM, Eichler J, et al. Influence of pulse duration on ultrashort laser pulse ablation of biological tissues. *J Biomed Opt*. (2001) 6:332–8. doi: 10.1117/1.1381561

12. Mayerhofer R. The shorter, the better: materials processing with ultra short pulsed lasers. *Laser Tech J*. (2011) 8:44–7. doi: 10.1002/latj.201190025

13. Mayerhofer R, May AB, Serbin J. Is it cold enough, yet? *Laser Tech J*. (2016) 13:20–3. doi: 10.1002/latj.201600008

14. Du D, Liu X, Korn G, Squier J, Mourou G. Laser-induced breakdown by impact ionization in SiO2 with pulse widths from 7 ns to 150 fs. *Appl Phys Lett*. (1994) 64:3071–3. doi: 10.1063/1.111350

15. Pronko PP, Dutta SK, Squier J, Rudd JV, Du D, Mourou G. Machining of sub-micron holes using a femtosecond laser at 800 nm. *Opt Commun*. (1995) 114:106–10. doi: 10.1016/0030-4018(94)00585-I

16. Chichkov BN, Momma C, Nolte S, von Alvensleben F, Tünnermann A. Femtosecond, picosecond and nanosecond laser ablation of solids. *Appl Phys A Mater Sci Process*. (1996) 63:109–15. doi: 10.1007/s003390050359

17. Cheng J, Liu CS, Shang S, Liu D, Perrie W, Dearden G, et al. A review of ultrafast laser materials micromachining. *Opt Laser Technol*. (2013) 46:88–102. doi: 10.1016/j.optlastec.2012.06.037

18. Palanker DV, Blumenkranz MS, Andersen D, Wiltberger M, Marcellino G, Gooding P, et al. Femtosecond laser-assisted cataract surgery with integrated optical coherence tomography. *Sci Transl Med*. (2010) 2:58ra85–11. doi: 10.1126/scitranslmed.3001305

19. Friedman NJ, Palanker DV, Schuele G, Andersen D, Marcellino G, Seibel BS, et al. Femtosecond laser capsulotomy. *J Cataract Refract Surg*. (2011) 37:1189–98. doi: 10.1016/j.jcrs.2011.04.022

20. Nagy ZZ, Kránitz K, Takacs AI, Miháltz K, Kovács I, Knorz MC. Comparison of intraocular lens decentration parameters after femtosecond and manual capsulotomies. *J Refract Surg*. (2011) 27:564–9. doi: 10.3928/1081597X-20110607-01

21. Donaldson KE, Braga-Mele R, Cabot F, Davidson R, Dhaliwal DK, Hamilton R, et al. Femtosecond laser-assisted cataract surgery. *J Cataract Refract Surg*. (2013) 39:1753–63. doi: 10.1016/j.jcrs.2013.09.002

22. Grewal DS, Schultz T, Basti S, Dick HB. Femtosecond laser-assisted cataract surgery-current status and future directions. *Surv Ophthalmol*. (2016) 61:103–31. doi: 10.1016/j.survophthal.2015.09.002

23. Kang MJ, Lee YE, Choi JS, Joo CK. Ideal parameters for femto-second laser-assisted anterior capsulotomy: animal studies. *PloS One*. (2018) 13:1–8. doi: 10.1371/journal.pone.0190858

24. Kohl H, Kulcsar G, Kopf D, Braun B. 12-ps megawatt peak power pulses out of a single laser oscillator with nonlinear pulse compression SPIE Photonics West - Solid State Lasers XXVIII - Sess 3 Pap. nr. 10896-19. (2019).

25. Giese A, Körber M, Kostourou K, Kopf D, Kottcke M, Lohbreier J, et al. Passively Q-switched sub-100 ps Yb3+:YAG/Cr4+:YAG microchip laser: experimental results and numerical analysis. Proc. SPIE 12399, solid state lasers XXXII Technol. *Dev Dent*. (2023) 123990S:9057. doi: 10.1117/12.2649057

26. Schmidbauer JM, Vargas LG, Peng Q, Escobar-Gomez M, Werner L, Arthur SN, et al. Posterior Capsule Opacification. *Int Ophtalmol Clin*. (2001) 41:109–31. doi: 10.1097/00004397-200107000-00010

27. Haug SJ, Bhisitkul RB. Risk factors for retinal detachment following cataract surgery. *Curr Opin Ophthalmol*. (2012) 23:7–11. doi: 10.1097/ICU.0b013e32834cd653

28. Choi A, Kim K, Lee C. Serous retinal detachment following laser peripheral Iridotomy for the angle closure secondary to posterior Scleritis. *Keimyung Med J*. (2017) 36:52–7. doi: 10.0000/kmj.2017.36.1.52

29. Lauterborn W. Optische Kavitation. *Phys J*. (1976) 32:553–63. doi: 10.1002/phbl.19760321208

30. Puliafito CA, Steinert RF. Short-pulsed Nd:YAG laser microsurgery of the eye: biophysical considerations. *IEEE J Quantum Electron*. (1984) 20:1442–8. doi: 10.1109/JQE.1984.1072343

31. Hammer DX, Thomas RJ, Noojin GD, Rockwell BA, Kennedy PK, Roach WP. Experimental investigation of ultrashort pulse laser-induced breakdown thresholds in aqueous media. *IEEE J Quantum Electron*. (1996) 32:670–8. doi: 10.1109/3.488842

32. Petkovšek R, Močnik G, Možina J. Optodynamic characterization of shock waves after laser induced breakdown in water. *Conf Lasers Electro-Optics Eur - Tech Dig*. (2005) 13:4107–12. doi: 10.1109/CLEOE.2005.1568419

33. Liang XX, Linz N, Freidank S, Paltauf G, Vogel A. Comprehensive analysis of spherical bubble oscillations and shock wave emission in laser-induced cavitation. *J Fluid Mech*. (2022) 940:A5. doi: 10.1017/jfm.2022.202

34. Schwartz AL, Anderson DR. Trabecular surgery. *Arch Ophthalmol*. (1974) 92:134–8. doi: 10.1001/archopht.1974.01010010140012

35. Kramer TR, Noecker RJ. Comparison of the morphologic changes after selective laser trabeculoplasty and argon laser trabeculoplasty in human eye bank eyes. *Ophthalmology*. (2001) 108:773–9. doi: 10.1016/S0161-6420(00)00660-6

36. Gupta M, Heo JY, Gong H, Cha E, Latina M, Rhee DJ. Morphologic and cellular changes induced by selective laser Trabeculoplasty. *Clin Ophthalmol*. (2022) 16:1383–90. doi: 10.2147/OPTH.S342787

37. Körber M. *Master's thesis - Iridotomy as glaucoma treatment using a novel ultrashort pulse laser source*. Technische Hochschule Nürnberg Georg Simon Ohm: Nürnberg (2019).

38. [Dataset] 'Divest'. Available at: www.vizaar-xtra.de Emissionsgrad-Tabelle - date Accessed: 19.09.2023 (2023).

39. Ansari MA, Zakeri M. Blind localization of heating in neural tissues induced by a train of the infrared pulse laser. *J Lasers Med Sci*. (2019) 10:264–7. doi: 10.15171/jlms.2019.43

40. Sacks ZS, Dobkin-Bekman M, Geffen N, Goldenfeld M, Belkin M. Non-contact direct selective laser trabeculoplasty: light propagation analysis. *Biomed Opt Express*. (2020) 11:2889–904. doi: 10.1364/boe.390849

41. Körber M, Fritsche M, Giese A, Kopf D, Kottcke M, Luciani F, et al. Ophthalmological surgeries with a novel ultrashort pulse laser source In:. *Paracelsus virtual Sci. Get together 2021*. Nürnberg: PMU Nürnberg (2021)

42. Wenk J. *Bachelor's thesis - quantitative analyse laserinduzierter Kavitationsblasen*. Nürnberg: Tech. rep., Technische Hochschule Nürnberg Georg Simon Ohm (2022).

43. Körber M, Fritsche M, Giese A, Kostourou K, Kopf D, Kottcke M, et al. Iridotomy and capsulotomy on porcine eyes with ultrashort laser pulses in the picosecond regime. Proc. SPIE 12360, *Ophthalmic Technol*. (2023) XXXIII:123600J. doi: 10.1117/12.2650151

44. Vogel A, Venugopalan V. Mechanisms of pulsed laser ablation of biological tissues. *Chem Rev*. (2003) 103:577–644. doi: 10.1021/cr010379n

45. Yakovlev E, Shandybina G, Shamova A. Modelling of the heat accumulation process during short and ultrashort pulsed laser irradiation of bone tissue. *Biomed Opt Express*. (2019) 10:3030–40. doi: 10.1364/boe.10.003030

frontiers | Frontiers in Ophthalmology

TYPE Original Research
PUBLISHED 14 February 2024
DOI 10.3389/fopht.2024.1357373

OPEN ACCESS

EDITED BY
Yongwei Guo,
Zhejiang University, China

REVIEWED BY
Luping Wang,
Capital Medical University, China
Lanying Zhao,
St. Jude Children's Research Hospital, United States

*CORRESPONDENCE
Michael Simmons
michael.a.simm@gmail.com

RECEIVED 18 December 2023
ACCEPTED 29 January 2024
PUBLISHED 14 February 2024

CITATION
Sather RN III, Molleti S, Moon JY, Chaudhry S, Montezuma SR and Simmons M (2024) Visual outcomes of the surgical rehabilitative process following open globe injury repair. *Front. Ophthalmol.* 4:1357373. doi: 10.3389/fopht.2024.1357373

Visual outcomes of the surgical rehabilitative process following open globe injury repair

Richard N. Sather III[1], Sanjana Molleti[1], Jade Y. Moon[1], Saliha Chaudhry[1], Sandra R. Montezuma[1] and Michael Simmons[1,2]*

[1]Department of Ophthalmology and Visual Neurosciences, University of Minnesota, Minneapolis, MN, United States, [2]Rocky Mountain Retina Consultants, Salt Lake City, UT, United States

Background: The path of rehabilitation of an eye after open globe injury (OGI) may require multiple additional secondary surgeries after the initial repair. Although much has been studied regarding the outcomes of secondary surgeries after open globe repair, it can be challenging to understand the possible implications of the surgical rehabilitative process. This retrospective study considers the benefits of the required additional secondary surgeries for a consecutive series of OGI patients.

Methods: OGI patients who had at least one additional surgery after the initial open globe repair (OGR) were studied retrospectively. Additional inclusion criteria included: follow up of at least 12 months since the initial injury and at least 3 months since their most recent surgery, and no additional planned interventions. Preoperative visual acuity was compared to final visual acuity. Additionally, the odds of achieving ambulatory vision (≥20/800) and reading vision (≥20/40) were calculated after each indicated consecutive surgery.

Results: A cohort of 74 eyes from 73 patients met our inclusion criteria. These patients underwent a mean of two additional surgeries. The mean logMAR VA improved from 2.3 (HM) at presentation to 1.4 (20/150), or a 9-line Snellen equivalent improvement. Upon reaching their final visit status, 50% of patients had achieved ambulatory vision and 30% of patients had achieved reading vision. The odds of achieving ambulatory vision after completion of all the rehabilitative surgical process compared to the vision prior to the secondary rehabilitative surgery were higher (OR: 19.1, 95% CI: 7.9 – 30.4, p = 0.0008) as were the odds of achieving reading vision (OR: 4.6, 95% CI: 0.2 – 9.0, p = 0.04). With subsequent second, third, and fourth additional surgeries, the odds of achieving either ambulatory or reading vision at the final visit compared to their preoperative visual acuities were not significant (p > 0.05) but the visual acuity continued to trend toward visual improvement.

Conclusion: Approximately 50% of individuals who required additional surgery at UMN achieved ambulatory vision and 30% achieved reading vision. The odds of visual improvement through the surgical rehabilitative process were very high, with the greatest gains generally achieved after the first surgery.

KEYWORDS

open globe injury (OGI), rehabilitation, trauma, visual outcome, open globe repair

1 Introduction

Open globe injuries (OGIs) continue to be one of the leading causes of monocular vision loss in the United States and worldwide (1). OGIs are considered emergencies, and surgery is usually recommended within 12–24 h of the injury (2, 3). The initial surgery includes proper wound closure, addressing prolapsed ocular tissue, and removing blood and tissue that may limit the view for further surgeries (3).

Many OGIs require additional secondary surgeries after the initial repair with the goal of maximizing or restoring vision. The possible interventions may include pars plana vitrectomy (PPV) (4, 5), penetrating keratoplasty (PKP) (6), iris reconstruction, glaucoma surgery (7), cataract surgery (8), and lens placement (9, 10), to name a few. Although much has been studied on the outcomes of anterior and posterior segment surgeries, the entire surgical rehabilitative process after OGI is less well documented. Each surgery poses an increased risk of endophthalmitis, inflammation, or other complications, with the possibility of diminishing returns with additional intervention. Thus, the question of whether to continue to offer surgery to patients with complications of OGI continues to pose a concern for surgeons and their patients (11).

The current literature also describes factors that predict the final visual acuity (VA), including delays in time to surgery, age of patient, preoperative VA, and modality of injury (12–17). Poor prognostic factors including globe rupture, zone III injuries, multimorbidity, history of PKP, retinal detachment (RD), vitreous hemorrhage (VH), and lens dislocation have shown similar results (16, 18, 19). Despite these in-depth findings, there has been increased recognition of the need to evaluate the VA outcomes for patients who undergo secondary surgeries (15).

The Birmingham Eye Trauma Terminology System (BETTS) was proposed by Kuhn et al. in 1996 to help identify all injury types and classify injuries within a comprehensive framework (20). Eye injury terminology is first divided into closed or open globe injuries. Closed globe injuries include either contusion or lamellar laceration. The focus of this study centers around OGIs, which are either rupture or laceration. A laceration is further subdivided into penetrating, perforating, or intraocular foreign body (IOFB). The differences will be addressed in *Methodology*.

The purpose of this study was to evaluate the VA benefits and qualitative results of secondary indicated surgeries (e.g., RD repair and glaucoma surgery), including surgeries for the rehabilitative process (e.g., cataract surgery and cornea transplant) after the initial open globe repair (OGR) to inform future care protocols for ocular trauma patients.

Abbreviations: OGI, open globe injury; OGR, open globe repair; Betts Classification, a classification system for open globe injuries; IOFB, intraocular foreign body; ED, emergency department; IRB, Institutional Review Board; REDCap, Research Electronic Data Capture; PKP, penetrating keratoplasty; BETT, Birmingham Eye Trauma Terminology; OTS, Ocular Trauma Score; VA, visual acuity; RD, retinal detachment; VH, vitreous hemorrhage; rAPD, relative afferent pupillary defect; PVR, proliferative vitreoretinopathy; NLP, no light perception; CF, count fingers; HM, hand motion; LP, light perception; SD, standard deviation; IU, international units (used in the figure); UMN, University of Minnesota; OR, odds ratio; CI, confidence interval.

2 Methodology

In this retrospective case series, all patients who underwent OGI at the University of Minnesota (UMN)/Minnesota Health System between September 1, 2012 (the date our institution implemented its current electronic medical record system) and October 20, 2022 (the date of IRB submission) were reviewed under our IRB approval STUDY00015830.

The inclusion criteria for this study were as follows: 1) had undergone subsequent surgeries following their OGR; 2) had no further planned surgical intervention; 3) with at least 12 months since their initial injury; and 4) with at least 3 months since their most recent surgery. Patients with non-traumatic globe compromise (e.g., perforation secondary to corneal ulceration) were excluded. Clinical information was gathered using our institution's Electronic Healthcare Record system. Data collection did not exclude patients based on age, ethnicity, or gender. Patients within our hospital system may opt out of inclusion in retrospective chart reviews at the time of the initial consent for service. All patients who opted out were excluded from this analysis.

2.1 Database construction

The REDCap software platform was used to curate the UMN Open Globe Database. An original survey was constructed to facilitate the retrospective collection of all OGIs between the dates mentioned previously. Each patient received a randomized numerical assignment, accompanied by their medical identification number and baseline demographics. Any question addressed in the survey that was not directly found in the patient chart was labeled as "not documented".

The data entry for each open globe patient included four surveys: 1) initial presentation; 2) initial surgical repair; 3) secondary surgeries; and 4) final outcome. The clinical characteristics of the initial OGI included the Birmingham Eye Trauma Terminology (BETT) classification of the type of globe injury (penetrating, perforating, IOFB, and globe rupture) and the zone of injury (20). Rupture was further divided into non-penetrating keratoplasty (non-PKP) and PKP dehiscence. Additional injury details recorded included the presence of RD, endophthalmitis, VH, relative afferent pupillary defect (rAPD) at presentation, mean laceration length, and the presence of laceration extending 13 mm posterior to the equator. The laceration length was calculated by adding all laceration lengths to determine the longest component. Small segments of branching lacerations were ignored.

2.2 Secondary surgeries and final outcome

The types and total number of ophthalmic operations undergone after the initial OGR were recorded. The incidence of

10.3389/fopht.2024.1357373

proliferative vitreoretinopathy (PVR), RD, eye evisceration/enucleation, and phthisis bulbi was also recorded. The final visual outcome measures included the final Snellen acuity, percentage of those who achieved reading vision (defined as VA ≥20/40), percentage of those who achieved ambulatory vision (defined as ≥20/800), and VA comparison from baseline. A patient was deemed to have reached their final VA if they 1) were at least 12 months out from the initial injury and 2) had no additional surgery planned.

2.3 Statistical analysis

Statistical analysis was performed using R v.3.6.3 (R Foundation for Statistical Computing) (21). Mixed effects logistic regression models were used to calculate the odds ratios (ORs) to interpret the likelihood of achieving the visual end points of both reading and ambulatory vision with each secondary surgery and to calculate confidence intervals. Confidence intervals were calculated at the 95th percentile, and statistical significance was set to $p < 0.05$. To calculate the OR, we assumed that, if the patient had not undergone any additional surgery, their final VA would have been equal to their preoperative VA for that surgery. Although we noted the change between the preoperative and postoperative vision for each surgery, we calculated the OR with the patient's final VA. The preoperative VA for any given surgery was compared to the patient's final VA (not to their postoperative VA) for that surgery regardless of the number of surgeries a given patient had. We also noted the visual changes that occurred following each surgery to provide a mixed effects regression model, which was used to account for the inclusion of each patient twice in the dataset, once as preoperative self and once as postoperative self. The Snellen VA was converted to a corresponding logMAR scale to reduce erroneous results and misrepresentative statistical analyses (22, 23). To convert low VA reference values [count fingers, hand motion (HM), light perception (LP), and no light perception (NLP)] to logMAR, we utilized the Excel conversion tool produced by Moussa et al. (24).

3 Results

3.1 Demographic information

A total of 229 patients with OGIs between September 2016 and October 2022 were evaluated. From these patients, a cohort of 74 eyes from 73 patients met the proposed inclusion criteria. The baseline demographic information for our patient cohort is displayed in Table 1. The cohort was predominantly men and Caucasian, with a median age of 38 years. The majority of injuries occurred at home (41.1%), at work (26.0%), or on a farm (6.8%). The mechanism of injury was widely dispersed, with the majority coming from ground-level fall/syncope (15.1%), operating a power tool (11.0%), and firearm/firework (11.0%). Approximately a third of the mechanisms did not fall into one of the categories listed.

TABLE 1 Baseline demographic information.

Epidemiological data	Number distribution	Percentage
1. Sex		
Male	63	86.3
Female	10	13.7
2. Age (years)		
Mean ± SD	42.5 ± 22.3	
Median	38	
Range	4–96	
3. Self-identified ethnicity		
Caucasian	63	82.9
Black/African American	8	10.5
Other: American Indian/ Alaska Native/Asian/Latin	5	6.6
4. Eye(s) affected		
OD	32	43.8
OS	40	54.8
OU	1	1.4
5. Injury location		
Home	30	41.1
Work	19	26.0
Farm	5	6.9
School	0	0.0
Other	19	26.0
6. Injury mechanism		
Ground-level fall/syncope	11	15.1
Hammering metal-on-metal	7	9.6
Power tool	8	11.0
Animal	3	4.0
Sport	1	1.4
Assault	6	8.2
Firearm/firework	8	11.0
Sharp stick	4	5.5
Other	25	34.2

OD, oculus dexter; OS, oculus sinister; OU, oculus uterque.

3.2 Initial injury and surgical management

The BETT classification system was first utilized at the beginning of each visit. The open globe clinical evaluation is displayed in Table 2. There was an almost equal distribution of penetrating (29.2%), IOFB (27.8%), and non-PKP rupture (27.8%) injury types that comprised the majority of our patient cohort. There were only three cases (4.2%) of perforating injury. The injury

10.3389/fopht.2024.1357373

TABLE 2 Clinical characteristics of the initial injury and intraoperative repair.

Preoperative status	Number distribution	Percentage
1. Injury type		
Penetrating	21	29.2
Perforating	3	4.1
IOFB	20	27.8
Rupture (non-PKP)	20	27.8
Rupture (PKP dehiscence)	8	11.1
2. Injury zone		
Zone I	46	63.9
Zone II	20	27.8
Zone III	15	20.8
3. OTS		
Mean ± SD	2.1 ± 1	
Median	2	
Range	1–5	
4. Laceration length (mm)		
Mean ± SD	9.5 ± 7.1	
Median	7.5	
Range	1–30	
5. Presenting VA logMAR (Snellen equivalent)		
Mean ± SD	2.3 ± 0.85 (~HM)	
Median	2.4 (HM)	
Range	0–3.0 (20/20–NLP)	
6. Clinical findings		
Vitreous hemorrhage	39	54.2
RD	22	30.1
Endophthalmitis	7	9.7
rAPD	9	12.3
Laceration posterior to the equator	6	8.7

IOFB, intraocular foreign body; PKP, penetrating keratoplasty; OTS, Ocular Trauma Score; RD, retinal detachment; rAPD, relative afferent pupillary defect; HM, hand motion; NLP, no light perception.

zone consisted mainly of zone I involvement (63.9%), with a near-equal distribution between zones II and III (27.8% and 20.8%, respectively). The mean Ocular Trauma Score (OTS) was ~2. The mean laceration length was ~9.5 mm, with a median of 7.5 mm. Laceration lengths ranged from 1 to 30 mm posterior to the limbus. The presenting VA ranged from 20/20 to NLP, with an average logMAR of 2.3 (equivalent to HM). The most common clinical findings on initial presentation were RD (30.1%) and VH (54.2%). Approximately 10% of patients had endophthalmitis, rAPD, or a laceration posterior to the equator.

3.3 Additional surgeries and final patient outcome

The patients in our cohort underwent a mean of two secondary surgeries after their initial globe repair. Figure 1 displays the total number of patients who underwent each secondary surgery with attention to each type of secondary surgery. Only two patients had five additional surgeries, and one patient had six. The majority of surgeries were retinal repair (49%), followed by lens management (28%), iris surgery (13%), corneal transplant (6%), and glaucoma surgery (3%). Strabismus surgery represented 1% of the secondary surgeries. The final visual and anatomic outcomes of this cohort are presented in Table 3. It should be noted that 12 patients (16.4%) did not get an initial VA. A final mean VA outcome of 1.4, or 20/500, was obtained for our patient cohort. This represents an average of 0.9 logMAR scale, or a nine-line Snellen VA, improvement from the presenting baseline VA. There were 39 patients (~65%) who had a final outcome VA improvement relative to their baseline VA. Subsequently, ~12% of the final VA outcome worsened and ~23% remained unchanged. The 14 patients who had an unchanged final VA included 10 NLP, 3 LP, and 1 HM. Overall, ~50% of our patient cohort achieved ambulatory vision and 30% achieved reading vision.

The retina remained attached for the majority of patients (~55%), while PVR developed in ~20%. Of those subjects who developed RD, re-attachment occurred in 62.5% of patients by their final visit. Overall, ~80% of the patients had their retina attached by the final visit. A total of 13 patients (17.8%) had their eye enucleated as a result of the trauma. Lastly, only two patients (3.0%) developed phthisis bulbi, and both of these were enucleated.

On crude analysis, there was an improvement in the median VA with each subsequent surgery, as demonstrated in Figure 2A. This upward trend in VA held true for the majority of individual patients included in our cohort, as demonstrated in Figure 2B.

Table 4 displays the ORs for achieving the visual end points of reading and ambulatory vision at the final visit, with each additional surgery compared to the preoperative VA for that surgery, controlling for OTS. The number of patients who underwent a secondary surgery is indicated by the denominator (i.e., 73 patients underwent the first secondary surgery, 41 patients underwent a second secondary surgery, etc.). The number of patients who needed additional surgery decreased by approximately half after each surgery. The number of patients who achieved ambulatory VA increased to more than double after their first additional surgery and nearly doubled following the second surgery. The number who attained reading VA increased from 2 to 20 and from 2 to 7 patients for secondary surgeries 1 and 2, respectively. It should be noted that the number of patients who achieved ambulatory VA after their third secondary surgery decreased postoperatively; however, the number who achieved reading VA postoperatively increased.

Only two patients required more than four surgeries. The ORs for the achievement of final visual end points were not calculated for

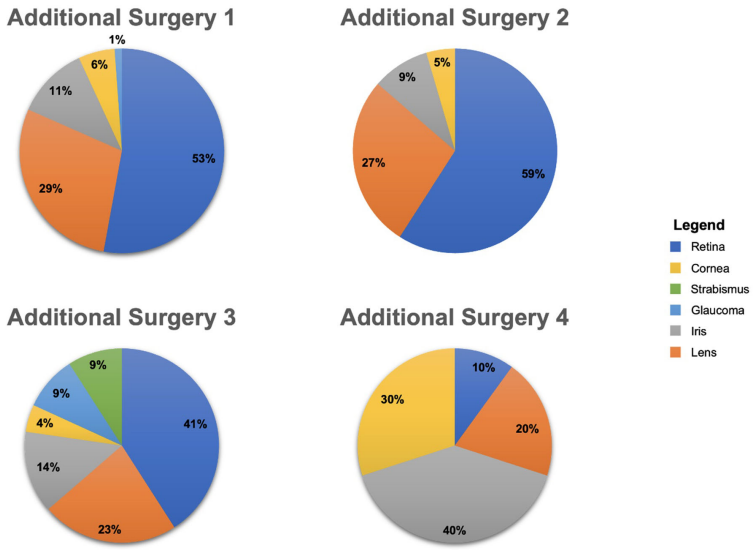

FIGURE 1
Graphical division of the different types of additional secondary surgeries.

TABLE 3 Secondary surgeries and final outcome.

Postoperative status	Number distribution	Percentage
1. Secondary surgeries		
Mean ± SD	2.08 ± 1.20	
Median	2	
Range	1–6	
2. Final VA logMAR (Snellen equivalent)		
Mean ± SD	1.4 ± 1.2 (20/500)	
Median	0.88 (20/150)	
Range	0–3 (20/20–NLP)	
Achieved:		
Reading vision ≥20/40	20	28.2
Ambulatory vision ≥20/800	38	53.5
From baseline VA:		
Improved	39	65.0
Worsened	7	11.7
Unchanged	14	23.3
3. Final surgical outcome		
RD incidence	32	44.4
PVR incidence	15	20.8
Retina attached	40	55.6
Retina re-attachment	20	62.5
Phthisis bulbi	2	3.0
Enucleation	13	17.8

VA, visual acuity; RD, retinal detachment; PVR, proliferative vitreoretinopathy.

these. A single patient who required five secondary surgeries had an IOFB removal with four subsequent retinal surgeries. There was an ~1.2 logMAR improvement between the initial and the final visit (CF → 20/150). Another patient underwent six secondary surgeries due to endophthalmitis complications. This patient underwent three retinal surgeries, one cornea surgery, one lens surgery, and one iris surgery. There was an ~0.8 logMAR improvement (20/800 → 20/60) for this patient at the final outcome. The data of these patients were excluded from Table 4, as there were insufficient eyes for statistical analysis.

The odds of achieving ambulatory and reading vision at the final visit after undergoing the first surgery were 19 times greater than without that procedure (OR = 19.1, 95% CI = 7.9–30.4, $p = 0.0008$). With subsequent second, third, and fourth additional surgeries, the odds of achieving ambulatory or reading vision were not significant ($p > 0.05$). The second additional surgery, however, did trend toward significance at $p = 0.06$ for ambulatory vision, with a favorable OR. It should be noted that having a third additional surgery lowered the odds of achieving either ambulatory or reading VA; however, the small sample size likely confounds this measurement. In addition, the small sample size limited the statistical analysis for reading vision after the fourth additional surgery.

4 Discussion

In this retrospective case series of patients who underwent additional surgeries after OGR, approximately one-half of our cohort achieved ambulatory vision, while a little over one-fourth achieved reading vision, with a mean of two surgeries by their final visit. For patients and their surgeons contemplating the implications of a recent OGI, these data suggest that, when indicated, the surgical rehabilitative process provided a functionally meaningful visual benefit in our population.

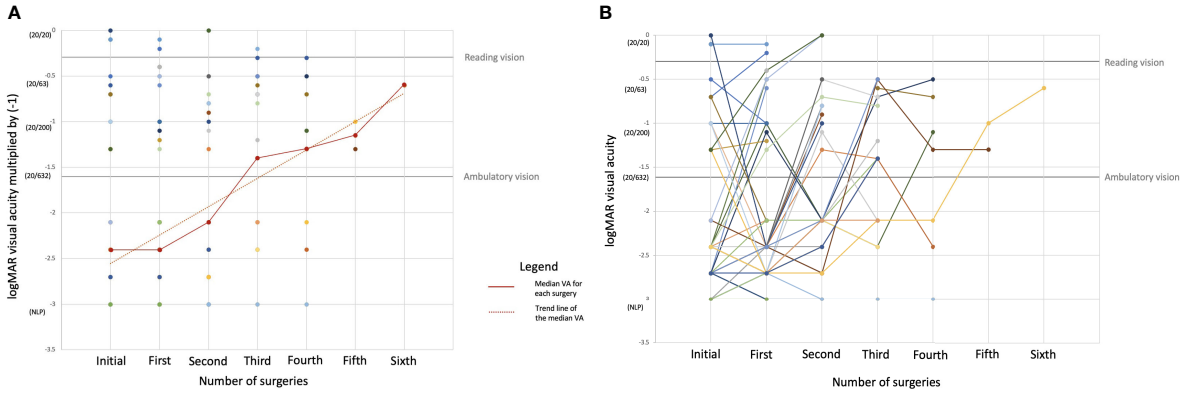

FIGURE 2
Changes in the preoperative visual acuity (VA) by number of subsequent surgeries. The *y*-axis represents the logMAR VA value multiplied by (−1). **(A)** All VA values with the median VA value for each surgery and the trend line for the median VA value superimposed. **(B)** Changes in the preoperative VA with each subsequent additional surgery by each individual patient. Each of the 73 *colored lines* with its associated *dots* corresponds to individual patients and changes in their VA with each subsequent surgery.

The mean VA on initial presentation in our cohort was logMAR 2.3 (roughly equivalent to HM) and improved to logMAR 1.4 (Snellen equivalent 20/150), which represents a 0.9 logMAR, or a nine-line ETDRS equivalent improvement. The OTS provides predictions of the final VA at 6 months after OGI (20), and these predictions have been validated in other cohorts (25). For our cohort, the mean OTS of approximately 2 on presentation, which corresponds to a 6-month estimated VA follow-up of ≥20/40 (15%), 20/50–20/200 (13%), 19/200–1/200 (18%), HM or LP (26%), and NLP (28%) (26). The patients in our cohort outperformed these predictions, but it should be noted that our cohort was inherently different from that in the OTS: we included only patients who underwent secondary surgeries, which likely biased our cohort to include patients with higher vision potential (i.e., patients who underwent additional surgery did so because their surgeons deemed their vision potential high enough to merit intervention).

In our cohort, the odds of achieving ambulatory and reading vision at the final visit were most favorable with the first additional surgery, and the majority of patients who achieved these end points did so after the first surgery. Following this first surgery, the odds of meeting the VA end

TABLE 4 Patient proportion and odds ratio of obtaining ambulatory and reading visual acuity (VA) with each secondary surgery controlling for the Ocular Trauma Score (OTS).

Secondary surgery no.	Proportion preoperatively	Proportion postoperatively[a]	Odds ratio[b]	95% Confidence interval	*p*-value
Surgery 1:					
Ambulatory	13/73	39/73	19.1	7.9–30.4	0.0008*
Reading	2/73	20/73	4.6	0.2–9.0	0.04*
Surgery 2:					
Ambulatory	12/41	21/41	1.6	−0.1 to 3.3	0.06
Reading	2/41	7/41	3.3	−8.0 to 14.7	0.56
Surgery 3:					
Ambulatory	13/23	12/23	−0.6	−2.5 to 1.4	0.58
Reading	2/23	4/23	−8.2	−72.4 to 55.9	0.80
Surgery 4:					
Ambulatory	5/9	6/9	12.6	−15.0 to 40.2	0.37
Reading[c]	1/9	1/9	–	–	–

*$p < 0.05$ (statistically significant relationship).
[a]The postoperative VA for surgery 1 was taken from the same visit as the preoperative VA for surgery 2, and likewise for each surgery.
[b]The odds ratio was calculated using the final VA. Postoperative proportions meeting the visit thresholds are provided for clarity.
[c]Statistics unable to perform the fourth surgery (reading) due to a small sample size.

points were not significant. A number of factors likely contributed to this. Firstly, the sample size decreased by approximately half with each consecutive surgery, making statistical significance harder to demonstrate. Secondly, the preoperative proportion of patients who had already met a given end point increased with each consecutive surgery so that the difference between preoperative and postoperative VA shrunk as patients underwent additional intervention. Lastly, the number of required surgeries may well reflect the severity of the initial injury: the more surgeries required, the worse the underlying pathology may have been, and the more limited the final visual prognosis.

The division among the different types of secondary surgeries that were performed is included in Figure 1. Approximately 50% of our patient cohort underwent at least one secondary retinal surgery. These surgeries were used to manage various posterior pathologies common after OGI, such as RD, VH, PVR, and endophthalmitis. A total of 46 patients (63%) had a PPV performed during the first surgery, and all of those patients had a postoperative VA improvement: 16 eyes improved to ambulatory vision and 11 eyes improved to reading vision. These data align with the findings of other groups whose research supports the importance of vitrectomy after OGR (25).

Approximately 43% of our cohort developed an RD. Given that our cohort was biased toward those who needed surgical intervention after OGI, this percentage is not directly comparable, but is likely consistent with the incidence of RD after OGI of 29.0% reported by the Massachusetts Eye and Ear Infirmary (4) and the Kellogg Eye Center for RD after OGI (27). In our cohort, 55% had their retina attached at the initial presentation. Conversely, 62.5% of patients who experienced RD had reattachment by the final visit. Over 80% of patients had their retina attached at their final visit.

One of the strengths of this study is our approach of calculating the OR for the final VA rather than the postoperative VA because this reflects the clinically relevant question that patients and their surgeons want to know: after sustaining an OGI, if an unknown number of surgeries will be needed to rehabilitate the eye, will taking the next step and undergoing the next indicated surgery be worth it in the end? Although multiple different surgeries may be indicated, using the OR for the final VA allows the ratio to reflect the entire rehabilitation process rather than the specific details of a single indicated surgery. Likewise, the structural outcomes we reported should be interpreted as the outcomes for a cohort who completed a surgical rehabilitative process after OGI.

One limitation of this study is that our categorical outcome markers of ambulatory and reading vision limited recognition of vision gains within these categories (i.e., clinically relevant gains of vision between 20/800 and 20/40 or from 20/40 to 20/20 were not captured in our ORs). Likewise, our results were limited by the extent our assumption is true that the final VA for a given patient would be equal to their preoperative VA if they never underwent any additional intervention. Many surgeries after OGI are performed with the intent of stabilizing the eye (for example in the setting of developing RD or glaucoma), so it is reasonable to assume that the final vision for patients would have been equal to or worse than their preoperative vision if they had not undergone surgery. Lastly, this was a retrospective cohort study from a single institution; thus, our results may not be generalizable to other populations and should be applied in clinical decisions with caution.

5 Conclusion

Patients at the University of Minnesota who underwent secondary surgeries after OGR experienced significant gains in vision. The odds of achieving ambulatory vision and reading vision through the surgical rehabilitative process were favorable, and the greatest gains for our cohort were attained through the first secondary surgery. The number of patients needing additional surgery decreased by approximately half with each surgery through the surgical rehabilitative process.

Data availability statement

The original contributions presented in the study are included in the article/supplementary material. Further inquiries can be directed to the corresponding author.

Ethics statement

The studies involving humans were approved by University of Minnesota Institutional Review Board. The studies were conducted in accordance with the local legislation and institutional requirements. Written informed consent for participation was not required from the participants or the participants' legal guardians/next of kin in accordance with the national legislation and institutional requirements.

Author contributions

RS: Conceptualization, Data curation, Formal analysis, Investigation, Methodology, Writing – original draft, Writing – review & editing. SM: Data curation, Formal analysis, Investigation, Methodology, Writing – review & editing. JM: Data curation, Formal analysis, Investigation, Methodology, Software, Writing – original draft, Writing – review & editing. SC: Data curation, Investigation, Methodology, Writing – review & editing. SM: Formal analysis, Funding acquisition, Investigation, Resources, Supervision, Validation, Writing – review & editing. MS: Conceptualization, Data curation, Formal analysis, Funding acquisition, Investigation, Methodology, Resources, Supervision, Validation, Visualization, Writing – original draft, Writing – review & editing.

Funding

The author(s) declare financial support was received for the research, authorship, and/or publication of this article. This work was supported by the Minnesota Lions Vision Foundation (1701-11820-20090-UMF0011830) and the Knobloch Chair Professorship (1701-11820-20231-UMF0014654) (SRM). The study sponsors were not involved in the study design, collection, analysis, interpretation of data, writing the report, or the decision to submit the report for publication.

Acknowledgments

To all UMN residents and attendings involved on these trauma patient's care.

Conflict of interest

The authors declare that the research was conducted in the absence of any commercial or financial relationships that could be construed as a potential conflict of interest.

Publisher's note

References

1. Chen A, McGwin G, Justin GA, Woreta FA. The United States eye injury registry: past and future directions. *Ophthalmology*. (2021) 128:647–8. doi: 10.1016/j.ophtha.2020.11.026

2. Makhoul KG, Bitar RA, Armstrong GW, Weinert MC, Ivanov A, Kahale F, et al. Effect of time to operative repair within twenty-four hours on visual acuity outcomes for open globe injuries. *Eye*. (2023) 37:2351–5. doi: 10.1038/s41433-022-02350-6

3. Zhou Y, DiSclafani M, Jeang L, Shah AA. Open globe injuries: review of evaluation, management, and surgical pearls. *Clin Ophthalmol*. (2022) 16:2545–59. doi: 10.2147/OPTH.S372011

4. Stryjewski TP, Andreoli CM, Eliott D. Retinal detachment after open globe injury. *Ophthalmology*. (2014) 121:327–33. doi: 10.1016/j.ophtha.2013.06.045

5. Ung C, Stryjewski TP, Eliott D. Indications, findings, and outcomes of pars plana vitrectomy after open globe injury. *Ophthalmol Retin*. (2020) 4:216–23. doi: 10.1016/j.oret.2019.09.003

6. Li KX, Durrani AF, Zhou Y, Zhao PY, Tannen BL, Mian SI, et al. Outcomes of penetrating keratoplasty after open globe injury. *Cornea*. (2022) 41:1345–52. doi: 10.1097/ICO.0000000000002918

7. Osman EA. Glaucoma after open globe injury. *Saudi J Ophthalmol Off J Saudi Ophthalmol Soc*. (2015) 29:222–4. doi: 10.1016/j.sjopt.2014.10.006

8. Tabatabaei SA, Rajabi MB, Tabatabaei SM, Soleimani M, Rahimi F, Yaseri M. Early versus late traumatic cataract surgery and intraocular lens implantation. *Eye (Lond)*. (2017) 31:1199–204. doi: 10.1038/eye.2017.57

9. Chuang L-H, Lai C-C. Secondary intraocular lens implantation of traumatic cataract in open-globe injury. *Can J Ophthalmol*. (2005) 40:454–9. doi: 10.1016/S0008-4182(05)80005-5

10. Thomas J, Armstrong G. Use of Yamane technique for secondary intraocular lens implantation following open globe injury. *BMJ Case Rep*. (2023) 16:e255995. doi: 10.1136/bcr-2023-255995

11. Andreoli MT, Andreoli CM. Surgical rehabilitation of the open globe injury patient. *Am J Ophthalmol*. (2012) 153:856–60. doi: 10.1016/j.ajo.2011.10.013

12. Fernandez EO, Miller HM, Pham VQ, Fleischman D. Comparison of time-to-surgery and outcomes in transferred vs non-transferred open globe injuries. *Clin Ophthalmol*. (2022) 16:2733–42. doi: 10.2147/OPTH.S378049

13. Agrawal R, Rao G, Naigaonkar R, Ou X, Desai S. Prognostic factors for vision outcome after surgical repair of open globe injuries. *Indian J Ophthalmol*. (2011) 59:465–70. doi: 10.4103/0301-4738.86314

14. Amro MY. Visual outcomes associated with delay from trauma to surgery for open globe eye injury in Palestine: a retrospective chart review study. *Lancet*. (2021) 398:S14. doi: 10.1016/S0140-6736(21)01500-2

15. Djalali-Talab Y, Mazinani B, Djalali-Talab Y. Traumatic open globe injury—epidemiology, risk factors and visual outcome at the University Hospital Aachen. *Spektrum der Augenheilkd*. (2021) 35:75–82. doi: 10.1007/s00717-020-00480-4

16. Fujikawa A, Mohamed YH, Kinoshita H, Matsumoto M, Uematsu M, Tsuiki E, et al. Visual outcomes and prognostic factors in open-globe injuries. *BMC Ophthalmol*. (2018) 18:138. doi: 10.1186/s12886-018-0804-4

17. Puodžiuvienė E, Valeišaitė G, Žemaitienė R. Clinical characteristics, visual outcomes, and prognostic factors of open globe injuries. *Medicina (B Aires)*. (2021) 57(11):1198. doi: 10.3390/medicina57111198

18. Bleicher ID, Tainsh LT, Gaier ED, Armstrong GW. Outcomes of zone 3 open globe injuries by wound extent: subcategorization of zone 3 injuries segregates visual and anatomic outcomes. *Ophthalmology*. (2023) 130:379–86. doi: 10.1016/j.ophtha.2022.10.027

19. Batchelor A, Lacy M, Hunt M, Lu R, Lee AY, Lee CS, et al. Predictors of long-term ophthalmic complications after closed globe injuries using the IRIS® registry (Intelligent research in sight). *Ophthalmol Sci*. (2023) 3(1):100237. doi: 10.1016/j.xops.2022.100237

20. Kuhn F, Morris R, Witherspoon CD, Heimann K, Jeffers JB, Treister G. A standardized classification of ocular trauma. *Ophthalmology*. (1996) 103:240–3. doi: 10.1016/S0161-6420(96)30710-0

21. R Core Team. R: A language and environment for statistical computing. *A Language and Environment for Statistical Computing*. Vienna, Austria (2020). Available online at https://www.R-project.org/.

22. HJ T. Proper method for calculating average visual acuity. *J Refract Surg*. (1997) 13:388–91. doi: 10.3928/1081-597X-19970701-16

23. Holladay JT. Visual acuity measurements. *J Cataract Refract Surg*. (2004) 30 (2):287–290. doi: 10.1016/j.jcrs.2004.01.014

24. Moussa G, Bassilious K, Mathews N. A novel excel sheet conversion tool from Snellen fraction to LogMAR including 'counting fingers', 'hand movement', 'light perception' and 'no light perception' and focused review of literature of low visual acuity reference values. *Acta Ophthalmol*. (2021) 99:e963–5. doi: 10.1111/aos.14659

25. Perez EA, Scott NL, Russell JF. Improved visual outcomes after severe open-globe injuries associated with perioperative vitreoretinal evaluation. *Ophthalmol Retin*. (2023) 7:771–8. doi: 10.1016/j.oret.2023.04.015

26. Kuhn F, Maisiak R, Mann L, Mester V, Morris R, Witherspoon CD. The ocular trauma score (OTS). *Ophthalmol Clin*. (2002) 15:163–5. doi: 10.1016/S0896-1549(02)00007-X

27. Durrani AF, Li K, Zhou Y, Toiv A, Zhao PYC, Huvard M, et al. Risk factors for retinal detachment following open globe injury and outcomes of retinal detachment repair following ocular trauma. *Invest Ophthalmol Vis Sci*. (2022) 63:4302.

frontiers | Frontiers in Medicine

TYPE Original Research
PUBLISHED 13 March 2024
DOI 10.3389/fmed.2024.1382100

OPEN ACCESS

EDITED BY
Georgios D. Panos,
Nottingham University Hospitals NHS Trust, United Kingdom

REVIEWED BY
Zhaotian Zhang,
Sun Yat-sen University, China
Katarzyna Krysik,
Wojewódzki Szpital Specjalistyczny nr 5 Sosnowiec, Poland

*CORRESPONDENCE
Peiquan Zhao
✉ zhaopeiquan@xinhuamed.com.cn

†These authors have contributed equally to this work and share first authorship

RECEIVED 05 February 2024
ACCEPTED 26 February 2024
PUBLISHED 13 March 2024

CITATION
Ye H, Wu M, Sun W, Lyu J, Xu Y, Fei P, Peng J, Jin H and Zhao P (2024) Clinical observation of a modified technique for intrascleral fixation of flanged three-piece foldable intraocular lenses through a Hoffman pocket. *Front. Med.* 11:1382100. doi: 10.3389/fmed.2024.1382100

Clinical observation of a modified technique for intrascleral fixation of flanged three-piece foldable intraocular lenses through a Hoffman pocket

Hongfei Ye[1†], Mengxiao Wu[1†], Wan Sun[1†], Jiao Lyu[1], Yu Xu[1], Ping Fei[1], Jie Peng[1], Haiying Jin[2] and Peiquan Zhao[1*]

[1]Department of Ophthalmology, Xinhua Hospital Affiliated to Shanghai Jiaotong University School of Medicine, Shanghai, China, [2]Department of Ophthalmology, Shanghai East Hospital, Tongji University School of Medicine, Shanghai, China

Purpose: To present the outcomes of a new technique for intrascleral fixation of a flanged three-piece foldable intraocular lens (IOL) without a conjunctival incision.

Materials and methods: We retrospectively reviewed a consecutive series of 12 eyes of 12 patients who underwent scleral IOL fixation using this technique.

Results: The follow-up period ranged 3–12 months. There was a significant improvement in best-corrected visual acuity, from 0.8 (1.6) logarithm of the minimum angle of resolution (logMAR) preoperatively to 0.45 (0.8) logMAR at the final postoperative follow-up ($p = 0.012$). Notable complications included one case of pupillary IOL capture and increased intraocular pressure.

Conclusion: Our novel technique is a viable solution for managing secondary IOL fixation, enabling the use of a wider variety of IOLs and simplifying the reposition process for dislocated three-piece IOLs. This approach has the potential to lower complication rates and enhance patients' recovery.

KEYWORDS

three-piece intraocular lens, scleral fixation, Hoffman pockets, flange, knotting

Introduction

Scleral fixation of posterior chamber intraocular lens (PCIOLs) is a popular technique for secondary IOL implantation in the absence of capsular support, which allows for IOL placement in the physiologic anatomic position and theoretically mitigates complications (1). Although sutureless scleral fixation techniques can mitigate the risk of complications associated with sutures, there remains a significant concern regarding the stability of IOLs, with generally unsatisfactory long-term outcomes (2). Thus far, scleral suture fixation of PCIOLs has demonstrated superior long-term durability and offers a comparatively simpler approach to manage potential surgical complications (1, 3).

Traditional sclerally-sutured IOLs, such as CZ70BD (Alcon Laboratories, Fort Worth, Texas, USA), are composed of polymethyl methacrylate (PMMA) and require a larger incision. This variety of IOLs have become less popular over recent years given the associated risks of

intraoperative damages and postoperative complications (4). Though the literatures have reported on the use of foldable IOLs for suture fixation, these studies were mostly designed with closed-loop haptics (5, 6). The option of using foldable IOLs remains limited for scleral fixation. In our previous study, a modified technique for scleral suture fixation of a three-piece PCIOL was proposed (7). While it is a general trend to develop novel fixation techniques for more flexible usage of various designs of IOLs.

In this study, we present observation outcomes of a modified technique, combining the Hoffman pocket, flanged IOL fixation technique, and a special knotting method for firm suturing and secure IOL fixation. This technique allows for flexible usage of three-piece PCIOLs under various conditions. For IOL dislocation cases, this method allows IOL reposition without the procedures of IOL explantation and reimplantation, which is highly effective and leads to a significant reduction in both intraoperative and postoperative complications. Below, we describe the utilization of this technique, its applications, and corresponding clinical results.

Materials and methods

This study was approved by the Ethical Review Board of Xinhua Hospital Affiliated to Shanghai Jiao Tong University School of Medicine and adhered to the principles of the Declaration of Helsinki. A retrospective chart review was performed consisting of 12 eyes of 12 patients who underwent this modified scleral suture fixation of a three-piece PCIOL [Tecnis ZA9003 (Johnson and Johnson, Santa Ana, California, USA) or MA60AC (Alcon Laboratories, Fort Worth, Texas, USA)] between January 2022 and December 2022. Patients were followed up for at least 3 months after surgery. Medical records included surgical indications, relevant ocular and systemic histories, and postoperative complications were collected. All patients had undergone ophthalmic evaluations including best-corrected visual acuity (BCVA), intraocular pressure (IOP), refraction, slit-lamp biomicroscopy, dilated fundus examination, optical coherence tomography measurement, axial length, and corneal endothelial density (ECD) preoperatively and at the last visit postoperatively.

Surgical technique

Two scleral pockets are created by a crescent blade posteriorly from the limbus at 3 o'clock and 9 o'clock. The pockets are extended perpendicular to the limbus and continued for 3.0 mm, keeping a uniform depth of 300 µm in the sclera (Figure 1A). Using a 20-G microvitreoretinal blade, a paracentesis is made at 4 o'clock for 20-G infusion, and two side paracenteses are made at 2:30 o'clock and 9:30 o'clock for sutures. A superior corneal incision is made using a 3.0 mm sharp-tip keratome. Subsequently, two puncture points are marked by calipers at the pocket beds' midline and 2.0 mm posterior to the limbus on both sides (Figure 1B). A double-armed 9–0 polypropylene suture (Mani, Tochigi, Tokyo, Japan) with one straight needle and one curved needle is used for IOL fixation. The straight needle is introduced at one puncture point at 9 o'clock through the conjunctiva and full thickness of the scleral pocket, passing through the anterior chamber and guided out via the side paracentesis at 2:30 o'clock with the assistance of a vitreoretinal forceps. Afterwards, the straight needle is again passed back through the same side paracentesis, threading through the anterior chamber and docked into the opening of a 30-G needle which is introduced at 1.0–2.0 mm adjacent to the puncture point at 9 o'clock and then removed externally (Figure 1C). The same manipulations are performed at the other puncture point at 3 o'clock. Next, the two suture-loops are dragged externally from the anterior chamber out of the superior incision by the forceps for IOL fixation (Figure 1D). Following this, the two haptic ends of the IOL are cauterized to create a flange (Figure 1E). The PCIOL is loaded in the cartridge and the leading haptic is pushed out. Then, the double sutures with its loop at 9 o'clock are wrapped around the flanged end of the leading haptic, passing behind the standing part, and the flanged end is tucked into the suture-loop, which is finally tightened to form a knot at the junction of the enlarged flange (Figure 1F). We illustrate four types of wrapping methods in Figure 2. After the leading haptic tied with the double sutures and the optic of the folded IOL is injected into the anterior chamber, the trailing haptic left externally is tied with the same knot using the double sutures with its loop at 3 o'clock (Figure 1G), and then pushed subsequently into the eye using a Sinskey hook. Thereafter, each suture end is retrieved through the scleral pocket opening by placing the Sinskey hook into the pocket and externalized after adjusting the suture tensions on both sides for the position of the PCIOL. The two pairs of suture ends are tied by tension adjustable knot to further center the optic of the PCIOL (Figure 1H). Finally, the superior incision is sutured with 10–0 threads and the side incisions are watertight (Figure 1I). An additional movie file shows this in more details (Supplementary Video 1).

All surgeries were performed by a singular experienced surgeon (PQ.Z), under general anesthesia for patients under 13 years old and retrobulbar anesthesia for the remaining. For cases with silicone oil retention, a complete pars plana vitrectomy (PPV) was performed to remove remnant silicone oil droplets prior to IOL fixation. Lensectomy was conducted beforehand to retrieve subluxated lenses or disintegrated lens capsules.

Statistical analysis

All statistic analysis was conducted using SPSS software version 26.0 for Windows (SPSS, Chicago, Illinois, USA). The Snellen VA measurements were converted to the logarithm of the minimum angle of resolution (logMAR) units for the statistical analyses. The Wilcoxon signed-rank test was used to identify the changes between the preoperative and postoperative BCVA. The changes of IOP and ECD before and after the operation were analyzed by paired *t*-test. The statistically significance was considered when p value was less than 0.05.

Results

Twelve eyes of twelve patients (9 males, 3 females) were included in this study. The mean patient age was 19.3 ± 14.6 years at the time of the surgery. The lenses of seven patients had been extracted in previous surgeries due to traumatic retinal detachment (4 eyes), rhegmatogenous retinal detachment (1 eye), intraocular foreign body (1 eye), and congenital lens subluxation (1 eye). Four patients had subluxated lenses (4 eyes) and one patient (1 eye) had a dislocated IOL

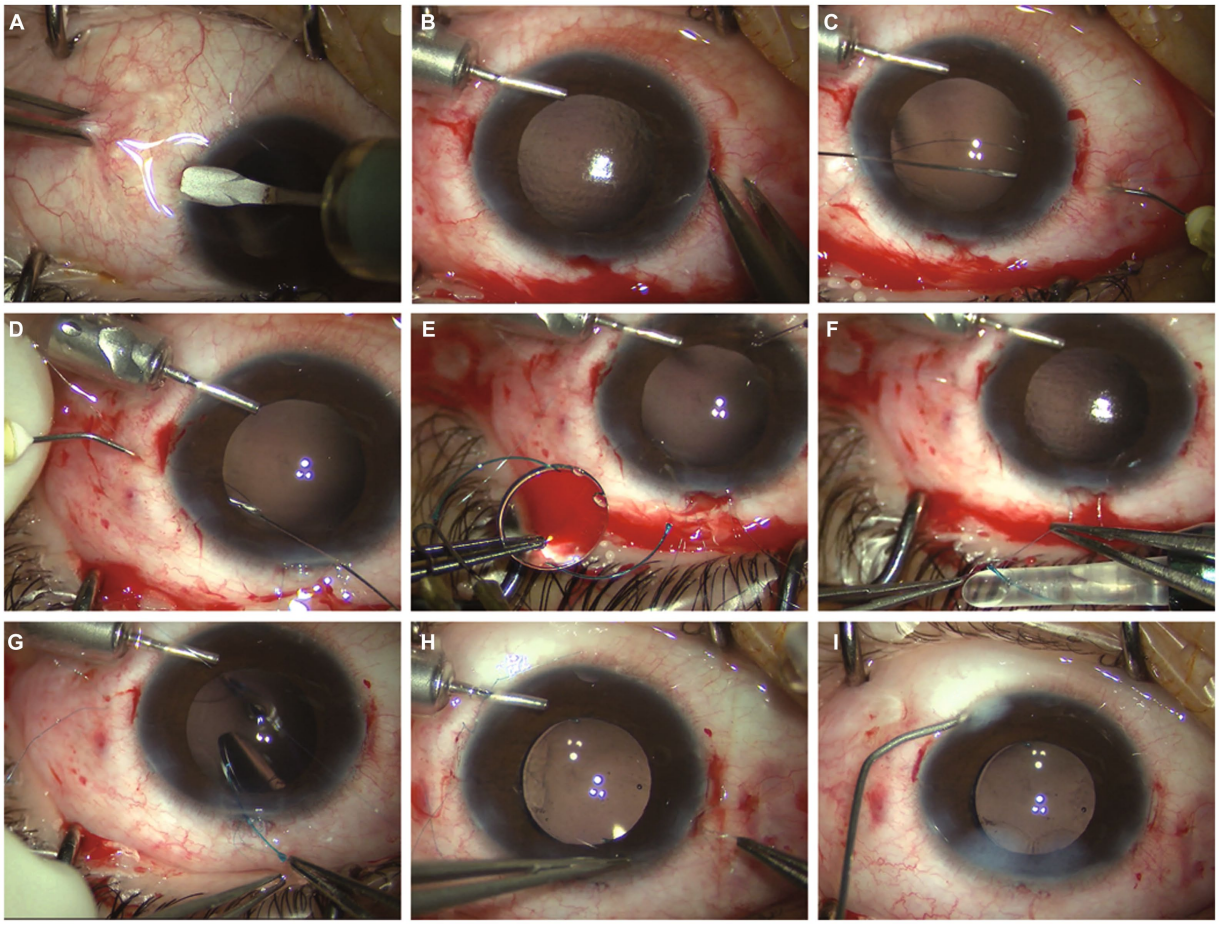

FIGURE 1
(A) Two scleral pockets are dissected by a crescent blade posteriorly from the limbus at 3 o'clock and 9 o'clock, achieving a thickness of 300 μm and a length of 3.0 mm. **(B)** After anterior chamber infusion, puncture points are marked at the middle line of the pocket beds 2.0 mm posterior to the limbus on both sides. **(C)** The straight needle of a double-armed 9–0 polypropylene suture is introduced at one puncture point at 9 o'clock through the conjunctiva and full thickness of the scleral pocket, passing through the anterior chamber and guided out via the side paracentesis at 2:30 o'clock. The straight needle is again passing backward through the same side paracentesis, threading through the anterior chamber and docked into the opening of a 30-G needle which is introduced at 1.0–2.0 mm adjacent to the puncture point at 9 o'clock and then removed externally. **(D)** The same manipulations are performed at the other puncture point at 3 o'clock, leaving two suture-loops externally through the superior incision. **(E)** The two haptic ends of the intraocular lens (IOL) are cauterized to make a flange. **(F)** The leading haptic of the IOL is pushed out of the cartridge and the suture loop at 9 o'clock is knotting at the junction of the enlarged flange. **(G)** The optic of the folded IOL is injected into the anterior chamber, the trailing haptic left externally is tied with the same knot using the double sutures with its loop at 3 o'clock. **(H)** The two pairs of suture ends are retrieved through the scleral pocket opening pulled out by the Sinskey hook and knotted by tension adjustable knot to center the optic of the IOL. **(I)** The superior incision is sutured with 10–0 threads and the side incisions are watertight.

due to ocular trauma. The mean follow-up time was 6.50 ± 2.97 months. Detailed patient characteristics are provided in Table 1 and detailed comparison of clinical data before and after surgery are provided in Table 2. Table 3 shows that the mean preoperative BCVA was 0.8 (1.6) logMAR, and improved to 0.45 (0.8) logMAR at the last visit ($p = 0.012$). Differences in IOP and ECD before and after surgery were, respectively, not statistically significant ($p = 0.395$ and $p = 0.813$) and generally remained in the normal range postoperatively. One pediatric patient with congenital lens subluxation experienced recurrent pupillary capture of the IOL optic as well as increased IOP during the follow-up period. Using a mydriatic agent, the patient's IOL capture was relieved, yet recurred after terminating medication. Ultimately, the IOL was repositioned using a 30-gauge needle under the slit lamp and a miotic agent was applied to prevent recurrence. IOP-lowering eye drops were used during this period and helped maintaining the IOP between 22 and 24 mmHg and were discontinued after the IOP returned to normal. No other intraoperative or postoperative complications were recorded till the last follow-up visit.

Discussion

Application of foldable three-piece IOLs have been reported in a handful of sutureless scleral fixation techniques (2, 8). Given that suture fixation of PCIOLs remains the most widely accepted method for significant long-term stability and safety, we modified it with a special designed foldable three-piece PCIOL in our previous study (7). The haptic ends of this PCIOL (PY60AD, HOYA Medicals, Shinjuku, Tokyo, Japan) is designed with an enlarged cone shape, which enables us to knot the suture directly at the junction of haptic ends and avoid

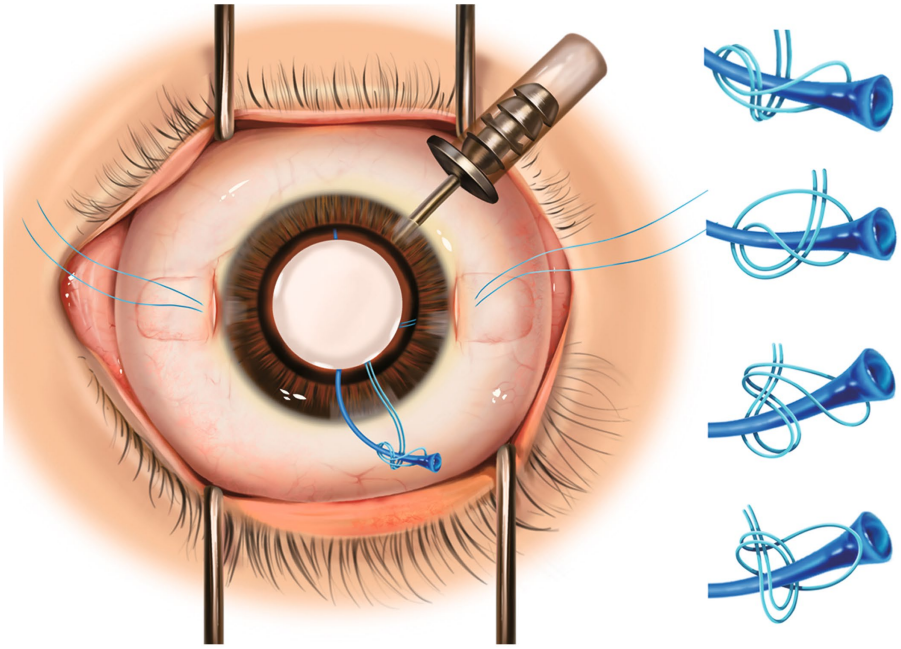

FIGURE 2
Left: Schematic figure demonstrating intrascleral fixation of flanged three-piece foldable intraocular lens with Hoffman pocket technique and special knots. Right: Four different types of wrapping methods for the knots.

TABLE 1 Individual patient characteristics.

Case	Gender	Age	Laterality	Axial Length	Indication for surgery	Ophthalmolmic comorbidities	Follow-up time
		years		mm			months
1	Male	10	Right	21.37	Postoperative aphakia	Traumatic RD	12
2	Male	29	Right	25.16	Traumatic aphakia	Traumatic lens subluxation	8
3	Female	5	Right	20.95	Postoperative aphakia	Traumatic RD	8
4	Female	14	Right	24.00	Postoperative aphakia	Traumatic RD	11
5	Male	11	Left	25.23	Postoperative aphakia	Intraocular foreign body	6
6	Male	11	Right	22.48	Traumatic aphakia	Traumatic lens subluxation	5
7	Male	15	Left	22.30	Postoperative aphakia	Traumatic RD; Stickler syndrome	3
8	Male	35	Right	23.42	Traumatic aphakia	Traumatic lens subluxation	3
9	Male	11	Right	26.52	Traumatic IOL dislocation	Congenital cataract	3
10	Male	13	Left	24.71	Postoperative aphakia	Congenital lens subluxation	5
11	Male	21	Left	23.21	Postoperative aphakia	RRD	7
12	Male	57	Right	23.30	Traumatic aphakia	Traumatic lens subluxation	7

RD, retinal detachment; IOL, intraocular lens; RRD, rhegmatogenous retinal detachment.

suture slippage. Based on this, we intended to improve upon this technique and broaden the usage of three-piece IOLs of other commonly designed varieties. The present study describes a modified suture scleral fixation approach combining Hoffman pocket technique and flanged IOL fixation technique, with a special knot. Clinical observation during the follow-up period reported improved BCVA without severe intraoperative and postoperative complications.

There are several advantages of to this technique. First, the scleral pocket technique eliminates the need for, and associated risks of, conjunctival dissection, scleral cauterization, and sutured wound closure. By bypassing these procedures, we posit to enhance patients' recovery and comfort. Additionally, it is also easier to perform in the distal location rather than via a triangular flap. More importantly, burying the suture knot in the pocket mitigates the risks of overlying conjunctiva erosion, subsequent endophthalmitis, and suture breakage (9). Second, previous studies involving sutured scleral fixation of foldable three-piece IOLs generally involve dialing a hole in the optic of the IOL (10). Our approach of creating a flange not only effectively prevents the scleral suture knots from becoming loose at haptic ends, but also enables flexible application of various types of foldable three-piece PCIOLs. Another noteworthy aspect is the flexibility of performing the knotting procedure, which can be accomplished with at least four different

TABLE 2 Comparison of clinical data before and after surgery.

Case	BCVA, logMAR		IOP, mmHg		ECD, cells/mm^3		Postoperative complications
	Pre	Post	Pre	Post	Pre	Post	
1	2.0	1.0	7.2	8.1	2,242	2,618	None
2	0.3	0.1	Tn	12.9	Unmeasurable	2,359	None
3	1.9	1.8	Tn	17.8	Unmeasurable	2,844	None
4	1.9	0.5	18.1	18.8	3,120	3,081	None
5	0.6	0.5	14.1	19.9	2,278	2,205	None
6	2.0	0.4	20.8	16.7	2,819	2,885	None
7	1.0	1.2	13.6	20.3	3,393	3,303	None
8	0.5	0.3	29.8	20.5	2,700	2,658	None
9	0.4	0.2	27.5	15.2	2,850	2,969	None
10	0.4	0.2	24.1	20.2	3,153	3,826	Pupillary IOL capture
11	2.0	0.9	14.3	16.8	2,513	2,507	None
12	0.2	0.2	14.8	10.3	2,339	1,628	None

BCVA, best-corrected visual acuity; IOP, intraocular pressure; ECD, endothelial cell density; IOL, intraocular lens.

TABLE 3 Analysis of clinical data before and after surgery.

Preoperative BCVA (logMAR)	
M (IQR)	0.8 (1.6)
Postoperative BCVA (logMAR)	
M (IQR)	0.45 (0.8)
P	**0.012***
Preoperative IOP (mmHg)	
MD ± SD	18.43 ± 7.05
Postoperative IOP (mmHg)	
MD ± SD	16.46 ± 4.12
P	0.395†
Preoperative ECD (cells/mm^3)	
MD ± SD	2740.70 ± 399.32
Preoperative ECD (cells/mm^3)	
MD ± SD	2740.25 ± 559.28
P	0.813†

*Wilcoxon signed-rank test for the analysis of BCVA.
†Paired *t*-test for the analysis of IOP and ECD.
BCVA, best-corrected visual acuity; IOP, intraocular pressure; ECD, endothelial cell density; P < 0.05 is marked in bold.

wrapping methods at the junction of the haptic ends (Figure 2). We note that this method is much easier for surgeons to master without the need to split the suture loop in half. Moreover, our technique streamlines surgical maneuvers and expedites the entire procedure for dislocated IOLs by eliminating the need to explant the posteriorly dislocated IOL via creating a new incision. This step, commonly associated with complications such as corneal injury, unstable IOP, and postoperative astigmatism, is thereby circumvented. Further, our approach strengthens the existing internal scleral fixation methods for repositioning dislocated IOLs within a closed-eye system, specifically designed for foldable three-piece IOLs (3, 4). Notably, compared to Yamane's method (2), our technique may be a more stable choice for patients with thinner sclera, such as pediatric or high myopic patients, as well as ones with scleral scarring due to PPV incisions, because of the potential sliding of flanged haptics under those conditions.

There are several important considerations to address during the surgical procedures. 1) For the main incision, it is feasible to opt for either a clear corneal incision or a scleral tunnel incision. 2) We recommend making scleral pockets before the three ports for PPV, as pre-existing PPV incisions may occupy the space required for the pockets. 3) Anterior and posterior infusion are both viable options, depending on specific surgical requirements for individual cases. 4) What we particularly emphasize is the necessity of creating a haptic flange. While some previous techniques have reported using a suture loop to secure the haptics without a flange for repositioning dislocated IOLs (11, 12), we observed postoperative suture slippage in two cases involving foldable three-piece IOLs where haptic flanges were not created (not reported in this study). 5) Additionally, it is worth noting that our technique is not suitable for IOLs with haptics made from polyimide, as the material cannot be cauterized.

Concerning postoperative complications, the patient who exhibited recurrent pupillary capture of the IOL optic, was suspected to have Marfan Syndrome (MFS) based on his ocular manifestations, while the parents of the patient declined gene test for a definitive diagnosis. A detailed examination of the patient's peripheral retina revealed lattice degeneration, which was subsequently lasered during PPV. In pseudophakic patients with MFS, it had been reported that myopathy affecting pupil constrictors and dilators can result in pliable iris and reverse pupillary block, which may induce a higher rate of pupillary capture (13). In such cases, we recommend relocating the IOL fixation plane from 2.0 to 2.5 mm posterior to the limbus, along with peripheral iridectomy. For patients with irreversible recurrent IOL capture, pupillary cerclage suturing is also a viable option.

In conclusion, this surgical technique innovatively combines the Hoffman pocket, flanged IOL, and knotting techniques, to enable flexible usage of three-piece IOLs with secure haptic fixation and achievement of improved visual outcomes with fewer complications. Future studies with larger sample sizes and extended follow-up are needed to validate long-term functional and anatomic outcomes.

Data availability statement

The raw data supporting the conclusions of this article will be made available by the authors, without undue reservation.

Ethics statement

The studies involving humans were approved by Ethical Review Board of Xinhua Hospital Affiliated to Shanghai Jiao Tong University School of Medicine. The studies were conducted in accordance with the local legislation and institutional requirements. Written informed consent for participation was not required from the participants or the participants' legal guardians/next of kin in accordance with the national legislation and institutional requirements. The need for participation consent was waived due to the retrospective nature of this.

Author contributions

HY: Conceptualization, Data curation, Formal analysis, Funding acquisition, Investigation, Methodology, Project administration, Resources, Software, Supervision, Validation, Visualization, Writing – original draft, Writing – review & editing. MW: Conceptualization, Data curation, Formal analysis, Funding acquisition, Investigation, Methodology, Project administration, Resources, Software, Supervision, Validation, Visualization, Writing – original draft, Writing – review & editing. WS: Conceptualization, Data curation, Formal analysis, Funding acquisition, Investigation, Methodology, Project administration, Resources, Software, Supervision, Validation, Visualization, Writing – original draft, Writing – review & editing. JL: Conceptualization, Investigation, Methodology, Project administration, Resources, Validation, Writing – review & editing. YX: Conceptualization, Data curation, Investigation, Methodology, Resources, Supervision, Validation, Visualization, Writing – review & editing. PF: Conceptualization, Investigation, Methodology, Project administration, Resources, Validation, Visualization, Writing – review & editing. JP: Methodology, Project administration, Validation, Visualization, Writing – review & editing. HJ: Conceptualization, Investigation, Methodology, Validation, Visualization, Writing – review & editing. PZ: Conceptualization, Data curation, Formal analysis, Funding acquisition, Investigation, Methodology, Project administration, Resources, Software, Supervision, Validation, Visualization, Writing – original draft, Writing – review & editing.

Funding

This work was supported by Shanghai Science and Technology Committee (no. 22015820200) and Interdisciplinary Program of Shanghai Jiao Tong University (no. YG2021QN52).

Conflict of interest

The authors declare that the research was conducted in the absence of any commercial or financial relationships that could be construed as a potential conflict of interest.

Publisher's note

All claims expressed in this article are solely those of the authors and do not necessarily represent those of their affiliated organizations, or those of the publisher, the editors and the reviewers. Any product that may be evaluated in this article, or claim that may be made by its manufacturer, is not guaranteed or endorsed by the publisher.

Supplementary material

The Supplementary material for this article can be found online at: https://www.frontiersin.org/articles/10.3389/fmed.2024.1382100/full#supplementary-material

SUPPLEMENTARY VIDEO 1
The surgical procedures of the technique.

References

1. Patel LG, Starr MR, Ammar MJ, Yonekawa Y. Scleral fixated secondary intraocular lenses: a review of recent literature. *Curr Opin Ophthalmol*. (2020) 31:161–6. doi: 10.1097/icu.0000000000000661

2. Yamane S, Sato S, Maruyama-Inoue M, Kadonosono K. Flanged intrascleral intraocular lens fixation with double-needle technique. *Ophthalmology*. (2017) 124:1136–42. doi: 10.1016/j.ophtha.2017.03.036

3. Kokame GT, Yanagihara RT, Shantha JG, Kaneko KN. Long-term outcome of pars plana vitrectomy and sutured scleral-fixated posterior chamber intraocular lens implantation or repositioning. *Am J Ophthalmol*. (2018) 189:10–6. doi: 10.1016/j.ajo.2018.01.034

4. Lyu J, Pq Z. Simplified ab externo fixation technique to treat late dislocation of scleral-sutured polymethyl methacrylate intraocular lenses. *Eye*. (2016) 30:668–72. doi: 10.1038/eye.2015.286

5. Zhang JTJ, Sun X, Yuan G. Closed continuous-loop suture: a novel surgical technique for transscleral fixation of intraocular lenses. *Retina*. (2022) 42:2221–4. doi: 10.1097/IAE.0000000000002644

6. Fan KC, Smiddy WE. Rescuing an Akreos 4-point haptic intraocular lens: a novel surgical technique. *Retina*. (2021) 43:1616–9. doi: 10.1097/IAE.0000000000003159

7. Ye H, Zhang S, Mi W, Fei P, Zhao P. One-year outcomes of modified technique for scleral fixation of a three-piece intraocular lens without conjunctival opening. *Front Med*. (2022) 9:856800. doi: 10.3389/fmed.2022.856800

8. Can E. Flapless and sutureless intrascleral fixation of posterior chamber intraocular lens for correction of aphakia. *J Cataract Refract Surg*. (2018) 44:929–31. doi: 10.1016/j.jcrs.2018.03.037

9. Hoffman RS, Fine HI, Packer M. Scleral fixation without conjunctival dissection. *J Cataract Refract Surg*. (2006) 32:1907–12. doi: 10.1016/j.jcrs.2006.05.029

10. Kumar Rajanna M, Konana VK, Kanakamedla A, Sagar P, Gudimetla J. A novel technique of internal scleral fixation of posteriorly dislocated intraocular lens. *Retina*. (2022) 42:1805–8. doi: 10.1097/IAE.0000000000002529

11. Li PH, Tseng GL, Wu SC, Liou SW. 27-guage needle-assisted technique for repositioning a dislocated intraocular lens. *Retina*. (2016) 36:1791–5. doi: 10.1097/IAE.0000000000001139

12. Hanemoto T, Ideta H, Kawasaki T. Luxated intraocular lens fixation using intravitreal cow hitch (girth) knot. *Ophthalmology*. (2002) 109:1118–22. doi: 10.1016/s0161-6420(02)01026-6

13. Choi SR, Jeon JH, Kang JW, Heo JW. Risk factors for and management of pupillary intraocular lens capture after intraocular lens transscleral fixation. *J Cataract Refract Surg*. (2017) 43:1557–62. doi: 10.1016/j.jcrs.2017.08.021

frontiers | Frontiers in Medicine

TYPE Original Research
PUBLISHED 13 March 2024
DOI 10.3389/fmed.2024.1344107

OPEN ACCESS

EDITED BY
Georgios D. Panos,
Nottingham University Hospitals NHS Trust, United Kingdom

REVIEWED BY
Zizhong Hu,
Nanjing Medical University, China
Xiaofei Wang,
Beihang University, China

*CORRESPONDENCE
Quangang Xu
✉ xuquangang@126.com
Baoke Hou
✉ hbk_science@126.com

†These authors have contributed equally to this work

RECEIVED 25 November 2023
ACCEPTED 01 February 2024
PUBLISHED 13 March 2024

CITATION
Jin X, Fu J, Lv R, Hao X, Wang S, Sun M, Xu G, Zhang Q, Zhang L, Li Y, Xu Q and Hou B (2024) Efficacy and safety of platelet-rich plasma for acute nonarteritic anterior ischemic optic neuropathy: a prospective cohort study.
Front. Med. 11:1344107.
doi: 10.3389/fmed.2024.1344107

Efficacy and safety of platelet-rich plasma for acute nonarteritic anterior ischemic optic neuropathy: a prospective cohort study

Xin Jin[1†], Junxia Fu[2†], Ruju Lv[3], Xiaolu Hao[1†], Song Wang[4†], Mingming Sun[1], Guangcan Xu[1], Qi Zhang[1], Lei Zhang[1], Yan Li[1], Quangang Xu[1*] and Baoke Hou[1*]

[1]Senior Department of Ophthalmology, The Third Medical Center of PLA General Hospital, Beijing, China, [2]Department of Ophthalmology, School of Medicine, Xinhua Hospital Affiliated to Shanghai Jiao Tong University, Shanghai, China, [3]Department of Ophthalmology, Jinan University, Jinan, China, [4]Department of Ophthalmology, The Second Affiliated Hospital of Anhui Medical University, Hefei, China

Background: As the most common acute optic neuropathy in older patients, nonarteritic anterior ischemic optic neuropathy (NAION) presents with varying degrees of visual acuity loss and visual field defect. However, there is no generally accepted treatment for NAION.

Objectives: To evaluate the efficacy and safety of platelet-rich plasma (PRP) for patients with acute NAION within 2 months.

Design: A prospective, nonrandomized controlled trial.

Methods: Twenty-five eyes of 25 patients were enrolled. Of them, 13 received anisodine hydrobromide and butylphthalide-sodium chloride injection continuously for 10 days as basic treatment in the control group, and 12 received two tenon capsule injections of PRP on a 10 days interval as an additional treatment in the PRP group. We compared the best-corrected visual acuity (BCVA) and capillary perfusion density (CPD) of radial peripapillary capillaries and the moth-eaten eara of the peripapillary superficial capillary plexus and deep capillary plexus at 1 day (D1) before the first PRP treatment and 7 days (D7), 14 days (D14), and 30 days (D30) after the first PRP injection. Ocular and systemic adverse effects were assessed.

Results: In the PRP group, a better BCVA occurred at D30 (adjusted $p = 0.005$, compared with D1, recovered from 0.67 ± 0.59 to 0.43 ± 0.59), and a significant improvement in CPD was observed at D30 (adjusted $p < 0.001$, $p = 0.027$, $p = 0.027$, compared with D1, D7, D14, in sequence, the value was 35.97 ± 4.65, 38.73 ± 4.61, 39.05 ± 5.26, 42.71 ± 4.72, respectively). CPD at D7 in the PRP group was better than that in the control group ($p = 0.043$). However, neither BCVA nor the moth-eaten area index were significantly different (all $p > 0.5$) between the two groups. The main adverse effect was local discomfort resolved within 1 week, and no other systemic adverse events occurred.

Conclusion: Tenon capsule injection of PRP was a safe treatment for AION and could improve capillary perfusion of the optic nerve head and might be helpful in increasing short-term vision in patients with acute NAION.

KEYWORDS

platelet-rich plasma, nonarteritic anterior ischemic optic neuropathy, prospective controlled trial, OCT angiography, efficacy and safety analyses

Introduction

As the most common acute optic neuropathy in older patients, nonarteritic anterior ischemic optic neuritis (NAION) is characterized by acute or subacute, painless, usually monocular vision loss that progresses over several hours to days and presents with diffuse or segmental optic disc edema often with peripapillary flame-shaped retinal hemorrhages (1, 2). It occurs worldwide with an annual incidence ranging from 2.3 to 10.3 cases per 100,000 persons among adults over age 50 years (1, 3, 4). With visual acuity loss from 20/20 to no light perception (NLP) and a typical arcuate or altitudinal visual field defect particularly in the inferior visual field and a limited improvement (2), a variety of therapies have been attempted, most of which are empirical, such as noninvasive or minimally invasive therapeutic options—oral glucocorticoids or anti-platelet agents, intravitreal injections of triamcinolone or anti-vascular endothelial growth factor (VEGF) agents and hyperbaric oxygen therapy, and surgical solutions—optic nerve decompression. Regrettably, there is no generally accepted treatment for NAION (5–7). To date, the exact cause of ischemia remains uncertain, and the acute hypoperfusion of vascular networks originating from the posterior ciliary arteries is the most widely accepted primary trigger. The main factors—vascular risk factors and a small, crowded optic nerve—contribute to the worsening of optic nerve ischemia (1, 2, 8). Most therapeutic interventions mainly target the possible causes of ischemia, including correction of vascular risk factors, treatment of thrombosis, vasodilation, neuroprotection, and treatment of compartment syndrome (7).

Platelet-rich plasma (PRP) is a preparation of autologous plasma enriched with a higher concentration of platelets, and it possesses high potential for regeneration, which allows for greater release of growth factors and biologically active proteins and then activates the wound-healing cascade by stimulating neoangiogenesis and collagen production (9). PRP preparation involves the collection of a small sample of an individual's blood and centrifugation to separate platelets from other components (10). Clinically, PRP can be used alone or in conjunction with topical and oral therapies. Due to the ease of use and generally high safety profile, it has propelled itself into mainstream tissue engineering, showing excellent potential for hair restoration, skin rejuvenation, and osteochondral lesions (11–13) and providing a wide range of prospects in ophthalmology from ocular surface—corneal epithelial wound healing such as ulcers, dry eye, and burns (14–18) to ocular fundus—retinitis pigmentosa (19), macular holes (20, 21), and retinal hole repair in recurrent retinal detachment (22).

However, research on the therapeutic effect of PRP on optic nerve diseases is scarce. Our study aimed to evaluate the effectiveness of PRP in improving short-term visual outcomes and the microcirculation of the optic nerve head in acute NAION patients, and the safety of local injection was also assessed.

Methods

Study design and participants

We conducted a single-center nonrandomized controlled trial that included all NAION subjects presenting at the Senior Department of Ophthalmology, the Third Medical Center of Chinese People's Liberation Army General Hospital between February 2022 and August 2022. Our study was in accordance with the tenets of the Helsinki Declaration and the ICH-GCP guidelines, and the study protocol was approved by the Ethics Committee for Human Research of the hospital (approval number KY2021-031). Written informed consent was obtained from all participants.

The diagnosis of acute NAION was primarily based on the clinical diagnosis (1). All patients underwent a comprehensive evaluation before enrollment, including best-corrected visual acuity (BCVA), visual field (when BCVA was more than 0.1), intraocular pressure (IOP), slit-lamp microscope, fundus color photo, optical coherence tomography (OCT), orbital magnetic resonance imaging (MRI) and hematological examination. The inclusion criteria were as follows: (1) age < 75 years, (2) acute and painless loss of vision or visual field defect, (3) optic disc swelling of the affected eye under the direct ophthalmoscope, (4) within 2 months from onset to treatment, and (5) complete follow-up evaluation including 7-, 14-, and 30 days follow-up. The exclusion criteria were as follows: (1) IOP higher than 20 mmHg, (2) concomitant other ophthalmic disorders, including but not limited to corneal opacity, severe cataract, vitreoretinal or other optic nerve diseases, (3) erythrocyte sedimentation rate and C-reactive protein examination suggested arteritic ischemic optic neuropathy, (4) previous history of ocular trauma or ophthalmic surgery, (5) combined with blood system diseases that may affect PRP preparation, and (6) combined with neurological diseases such as neuromyelitis optica spectrum disorders, myelin oligodendrocyte glycoprotein antibody-associated diseases, Alzheimer's disease, and Parkinson's disease, which may affect the optic nerve.

All recruited patients were intravenously administered an iodine hydrobromide and butylphthalide-sodium chloride injection for 10 consecutive days as basic treatment. For the PRP group, the first tenon capsule injection of PRP was given on the first day, and the second PRP administration was given on the last day during the basic treatment period as an intensive treatment and without any other additional treatment.

Visual function examination

All patients underwent a visual function evaluation using a standard logarithmic visual acuity chart at each visit, including 1 day before the first PRP injection (D1) and 7- (D7), 14- (D14), and 30 days (D30) follow-ups after the first PRP injection, and the decimal visual

acuity was converted into the logarithm of the minimum angle of resolution (logMAR) scale for statistical analysis.

Optical coherence tomography angiography imaging and assessment

All recruited subjects underwent optical coherence tomography angiography (OCTA) scan with a swept-source OCT (YG-100K Yalkaid, TowardPi Medical Technology, Beijing, China) with their eyes dilated and with room lighting turned off. Raster-pattern retinal scans were obtained through the optic nerve head, using scanning patterns of $6 \times 6\,mm^2$ in all patients. Images with a quality score below 40 or images with obvious motion artifacts or signal loss were excluded. Obvious motion artifacts were defined subjectively as image artifacts seen on the retinal scans, such as a horizontal frame shift larger than the average diameter of retinal vessels or a distorted oval appearance of the optic nerve head. The vascular scanning model of the TowardPi OCTA revealed precise perfusion in four disparate layers: the optic nerve head layer, vitreous layer, radial peripapillary capillaries (RPC), and choroid. Specifically, the optic nerve head layer encompasses the area between the retinal pigment epithelium (RPE) and the inner limiting membrane (ILM). Furthermore, using the TowardPi OCTA, the optic nerve head layer can be further divided into the surface capillary plexus (SCP) and deep capillary plexus (DCP). In our study, the optic nerve head layer and RPC were chosen to assess optic disc blood flow. The graphs were analysed using ImageJ software (1.8.0_112, https://imagej.nih.gov/ij/, National Institutes of Health, Bethesda, Maryland, United States). We calculated the capillary perfusion density (CPD) of RPC as described in a previous study (23) and the moth-eaten area index for the peripapillary SCP and DCP. We selected the optic disc margin threshold (Figure 1A), showing perfusion areas (Figure 1B), and the optic disc region, except for the major branch retinal blood vessels (Figure 1C). The moth-eaten area index was defined as the total weighted area of nonperfused vasculature per unit area in a measurement area by means of marking no-perfusion areas (Figure 1E) and the optic disc region, with the exception of the major branch retinal blood vessels and optic disc (Figure 1F).

Tenon capsule injection of PRP

PRP administration was performed on all case group patients, who received two capsule injections on a 10 days interval during hospitalization. During the preparation session, PRP was obtained by differential centrifugation from approximately 10 mL of autologous blood collected in the operating room. During the treatment session, each patient received 1.5 mL of PRP fluid on the nasal and temporal side of the optic nerve in the Tenon capsule near the inner part of the ball by an experienced ophthalmologist (by BH). As shown in Figure 2, hyperintensity on T2-weighted imaging and enhancement

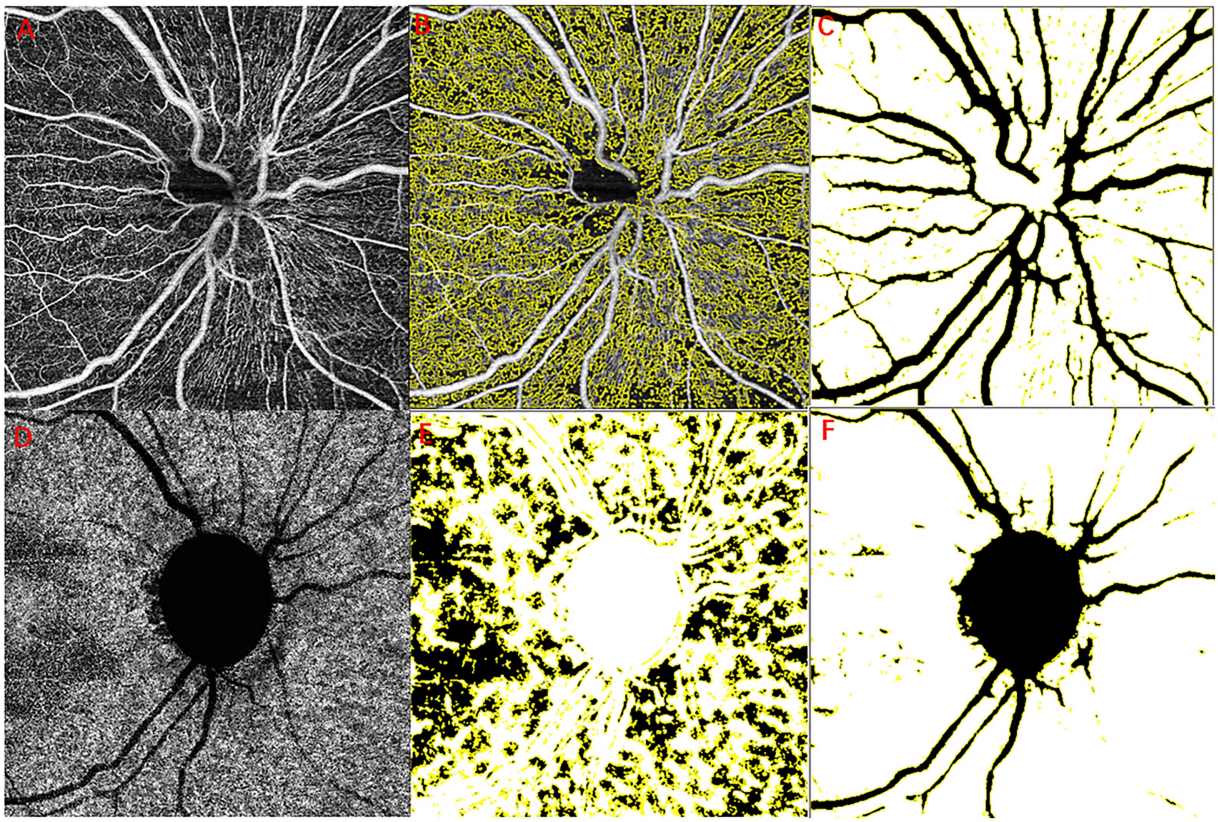

FIGURE 1
Example images for retinal layer segmentation and large vessel removal. RPC layer blood flow diagram **(A–C)**, original optic disc margin threshold **(A)**, optic perfusion areas **(B)**, and the major branch retinal blood vessels **(C)**. Choroidal capillary blood flow diagram **(D–F)**, original chorioidal capillary layer **(A)**, no-perfusion areas **(E)**, and the major branch retinal blood vessels and optic disc **(F)**. RPC, radial peripapillary capillaries.

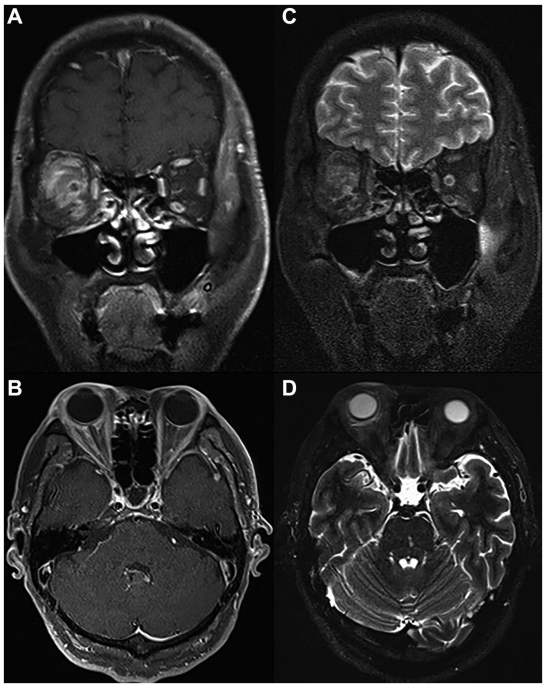

FIGURE 2
MRI scan of the same patient on the day of PRP injection. Coronal **(A)** and **(B)** axial T1 postcontrast images showing successful injection of PRP in the right Tenon capsule near the inner part of the ball with marked postcontrast enhancement. Coronal **(C)** and **(D)** axial T2-weighted images showing extensive T2 high signal in the fascia tissue behind the ball of the right eye. PRP, platelet-rich plasma; MRI, magnetic resonance imaging.

on T1-enhanced scanning were observed after PRP administration, which hinted at successful delivery of the drug to the Tennon capsule.

Statistical analysis

For patients with simultaneous bilateral eye attack, only one eye was randomly selected using a random number table to avoid selective bias. Statistical analysis was performed with SPSS version 22.0 (IBM Corp., Armonk, NY, United States). Continuous data are presented as the mean ± standard deviation, and categorical variables are expressed as rates and percentages. We used the Mann–Whitney U test to compare the differences for continuous variables and the chi-square test, correct chi-square test, or Fisher's exact test to compare categorical variables between the two groups. The Friedman test, together with the *post hoc* Wilcoxon signed-rank test, was used to compare BCVA, CPD, and moth-eaten area index at the four time points in each group. Statistical significance in the Wilcoxon signed-rank test was adjusted by Bonferroni correction. We defined $p < 0.05$ as statistically significant.

Results

Baseline characteristics of recruited NAION patients

The study flow is shown in Figure 3. Finally, a total of 25 consecutive patients, consisting of 13 (52%) in the control group and 12 (48%) in the PRP group, were included in our study. The baseline characteristics of the two groups are shown in Table 1. Among them, 21 (84%) were male, the mean age of onset was 50.84 ± 9.64 years, the mean body mass index (BMI) was 24.56 ± 1.84 kg/m^2, 24 (96%) were unilaterally involved, 12 (48%) had a history of NAION, and 12 presented a small cup-to-disc ratio or a crowded optic nerve. In terms of the subtypes of visual field defects, 15 presented diffuse defects, 10 presented quadrant defects, and none of them presented central or paracentral scotoma. Compared with the PRP group, a greater proportion of small cup-to-disc ratio or a crowded optic nerve appeared in the control group ($p = 0.003$). No significant differences were found in other clinical characteristics between the two groups (all $p > 0.05$). For the PRP group, the median time from onset to PRP window was 25.5 days.

As depicted in Table 1, nearly half of the patients had hypertension, diabetes mellitus, hyperlipidemia, and obstructive sleep apnea, one had a history of ischemic heart disease, 2 had hyperhomocysteinaemia, and 4 had nocturnal hypotension overall. None of them had a history of stroke or malignant tumor. There were no significant differences (all $p > 0.05$) in systemic diseases between the two groups.

Changes in visual function

When comparing the mean logMAR visual acuity at the same time points, no difference was found between the two groups (all $p > 0.05$, Table 2). As expected, no significant difference was found in the mean logMAR VA of the studied eyes at four time points in the control group (Friedman $p = 0.852$, Table 3). In the PRP group, the VA at D1 and D7 ranged from 0.67 ± 0.59 to 0.59 ± 0.56 and did not change significantly after the first PRP treatment (adjusted $p > 0.999$, Table 4). Although no significant change was found after 14 days of follow-up (adjusted $p = 0.347$, Table 4), a better BCVA occurred at the 30 days follow-up than at D1 (adjusted $p = 0.005$, Table 4), and the mean logMAR BCVA recovered to 0.43 ± 0.59. For BCVA at three time points, D7, D14, and D30, no significant difference was found between each other (all adjusted $p > 0.05$, Table 4).

Changes in OCTA parameters

Excitingly, the CPD of RPC at D7 in the PRP group was better than that in the control group ($p = 0.043$, Table 2), but no statistically significant difference was found for the remaining three time points between the two groups ($p > 0.05$, Table 2). Similarly, no significant difference was observed for the moth-eaten area index of the peripapillary SCP and DCP at four time points between the two groups (all $p > 0.05$, Table 2).

Surprisingly, when compared with the CPD value at other time points (D1, D7, D14) in sequence, a significant improvement of CPD occurred at D30 in the PRP treatment group (adjusted $p < 0.001$, $p = 0.027$, $p = 0.027$, Table 4), and the CPD values among the other three time points, D1, D7, and D14, were equivalent, ranging from 35.97 ± 4.65 to 39.05 ± 5.26 (adjusted $p = 0.683$, $p = 0.068$, $p > 0.999$, Table 4). The CPD value in the control group was equal at the four time points ($p = 0.139$, Table 3).

In contrast, the moth-eaten area index at four time points in neither the control group nor the PRP group was statistically significant (Friedman $p = 0.960$, $p = 0.231$, respectively, Table 3).

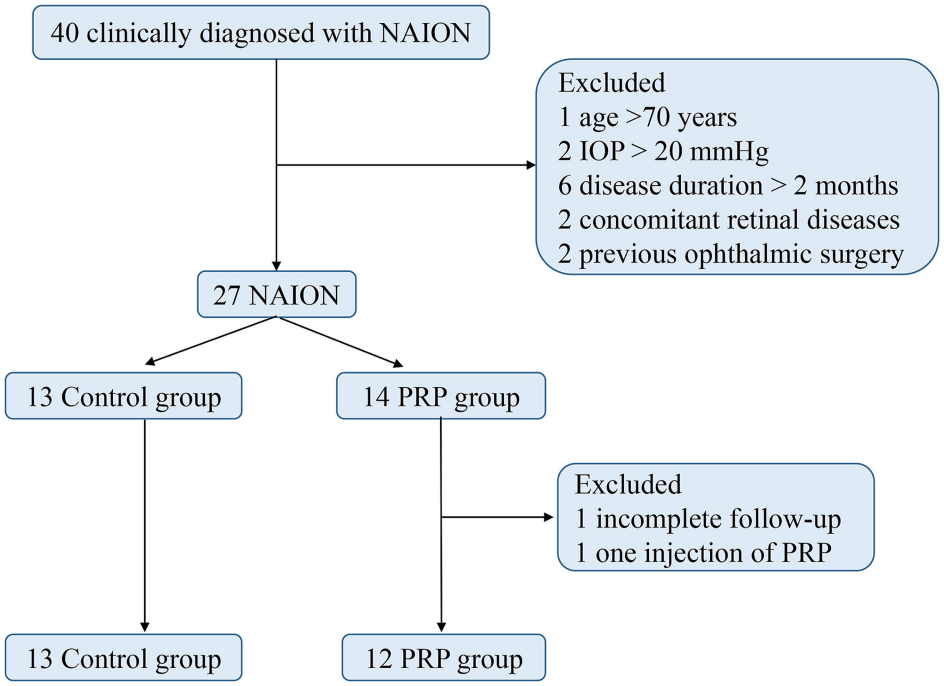

FIGURE 3
Study flow chart. NAION, nonarteritic anterior ischemic optic neuropathy; PRP, platelet-rich plasma; IOP, intraocular pressure.

Safety data

Among the 12 eyes that received PRP injection in our study, subconjunctival haemorrhage occurred in 10 eyes, periorbital or bulbar conjunctival bruising and swelling occurred in 5 eyes, and 3 patients felt eye distention and discomfort, but the symptoms were relieved within 1 week. Two patients had transient vision loss: one declined from 1 to 0.6, the other from 1 to 0.3, and one had a temporary IOP elevated to 46 mmHg. No other systemic adverse events occurred in the recruited subjects. At the stage of subject grouping, 1 patient in the PRP group did not receive a second PRP treatment due to personal economic problems.

Discussion

In this study, we developed the first attempt, to our knowledge, to show that Tenon capsule injection of PRP is safe and may be capable of short-term visual acuity improvement for acute NAION patients. Our study revealed the possibility that PRP treatment may improve impaired visual function by improving the blood supply of radial peripapillary capillaries.

Studies of ocular circulation help us better understand the pathogenesis of NAION. The eyeball receives a dual vascular supply, and the ciliary artery and central retinal artery provide arterial contributions, both of which originate from the ophthalmic artery, a main branch of the internal carotid artery. The central retinal artery, an end artery, enters the optic nerve approximately 1 cm behind the eye, goes along with the optic nerve to the retina, and finally supplies the inner part of the retina (24). The outer part of the retina is separately supplied by choroidal arteries stemming from the posterior ciliary arteries (2, 8). As part of the central nervous system, the optic nerve, approximately 50 mm long from the globe to the chiasm, can be divided into four segments: the intraocular segment, intraorbital segment, intracanalicular segment, and intracranial segment. The intraocular segment can be further subdivided into three parts: prelaminar, laminar and posterior portions by the lamina cribrosa of the sclera. The laminar and prelaminar portions are supplied primarily by branches of the short posterior ciliary arteries (2, 8, 24). The posterior part receives its arterial blood from the surrounding pial plexus derived from small penetrating branches off the ophthalmic and posterior ciliary arteries (2, 8, 24). The side branches of the short posterior ciliary arteries, branches from the nearby pial arterial plexus, and choroidal vessels compose the Zinn-Haller anastomotic arterial circle, which provides arterial blood for the optic nerve head (2).

As a small-vessel disease of the anterior portion of the optic nerve, the exact cause of NAION remains unknown, and a series of vascular risk factors, such as tissue hypoxia, anemia, blood loss, relative hypotension, elevation of IOP, and thrombotic risk factors, result in acute hypoperfusion of the posterior ciliary arteries (1, 25). Systemic diseases, including systemic hypertension, diabetes mellitus, ischemic heart disease, hypercholesterolemia, nocturnal hypotension, obstructive sleep apnea, and systemic atherosclerosis, have been associated with an increased risk of NAION (1, 7, 25). In addition, individual anatomical susceptibilities, such as optic nerve drusen, papilledema, and a small, crowded optic nerve head with a small physiological cup, presumably make patients prone to worsening ischemia of the anterior optic nerve (1, 25). Following swelling of the optic nerve head, which triggers axonal and capillary compression via compartment syndrome, subsequent vasogenic and cytotoxic optic nerve edema aggravates the impairment of axonal flow and capillary perfusion of the optic nerve head with subsequent axonal degeneration

TABLE 1 Baseline characteristics of the recruited NAION patitents.

	Total	Control group	PRP group	*p*
Study subjects (eyes)	25	13	12	
Male (*n*, %)	21 (84%)	10 (76.9%)	11 (91.7%)	0.647[c]
Age of onset (mean ± SD, years)	50.84 ± 9.64	51.08 ± 11.44	50.58 ± 7.74	0.806[a]
BMI (mean ± SD, kg/m^2)	24.56 ± 1.84	24.62 ± 1.32	24.48 ± 2.35	0.605[a]
Unilateral eye onset (*n*, %)	24 (96%)	12 (92.3%)	12 (100%)	0.999[d]
History of NAION (*n*, %)	12 (48%)	5 (38.5%)	7 (58.3%)	0.320[b]
Presence of small cup-to-disc ratio or a crowded optic nerve (*n*, %)	12 (48%)	10 (76.9%)	2 (16.7%)	**0.003**[b]
Type of visual field defect (*n*, %)				
Diffuse defect	15 (60%)	8 (61.5%)	7 (58.3%)	0.999[c]
Quadrant defect	10 (40%)	5 (38.5%)	5 (41.7%)	
Central or paracentral scotoma	0	0	0	
Onset to PRP window (median, IQR, days)	—	—	25.5 (18.8, 37)	—
Systemic diseases				
Hypertension (*n*, %)	11 (44%)	6 (46.2%)	5 (41.7%)	0.821[b]
Diabetes mellitus (*n*, %)	12 (48%)	6 (46.2%)	6 (50%)	0.848[b]
Hyperlipidemia (*n*, %)	10 (40%)	3 (23.1%)	7 (58.3%)	0.165[c]
Hyperhomocysteinemia (*n*, %)	2 (8%)	0	2 (16.7%)	0.220[d]
Nocturnal hypotension (*n*, %)	4 (16%)	3 (23.1%)	1 (8.3%)	0.647[c]
Obstructive sleep apnea (*n*, %)	10 (40%)	6 (46.2%)	4 (33.3%)	0.806[c]
History of ischemic heart disease (*n*, %)	1 (4%)	1 (0.7%)	0	0.999[d]
History of stroke (*n*, %)	0	0	0	—
History of malignant tumor (*n*, %)	0	0	0	—

NAION, nonarteritic anterior ischemic optic neuropathy; PRP, platelet rich plasma; BMI, body mass index; *n*, number; SD, standard deviation; IQR, interquartile range.
Bold: $p < 0.05$.
[a]Mann–Whitney test.
[b]Chi-square test.
[c]Correct chi-square test.
[d]Fisher's exact test.

and loss of retinal ganglion cells through apoptosis (1). As these cells die off, they are unable to create new connections with other neurons, leading to further deterioration of vision over time.

As a tissue regeneration technique, PRP treatment can delay aging in the presence of cytokines and growth factors and promote the production of type 1 procollagen and hyaluronic acid, which in turn improves the skin texture, firmness, and color homogeneity and exhibits efficacy in facial plastic surgery (12). In ophthalmology, it has been employed for ocular surface (14–17, 26–30) and as adjuvant therapy in pathogenic myopic retinal holes or idiopathic large macular holes (21, 22), showing encouraging results in the improvements of visual field (VF), multifocal electroretinography (mfERG), and microperimetry (MP) in retinitis pigmentosa (RP) patients (31).

Benefiting from the emergence of OCTA, which provides detailed images of retinal and choroidal blood flow, allows us to noninvasively visualize microvascular flow impairment. Chen found decreased retinal nerve fibre layer (RNFL) microcirculation in eyes with open-angle glaucoma and in the normal hemisphere of eyes with glaucoma, as measured by blood flux index and vessel area density, and both were significantly correlated with visual field loss and RNFL thinning, which suggests that vascular dysfunction may precede structural changes in glaucoma and that microcirculation measurement may help physicians monitor glaucoma (23, 32). Similarly, as an optic neuropathy, poor blood flow recovery of the optic disc coincided with the poor visual function prognosis in nonacute phase NAION (33). Wright Mayes discovered that both the RPC and peripapillary choriocapillaris (PCC) were affected in patients with NAION (34). Due to the decrease in accuracy of PCC caused by papilledema and the decrease in visual field credibility caused by low vision, PCC and visual field indicators were not included in our study for analysis.

In our study, we exhibited an improvement in radial peripapillary capillaries after PRP injection, as shown by a significant improvement in CPD observed at D30 in the PRP group (adjusted $p < 0.001$, $p = 0.027$, $p = 0.027$, compared with D1, D7, D14, Table 4); correspondingly, a better BCVA occurred at D30 compared with BCVA at D1 (adjusted $p = 0.005$, Table 4). Although no significant change was found at D7 or D14 (adjusted $p > 0.999$, $p = 0.347$, respectively, Table 4), ocular adverse effects cannot be ignored within the first week after PRP injection, which may affect the assessment of visual acuity. Interestingly, a better CPD occurred at D7 in the PRP group than in the control group ($p = 0.043$, Table 2); regrettably, no statistically significant difference was found for the BCVA between the two groups (all $p > 0.05$, Table 2). The possible reason may be that the improvement in visual function within the group was not sufficient to

TABLE 2 Visual acuity and OCTA parameter of the studied eyes in two group during different time points.

	Total	Control group	PRP group	*p*
BCVA (logMAR, mean + SD)				
D1				0.526
Mean + SD	0.57 ± 0.51	0.48 ± 0.42	0.67 ± 0.59	
Median (Range)	0.60 (0–2)	0.40 (0–1.22)	0.71 (0–2)	
D7				0.978
Mean + SD	0.57 ± 0.48	0.54 ± 0.41	0.59 ± 0.56	
Median (Range)	0.52 (0–2)	0.52 (0–1.3)	0.56 (0–2)	
D14				0.397
Mean + SD	0.52 ± 0.49	0.54 ± 0.39	0.49 ± 0.60	
Median (Range)	0.40 (0–2)	0.52 (0–1.3)	0.30 (0–2)	
D30				0.188
Mean + SD	0.50 ± 0.50	0.56 ± 0.41	0.43 ± 0.59	
Median (Range)	0.40 (0–2)	0.40 (0–1.3)	0.22 (0–2)	
CPD (mean + SD)				
D1				0.356
Mean + SD	36.99 ± 4.34	38.00 ± 3.94	35.97 ± 4.65	
Median (Range)	37.48 (28.22–43.70)	39.06 (31.72–43.70)	35.01 (28.22–42.86)	
D7				**0.043**
Mean + SD	36.85 ± 4.89	34.97 ± 4.59	38.73 ± 4.61	
Median (Range)	37.20 (30.89–48.74)	33.10 (30.89–45.02)	38.42 (32.11–48.74)	
D14				0.603
Mean + SD	38.02 ± 5.06	36.98 ± 4.85	39.05 ± 5.26	
Median (Range)	37.63 (30.84–50.37)	38.06 (30.84–43.50)	37.63 (32.21–50.37)	
D30				0.166
Mean + SD	40.78 ± 5.10	38.85 ± 4.89	42.71 ± 4.72	
Median (Range)	40.10 (30.16–52.15)	39.24 (30.16–47.37)	40.20 (38.01–52.15)	
Moth-eaten area index (mean + SD)				
D1				0.817
Mean + SD	0.50 ± 0.05	0.50 ± 0.04	0.50 ± 0.06	
Median (Range)	0.49 (0.42–0.61)	0.49 (0.44–0.55)	0.49 (0.42–0.61)	
D7				0.356
Mean + SD	0.46 ± 0.06	0.47 ± 0.05	0.44 ± 0.07	
Median (Range)	0.46 (0.31–0.56)	0.46 (0.42–0.56)	0.45 (0.31–0.52)	
D14				0.299
Mean + SD	0.47 ± 0.07	0.48 ± 0.05	0.46 ± 0.09	
Median (Range)	0.47 (0.30–0.59)	0.48 (0.40–0.57)	0.45 (0.30–0.59)	
D30				0.149
Mean + SD	0.47 ± 0.08	0.49 ± 0.06	0.45 ± 0.08	
Median (Range)	0.48 (0.32–0.57)	0.49 (0.40–0.57)	0.46 (0.32–0.56)	

Mann–Whitney test was used for the comparison between the two groups. NAION, nonarteritic anterior ischemic optic neuropathy; PRP, platelet rich plasma; BCVA, best-corrected visual acuity; CPD, capillary perfusion density; logMAR, logarithm of the minimum angle of resolution; SD, standard deviation; D1, 1 day before first PRP or basic treatment injection; D7, 7 days after first PRP injection or basic treatment; D14, 14 days after first PRP injection or basic treatment; D30, 30 days after first PRP injection basic treatment.
Bold: $p < 0.05$.

achieve a group difference. Furthermore, a smaller sample size, 12 for the PRP group and 13 for the control group, may also cause a bias in our results.

Although an increasing number of studies have reported that PRP injection is a safe, virtually pain-free, simple, and rapid treatment (14), with no risk of infection and transmission of

TABLE 3 Visual acuity of the studied eyes in NAION patients during different time points.

	Control group	PRP group
P of BCVA	0.852	**<0.001**
P of CPD	0.139	**<0.001**
P of moth-eaten area index	0.960	0.231

NAION, nonarteritic anterior ischemic optic neuropathy; PRP, platelet rich plasma; BCVA, best-corrected visual acuity; CPD, capillary perfusion density.
Bold: $P < 0.05$.

TABLE 4 The comparation of visual acuity and CPD of the studied eyes in the PRP group between two each time points.

Time point	BCVA	CPD
D1–D7	>0.999	0.683
D1–D14	0.347	0.683
D1–D30	**0.005**	**<0.001**
D7–D14	>0.999	>0.999
D7–D30	0.068	**0.027**
D14–D30	0.928	**0.027**

(Adjust *p*-value). AION, nonarteritic anterior ischemic optic neuropathy; PRP, platelet rich plasma; BCVA, best-corrected visual acuity; CPD, capillary perfusion density; logMAR, logarithm of the minimum angle of resolution; SD, standard deviation; D1, 1 day before first PRP or basic treatment injection; D7, 7 days after first PRP injection or basic treatment; D14, 14 days after first PRP injection or basic treatment; D30, 30 days after first PRP injection basic treatment.
Bold: $p < 0.05$.

disease, minor adverse effects such as discomfort, small prick bleeding, and swelling can occasionally occur (35), and a rare but devastating complication—irreversible visual loss due to occlusion or impairment of the central retinal artery and the posterior ciliary artery secondary to PRP injection—should not be overlooked (23, 36–38).

Our study surely has several limitations. First, only twelve patients were included in the PRP group with a wide range of unequal logMAR VA before PRP injection from 0 to 2, which may cause a bias in our results. The number of patients in the control group was also relatively small, and an expanded sample size study is still needed to verify our conclusions. Second, as a human-based experimental study, although two groups with equivalent baselines were included in our study, we assigned patients largely dependent on personal preference, and it is difficult to perform a random double-blind test. An interaction effect between basic treatment and PRP injection is unavoidable. Third, due to the impact of the novel coronavirus, we did not complete a continuous follow-up, and it is essential to assess the long-term effect of PRP injection for NAION patients. Last, because of the poor reliability of visual field assessments, we only chose visual acuity as a single functional indicator and OCTA parameters as the unique structural indicator. A further comprehensive assessment is indispensable to provide more information about whether PRP treatment could improve visual acuity by improving blood perfusion of the optic nerve.

The most prominent points of this study are providing an opening for NAION's new treatment, Tenon capsule injection of PRP, which can significantly improve capillary perfusion of the optic nerve head and might be helpful in increasing short-term vision in patients with acute NAION.

Data availability statement

The original contributions presented in the study are included in the article/supplementary materials, further inquiries can be directed to the corresponding authors.

Ethics statement

The studies involving humans were approved by The Third Medical Center of the Chinese People's Liberation Army General Hospital is affiliated with the Third Medical Center of the Chinese People's Liberation Army General Hospital. The studies were conducted in accordance with the local legislation and institutional requirements. The participants provided their written informed consent to participate in this study.

Author contributions

XJ: Conceptualization, Investigation, Writing – review & editing, Project administration, Supervision. JF: Writing – original draft, Formal analysis, Validation. SW: Data curation, Investigation, Writing – review & editing. RL: Investigation, Writing – original draft. XH: Investigation, Writing – original draft. MS: Investigation, Writing – original draft. GX: Investigation, Writing – original draft. QZ: Investigation, Writing – original draft. LZ: Resources, Writing – original draft. YL: Resources, Writing – original draft. QX: Project administration, Writing – original draft. BH: Formal analysis, Investigation, Visualization, Project administration, Writing – original draft.

Funding

The author(s) declare that no financial support was received for the research, authorship, and/or publication of this article.

Acknowledgments

A platelet-rich plasma preparation kit was provided by Shandong Weigao Xinsheng Medical Device Co., Ltd. We are grateful to all participants in this study. We would like to thank all optometrists and nurses at the Senior Department of Ophthalmology in the Third Medical Center of PLA General Hospital.

Conflict of interest

The authors declare that the research was conducted in the absence of any commercial or financial relationships that could be construed as a potential conflict of interest.

Publisher's note

References

1. Biousse V, Newman NJ. Ischemic optic neuropathies. *N Engl J Med*. (2015) 372:2428–36. doi: 10.1056/NEJMra1413352

2. Luneau K. Newman N and Biousse VJTn. *Ischemic Opt Neuropath*. (2008) 14:341–54. doi: 10.1097/NRL.0b013e318177394b

3. Hattenhauer MG, Leavitt JA, Hodge DO, Grill R, Gray DT. Incidence of nonarteritic anterior ischemic optic neuropathy. *Am J Ophthalmol*. (1997) 123:103–7. doi: 10.1016/s0002-9394(14)70999-7

4. Johnson LN, Arnold AC. Incidence of nonarteritic and arteritic anterior ischemic optic neuropathy. Population-based study in the state of Missouri and Los Angeles County, California. *J Neuro-Ophthal*. (1994) 14:38–44.

5. Zhou P, Zhang J, Qi Y. The efficacy of glucocorticoids in the treatment of Nonarteritic anterior ischemic optic neuropathy: a systematic review and meta-analysis. *Comput Math Methods Med*. (2022) 2022:2935992. doi: 10.1155/2022/2935992

6. Huang HM, Kuo HK, Chiang WY, Wu PC, Poon LYC. Combination therapy with intravitreal triamcinolone Acetonide and Oral levodopa for the treatment of Nonarteritic anterior ischemic optic neuropathy: a pilot study. *J Ocular Pharmacol Therapeut*. (2022) 38:167–75. doi: 10.1089/jop.2021.0081

7. Atkins EJ, Bruce BB, Newman NJ, Biousse V. Treatment of nonarteritic anterior ischemic optic neuropathy. *Surv Ophthalmol*. (2010) 55:47–63. doi: 10.1016/j.survophthal.2009.06.008

8. Rucker J, Biousse V, Newman NJ. Ischemic optic neuropathies. *Curr Opin Neurol*. (2004) 17:27–35. doi: 10.1097/00019052-200402000-00006

9. Wu PI, Diaz R, Borg-Stein J. Platelet-rich plasma. *Phys Med Rehabil Clin N Am*. (2016) 27:825–53. doi: 10.1016/j.pmr.2016.06.002

10. Cengiz IF, Oliveira JM, Reis RL. PRP therapy. *Adv Exp Med Biol*. (2018) 1059:241–53. doi: 10.1007/978-3-319-76735-2_11

11. Justicz N, Derakhshan A, Chen JX, Lee LN. Platelet-rich plasma for hair restoration. *Facial Plast Surg Clin North Am*. (2020) 28:181–7. doi: 10.1016/j.fsc.2020.01.009

12. Peng GL. Platelet-rich plasma for skin rejuvenation: facts, fiction, and pearls for practice. *Facial Plast Surg Clin North Am*. (2019) 27:405–11. doi: 10.1016/j.fsc.2019.04.006

13. Annaniemi JA, Pere J, Giordano S. Platelet-rich plasma versus hyaluronic acid injections for knee osteoarthritis: a propensity-score analysis. *Scand J Surg*. (2019) 108:329–37. doi: 10.1177/1457496918812218

14. Rawat P, Agrawal R, Bhaisare V, Walia S, Kori N, Gupta R. Autologous platelet-rich plasma eye drop versus artificial tear eye drop for symptomatic dry eye disease: a prospective comparative interventional study. *Indian J Ophthalmol*. (2022) 70:1549–53. doi: 10.4103/ijo.IJO_2595_21

15. Okumura Y, Inomata T, Fujimoto K, Fujio K, Zhu J, Yanagawa A. Biological effects of stored platelet-rich plasma eye-drops in corneal wound healing. *Br J Ophthalmol*. (2022) 108:37–44. doi: 10.1136/bjo-2022-322068

16. Murtaza F, Toameh D, Chiu HH, Tam ES, Somani S. Autologous platelet-rich plasma drops for evaporative dry eye disease from Meibomian gland dysfunction: a pilot study. *Clin Ophthal*. (2022) 16:2199–208. doi: 10.2147/opth.S367807

17. Mohammed MA, Allam IY, Shaheen MS, Lazreg S, Doheim MF. Lacrimal gland injection of platelet rich plasma for treatment of severe dry eye: a comparative clinical study. *BMC Ophthalmol*. (2022) 22:343. doi: 10.1186/s12886-022-02554-0

18. Cecerska-Heryć E, Goszka M, Serwin N, Roszak M, Grygorcewicz B, Heryć R. Applications of the regenerative capacity of platelets in modern medicine. *Cytokine Growth Factor Rev*. (2022) 64:84–94. doi: 10.1016/j.cytogfr.2021.11.003

19. Sahli E, Arslan U, Özmert E, İdil A. Evaluation of the effect of subtenon autologous platelet-rich plasma injections on visual functions in patients with retinitis pigmentosa. *Regen Med*. (2021) 16:10.2217/rme-2020-0075:131–43. doi: 10.2217/rme-2020-0075

20. Hagenau F, Nobl M, Vogt D, Schworm B, Siedlecki J, Kreutzer T. Highly concentrated autologous platelet-rich plasma restores foveal anatomy in lamellar macular hole surgery. *Klinische Monatsblatter fur Augenheilkunde*. (2021) 238:885–92. doi: 10.1055/a-1409-9268

21. Babu N, Kohli P, Ramachandran NO, Adenuga OO, Ahuja A, Ramasamy K. Comparison of platelet-rich plasma and inverted internal limiting membrane flap for the management of large macular holes: a pilot study. *Indian J Ophthalmol*. (2020) 68:880–4. doi: 10.4103/ijo.IJO_1357_19

22. di Tizio F, Gattazzo I, di Staso F, di Pippo M, Guglielmelli F, Scuderi G. Human amniotic membrane patch and platelet-rich plasma to promote retinal hole repair in a recurrent retinal detachment. *Eur J Ophthalmol*. (2021) 31:1479–82. doi: 10.1177/1120672120953314

23. Zhou T, Ran J, Xu P, Shen L, He Y, Ye J. A hyaluronic acid/platelet-rich plasma hydrogel containing MnO(2) nanozymes efficiently alleviates osteoarthritis in vivo. *Carbohydr Polym*. (2022) 292:119667. doi: 10.1016/j.carbpol.2022.119667

24. Onda E, Cioffi GA, Bacon DR, van Buskirk EM. Microvasculature of the human optic nerve. *Am J Ophthalmol*. (1995) 120:92–102. doi: 10.1016/s0002-9394(14)73763-8

25. Chang MY, Keltner JL. Risk factors for fellow eye involvement in nonarteritic anterior ischemic optic neuropathy. *J Neuro Ophthalmol*. (2019) 39:147–52. doi: 10.1097/wno.0000000000000715

26. Nadelmann JB, Bunya VY, Ying GS, Hua P, Massaro-Giordano M. Effect of autologous platelet-rich plasma drops in the treatment of ocular surface disease. *Clin Ophthal*. (2022) 16:4207–13. doi: 10.2147/opth.S391536

27. Avila MY, Igua AM, Mora AM. Randomised, prospective clinical trial of platelet-rich plasma injection in the management of severe dry eye. *Br J Ophthalmol*. (2018) 103:648–53. doi: 10.1136/bjophthalmol-2018-312072

28. Alio JL, Rodriguez AE, Ferreira-Oliveira R, Wróbel-Dudzińska D, Abdelghany AA. Treatment of dry eye disease with autologous platelet-rich plasma: a prospective, interventional. *Non-Randomized Study Ophthalmology therapy*. (2017) 6:285–93. doi: 10.1007/s40123-017-0100-z

29. Alio JL, Rodriguez AE, Abdelghany AA, Oliveira RF. Autologous platelet-rich plasma eye drops for the treatment of post-LASIK chronic ocular surface syndrome. *J Ophthalmol*. (2017) 2017:2457620. doi: 10.1155/2017/2457620

30. Alio JL, Abad M, Artola A, Rodriguez-Prats JL, Pastor S, Ruiz-Colecha J. Use of autologous platelet-rich plasma in the treatment of dormant corneal ulcers. *Ophthalmology*. (2007) 114:1286–1293.e1. doi: 10.1016/j.ophtha.2006.10.044

31. Arslan U, Özmert E, Demirel S, Örnek F, Şermet F. Effects of subtenon-injected autologous platelet-rich plasma on visual functions in eyes with retinitis pigmentosa: preliminary clinical results. *Graefes Arch Clin Exp Ophthalmol*. (2018) 256:893–908. doi: 10.1007/s00417-018-3953-5

32. Chen CL, Zhang A, Bojikian KD, Wen JC, Zhang Q, Xin C. Peripapillary retinal nerve Fiber layer vascular microcirculation in Glaucoma using optical coherence tomography-based microangiography. *Invest Ophthalmol Vis Sci*. (2016) 57:475. doi: 10.1167/iovs.15-18909

33. Ling JW, Yin X, Lu QY, Chen YY, Lu PR. Optical coherence tomography angiography of optic disc perfusion in non-arteritic anterior ischemic optic neuropathy. *Int J Ophthalmol*. (2017) 10:1402–6. doi: 10.18240/ijo.2017.09.12

34. Wright Mayes E, Cole ED, Dang S, Novais EA, Vuong L, Mendoza-Santiesteban C. Optical coherence tomography angiography in nonarteritic anterior ischemic optic neuropathy. *J Neuro Ophthal*. (2017) 37:358–64. doi: 10.1097/wno.0000000000000493

35. Aust M, Pototschnig H, Jamchi S, Busch KH. Platelet-rich plasma for skin rejuvenation and treatment of actinic elastosis in the lower eyelid area. *Cureus*. (2018) 10:e2999. doi: 10.7759/cureus.2999

36. Karam EZ, Gan A, Muci Mendoza R, Martinez E, Perez E. Visual loss after platelet-rich plasma injection into the face. *Neuro Ophthal*. (2020) 44:371–8. doi: 10.1080/01658107.2020.1740936

37. Maslan N, Wan Abdul Halim WH, Din NM, Tang SF. Central retinal artery occlusion and optic neuropathy secondary to platelet rich plasma injection: a case report. *Int J Ophthalmol*. (2021) 14:945–7. doi: 10.18240/ijo.2021.06.23

38. Wu SZ, He X, Weiss RA. Vision loss after platelet-rich plasma injection: a systematic review. *Dermatol Surg*. (2022) 48:697–8. doi: 10.1097/dss.0000000000003451

frontiers | Frontiers in Medicine

TYPE Review
PUBLISHED 04 April 2024
DOI 10.3389/fmed.2024.1384500

OPEN ACCESS

EDITED BY
Georgios D. Panos,
Nottingham University Hospitals NHS Trust, United Kingdom

REVIEWED BY
Ruchi Shah,
Cedars Sinai Medical Center, United States
Brian Paul Ceresa,
University of Louisville, United States
Qingjian Ou,
Tongji University, China
Ajay Sharma,
Chapman University, United States
Bilian Ke,
Shanghai General Hospital, China
Bijorn Omar Balzamino,
GB Bietti Foundation (IRCCS), Italy
Peter S. Reinach,
Wenzhou Medical University, China

*CORRESPONDENCE
Chenming Zhang
✉ chenming-zhang@163.com
Aijun Deng
✉ dengaijun@hotmail.com

RECEIVED 09 February 2024
ACCEPTED 21 March 2024
PUBLISHED 04 April 2024

CITATION
Gong J, Ding G, Hao Z, Li Y, Deng A and Zhang C (2024) Elucidating the mechanism of corneal epithelial cell repair: unraveling the impact of growth factors.
Front. Med. 11:1384500.
doi: 10.3389/fmed.2024.1384500

Elucidating the mechanism of corneal epithelial cell repair: unraveling the impact of growth factors

Jinjin Gong[1,2], Gang Ding[2], Zhongkai Hao[1,2], Yuchun Li[3], Aijun Deng[1]* and Chenming Zhang[1,2]*

[1]School of Clinical Medicine, Shandong Second Medical University, Weifang, China, [2]Department of Ophthalmology, Jinan Second People's Hospital, Jinan, China, [3]Wuxi No. 2 Chinese Medicine Hospital, Wuxi, China

The repair mechanism for corneal epithelial cell injuries encompasses migration, proliferation, and differentiation of corneal epithelial cells, and extracellular matrix remodeling of the stromal structural integrity. Furthermore, it involves the consequential impact of corneal limbal stem cells (LSCs). In recent years, as our comprehension of the mediating mechanisms underlying corneal epithelial injury repair has advanced, it has become increasingly apparent that growth factors play a pivotal role in this intricate process. These growth factors actively contribute to the restoration of corneal epithelial injuries by orchestrating responses and facilitating specific interactions at targeted sites. This article systematically summarizes the role of growth factors in corneal epithelial cell injury repair by searching relevant literature in recent years, and explores the limitations of current literature search, providing a certain scientific basis for subsequent basic research and clinical applications.

KEYWORDS

cornea, corneal epithelial cells, growth factors, growth factor receptor, repair mechanism

1 Introduction

The cornea, in direct contact with the external environment, stands out as one of the body's tissues with the most dense innervation (1). Its structure is crucial for preserving the health and functionality of the ocular surface (Figure 1 shows the anatomical structure of the cornea). Damage to the corneal epithelium can result in corneal infections, ulcers, scar formation and vision loss ultimately. In recent years, factors such as surgical trauma, drug use, and infection have contributed to a rising number of patients with corneal epithelial injuries. As a result, the repair of corneal epithelial injuries has emerged not only as a prominent topic in basic scientific research but also as an urgent clinical problem that requires attention.

The corneal epithelium plays a crucial role in safeguarding the eye's barrier, stabilizing the tear film and maintaining the microenvironment of the ocular surface (2). Currently, the model governing corneal epithelial homeostasis relies on the XYZ hypothesis. According to this framework, the migration of limbal stem cells (LSCs) towards the central region of the cornea (X), combined with the vertical proliferation and differentiation of basal cells (Y), balances with the shedding of squamous cells (Z) from the epithelial surface. Healthy eyes are continuously bathed in tears containing growth factors, essential substances for maintaining

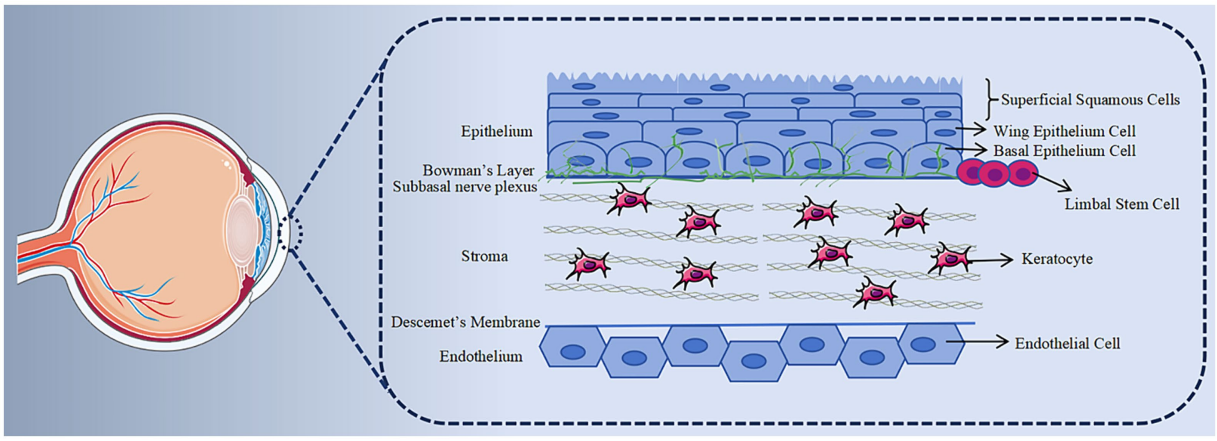

FIGURE 1
Histology of cornea. The cornea is structurally divided into five layers. The anterior epithelial layer comprises 5–7 layers of renewable epithelial cells. Behind the epithelial basement membrane lies the Bowman membrane, consisting of collagen fibers. The thickest layer, the stroma, primarily consists of keratocytes and collagen fibers, crucial for maintaining corneal transparency. Descemet, generated by the endothelium, is a transparent, elastic thin film with no distinct structure but possesses strong resistance. The endothelium is formed by a layer of hexagonal endothelial cells, incapable of regeneration.

the normal function of ocular surface tissue (3). Due to the unique anatomical location of the cornea, it is particularly susceptible to various injuries (4). When damaged, there is an upregulation of growth factors in tears, which target the cornea through relevant signaling pathways, thereby promoting corneal epithelial repair (5) and maintaining corneal epithelial homeostasis. Therefore, growth factors play a pivotal role in repairing corneal epithelial injuries and maintaining the normal microenvironment of the corneal epithelium.

In consideration of the aforementioned, this review aims to elucidate the roles played by various growth factors in the repair of corneal epithelial cells and comprehensively analyze their respective mechanisms of action. The overarching objective is to establish a robust scientific foundation that can serve as a springboard for subsequent basic research endeavors and clinical applications. The ensuing discussion will delve into the intricate interplay of growth factors within the context of repair mechanisms.

2 Growth factors involved In repair mechanisms

2.1 Epidermal growth factor

Epidermal growth factor (EGF) stands as one of the earliest identified single-chain peptides recognized for its ability to stimulate cell growth, playing a pivotal role in wound healing and maintaining tissue homeostasis by regulating cell survival, growth, motility and differentiation (6). In instances of corneal epithelial cell damage resulting from trauma, surgery or infection, EGF facilitates the migration and proliferation of corneal epithelial cells through the activation of its receptor EGFR/ErbB and subsequent binding. Consequently, this process promotes the effective repair of corneal epithelial injuries (7, 8). During the initial phases of corneal epithelial damage healing, EGFR1/ErbB1 tyrosine kinase instigates cellular signaling, activating downstream effectors such as the type III phosphoinositide 3-kinase (PI3K)—protein kinase B (Akt) axis and extracellular signal-regulated kinase (ERK). This orchestrated activation contributes significantly to the overall repair mechanism of corneal epithelial injuries (9). Furthermore, substance P also emerges as a noteworthy contributor to corneal epithelial injury repair, operating through the activation of EGFR and downstream signaling molecules, such as Akt (10). Abnormal activation of the EGFR-PI3K-AKT and ERK signaling pathways may result in increased cell apoptosis, decreased cell proliferation and delayed wound closure (11). The EGFR signaling pathway can further activate nuclear factor kappa-B (NF-κB) and histone deacetylase 6 (HDAC6). NF-κB, in turn, activates the transcription inhibitor CCCTC binding factor (CTCF) while downregulating the paired box gene 6 (PAX6), mediating the migration and proliferation of corneal epithelial cells. Simultaneously, HDAC6 promotes the migration of corneal epithelial cells and contributes to injury repair (12, 13).

There are four EGF receptors, with EGFR1 showing relatively high expression in corneal epithelial cells and demonstrating a reparative effect on the cornea during epithelial injury (14). EGFR2/ErbB2 and EGFR3/ErbB3 have also been confirmed to be expressed in the corneal epithelium, sharing a distribution pattern similar to EGFR1. Among them, the EGFR2/ErbB2 receptor enhances the corneal epithelial wound healing process by activating the ERK and PI3K signaling pathways (15). While the role of EGFR3/ErbB3 has not been fully elucidated, the existence of specific antibody inhibitors for EGFR3/ErbB3 has been confirmed. Utilizing these inhibitors and genetic techniques, studies have demonstrated that EGFR3/ErbB3 signaling can assist in the migration of corneal epithelial cells (16, 17). It's worth noting that EGFR4/ErbB4 is not expressed in the corneal epithelium (18).

Presently, seven EGFR ligands have been identified. In addition to EGF, six other endogenous ligands capable of binding to EGFR have been recognized, including heparin-binding EGF-like growth factor (HB-EGF), transforming growth factor-α (TGF-α), betacellulin (BTC), epiregulin, amphiregulin, and epigen. HB-EGF, integral in promoting growth and development, plays a crucial role, as evidenced by the fact that knockout mice perish shortly after birth (19).

Functioning as a soluble transmembrane protein, HB-EGF binds to an additional domain of negatively charged polysaccharides, thereby enhancing *in vitro* cell adhesion and promoting corneal epithelial injury repair (20). A notable discovery in the study indicates that HB-EGF exhibits prolonged cell attachment compared to EGF, resulting in a sustained impact on wound healing following brief therapy (21). TGF-α, a member of the epidermal growth factor family, is produced by both epidermal cells and macrophages. It plays a crucial role in the repair of corneal epithelial injuries by initiating multiple signaling cascade reactions upon binding with the EGFR (18, 22). The bidirectional interaction facilitated by TGF-α between corneal epithelial cells and mesenchymal cells assumes a pivotal morphological role in both corneal development and tissue repair. Any disruption in this intricate interplay can result in ocular lesions. Notably, TGF-α knockout mice exhibit significant ocular abnormalities, characterized by corneal epithelial thinning, inflammation, and edema (23, 24). TGF-α also promotes the proliferation of corneal epithelial and stromal cells (25). Additionally, TGF-α stimulates EGFR, facilitating the internalization and recycling of ligand-receptor complexes (22). Conversely, overexpression of TGF-α has been observed to induce corneal damage by activating EGFR in both corneal epithelium and stroma. This pathological manifestation is evident through a reduction in the number of corneal epithelial cell layers, corneal epithelial degeneration, conjunctivalization of the cornea, inhibition of the expression of the corneal pigment protein Kera, and a marked decrease in fibrocollagen types I and V collagen. Simultaneously, TGF-α overexpression can lead to corneal opacity by upregulating α-SMA and Wnt5a, while downregulating Col1a1, Col1a2, and Col5a1 (25–28). Some *in vitro* analysis of BTC indicates that BTC can expedite corneal epithelial injury repair and may even possess advantages over EGF in promoting corneal epithelial injury repair (18). LSCs, primarily located at the corneal-scleral junction, possess lifelong self-renewal capabilities and can produce transient amplifying cells (TACs). During corneal epithelial injury repair, TACs migrate towards the corneal center, proliferate, and differentiate into corneal epithelial cells, thereby promoting the healing of corneal epithelial wounds (29). Research has shown that treating injured mouse eyes with BTC results in significant increases in the expression of putative stem cell markers, such as DNp63α, ABCB5 and CK14. This suggests that BTC accelerates corneal LSCs proliferation and enhances mouse corneal epithelial repair by phosphorylating erk1/2 (30, 31). Despite the efficacy of various EGFR ligands in *in vitro* settings, *in vivo* wound healing is uniquely facilitated by EGF among the seven mentioned ligands. EGF also stands out as the sole ligand in human tears with an EGFR concentration closely aligned with the ligand Kd (18). Furthermore, EGFR can be reactivated through various effectors, such as phospholipase D (PLD) and extracellular ATP, to foster the migration and proliferation of cells during the wound healing process (32). Transient receptor potential (TRP) non-selective cation channels constitute a superfamily, which contains 28 different genes, and widely distributed in corneal epithelial cells and endothelial cells, its expression in the corneal epithelial layer contributes to the maintenance of corneal transparency and barrier function of the corneal epithelium. Research has shown that TRPV1 stimulation also induces increases in the proliferation and migration of corneal epithelial cells and the release of IL-6 and IL-8, and reduces the formation and of corneal neovascularization (CNV) and scar through transactivation of the EGFR. Meanwhile, TRPC4 stimulates corneal epithelial proliferation and migration by transactivation of the EGFR. TRPV in corneal epithelium can also promote homeostasis under thermal stimulation (33, 34).

While EGF holds the potential to stimulate the migration and proliferation of corneal epithelial cells, caution is warranted, as excessively increasing the intensity and duration of EGF may not yield positive effects. An experiment assessing EGF's effectiveness has revealed potential harm from continuous daily injections in rats (35). Furthermore, injecting recombinant EGF into the cornea post-corneal epithelial cell injury can lead to CNV (36). Elevated tear EGF levels are also associated with meibomian duct hypertrophy, contributing to meibomian gland hyperplasia (37). These findings underscore the need for caution when employing exogenous EGF in treating corneal injuries. Additionally, EGFR activity is a critical determinant in maintaining corneal epithelial homeostasis and plays a pivotal role in restoring damaged corneal epithelial cells. Despite the inherent regulatory mechanisms preventing sustained EGFR signal transduction, a deeper understanding of the molecular mechanisms governing EGFR signaling holds promise for developing new methods to overcome these regulatory barriers and enhance the efficacy of EGF (Figure 2 shows the EGF signaling pathway).

2.2 Hepatocyte growth factor

Hepatocyte growth factor (HGF) is a growth factor originating from fibroblasts, predominantly produced by mesenchymal cells, and expressed in various cell types, including corneal epithelial cells, keratocytes and endothelial cells. Its mode of action is paracrine, exerting its effects on adjacent cells (38). Structurally, HGF consists of α- and β-chains and serves as a mitogen and motility factor. In the cornea, HGF plays a significant role by binding to its receptor c-met and primarily participating in the proliferation, mitosis, and morphogenesis of corneal epithelial cells (39–41).

When the corneal epithelium undergoes damage, the expression of HGF in corneal epithelial cells and keratocytes is upregulated. This upregulation activates the signal mediators phosphatidylinositol of PI3K/Akt, phosphoprotein 70 ribosomal protein S6 kinase (p70s6K), and ERK. Consequently, it controls the cell cycle, promoting cell division and proliferation of corneal epithelial cells by triggering the activity of NF-κB. Simultaneously, it reverses the anti-proliferative effect of pro-inflammatory cytokines interleukin-1β (IL-1β) and TNF-α on these cells in the inflammatory environment, mediating corneal epithelial injury repair (42–46). HGF also exhibits wound repair effects by inhibiting the inflammatory response of corneal epithelial cells. Studies have demonstrated that HGF can inhibit the activation of immune cells and the expression of inflammatory factors. It further suppresses the expression of TNF-α, monocyte chemotactic protein-1 (MCP-1), and IL-6 in the macrophage system *in vitro*. Additionally, it promotes the production of the anti-inflammatory cytokine IL-10 in bone marrow-derived macrophages and dendritic cells stimulated by lipopolysaccharide (LPS) (43, 47–49). Evidence supports that HGF significantly inhibits cell apoptosis, temporarily downregulates the expression of cell cycle inhibitors in corneal epithelial cells, and upregulates cyclin and cyclin-dependent kinases. It also influences tumor suppressor proteins Rb and p53, which regulate cell cycle and apoptosis. Through these mechanisms, HGF

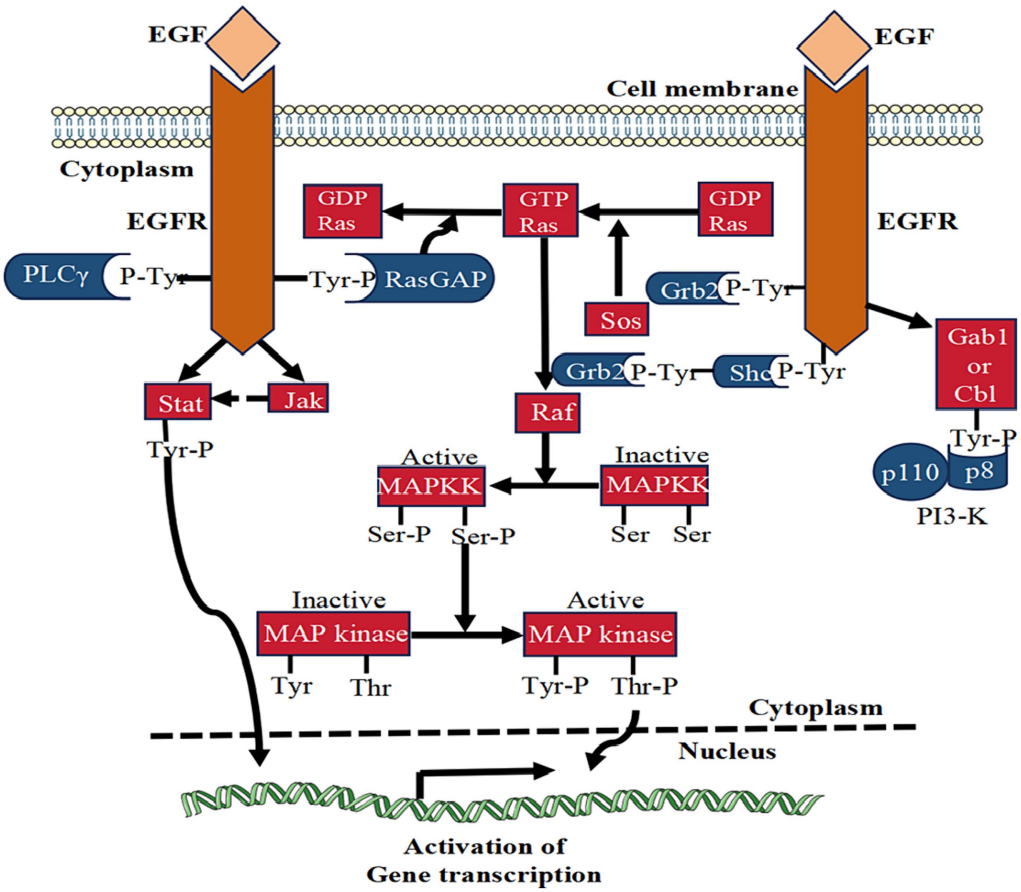

FIGURE 2
The signaling pathway of EGF. This figure illustrates the signal transduction mechanism of EGF in corneal epithelial injury repair. EGF binding activates EGFR, stimulating various signaling pathways like PLCγ, Ras-GAP, Grb2, and Shc. These pathways collectively contribute to the reparative effects on corneal epithelial injuries.

actively participates in corneal epithelial injury repair (50, 51). HGF also has the capability to penetrate through LPS-induced corneal opacity, promoting recovery, diminishing corneal fibrosis, restoring normal corneal tissue structure, and reestablishing immune quiescence after keratitis (52). In cases of diabetes-related corneal epithelial damage, HGF exhibits a reparative effect by restoring the level of c-met in the cornea of diabetic patients through downstream activation of p38 mitogen-activated protein kinase (MAPK) and the production of several putative stem cell markers. Importantly, this positive effect is observed in cultured corneas, regardless of whether gene therapy is applied to the entire corneal epithelial cells or only to the corneal edge area containing stem cells (53). Research indicates that silencing the HGF gene inhibits corneal epithelial proliferation and UVR-induced CNV. Additionally, HGF contributes to the upregulation of vascular endothelial growth factor (VEGF) and plays a role in angiogenesis regulation. These findings open up new avenues for exploring treatment strategies for CNV (54, 55).

2.3 Insulin-like growth factor

Insulin-like growth factor (IGF) belongs to the multifunctional cell proliferation regulatory factor, representing a group of peptide substances capable of promoting growth. Its secretory cells are widely distributed in various tissues, including the liver, kidneys, heart and eyes of the human body. The IGF family comprises two peptide ligands (IGF-1 and IGF-2), three receptors, and six binding proteins, collectively maintaining tissue homeostasis by regulating metabolism and/or mitotic pathways at the level of all corneal cells (56).

IGF-1, a multifunctional cytokine with broad biological activity, holds considerable promise for applications in corneal epithelial injury repair. By binding to the insulin-like growth factor 1 receptor (IGF-1R), IGF-1 actively maintains and regulates corneal epithelial cell growth, proliferation, differentiation, maturation, migration, regeneration, and energy metabolism. It promotes corneal epithelial cell proliferation through the activation of the hybrid of IGF-1R and insulin receptor (INSR), leading to subsequent Akt phosphorylation. Additionally, IGF-1 mediates corneal epithelial cell migration through the PI3K/AKT pathway. Furthermore, IGF-1 promotes the expression of IGF receptors in corneal limbal cells, stimulating LSCs to differentiate into corneal epithelial cells (57, 58). Beyond its role in cell proliferation and migration, IGF-1 serves as a crucial neurotrophic factor facilitating the regeneration and restoration of nerves following peripheral nerve damage in the cornea (59). In combination with substance P, IGF-1 demonstrates a synergistic effect in promoting corneal epithelial injury repair. The co-application accelerates the *ex*

vivo migration of corneal epithelial cells in the injured corneal stroma. Mediated by the interaction between substance P and tachykinin receptors, it enhances the adhesion of corneal epithelium to fibronectin (FN) and type IV collagen, thereby augmenting the protective role of the corneal epithelium through the stimulation of wound healing (60–64). The low levels of IGF-1 in tears, particularly the reduced proportion of IGF-1 and IGF binding protein 3 (IGFBP-3) in tears of diabetic patients, have been associated with decreased proliferation of corneal epithelial cells and delayed wound repair. This change inhibits the capacity of IGF-1 to induce IGF-1R or hybrid R phosphorylation (65, 66). Research has demonstrated that mRNA of adipose-derived stem cells (ADSCs) modified with IGF-1 exhibits stronger cell proliferation and migration abilities, promoting wound repair, morphological and functional recovery, corneal nerve regeneration, and maintenance of corneal homeostasis after acute alkali burns. Importantly, it can prevent the generation of CNV and corneal lymphatic vessels, highlighting the crucial role of IGF-1 in the repair of corneal epithelial injury (60). However, the application of IGF-1 protein to the cornea in the form of eye drops faces limitations, including a limited duration of effect, elevated attrition rates, and the need for repeated administration. Further research is expected to explore new carrier forms that can overcome these shortcomings and enhance the effectiveness of IGF-1 in corneal injury repair. The expression of IGF-2 and its receptors significantly increases after corneal epithelial cell injury, promoting the transformation of LSCs in the basal layer of the cornea into corneal epithelial cells and subsequently supporting corneal epithelial cell repair (67). Additionally, both IGF-1 and IGF-2 play roles in promoting the proliferation of keratocytes and collagen synthesis (68).

IGFBP primarily exists in the aqueous humor and vitreous body, exerting unique, cell- and tissue-dependent effects through interactions with the IGF family via binding (69–71). The primary function of IGFBP is to bind to IGF-1, extending its half-life in circulation and preventing IGF-1R activation induced by IGF-1 (72, 73). IGFBP-2 and IGFBP-3 play pivotal roles in corneal tissue homeostasis, particularly in regulating the growth of corneal epithelial cells and the localization of intracellular receptors (74, 75). The mutual regulation between IGFBP-3 and IGF-1R maintains corneal epithelial homeostasis. Previous studies have shown that IGFBP-3 is essential for inducing the transport of IGF-1R, and the absence of IGF-1R will downregulate IGFBP-3 in turn (76). During conditions such as hypoxia and hyperglycemia, the secretion of IGFBP-3 increases. For instance, the level of IGFBP-3 in the tears of diabetic patients rises, suggesting its potential role in regulating eye homeostasis in diabetic patients and indicating therapeutic potential in ocular surface diseases associated with diabetes (66).

Moreover, IGF and insulin share a close relationship, with the former mediating the action of insulin to promote the growth of corneal epithelial cells. This suggests a potential collaborative repair effect between the two, offering a promising avenue for future research exploration (77, 78).

2.4 Neurogenic growth factor

Neurogenic growth factor (NGF) belongs to the family of neurotrophic factors, exhibiting dual biological functions of neuronal nourishment and promoting synaptic growth (79). In the context of the cornea, signals mediated by NGF propagate through the high-affinity receptor tropomyosin receptor kinase A (TrkA) and the low-affinity non-selective transmembrane glycoprotein receptor p75NTR. When combined with NGF, TrkA activates Ras MAPK, ERK, phospholipase C-γ (PLC-γ), and PI3K. This activation includes stimulating D-type cell cycle regulatory proteins through PI3K/Akt and MAPK/ERK, subsequently promoting corneal epithelial cell cycle progression. Simultaneously, p75NTR activates the c-Jun kinase and NF-kB signaling pathway, exhibiting a protective effect on corneal epithelial cells by inhibiting the inflammatory signaling pathway of NF-kB (80–82).

Research has demonstrated that NGF participates in the repair process of corneal epithelial and stromal damage by upregulating matrix metalloproteinase-9 (MMP-9) and cleaving integrins β4 to stimulate the migration of corneal epithelial cells, promotes the differentiation of keratocytes into myofibroblasts, and reduces the formation of corneal haze (83–85). Moreover, NGF induces the differentiation of goblet cells and the production of mucin through receptors expressed in the lacrimal gland and neural reflexes, thereby contributing to the maintenance of corneal epithelial function (86). In addition to its role in cellular functions, NGF regulates immune function through Toll-like receptors (TLRs) in corneal physiology and pathology, playing a crucial role in maintaining corneal homeostasis both *in vivo* and *in vitro* settings (87). NGF has also been identified as a key promoter for the proliferation of LSCs, the formation of colonies in LSCs, and the maintenance of the LSC phenotype (79). For patients with corneal ulcers, local application of NGF eye drops has been shown to improve the speed of corneal epithelial repair and the sensitivity of the cornea. In cases of herpes simplex keratitis (HSK), endogenous NGF, akin to acyclovir, significantly improves the condition and inhibits recurrence. Clinical studies indicate that eye drops containing NGF can induce complete healing in HSK patients resistant to acyclovir (88, 89). Treatment with recombinant human NGF (rhNGF) has proven effective in enhancing corneal perception in patients with neurotrophic keratitis (NK) by increasing the density and number of nerve fibers in the basal layer of the corneal epithelium. It also promotes the healing of persistent corneal epithelial defects and ulcers. Furthermore, rhNGF provides lubrication and natural protection against pathogen damage to the corneal epithelium by promoting tear secretion from the lacrimal gland. RhNGF has received approval as a primary therapeutic drug for NK (87, 88). Additionally, NGF exhibits the ability to inhibit oxidative damage caused by hyperosmotic stress or high glucose levels. This finding suggests its potential therapeutic effect on conditions such as dry eye syndrome and diabetic keratopathy (DK) (90, 91).

2.5 TGF-β

TGF is a protein composed of amino acids in the cytoplasm, belonging to the family of peptide growth factors. It includes two main types: TGF-α and TGF-β (92). TGF-α has been described in the EGF section. TGF-β is a multifunctional growth factor, further divided into three subtypes: TGF-β1, TGF-β2 and TGF-β3. All three subtypes and their receptors are expressed in corneal epithelium and keratocytes (93). TGF-β assumes a pivotal role in orchestrating and coordinating the response to corneal injury repair, exerting influence over various facets such as the proliferation, motility, and differentiation of corneal

epithelial cells. Moreover, TGF-β modulates the activity and apoptosis of keratocytes, as well as the development of myofibroblasts (94). By stimulating the migration of corneal epithelial cells through integrin β1, TGF-β enhances the fluidity of these cells (95). Notably, the conditional ablation of its type II receptor has been found to impede the repair of corneal epithelial wounds and the activation of p38 MAPK, thereby hindering the migration of corneal epithelial cells (96). Furthermore, TGF-β2 has been substantiated to expedite the repair of corneal epithelial wounds in rabbits, augmenting barrier integrity by promoting cell adhesion to substrates and enhancing the functionality of corneal endothelial cells (CECs) (97). Tgfbr-2 also plays a crucial role in maintaining corneal stromal homeostasis, as studies have demonstrated that Tgfbr-2 knockout mice display significant corneal thinning and a potential for corneal ectasia (98). TGF-β3 exhibits the capability to mitigate interstitial scars induced by the activity of TGF-β1 and TGF-β2. Moreover, it demonstrates potential therapeutic effects in addressing corneal and skin wounds in diabetic patients, acting through the PI3K-Akt and SMAD signaling pathways, along with their target genes (99). Additionally, if the Bowman layer is damaged, corneal cells are highly susceptible to exposure to TGF-β. In such cases, TGF-β promotes damage repair through various mechanisms (100). Despite its essential role in corneal epithelial injury repair, TGF-β also has negative effects on the cornea. For instance, it can promote the aging of corneal epithelial cells through the NF-κB signaling pathway. This aging process can be alleviated by inhibiting the NF-κB signaling pathway (101). TGF-β is implicated in the pathogenesis of various eye diseases, including pterygium, vernal keratoconjunctivitis (VKC), atopic keratoconjunctivitis (AKC), and graft-versus-host disease (GVHD). Elevated levels of TGF-β are observed in the corneas of individuals with these diseases (102). Additionally, TGF-β regulates the transformation of corneal epithelial cells and corneal fibroblasts into myofibroblasts, and the high expression of α-SMA and F-actin in myofibroblasts can lead to the loss of corneal transparency and corresponding corneal haze (103). Moreover, TGF-β1 and TGF-β2 can prevent corneal epithelial cells from proliferating *in vitro* (104).

2.6 Platelet-derived growth factor

Platelet-derived growth factor (PDGF), secreted by epithelial cells, endothelial cells and inflammatory cells, serves as a potent mitogenic factor, existing in diverse isoforms, namely PDGF-AA, PDGF-BB, PDGF-CC, PDGF-DD, and PDGF-AB (105). Featuring both α and β types of receptors, PDGF exerts its cellular effects by inducing the complex formation of α-tyrosine kinase receptors and β-tyrosine kinase receptors. This induction, in turn, triggers processes such as cell growth, chemotaxis, actin recombination and protection against apoptosis. Analogous to TGF-β, PDGF assumes a pivotal role in regulating and coordinating the response to corneal wound repair. It influences the proliferation, motility and differentiation of corneal epithelial cells, while also modulating the activity and apoptosis of keratocytes and contributing to the development of myofibroblasts (94). Corneal epithelial cells express PDGF AA, PDGF BB and PDGF AB, which regulate the migration and proliferation of keratocytes. In the presence of FN, these isoforms can enhance the migration of corneal epithelial cells (106–108). Research indicates that PDGF-AB and PDGF-BB promote the migration of corneal fibroblasts *in vitro*, leading to an increase in the concentration of cytosolic free Ca^{2+}. PDGF-BB also significantly stimulates DNA synthesis in bovine corneal endothelial cells (BCEC) and human corneal fibroblasts (HCF) in a dose-dependent manner (108–110). Moreover, under high fibroblast density, PDGF isomers act as mitogens for interstitial fibroblasts during wound healing, conversely, at low cell density, PDGF-AA and PDGF-AB can prevent cell loss during the corneal homeostasis process (111). The secretion of PDGF is activated during corneal trauma, infection, or inflammation, providing significant stimulation for tissue repair. However, hyperstimulation can have negative effects. For instance, PDGF-α hyperstimulation can promote the proliferation and migration of lens epithelial cells, leading to epithelial-mesenchymal transition (EMT) (112, 113).

2.7 Fibroblast growth factor

Fibroblast growth factor (FGF) is secreted by the hypothalamus and pituitary gland, serving as a broad-spectrum mitogen, currently, at least 23 FGF families have been identified, stimulating or maintaining specific cellular functions required for tissue metabolism, homeostasis and development through signaling axes mediated by their receptors (114). Corneal epithelial changes, accompanied by decreased vision and dry eye symptoms, have been observed after treatment with inhibitors of the FGF receptor (FGFR), indirectly indicating FGF's involvement in corneal epithelial homeostasis (115). Basic FGF (b-FGF/FGF2), approved for the treatment of corneal damage, accelerates the repair of corneal epithelial cell damage and reduces keratitis by promoting the proliferation, differentiation and migration of corneal epithelial cells (116, 117). In experiments involving FGFR2 knockout mice, observations reveal localized central corneal thinning, along with the loss of collagen fibers and apoptosis of keratocytes (118). In addition, the signal transduction of FGFR2b promotes corneal epithelial injury repair, studies have found that FGFR2b knockout mice exhibit reduced proliferation of corneal epithelial cells, as well as loss of lacrimal gland and meibomian gland. FGFR2b is also necessary for the development of submandibular glands (119). FGF-10 plays a crucial role in the development of the cornea, morphogenesis and growth of the lens and induction and branching of the lacrimal gland and meibomian gland. Research has shown that FGF-10 is essential for the development of lacrimal glands in humans and mice (120, 121). FGF-10 can upregulate the expression of mucin in conjunctival epithelial cells, protecting the ocular surface in a dry eye model of rabbits and controlling the migration of epithelial cells during the process of embryonic eyelid closure (122, 123). Additionally, FGF-10 is associated with adult tissue homeostasis and the function of stem cells (124). In an experimental study of DK, it has been found that rhFGF-21 can improve the vitality and migration of human corneal epithelial cells, promote the healing of corneal wounds and the production of tears, and improve corneal edema. RhFGF-21 significantly reduces the expression of pro-inflammatory cytokines such as TNF-α and MMPs in corneal epithelial cells, while increasing the level of anti-inflammatory molecules IL-10 and SOD-1. RhFGF-21 also inhibits excessive production of reactive oxygen species (ROS) and alleviates oxidative stress induced by hyperglycemia in corneal epithelial cells. Therefore, the application of drugs containing FGF-21 may be a potential treatment method for DK (125, 126).

2.8 Keratinocyte growth factor

Keratinocyte growth factor (KGF) belongs to the FGF family, officially known as FGF-7. It is produced by mesenchymal cells and acts on adjacent cells in a paracrine manner. KGF promotes the repair of corneal epithelial wounds through the signaling cascade of MAPK and PI3K/p70 S6 in corneal epithelial cells. It also inhibits the destruction of the barrier function caused by hypoxia in corneal epithelial cells by activating ERK (46, 127, 128). *In vitro* experiments have shown that KGF can protect cells from apoptosis for an extended period, with the final percentage of apoptosis in cells treated with KGF being only 10% (129). Similar to HGF, KGF has the capacity to inhibit UVR-induced corneal epithelial proliferation. Through gene silencing, it downregulates the expression of VEGF and its receptors, consequently mitigating CNV (48, 49). Additionally, KGF-2 exhibits certain effects in re-epithelialization, accelerating migration, reducing scar formation and edema. It is considered superior to b-FGF and holds potential as a new drug for treating corneal injuries (116). KGF also can promote the migration of LSCs, thereby promoting the repair of corneal epithelial damage (36).

2.9 Opioid growth factor

Opioid growth factor (OGF) is an endogenous peptide found together with its receptor OGFr in or on the basal layer of many species' corneas, when combined, OGF regulates DNA synthesis in corneal epithelial cells and influences cell migration (130). Experimental evidence suggests that OGF inhibits cell overgrowth by upregulating cyclin-dependent inhibitory kinases p16 and p21, contributing to the maintenance of corneal epithelial homeostasis (131). Studies conducted on patients and rats with diabetes have indicated elevated levels of OGF and OGFr in serum and corneal epithelium. This elevation has been associated with ocular surface complications, including dry eyes, abnormal sensitivity of the corneal surface, and delayed corneal epithelial repair. In rats, an OGF-OGFr axis is present in the corneal limbus, and its dysregulation in hyperglycemia impacts the morphology of the corneal limbus, exacerbating diabetes-related complications on the corneal surface. Local application of the opioid antagonist naltrexone (NTX) has demonstrated improvement in this situation (132, 133). NTX disrupts the OGF-OGFr interaction, resulting in increased DNA synthesis in epithelial cells of the peripheral cornea and limbus corneae, as well as the proliferation of fibroblast cells. The latter plays a crucial role in corneal wound healing (134, 135). Additionally, the application of NTX significantly promotes corneal re-epithelialization and increases tear production (136–138). In summary, the use of eye drops containing opioid antagonists, such as NTX, holds promise as a novel therapy for treating wound repair disorders of the corneal epithelium.

2.10 VEGF

VEGF, recognized as a highly specific mitogen promoting endothelial cell growth, is also referred to as vascular permeability factor (VPF) due to its ability to significantly enhance vascular permeability (139). The VEGF family comprises seven subtypes: VEGF-A, VEGF-B, VEGF-C, VEGF-D, VEGF-E, VEGF-F, and placental growth factor (PLGF). Additionally, there are three receptors, VEGFR-1, VEGFR-2, and VEGFR-3. Among these, VEGF-A stands out for its profound ability to promote angiogenesis and is the most prevalent subtype in the eyes (140). The VEGF family and its receptors are expressed in the corneal epithelium (4). Under normal circumstances, a delicate balance is maintained between ocular angiogenic factors and anti-angiogenic factors to prevent pathological CNV production. However, factors such as wearing contact lenses, inflammation, and infection can disrupt this balance and lead to CNV (141). Research has highlighted the crucial role of VEGF in the pathogenesis of CNV, making the use of anti-VEGF drugs a feasible therapeutic approach (142, 143). Additionally, VEGF is implicated in non-angiogenic functions, such as neuroprotection and serving as a nutritional factor for corneal nerves (144). VEGF also plays a role in wound repair; studies have shown that VEGF accelerates corneal epithelial wound healing by stimulating corneal nerve regeneration (145). VEGF may be linked to the pathogenesis of pterygium, with higher expression detected in pterygium compared to normal tissue (146). Pigment epithelial-derived factors (PEDFs) are closely related to VEGF, sharing anti-angiogenic functions and a protective role for corneal nerves (147). Both factors exhibit synergistic therapeutic effects in certain diseases. However, in pterygium, a decrease in PEDF expression has been observed (146). Moreover, PEDF has been found to promote the self-renewal and migration of LSCs, thereby facilitating corneal epithelial repair (148). (The expression of growth factors in the corneal epithelium is depicted in Figure 3, and the biological effects of corneal epithelial growth factor receptors are summarized in Table 1).

3 Discussion and outlook

Eye injuries often involve damage to the corneal epithelial layer, leading to symptoms such as eye pain, bleeding, ulcers, and vision loss, significantly impacting quality of life (151, 152). The repair of corneal epithelial injuries has emerged as a prominent research focus, with growing recognition of the crucial role played by growth factors in this process. These growth factors contribute to the wound healing of corneal epithelium through intricate mechanisms.

Despite the significant role of growth factors in corneal epithelial injury repair, there are existing limitations. The current understanding of the signal transduction pathways of various growth factors is not yet comprehensive, and their full potential as a treatment method for corneal epithelial injury remains to be realized. Some growth factors, like TGF, have stringent usage and dosage guidelines in corneal epithelium treatment—only within a safe usage range can they effectively repair the corneal epithelium. This presents a crucial and challenging aspect in utilizing growth factors for corneal epithelium treatment. For targeted repair effects of growth factors, many studies focus on single targets or signal pathways. The comprehensive repair mechanisms involving different growth factors still require further exploration. Additionally, some growth factors are primarily limited to basic research, and their potential for improving corneal epithelial cells in clinical practice needs further validation. Growth factors can be categorized into endogenous and exogenous types, with exogenous growth factors often utilized in experimental studies involving mice. However, when it comes to the role of growth factors in corneal epithelial injury repair, there is a noticeable gap in research and discussion regarding whether the mechanisms differ between the two types. Furthermore, in the case of the growth factor VEGF, exploring more suitable drug carriers could potentially enhance its therapeutic

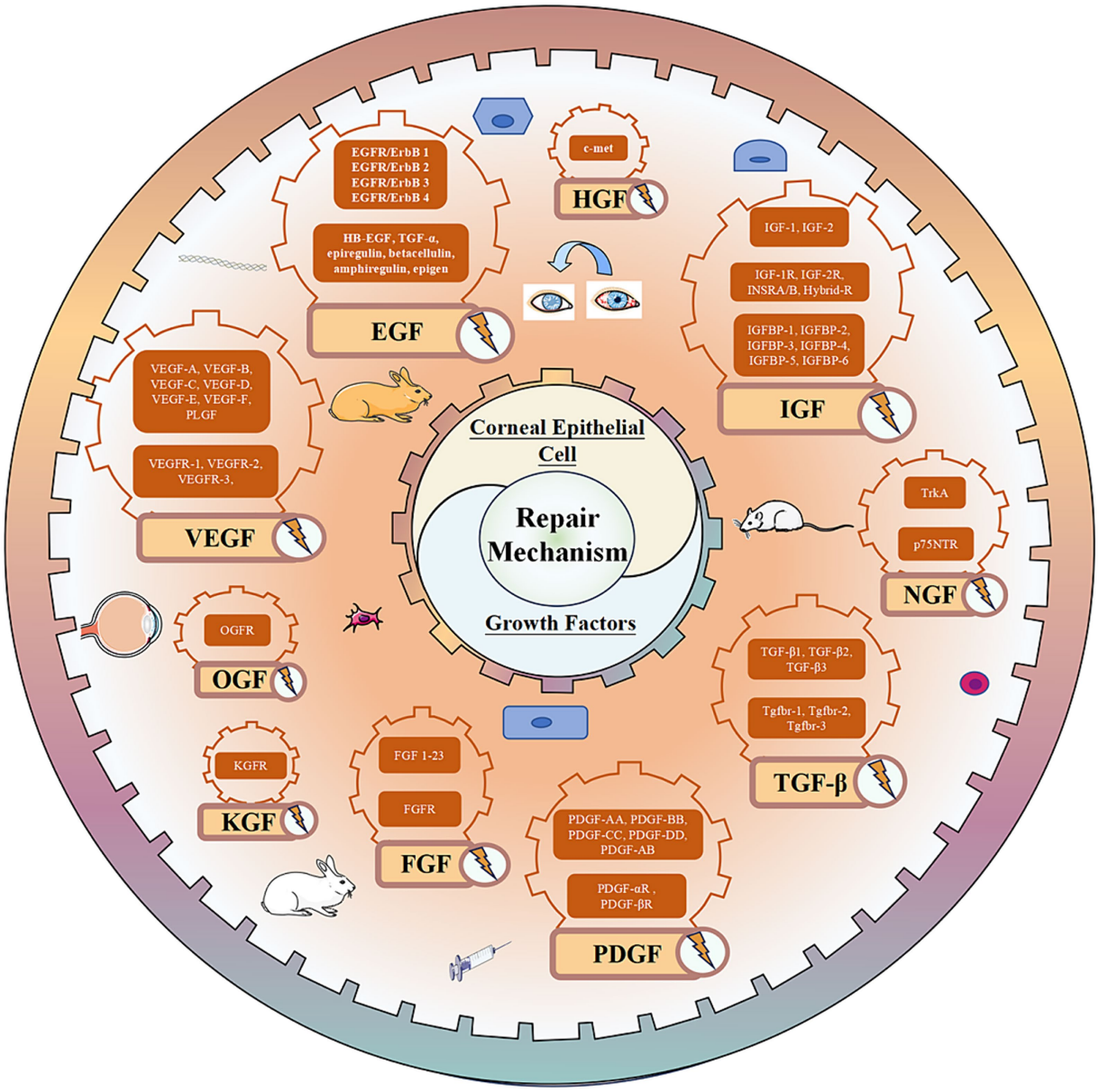

FIGURE 3
Growth factor mediated repair mechanism of corneal epithelial cell injury.

efficacy. This avenue of research could lead to the development of more effective delivery systems for VEGF, optimizing its impact on corneal epithelial repair.

Future research endeavors should leverage current multi-omics techniques to explore and study the signaling mechanisms and synergistic effects of different growth factors, aiming to enhance their roles in corneal epithelial injury repair. Simultaneously, through in-depth basic and clinical research, optimizing the dosage and understanding side effects of growth factors can contribute to revealing their basic mechanisms and optimal usage methods. This foundational work will pave the way for the development of new treatment methods involving growth factors. Further research and exploration are essential to determine potential differences in the roles of endogenous and exogenous growth factors in corneal epithelial repair, a facet not addressed in the current study. Additionally, investigating ways to enhance exogenous growth factors and identifying more suitable drug carriers are critical for optimizing the use of growth factors in the future.

Author contributions

JG: Writing – original draft. GD: Writing – review & editing. ZH: Writing – review & editing. YL: Writing – review & editing. AD: Writing – review & editing. CZ: Writing – review & editing.

Funding

The author(s) declare that financial support was received for the research, authorship, and/or publication of this article. This study was supported by Jinan Clinical Medical Technology Innovation Project

TABLE 1 Biological effects of corneal epithelial growth factor receptor.

Factor	Receptor	Effects on corneal wound healing	References
EGF	EGFR	• Promotes migration and proliferation of epithelial cells • EGFR can be reactivated through various effectors	(7, 8, 12, 13, 17, 32)
HB-EGF		• Enhances cell adhesion	(19)
BTC		• Accelerates corneal epithelial injury repair • Accelerates the proliferation of LSCs	(18, 30)
TGF-α		• Promotes the proliferation of corneal epithelial and stromal cells • Facilitates the internalization and recycling of ligand-receptor complexes	(22, 25)
HGF	c-Met	• Participates in the mitosis and morphogenesis of corneal epithelial cells • Promotes cell division and proliferation of corneal epithelial cells by controlling the cell cycle • Reverses the anti-proliferative effect of pro-inflammatory cytokines in the inflammatory environment • Inhibits the activation of immune cells and the expression of inflammatory factors • Promotes the production of anti-inflammatory cytokines • Suppresses apoptosis of corneal epithelial cells • Promotes corneal opacity recovery, reduces corneal fibrosis, normalize corneal tissue structure and reestablish immune quiescence post-keratitis • Restores the level of c-met in the cornea of diabetic patients • Inhibits UVR-induced corneal epithelial proliferation and CNV by HGF gene silencing • Participates in angiogenesis	(39–55)
IGF/INS	IGF-1R、IGF-2R、INSR、Hybrid-R	• Regulates metabolism and/or mitotic pathways • Promotes the migration and proliferation of epithelial cells • Facilitates the regeneration and restoration of corneal nerves • Accelerates the *ex vivo* migration of corneal epithelial cells in the injured corneal stroma • Enhances the adhesion of corneal epithelium to FN and type IV collagen • Promotes the transformation of LSCs in the basal layer of the cornea into corneal epithelial cells • Promotes the proliferation of keratocytes and collagen synthesis • Plays pivotal roles in corneal tissue homeostasis	(56–64, 67, 68, 74, 75)
NGF	TrkA, p75NTR	• Stimulates the migration of corneal epithelial cells, promotes the differentiation of keratocytes into myofibroblasts and reduces the formation of corneal haze • Induces the differentiation of goblet cells and the production of mucin regulates immune function • Be identified as a key promoter for the proliferation of LSCs, the formation of colonies in LSCs and the maintenance of the LSCs phenotype • Improves the speed of corneal epithelial repair and the sensitivity of the cornea of patients with corneal ulcers, significantly improves the condition and inhibits recurrence of HSK • Increases the density and number of nerve fibers in the basal layer of the corneal epithelium, promotes tear secretion • Inhibits oxidative damage caused by hyperosmotic stress or high glucose levels	(79, 83–91, 149, 150)
TGF-β	Tgfbr-1, Tgfbr-2, Tgfbr-3	• Modulates the activity and apoptosis of keratocytes, modulates the development of myofibroblasts • Stimulates the migration of corneal epithelial cells • Augments barrier integrity by promoting cell adhesion to substrates and enhancing the functionality of corneal endothelial cells (CECs) • Plays an important role in corneal stromal homeostasis • Reduces interstitial scars promotes damage repair of Bowman layer • Promotes the aging of corneal epithelial cells • Be implicated in the pathogenesis of various eye diseases, such as pterygium • Regulates the transformation of corneal epithelial cells and corneal fibroblasts into myofibroblasts • Prevents corneal epithelial cells from proliferating *in vitro*	(94–103)
(PDGF)	PDGF-αR, PDGF-βR	• Promotes the proliferation, motility and differentiation of corneal epithelial cells • Modulates the activity and apoptosis of keratocytes and contributes to the development of myofibroblasts • Stimulates DNA synthesis in BCEC and HCF • Acts as mitogens for interstitial fibroblasts during wound healing • Prevents cell loss during the corneal homeostasis process	(94, 105–110)

(Continued)

TABLE 1 (Continued)

Factor	Receptor	Effects on corneal wound healing	References
FGF	FGFR	• Participates in corneal epithelial homeostasis • Promotes the proliferation, differentiation and migration of corneal epithelial cells • Promotes the regeneration of the lacrimal gland, submandibular gland and meibomian gland • Promotes the development of the cornea and morphogenesis and growth of the lens • Be associated with adult tissue homeostasis and the function of stem cells • Improves the vitality of human corneal epithelial cells • Improves corneal edema • Reduces the expression of pro-inflammatory cytokines and increases the level of anti-inflammatory molecules • Suppresses excessive production of ROS and alleviates oxidative stress	(114–120, 123–125)
(KGF)	KGFR	• Inhibits the destruction of the barrier function caused by hypoxia in corneal epithelial cells • Suppresses apoptosis of corneal epithelial cells • Inhibits UVR-induced corneal epithelial proliferation and CNV by HGF gene silencing • Enhances re-epithelialization rates • Promotes the migration and proliferation of epithelial cells • Reduces corneal scars and edema • Promotes the proliferation of LSCs	(36, 48, 49, 115, 127, 128)
OGF	OGFr	• Regulates DNA synthesis in corneal epithelial cells and influences the migration of corneal cells • Inhibits the overgrowth of corneal cells and maintains of corneal epithelial homeostasis	(129, 130)
VEGF	VEGFR-1, VEGFR-2, VEGFR-3	• Promotes the growth of endothelial cell • Promote corneal angiogenesis • Protecting corneal nerves • Be related to the pathogenesis of pterygium	(138, 139, 143, 145)

EGF, epidermal growth factor; EGFR, epidermal growth factor receptor; HB-EGF, heparin-binding EGF-like growth factor; BTC, betacellulin; TGF-α, transforming growth factor-α; HGF, hepatocyte growth factor; c-Met, hepatocyte growth factor receptor; IGF, insulin-like growth factor; INS, insulin; IGF-1R, insulin-like growth factor-1 receptor; IGF-2R, insulin-like growth factor-2 receptor; INSR, insulin receptor; Hybrid-R, IGF-1R and INSR hybrid; NGF, nerve growth factor; TrkA, tropomyosin receptor kinase A; p75NTR, low-affinity non-selective transmembrane glycoprotein receptor; TGF-β, transforming growth factor-β; Tgfbr-1, transforming growth factor beta receptor-1; Tgfbr-2, transforming growth factor beta receptor-2; Tgfbr-3, transforming growth factor beta receptor-3; PDGF, platelet derived growth factor; PDGF-αR, platelet derived growth factor receptor-α; PDGF-βR, platelet derived growth factor receptor-β; FGF, fibroblast growth factor; FGFR, fibroblast growth factor receptor; KGF, keratinocyte growth factor; KGFR, keratinocyte growth factor receptor; OGF, opioid growth factor; OGFr, opioid growth factor receptor.

(No. 202225058) and Shandong Province Medical and Health Technology Project (No. 202307021389).

Conflict of interest

The authors declare that the research was conducted in the absence of any commercial or financial relationships that could be construed as a potential conflict of interest.

Publisher's note

References

1. Ludwig PE, Lopez MJ, Sevensma KE. Anatomy, head and neck, eye cornea In: *StatPearls*. Treasure Island, FL: StatPearls Publishing (2023).

2. Downie LE, Bandlitz S, Bergmanson JPG, Craig JP, Dutta D, Maldonado-Codina C, et al. CLEAR—anatomy and physiology of the anterior eye. *Cont Lens Anterior Eye*. (2021) 44:132–56. doi: 10.1016/j.clae.2021.02.009

3. Koh S, Rao SK, Srinivas SP, Tong L, Young AL. Evaluation of ocular surface and tear function—a review of current approaches for dry eye. *Indian J Ophthalmol*. (2022) 70:1883–91. doi: 10.4103/ijo.IJO_1804_21

4. Tarvestad-Laise KE, Ceresa BP. Modulating growth factor receptor signaling to promote corneal epithelial homeostasis. *Cells*. (2023) 12:2730. doi: 10.3390/cells12232730

5. Klenkler B, Sheardown H, Jones L. Growth factors in the tear film: role in tissue maintenance, wound healing, and ocular pathology. *Ocul Surf*. (2007) 5:228–39. doi: 10.1016/s1542-0124(12)70613-4

6. Shin SH, Koh YG, Lee WG, Seok J, Park KY. The use of epidermal growth factor in dermatological practice. *Int Wound J*. (2023) 20:2414–23. doi: 10.1111/iwj.14075

7. Zieske JD, Takahashi H, Hutcheon AE, Dalbone AC. Activation of epidermal growth factor receptor during corneal epithelial migration. *Invest Ophthalmol Vis Sci*. (2000) 41:1346–55.

8. Wilson SE. Corneal wound healing. *Exp Eye Res*. (2020) 197:108089. doi: 10.1016/j.exer.2020.108089

9. Zhang Y, Akhtar RA. Epidermal growth factor stimulation of phosphatidylinositol 3-kinase during wound closure in rabbit corneal epithelial cells. *Invest Ophthalmol Vis Sci*. (1997) 38:1139–48.

10. Yang L, Di G, Qi X, Qu M, Wang Y, Duan H, et al. Substance P promotes diabetic corneal epithelial wound healing through molecular mechanisms mediated via the neurokinin-1 receptor. *Diabetes*. (2014) 63:4262–74. doi: 10.2337/db14-0163

11. Xu K, Yu FS. Impaired epithelial wound healing and EGFR signaling pathways in the corneas of diabetic rats. *Invest Ophthalmol Vis Sci*. (2011) 52:3301–8. doi: 10.1167/iovs.10-5670

12. Li T, Lu L. Epidermal growth factor-induced proliferation requires down-regulation of Pax 6 in corneal epithelial cells. *J Biol Chem*. (2005) 280:12988–95. doi: 10.1074/jbc.M412458200

13. Imanishi J, Kamiyama K, Iguchi I, Kita M, Sotozono C, Kinoshita S. Growth factors: importance in wound healing and maintenance of transparency of the cornea. *Prog Retin Eye Res*. (2000) 19:113–29. doi: 10.1016/s1350-9462(99)00007-5

14. Liu Z, Carvajal M, Carraway CA, Carraway K, Pflugfelder SC. Expression of the receptor tyrosine kinases, epidermal growth factor receptor, ErbB2, and ErbB3, in human ocular surface epithelia. *Cornea*. (2001) 20:81–5. doi: 10.1097/00003226-200101000-00016

15. Xu KP, Riggs A, Ding Y, Yu FS. Role of ErbB2 in corneal epithelial wound healing. *Invest Ophthalmol Vis Sci*. (2004) 45:4277–83. doi: 10.1167/iovs.04-0119

16. Huang J, Wang S, Lyu H, Cai B, Yang XH, Wang J, et al. The anti-ErbB3 antibody MM-121/SAR256212 in combination with trastuzumab exerts potent antitumor activity against trastuzumab-resistant breast cancer cells. *Mol Cancer*. (2013) 12:134. doi: 10.1186/1476-4598-12-134

17. Schoeberl B, Faber AC, Li D, Liang MC, Crosby K, Onsum M, et al. An ErbB3 antibody, MM-121, is active in cancers with ligand-dependent activation. *Cancer Res*. (2010) 70:2485–94. doi: 10.1158/0008-5472.CAN-09-3145

18. Peterson JL, Phelps ED, Doll MA, Schaal S, Ceresa BP. The role of endogenous epidermal growth factor receptor ligands in mediating corneal epithelial homeostasis. *Invest Ophthalmol Vis Sci*. (2014) 55:2870–80. doi: 10.1167/iovs.13-12943

19. Iwamoto R, Yamazaki S, Asakura M, Takashima S, Hasuwa H, Miyado K, et al. Heparin-binding EGF-like growth factor and ErbB signaling is essential for heart function. *Proc Natl Acad Sci USA*. (2003) 100:3221–6. doi: 10.1073/pnas.0537588100

20. Block ER, Matela AR, Sundar Raj N, Iszkula ER, Klarlund JK. Wounding induces motility in sheets of corneal epithelial cells through loss of spatial constraints: role of heparin-binding epidermal growth factor-like growth factor signaling. *J Biol Chem*. (2004) 279:24307–12. doi: 10.1074/jbc.M401058200

21. Tolino MA, Block ER, Klarlund JK. Brief treatment with heparin-binding EGF-like growth factor, but not with EGF, is sufficient to accelerate epithelial wound healing. *Biochim Biophys Acta*. (2011) 1810:875–8. doi: 10.1016/j.bbagen.2011.05.011

22. Roepstorff K, Grandal MV, Henriksen L, Knudsen SLJ, Lerdrup M, Grøvdal L, et al. Differential effects of EGFR ligands on endocytic sorting of the receptor. *Traffic*. (2009) 10:1115–27. doi: 10.1111/j.1600-0854.2009.00943.x

23. Singh B, Coffey RJ. From wavy hair to naked proteins: the role of transforming growth factor alpha in health and disease. *Semin Cell Dev Biol*. (2014) 28:12–21. doi: 10.1016/j.semcdb.2014.03.003

24. Luetteke NC, Qiu TH, Peiffer RL, Oliver P, Smithies O, Lee DC. TGF alpha deficiency results in hair follicle and eye abnormalities in targeted and waved-1 mice. *Cell*. (1993) 73:263–78. doi: 10.1016/0092-8674(93)90228-i

25. Zhang L, Yuan Y, Yeh LK, Dong F, Zhang J, Okada Y, et al. Excess transforming growth factor-α changed the cell properties of corneal epithelium and stroma. *Invest Ophthalmol Vis Sci*. (2020) 61:20. doi: 10.1167/iovs.61.8.20

26. Reneker LW, Silversides DW, Xu L, Overbeek PA. Formation of corneal endothelium is essential for anterior segment development—a transgenic mouse model of anterior segment dysgenesis. *Development*. (2000) 127:533–42. doi: 10.1242/dev.127.3.533

27. Liu CY, Shiraishi A, Kao CW, Converse RL, Funderburgh JL, Corpuz LM, et al. The cloning of mouse keratocan cDNA and genomic DNA and the characterization of its expression during eye development. *J Biol Chem*. (1998) 273:22584–8. doi: 10.1074/jbc.273.35.22584

28. Chen S, Mienaltowski MJ, Birk DE. Regulation of corneal stroma extracellular matrix assembly. *Exp Eye Res*. (2015) 133:69–80. doi: 10.1016/j.exer.2014.08.001

29. Lehrer MS, Sun TT, Lavker RM. Strategies of epithelial repair: modulation of stem cell and transit amplifying cell proliferation. *J Cell Sci*. (1998) 111:2867–75. doi: 10.1242/jcs.111.19.2867

30. Jeong WY, Yoo HY, Kim CW. β-cellulin promotes the proliferation of corneal epithelial stem cells through the phosphorylation of erk1/2. *Biochem Biophys Res Commun*. (2018) 496:359–66. doi: 10.1016/j.bbrc.2018.01.054

31. Seyed-Safi AG, Daniels JT. The limbus: structure and function. *Exp Eye Res*. (2020) 197:108074. doi: 10.1016/j.exer.2020.108074

32. Zhang F, Yang H, Pan Z, Wang Z, Wolosin JM, Gjorstrup P, et al. Dependence of resolvin-induced increases in corneal epithelial cell migration on EGF receptor transactivation. *Invest Ophthalmol Vis Sci*. (2010) 51:5601–9. doi: 10.1167/iovs.09-4468

33. Pan Z, Yang H, Reinach PS. Transient receptor potential (TRP) gene superfamily encoding cation channels. *Hum Genomics*. (2011) 5:108–16. doi: 10.1186/1479-7364-5-2-108

34. Yang Y, Yang H, Wang Z, Okada Y, Saika S, Reinach PS. Wakayama symposium: dependence of corneal epithelial homeostasis on transient receptor potential function. *Ocul Surf*. (2013) 11:8–11. doi: 10.1016/j.jtos.2012.09.001

35. Hennessey PJ, Nirgiotis JG, Shinn MN, Andrassy RJ. Continuous EGF application impairs long-term collagen accumulation during wound healing in rats. *J Pediatr Surg*. (1991) 26:362–6. doi: 10.1016/0022-3468(91)90980-8

36. Nezu E, Ohashi Y, Kinoshita S, Manabe R. Recombinant human epidermal growth factor and corneal neovascularization. *Jpn J Ophthalmol*. (1992) 36:401–6.

37. Rao K, Farley WJ, Pflugfelder SC. Association between high tear epidermal growth factor levels and corneal subepithelial fibrosis in dry eye conditions. *Invest Ophthalmol Vis Sci*. (2010) 51:844–9. doi: 10.1167/iovs.09-3875

38. Bottaro DP, Rubin JS, Faletto DL, Chan AML, Kmiecik TE, Vande Woude GF, et al. Identification of the hepatocyte growth factor receptor as the c-met proto-oncogene product. *Science*. (1991) 251:802–4. doi: 10.1126/science.1846706

39. Pai P, Kittur SK. Hepatocyte growth factor: a novel tumor marker for breast cancer. *J Cancer Res Ther*. (2023) 19:S0. doi: 10.4103/jcrt.JCRT_1084_16

40. Nakamura T, Nishizawa T, Hagiya M, Seki T, Shimonishi M, Sugimura A, et al. Molecular cloning and expression of human hepatocyte growth factor. *Nature*. (1989) 342:440–3. doi: 10.1038/342440a0

41. Wright JW, Church KJ, Harding JW. Hepatocyte growth factor and macrophage-stimulating protein "hinge" analogs to treat pancreatic cancer. *Curr Cancer Drug Targets*. (2019) 19:782–95. doi: 10.2174/1568009619666190326130008

42. Chandrasekher G, Kakazu AH, Bazan HE. HGF- and KGF-induced activation of PI-3K/p 70 s6 kinase pathway in corneal epithelial cells: its relevance in wound healing. *Exp Eye Res*. (2001) 73:191–202. doi: 10.1006/exer.2001.1026

43. Omoto M, Suri K, Amouzegar A, Li M, Katikireddy KR, Mittal SK, et al. Hepatocyte growth factor suppresses inflammation and promotes epithelium repair in corneal injury. *Mol Ther*. (2017) 25:1881–8. doi: 10.1016/j.ymthe.2017.04.020

44. Okunishi K, Dohi M, Fujio K, Nakagome K, Tabata Y, Okasora T, et al. Hepatocyte growth factor significantly suppresses collagen-induced arthritis in mice. *J Immunol*. (2007) 179:5504–13. doi: 10.4049/jimmunol.179.8.5504

45. Benkhoucha M, Santiago-Raber ML, Schneiter G, Chofflon M, Funakoshi H, Nakamura T, et al. Hepatocyte growth factor inhibits CNS autoimmunity by inducing tolerogenic dendritic cells and $CD25^+$ $Foxp3^+$ regulatory T cells. *Proc Natl Acad Sci USA*. (2010) 107:6424–9. doi: 10.1073/pnas.0912437107

46. Giannopoulou M, Dai C, Tan X, Wen X, Michalopoulos GK, Liu Y. Hepatocyte growth factor exerts its anti-inflammatory action by disrupting nuclear factor-kappa B signaling. *Am J Pathol*. (2008) 173:30–41. doi: 10.2353/ajpath.2008.070583

47. Kusunoki H, Taniyama Y, Otsu R, Rakugi H, Morishita R. Anti-inflammatory effects of hepatocyte growth factor on the vicious cycle of macrophages and adipocytes. *Hypertens Res*. (2014) 37:500–6. doi: 10.1038/hr.2014.41

48. Coudriet GM, He J, Trucco M, Mars WM, Piganelli JD. Hepatocyte growth factor modulates interleukin-6 production in bone marrow derived macrophages: implications for inflammatory mediated diseases. *PLoS One*. (2010) 5:e15384. doi: 10.1371/journal.pone.0015384

49. Rutella S, Bonanno G, Procoli A, Mariotti A, de Ritis DG, Curti A, et al. Hepatocyte growth factor favors monocyte differentiation into regulatory interleukin (IL)-10++IL-12low/neg accessory cells with dendritic-cell features. *Blood*. (2006) 108:218–27. doi: 10.1182/blood-2005-08-3141

50. Chandrasekher G, Pothula S, Maharaj G, Bazan HE. Differential effects of hepatocyte growth factor and keratinocyte growth factor on corneal epithelial cell cycle protein expression, cell survival, and growth. *Mol Vis*. (2014) 20:24–37.

51. Sherr CJ, McCormick F. The RB and p 53 pathways in cancer. *Cancer Cell*. (2002) 2:103–12. doi: 10.1016/s1535-6108(02)00102-2

52. Elbasiony E, Cho W, Mittal SK, Chauhan SK. Suppression of lipopolysaccharide-induced corneal opacity by hepatocyte growth factor. *Sci Rep*. (2022) 12:494. doi: 10.1038/s41598-021-04418-x

53. Sharma GD, He J, Bazan HE. p38 and ERK1/2 coordinate cellular migration and proliferation in epithelial wound healing: evidence of cross-talk activation between MAP kinase cascades. *J Biol Chem*. (2003) 278:21989–97. doi: 10.1074/jbc.M302650200

54. He M, Han T, Wang Y, Wu YH, Qin WS, du LZ, et al. Effects of HGF and KGF gene silencing on vascular endothelial growth factor and its receptors in rat ultraviolet radiation-induced corneal neovascularization. *Int J Mol Med*. (2019) 43:1888–99. doi: 10.3892/ijmm.2019.4114

55. Matsumura A, Kubota T, Taiyoh H, Fujiwara H, Okamoto K, Ichikawa D, et al. HGF regulates VEGF expression via the c-met receptor downstream pathways, PI3K/Akt, MAPK and STAT3, in CT26 murine cells. *Int J Oncol*. (2013) 42:535–42. doi: 10.3892/ijo.2012.1728

56. Baxter RC. Signaling pathways of the insulin-like growth factor binding proteins. *Endocr Rev*. (2023) 44:753–78. doi: 10.1210/endrev/bnad008

57. Stuard WL, Titone R, Robertson DM. The IGF/insulin-IGFBP axis in corneal development, wound healing, and disease. *Front Endocrinol*. (2020) 11:24. doi: 10.3389/fendo.2020.00024

58. Trosan P, Svobodova E, Chudickova M, Krulova M, Zajicova A, Holan V. The key role of insulin-like growth factor I in limbal stem cell differentiation and the corneal wound-healing process. *Stem Cells Dev*. (2012) 21:3341–50. doi: 10.1089/scd.2012.0180

59. Slavin BR, Sarhane KA, von Guionneau N, Hanwright PJ, Qiu C, Mao HQ, et al. Insulin-like growth factor-1: a promising therapeutic target for peripheral nerve injury. *Front Bioeng Biotechnol*. (2021) 9:695850. doi: 10.3389/fbioe.2021.695850

60. Yu F, Gong D, Yan D, Wang H, Witman N, Lu Y, et al. Enhanced adipose-derived stem cells with IGF-1-modified mRNA promote wound healing following corneal injury. *Mol Ther*. (2023) 31:2454–71. doi: 10.1016/j.ymthe.2023.05.002

61. Nakamura M, Chikama TI, Nishida T. Characterization of insulin-like growth factor-1 receptors in rabbit corneal epithelial cells. *Exp Eye Res*. (2000) 70:199–204. doi: 10.1006/exer.1999.0775

62. Todorović V, Peško P, Micev M, Bjelović M, Budeč M, Mićić M, et al. Insulin-like growth factor-I in wound healing of rat skin. *Regul Pept*. (2008) 150:7–13. doi: 10.1016/j.regpep.2008.05.006

63. Ghiasi Z, Gray T, Tran P, Dubielzig R, Murphy C, McCartney D, et al. The effect of topical substance-P plus insulin-like growth factor-1 (IGF-1) on epithelial healing after photorefractive keratectomy in rabbits. *Transl Vis Sci Technol*. (2018) 7:12. doi: 10.1167/tvst.7.1.12

64. Nagano T, Nakamura M, Nakata K, Yamaguchi T, Takase K, Okahara A, et al. Effects of substance P and IGF-1 in corneal epithelial barrier function and wound healing in a rat model of neurotrophic keratopathy. *Invest Ophthalmol Vis Sci*. (2003) 44:3810–5. doi: 10.1167/iovs.03-0189

65. Patel R, Zhu M, Robertson DM. Shifting the IGF-axis: an age-related decline in human tear IGF-1 correlates with clinical signs of dry eye. *Growth Hormon IGF Res*. (2018) 40:69–73. doi: 10.1016/j.ghir.2018.02.001

66. Wu YC, Buckner BR, Zhu M, Cavanagh HD, Robertson DM. Elevated IGFBP3 levels in diabetic tears: a negative regulator of IGF-1 signaling in the corneal epithelium. *Ocul Surf*. (2012) 10:100–7. doi: 10.1016/j.jtos.2012.01.004

67. Jiang Y, Ju Z, Zhang J, Liu X, Tian J, Mu G. Effects of insulin-like growth factor 2 and its receptor expressions on corneal repair. *Int J Clin Exp Pathol*. (2015) 8:10185–91.

68. Hassell JR, Birk DE. The molecular basis of corneal transparency. *Exp Eye Res*. (2010) 91:326–35. doi: 10.1016/j.exer.2010.06.021

69. Ferry RJ Jr, Katz LE, Grimberg A, Cohen P, Weinzimer SA. Cellular actions of insulin-like growth factor binding proteins. *Horm Metab Res*. (1999) 31:192–202. doi: 10.1055/s-2007-978719

70. Arnold DR, Moshayedi P, Schoen TJ, Jones BE, Chader GJ, Waldbillig RJ. Distribution of IGF-I and -II, IGF binding proteins (IGFBPs) and IGFBP mRNA in ocular fluids and tissues: potential sites of synthesis of IGFBPs in aqueous and vitreous. *Exp Eye Res*. (1993) 56:555–65. doi: 10.1006/exer.1993.1069

71. Titone R, Zhu M, Robertson DM. Insulin mediates *de novo* nuclear accumulation of the IGF-1/insulin hybrid receptor in corneal epithelial cells. *Sci Rep*. (2018) 8:4378. doi: 10.1038/s41598-018-21031-7

72. Conover CA, Oxvig C. PAPP-A: a promising therapeutic target for healthy longevity. *Aging Cell*. (2017) 16:205–9. doi: 10.1111/acel.12564

73. Argente J, Chowen JA, Pérez-Jurado LA, Frystyk J, Oxvig C. One level up: abnormal proteolytic regulation of IGF activity plays a role in human pathophysiology. *EMBO Mol Med*. (2017) 9:1338–45. doi: 10.15252/emmm.201707950

74. Park SH, Kim KW, Kim JC. The role of insulin-like growth factor binding protein 2 (IGFBP2) in the regulation of corneal fibroblast differentiation. *Invest Ophthalmol Vis Sci*. (2015) 56:7293–302. doi: 10.1167/iovs.15-16616

75. Rao P, Suvas PK, Jerome AD, Steinle JJ, Suvas S. Role of insulin-like growth factor binding protein-3 in the pathogenesis of herpes stromal keratitis. *Invest Ophthalmol Vis Sci*. (2020) 61:46. doi: 10.1167/iovs.61.2.46

76. Titone R, Zhu M, Robertson DM. Mutual regulation between IGF-1R and IGFBP-3 in human corneal epithelial cells. *J Cell Physiol*. (2019) 234:1426–41. doi: 10.1002/jcp.26948

77. Lima MH, Caricilli AM, de Abreu LL, Araújo EP, Pelegrinelli FF, Thirone ACP, et al. Topical insulin accelerates wound healing in diabetes by enhancing the AKT and ERK pathways: a double-blind placebo-controlled clinical trial. *PLoS One*. (2012) 7:e36974. doi: 10.1371/journal.pone.0036974

78. Wirostko B, Rafii M, Sullivan DA, Morelli J, Ding J. Novel therapy to treat corneal epithelial defects: a hypothesis with growth hormone. *Ocul Surf*. (2015) 13:204–212.e1. doi: 10.1016/j.jtos.2014.12.005

79. Kolli S, Bojic S, Ghareeb AE, Kurzawa-Akanbi M, Figueiredo FC, Lako M. The role of nerve growth factor in maintaining proliferative capacity, colony-forming efficiency, and the limbal stem cell phenotype. *Stem Cells*. (2019) 37:139–49. doi: 10.1002/stem.2921

80. Huang EJ, Reichardt LF. Trk receptors: roles in neuronal signal transduction. *Annu Rev Biochem*. (2003) 72:609–42. doi: 10.1146/annurev.biochem.72.121801.161629

81. Lambiase A, Manni L, Bonini S, Rama P, Micera A, Aloe L. Nerve growth factor promotes corneal healing: structural, biochemical, and molecular analyses of rat and human corneas. *Invest Ophthalmol Vis Sci*. (2000) 41:1063–9.

82. Chen H, Zhang J, Dai Y, Xu J. Nerve growth factor inhibits TLR3-induced inflammatory cascades in human corneal epithelial cells. *J Inflamm*. (2019) 16:27. doi: 10.1186/s12950-019-0232-0

83. Micera A, Lambiase A, Puxeddu I, Aloe L, Stampachiacchiere B, Levi-Schaffer F, et al. Nerve growth factor effect on human primary fibroblastic-keratocytes: possible mechanism during corneal healing. *Exp Eye Res*. (2006) 83:747–57. doi: 10.1016/j.exer.2006.03.010

84. Blanco-Mezquita T, Martinez-Garcia C, Proença R, Zieske JD, Bonini S, Lambiase A, et al. Nerve growth factor promotes corneal epithelial migration by enhancing expression of matrix metalloprotease-9. *Invest Ophthalmol Vis Sci*. (2013) 54:3880–90. doi: 10.1167/iovs.12-10816

85. Anitua E, Muruzabal F, Alcalde I, Merayo-Lloves J, Orive G. Plasma rich in growth factors (PRGF-endoret) stimulates corneal wound healing and reduces haze formation after PRK surgery. *Exp Eye Res*. (2013) 115:153–61. doi: 10.1016/j.exer.2013.07.007

86. Muzi S, Colafrancesco V, Sornelli F, Mantelli F, Lambiase A, Aloe L. Nerve growth factor in the developing and adult lacrimal glands of rat with and without inherited retinitis pigmentosa. *Cornea*. (2010) 29:1163–8. doi: 10.1097/ICO.0b013e3181d3d3f9

87. Aloe L, Tirassa P, Lambiase A. The topical application of nerve growth factor as a pharmacological tool for human corneal and skin ulcers. *Pharmacol Res*. (2008) 57:253–8. doi: 10.1016/j.phrs.2008.01.010

88. Aloe L, Rocco ML, Balzamino BO, Micera A. Nerve growth factor: a focus on neuroscience and therapy. *Curr Neuropharmacol*. (2015) 13:294–303. doi: 10.2174/1570159x13666150403231920

89. Wu D, Qian T, Hong J, Li G, Shi W, Xu J. Micro RNA-494 inhibits nerve growth factor-induced cell proliferation by targeting cyclin D1 in human corneal epithelial cells. *Mol Med Rep*. (2017) 16:4133–42. doi: 10.3892/mmr.2017.7083

90. Sun Z, Hu W, Yin S, Lu X, Zuo W, Ge S, et al. NGF protects against oxygen and glucose deprivation-induced oxidative stress and apoptosis by up-regulation of HO-1 through MEK/ERK pathway. *Neurosci Lett*. (2017) 641:8–14. doi: 10.1016/j.neulet.2017.01.046

91. Park JH, Kang SS, Kim JY, Tchah H. Nerve growth factor attenuates apoptosis and inflammation in the diabetic cornea. *Invest Ophthalmol Vis Sci*. (2016) 57:6767–75. doi: 10.1167/iovs.16-19747

92. Ding Z, Jiang M, Qian J, Gu D, Bai H, Cai M, et al. Role of transforming growth factor-β in peripheral nerve regeneration. *Neural Regen Res*. (2024) 19:380–6. doi: 10.4103/1673-5374.377588

93. Nishida K, Kinoshita S, Yokoi N, Kaneda M, Hashimoto K, Yamamoto S. Immunohistochemical localization of transforming growth factor-beta 1, -beta 2, and -beta 3 latency-associated peptide in human cornea. *Invest Ophthalmol Vis Sci*. (1994) 35:3289–94.

94. Singh V, Jaini R, Torricelli AA, Santhiago MR, Singh N, Ambati BK, et al. TGFβ and PDGF-B signaling blockade inhibits myofibroblast development from both bone marrow-derived and keratocyte-derived precursor cells in vivo. *Exp Eye Res*. (2014) 121:35–40. doi: 10.1016/j.exer.2014.02.013

95. Bhowmick NA, Zent R, Ghiassi M, McDonnell M, Moses HL. Integrin beta 1 signaling is necessary for transforming growth factor-beta activation of p38MAPK and epithelial plasticity. *J Biol Chem*. (2001) 276:46707–13. doi: 10.1074/jbc.M106176200

96. Terai K, Call MK, Liu H, Saika S, Liu CY, Hayashi Y, et al. Crosstalk between TGF-beta and MAPK signaling during corneal wound healing. *Invest Ophthalmol Vis Sci*. (2011) 52:8208–15. doi: 10.1167/iovs.11-8017

97. Er H, Uzmez E. Effects of transforming growth factor-beta 2, interleukin 6 and fibronectin on corneal epithelial wound healing. *Eur J Ophthalmol*. (1998) 8:224–9. doi: 10.1177/112067219800800404

98. Wang YC, Zolnik OB, Yasuda S, Yeh LK, Yuan Y, Kao W, et al. Transforming growth factor beta receptor 2 (Tgfbr 2) deficiency in keratocytes results in corneal ectasia. *Ocul Surf*. (2023) 29:557–65. doi: 10.1016/j.jtos.2023.06.014

99. Bettahi I, Sun H, Gao N, Wang F, Mi X, Chen W, et al. Genome-wide transcriptional analysis of differentially expressed genes in diabetic, healing corneal epithelial cells: hyperglycemia-suppressed TGFβ3 expression contributes to the delay of epithelial wound healing in diabetic corneas. *Diabetes*. (2014) 63:715–27. doi: 10.2337/db13-1260

100. Rocher M, Robert PY, Desmoulière A. The myofibroblast, biological activities and roles in eye repair and fibrosis. A focus on healing mechanisms in avascular cornea. *Eye*. (2020) 34:232–40. doi: 10.1038/s41433-019-0684-8

101. Li ZY, Chen ZL, Zhang T, Wei C, Shi WY. TGF-β and NF-κB signaling pathway crosstalk potentiates corneal epithelial senescence through an RNA stress response. *Aging*. (2016) 8:2337–54. doi: 10.18632/aging.101050

102. Benito MJ, Calder V, Corrales RM, García-Vázquez C, Narayanan S, Herreras JM, et al. Effect of TGF-β on ocular surface epithelial cells. *Exp Eye Res*. (2013) 107:88–100. doi: 10.1016/j.exer.2012.11.017

103. Fink MK, Giuliano EA, Tandon A, Mohan RR. Therapeutic potential of pirfenidone for treating equine corneal scarring. *Vet Ophthalmol*. (2015) 18:242–50. doi: 10.1111/vop.12194

104. Saikia P, Thangavadivel S, Medeiros CS, Lassance L, de Oliveira RC, Wilson SE. IL-1 and TGF-β modulation of epithelial basement membrane components perlecan and nidogen production by corneal stromal cells. *Invest Ophthalmol Vis Sci*. (2018) 59:5589–98. doi: 10.1167/iovs.18-25202

105. Heldin CH, Westermark B. Platelet-derived growth factor: mechanism of action and possible *in vivo* function. *Cell Regul*. (1990) 1:555–66. doi: 10.1091/mbc.1.8.555

106. Daniels JT, Khaw PT. Temporal stimulation of corneal fibroblast wound healing activity by differentiating epithelium *in vitro*. *Invest Ophthalmol Vis Sci*. (2000) 41:3754–62.

107. Nishida T. Translational research in corneal epithelial wound healing. *Eye Contact Lens*. (2010) 36:300–4. doi: 10.1097/ICL.0b013e3181f016d0

108. Kamiyama K, Iguchi I, Wang X, Imanishi J. Effects of PDGF on the migration of rabbit corneal fibroblasts and epithelial cells. *Cornea*. (1998) 17:315–25. doi: 10.1097/00003226-199805000-00013

109. Hoppenreijs VP, Pels E, Vrensen GF, Felten PC, Treffers WF. Platelet-derived growth factor: receptor expression in corneas and effects on corneal cells. *Invest Ophthalmol Vis Sci*. (1993) 34:637–49.

110. Williamson JR, Monck JR. Hormone effects on cellular Ca^{2+} fluxes. *Annu Rev Physiol*. (1989) 51:107–24. doi: 10.1146/annurev.ph.51.030189.000543

111. Denk PO, Knorr M. The in vitro effect of platelet-derived growth factor isoforms on the proliferation of bovine corneal stromal fibroblasts depends on cell density. *Graefes Arch Clin Exp Ophthalmol*. (1997) 235:530–4. doi: 10.1007/BF00947012

112. Schultz T, Conrad-Hengerer I, Hengerer FH, Dick HB. Intraocular pressure variation during femtosecond laser-assisted cataract surgery using a fluid-filled interface. *J Cataract Refract Surg*. (2013) 39:22–7. doi: 10.1016/j.jcrs.2012.10.038

113. Wei J, Tang H, Xu ZQ, Li B, Xie LQ, Xu GX. Expression and function of PDGF-α in columnar epithelial cells of age-related cataracts patients. *Genet Mol Res*. (2015) 14:13320–7. doi: 10.4238/2015.October.26.28

114. Jin L, Yang R, Geng L, Xu A. Fibroblast growth factor-based pharmacotherapies for the treatment of obesity-related metabolic complications. *Annu Rev Pharmacol Toxicol*. (2023) 63:359–82. doi: 10.1146/annurev-pharmtox-032322-093904

115. Shin E, Lim DH, Han J, Nam DH, Park K, Ahn MJ, et al. Markedly increased ocular side effect causing severe vision deterioration after chemotherapy using new or investigational epidermal or fibroblast growth factor receptor inhibitors. *BMC Ophthalmol*. (2020) 20:19. doi: 10.1186/s12886-019-1285-9

116. Cai J, Zhou Q, Wang Z, Guo R, Yang R, Yang X, et al. Comparative analysis of KGF-2 and bFGF in prevention of excessive wound healing and scar formation in a corneal alkali burn model. *Cornea*. (2019) 38:1430–7. doi: 10.1097/ICO.0000000000002134

117. Reneker LW, Irlmeier RT, Shui YB, Liu Y, Huang AJW. Histopathology and selective biomarker expression in human meibomian glands. *Br J Ophthalmol*. (2020) 104:999–1004. doi: 10.1136/bjophthalmol-2019-314466

118. Zhang J, Upadhya D, Lu L, Reneker LW. Fibroblast growth factor receptor 2 (FGFR2) is required for corneal epithelial cell proliferation and differentiation during embryonic development. *PLoS One*. (2015) 10:e0117089. doi: 10.1371/journal.pone.0117089

119. Joseph R, Boateng A, Srivastava OP, Pfister RR. Role of fibroblast growth factor receptor 2 (FGFR2) in corneal stromal thinning. *Invest Ophthalmol Vis Sci*. (2023) 64:40. doi: 10.1167/iovs.64.12.40

120. Qu X, Carbe C, Tao C, Powers A, Lawrence R, van Kuppevelt TH, et al. Lacrimal gland development and Fgf 10-Fgfr2b signaling are controlled by 2-O- and 6-O-sulfated heparan sulfate. *J Biol Chem*. (2011) 286:14435–44. doi: 10.1074/jbc.M111.225003

121. Tsau C, Ito M, Gromova A, Hoffman MP, Meech R, Makarenkova HP. Barx 2 and Fgf 10 regulate ocular glands branching morphogenesis by controlling extracellular matrix remodeling. *Development*. (2011) 138:3307–17. doi: 10.1242/dev.066241

122. Ma M, Zhang Z, Niu W, Zheng W, Kelimu J, Ke B. Fibroblast growth factor 10 upregulates the expression of mucins in rat conjunctival epithelial cells. *Mol Vis*. (2011) 17:2789–97.

123. Tao H, Shimizu M, Kusumoto R, Ono K, Noji S, Ohuchi H. A dual role of FGF10 in proliferation and coordinated migration of epithelial leading edge cells during mouse eyelid development. *Development*. (2005) 132:3217–30. doi: 10.1242/dev.01892

124. Thotakura S, Basova L, Makarenkova HP. FGF gradient controls boundary position between proliferating and differentiating cells and regulates lacrimal gland growth dynamics. *Front Genet*. (2019) 10:362. doi: 10.3389/fgene.2019.00362

125. Li J, Zhang R, Wang C, Wang X, Xu M, Ma J, et al. Activation of the small GTPase rap 1 inhibits choroidal neovascularization by regulating cell junctions and ROS generation in rats. *Curr Eye Res*. (2018) 43:934–40. doi: 10.1080/02713683.2018.1454477

126. Li L, Wang H, Pang S, Wang L, Fan Z, Ma C, et al. Rh FGF-21 accelerates corneal epithelial wound healing through the attenuation of oxidative stress and inflammatory mediators in diabetic mice. *J Biol Chem*. (2023) 299:105127. doi: 10.1016/j.jbc.2023.105127

127. Wilson SE, Li Q, Mohan RR, Tervo T, Vesaluoma M, Bennett GL, et al. Lacrimal gland growth factors and receptors: lacrimal fibroblastic cells are a source of tear HGF. *Adv Exp Med Biol*. (1998) 438:625–8. doi: 10.1007/978-1-4615-5359-5_88

128. Teranishi S, Kimura K, Kawamoto K, Nishida T. Protection of human corneal epithelial cells from hypoxia-induced disruption of barrier function by keratinocyte growth factor. *Invest Ophthalmol Vis Sci*. (2008) 49:2432–7. doi: 10.1167/iovs.07-1464

129. Wilson SE, Walker JW, Chwang EL, He YG. Hepatocyte growth factor, keratinocyte growth factor, their receptors, fibroblast growth factor receptor-2, and the cells of the cornea. *Invest Ophthalmol Vis Sci*. (1993) 34:2544–61.

130. Kareem ZY, McLaughlin PJ, Kumari R. Opioid growth factor receptor: anatomical distribution and receptor colocalization in neurons of the adult mouse brain. *Neuropeptides*. (2023) 99:102325. doi: 10.1016/j.npep.2023.102325

131. Cheng F, McLaughlin PJ, Verderame MF, Zagon IS. The OGF-OGFr axis utilizes the p16INK4a and p21WAF1/CIP1 pathways to restrict normal cell proliferation. *Mol Biol Cell*. (2009) 20:319–27. doi: 10.1091/mbc.e08-07-0681

132. McLaughlin PJ, Sassani JW, Titunick MB, Zagon IS. Efficacy and safety of a novel naltrexone treatment for dry eye in type 1 diabetes. *BMC Ophthalmol*. (2019) 19:35. doi: 10.1186/s12886-019-1044-y

133. McLaughlin PJ, Sassani JW, Diaz D, Zagon IS. Elevated opioid growth factor alters the limbus in type 1 diabetic rats. *J Diabetes Clin Res*. (2023) 5:1–10. doi: 10.33696/diabetes.4.054

134. Zagon IS, Sassani JW, Purushothaman I, McLaughlin PJ. Blockade of OGFr delays the onset and reduces the severity of diabetic ocular surface complications. *Exp Biol Med*. (2021) 246:629–36. doi: 10.1177/1535370220972060

135. Immonen JA, Zagon IS, McLaughlin PJ. Selective blockade of the OGF-OGFr pathway by naltrexone accelerates fibroblast proliferation and wound healing. *Exp Biol Med*. (2014) 239:1300–9. doi: 10.1177/1535370214543061

136. Zagon IS, Sassani JW, Purushothaman I, McLaughlin PJ. Dysregulation of the OGF-OGFr pathway correlates with elevated serum OGF and ocular surface complications in the diabetic rat. *Exp Biol Med*. (2020) 245:1414–21. doi: 10.1177/1535370220940273

137. Zagon IS, Klocek MS, Sassani JW, McLaughlin PJ. Dry eye reversal and corneal sensation restoration with topical naltrexone in diabetes mellitus. *Arch Ophthalmol*. (2009) 127:1468–73. doi: 10.1001/archophthalmol.2009.270

138. Klocek MS, Sassani JW, McLaughlin PJ, Zagon IS. Naltrexone and insulin are independently effective but not additive in accelerating corneal epithelial healing in type I diabetic rats. *Exp Eye Res*. (2009) 89:686–92. doi: 10.1016/j.exer.2009.06.010

139. Bussolino F, di Renzo MF, Ziche M, Bocchietto E, Olivero M, Naldini L, et al. Hepatocyte growth factor is a potent angiogenic factor which stimulates endothelial cell motility and growth. *J Cell Biol*. (1992) 119:629–41. doi: 10.1083/jcb.119.3.629

140. Beheshtizadeh N, Gharibshahian M, Bayati M, Maleki R, Strachan H, Doughty S, et al. Vascular endothelial growth factor (VEGF) delivery approaches in regenerative medicine. *Biomed Pharmacother*. (2023) 166:115301. doi: 10.1016/j.biopha.2023.115301

141. Giannaccare G, Pellegrini M, Bernabei F, Scorcia V, Campos E. Ocular surface system alterations in ocular graft-versus-host disease: all the pieces of the complex puzzle. *Graefes Arch Clin Exp Ophthalmol*. (2019) 257:1341–51. doi: 10.1007/s00417-019-04301-6

142. Amano S, Rohan R, Kuroki M, Tolentino M, Adamis AP. Requirement for vascular endothelial growth factor in wound- and inflammation-related corneal neovascularization. *Invest Ophthalmol Vis Sci*. (1998) 39:18–22.

143. Giannaccare G, Pellegrini M, Bovone C, Spena R, Senni C, Scorcia V, et al. Anti-VEGF treatment in corneal diseases. *Curr Drug Targets*. (2020) 21:1159–80. doi: 10.2174/1389450121666200319111710

144. Goldhardt R, Batawi HIM, Rosenblatt M, Lollett IV, Park JJ, Galor A. Effect of anti-vascular endothelial growth factor therapy on corneal nerves. *Cornea*. (2019) 38:559–64. doi: 10.1097/ICO.0000000000001871

145. Pan Z, Fukuoka S, Karagianni N, Guaiquil VH, Rosenblatt MI. Vascular endothelial growth factor promotes anatomical and functional recovery of injured peripheral nerves in the avascular cornea. *FASEB J*. (2013) 27:2756–67. doi: 10.1096/fj.12-225185

146. Jin J, Guan M, Sima J, Gao G, Zhang M, Liu Z, et al. Decreased pigment epithelium-derived factor and increased vascular endothelial growth factor levels in pterygia. *Cornea*. (2003) 22:473–7. doi: 10.1097/00003226-200307000-00015

147. Yeh SI, Yu SH, Chu HS, Huang CT, Tsao YP, Cheng CM, et al. Pigment epithelium-derived factor peptide promotes corneal nerve regeneration: an *in vivo* and *in vitro* study. *Invest Ophthalmol Vis Sci*. (2021) 62:23. doi: 10.1167/iovs.62.1.23

148. Ho TC, Chen SL, Wu JY, Ho MY, Chen LJ, Hsieh JW, et al. PEDF promotes self-renewal of limbal stem cell and accelerates corneal epithelial wound healing. *Stem Cells*. (2013) 31:1775–84. doi: 10.1002/stem.1393

149. Versura P, Giannaccare G, Pellegrini M, Sebastiani S, Campos EC. Neurotrophic keratitis: current challenges and future prospects. *Eye Brain*. (2018) 10:37–45. doi: 10.2147/EB.S117261

150. Hao M, Cheng Y, Wu J, Cheng Y, Wang J. Clinical observation of recombinant human nerve growth factor in the treatment of neurotrophic keratitis. *Int J Ophthalmol*. (2023) 16:60–6. doi: 10.18240/ijo.2023.01.09

151. Sridhar MS. Anatomy of cornea and ocular surface. *Indian J Ophthalmol*. (2018) 66:190–4. doi: 10.4103/ijo.IJO_646_17

152. Sun X, Song W, Teng L, Huang Y, Liu J, Peng Y, et al. MiRNA 24-3p-rich exosomes functionalized DEGMA-modified hyaluronic acid hydrogels for corneal epithelial healing. *Bioact Mater*. (2022) 25:640–56. doi: 10.1016/j.bioactmat.2022.07.011

Glossary

EGF	Epidermal growth factor
EGFR/ErbB	Epidermal growth factor receptor
EGFR1/ErbB1	Epidermal growth factor receptor 1
PI3K	Type III phosphoinositide 3-kinase
Akt	Protein kinase B
ERK	Extracellular signal-regulated kinase
NF-kB	Nuclear factor kappa-B
HDAC6	Histone deacetylase 6
CTCF	CCCTC binding factor
PAX6	Paired box gene 6
EGFR2/ErbB2	Epidermal growth factor receptor 2
EGFR3/ErbB3	Epidermal growth factor receptor 3
EGFR4/ ErbB4	Epidermal growth factor receptor 4
HB-EGF	Heparin-binding EGF-like growth factor
TGF-α	Transforming growth factor-α
BTC	Betacellulin
PLD	Phospholipase D
CNV	Corneal neovascularization
HGF	Hepatocyte growth factor
p70s6K	Phosphoprotein 70 ribosomal protein S6 kinase
IL-1β	Interleukin-1β
MCP-1	Monocyte chemotactic protein-1
LPS	Lipopolysaccharide
MAPK	Mitogen-activated protein kinase
VEGF	Vascular endothelial growth factor
IGF	Insulin-like growth factor
IGFBP	IGF binding protein
IGF-1R	Insulin-like growth factor 1 receptor
INSR	Insulin receptor
LSCs	Corneal LSCs
FN	Fibronectin
IGFBP-3	IGF binding protein-3
ADSCs	Adipose-derived stem cells
IGFBP-2	IGF binding protein-2
TrkA	Tropomyosin receptor kinase A
PLC-γ	Phospholipase C-γ
MMP-9	Matrix metalloproteinase-9
TLRs	Toll-like receptors
HSK	Herpes simplex keratitis
rhNGF	Recombinant human NGF
NK	Neurotrophic keratitis
DK	Diabetic keratopathy
TGF	Transforming growth factor
CECs	Corneal endothelial cells
VKC	Vernal keratoconjunctivitis

(Continued)

GLOSSARY (Continued)

AKC	Atopic keratoconjunctivitis
GVHD	Graft-versus-host disease
PDGF	Platelet-derived growth factor
BCEC	Bovine corneal endothelial cells
HCF	Human corneal fibroblasts
EMT	Epithelial-mesenchymal transition
FGF	Fibroblast growth factor
FGFR	Fibroblast growth factor receptor
b-FGF/FGF2	Basic FGF
ROS	Reactive oxygen species
KGF	Keratinocyte growth factor
OGF	Opioid growth factor
OGFr	Opioid growth factor receptor
NTX	Naltrexone

frontiers | Frontiers in Medicine

TYPE Review
PUBLISHED 08 April 2024
DOI 10.3389/fmed.2024.1391327

OPEN ACCESS

EDITED BY
Georgios D. Panos,
Nottingham University Hospitals NHS Trust, United Kingdom

REVIEWED BY
Jinhai Huang,
Fudan University, China
Ioanna Mylona,
General Hospital of Serres, Greece

*CORRESPONDENCE
Lijun Zhang
✉ lijunzhangw1970@163.com

†These authors have contributed equally to this work and share first authorship

RECEIVED 25 February 2024
ACCEPTED 27 March 2024
PUBLISHED 08 April 2024

CITATION
Ning J, Zhang Q, Liang W, Zhang R, Xing Z, Jin L and Zhang L (2024) Bibliometric and visualized analysis of posterior chamber phakic intraocular lens research between 2003 and 2023.
Front. Med. 11:1391327.
doi: 10.3389/fmed.2024.1391327

Bibliometric and visualized analysis of posterior chamber phakic intraocular lens research between 2003 and 2023

Jiliang Ning[1,2,3,4†], Qiaosi Zhang[1,2,3,4†], Wei Liang[1,2,3,4], Rui Zhang[1,2,3,4], Zequn Xing[1,2,3,4], Lin Jin[1,2,3,4] and Lijun Zhang[1,2,3,4*]

[1]Department of Ophthalmology, The Third People's Hospital of Dalian, Dalian, China, [2]Department of Ophthalmology, Dalian Municipal Eye Hospital, Dalian, China, [3]Liaoning Provincial Key Laboratory of Cornea and Ocular Surface Diseases, Dalian, China, [4]Liaoning Provincial Optometry Technology Engineering Research Center, Dalian, China

Introduction: Myopia is causing a major public health concern, with its prevalence increasing globally. This study aimed to discuss posterior chamber phakic intraocular lens (pIOL) research publication trends and hotspots over the past 20 years.

Methods: Bibliometric analysis was performed using the Web Science Core Collection to investigate posterior-chamber pIOL research publication trends. The extracted records were analyzed, and a knowledge map was built using VOSviewer v.1.6.20. The analysis included visualizing the annual publication count, countries/regions distribution, international and institutional collaborations, author productivity, and journal contribution, in addition to identifying knowledge bases and hotspots. Burst keywords were extracted using CiteSpace v.6.1.R.

Results: In total, 791 articles on posterior chamber pIOLs published between 2003 and 2023 were retrieved. China had the highest number of publications, whereas Japanese papers received the most citations. Fudan University had the highest number of publications, with articles from Kitasato University having the highest number of citations. Regarding individual research, Xingtao Zhou has published the most significant number of articles, and Shimizu Kimiya had the highest number of citations. The top productive/influential journal was 'Journal of Cataract & Refractive Surgery'. The top cited references primarily focused on reporting the clinical outcomes of implantable collamer lens (ICL) for individuals with moderate to high myopia. The keywords primarily formed four clusters: posterior chamber pIOL clinical outcomes for myopic astigmatism correction, posterior chamber pIOL implantation complications, ICL size selection and postoperative vault predictions, and postoperative visual quality following posterior chamber pIOL implantation.

Conclusion: This study presents the first bibliometric analysis of research trends in posterior chamber pIOL over the past two decades. We investigated the current state and emerging trends of global collaboration and research focal points in this field, offering fresh insights and guidance for researchers.

KEYWORDS

posterior chamber phakic intraocular lens, implantable collamer lens, bibliometric analysis, VOSviewer, CiteSpace

1 Introduction

The prevalence of myopia is increasing globally, causing a major public health concern. It is estimated that billions of individuals will be affected by myopia by 2050 (1). Refractive surgery is crucial in myopia treatment; it enhances patients' quality of life, productivity, and overall daily performance (2). There are three main types of refractive surgery: laser refractive surgery, implantation and refractive lens exchange, and phakic intraocular lens implantation (pIOL) (3). Implantation using pIOL is reversible, unlike the other two surgeries. Posterior chamber pIOLs are positioned further away from the corneal endothelium, inflicting less harm than early anterior chamber angle-supported pIOLs and anterior chamber iris-fixated pIOLs (3). The Visian implantable collamer lens (ICL) (STAAR Surgical, Nidau, Switzerland) is the most widely used type of pIOL globally. It is safe and effective and corrects myopia, hyperopia, and astigmatism (4, 5). Over the last two decades, significant progress has been made in posterior chamber pIOL implantation research.

Bibliometric analysis enables the scientific and quantitative analysis of publications. It was first introduced by Pritchard in 1969 and was later expanded by Van Raan's infographics in 2004 (6, 7). This method allows for citation, coauthor, and keyword co-occurrence analyses, which can create knowledge maps. These knowledge maps can be visualized using tools such as CiteSpace and VOSviewer.

This study evaluated growth in the annual distribution of publications, international and institutional collaborations, author productivity, journal contribution, and identifying knowledge bases and hotspots related to posterior chamber pIOLs research. Assessing research trends in the academic field is crucial in identifying gaps that require attention in future studies. Therefore, our study used bibliometric techniques to comprehensively assess the current developmental status and future trends in posterior chamber pIOLs.

2 Materials and methods

2.1 Data sources and search strategies

The Science Citation Index Extension database of the Online Web of Science Core Collection (WoSCC) was used as the research source. The search keywords were "Posterior chamber phakic intraocular lens" or "Implantable collamer lens." The search time was between 2003 and 2023; the specified document types were articles. Language restrictions were not imposed. The search results were obtained as plain-text files and complete records with cited references. The search was conducted on January 31, 2024, and basic information on each article was collected, including the author, title, abstract, institution, journal, country, keywords, and references.

Abbreviations: D, Diopters; HOA, High-order aberrations; ICL, Implantable collamer lens; LASIK, Laser *in situ* keratomileusis; OCT, Optical coherence tomography; pIOL, Phakic intraocular lens; SMILE, Small incision lenticule extraction; TICL, Toric intraocular lens; UBM, Ultrasound biomicroscopy; WoSCC, Web of science core collection.

2.2 Analytical tools and methods

Visualization software can be used to analyze the publication data and generate knowledge graphs. This study analyzed publication data, including publication year, author, country/region, research institution, journals, citations, and keywords, using VOSviewer v.1.6.20. VOSviewer,[1] developed by van Eck and Waltman, is a literature visualization software that displays cluster analysis results (8). The knowledge graph generated by VOSviewer represents items as nodes and links. The sizes of the nodes and links correspond to the weights of the analyzed components. Node size indicates the number of publications, whereas the length and thickness of the connections between nodes represent the strength of the relationships between the analyzed components. Citation burst analysis on keywords was performed using CiteSpace 6.2.1, developed by Drexel University in Philadelphia, PA, United States. The burst map showed the burst intensity, with the red portion indicating the period during which the keywords emerged. This study utilized software to perform countries, authors, and institutional collaboration network coauthor analysis. In addition, it conducted reference co-citation analysis, co-occurrence analysis, and citation bursts of keywords (Figure 1).

3 Results

3.1 Annual quantitative distribution of literature

WoSCC indexed 791 articles published between 2003 and 2023 based on the selection criteria. The posterior chamber pIOL annual publication volume is shown in Figure 2. Over the past 20 years, posterior chamber pIOL publications have increased consistently, with a significant surge in the last four years. There were 103 publications in 2023, highlighting the rapid research development in this field.

3.2 Distribution and co-authorship of countries/regions

Figure 3 shows WoSCC search results of 791 articles identified from 62 countries. The top 10 countries involved in posterior chamber pIOL research published 739 articles, accounting for 93.4% of the published papers (Table 1). Regarding publication count, China produced the highest number of publications (235 publications, 29.7%), followed by Spain (123 publications, 15.5%) and the United States (92 publications, 11.6%). With respect to publication influence, Japanese publications received the highest number of citations (2,942 citations, 23%), followed by Spain (2,928 citations, 22.9%) and the United States (2,707 citations, 21.2%). A country/regional collaboration network, as illustrated in Figure 4, was created using the coauthor analysis method. The size of each node represents the number of articles published by the respective country, and the links between nodes represent collaborations. The strength of the link indicates the intensity of cooperation.

1 www.vosviewer.com

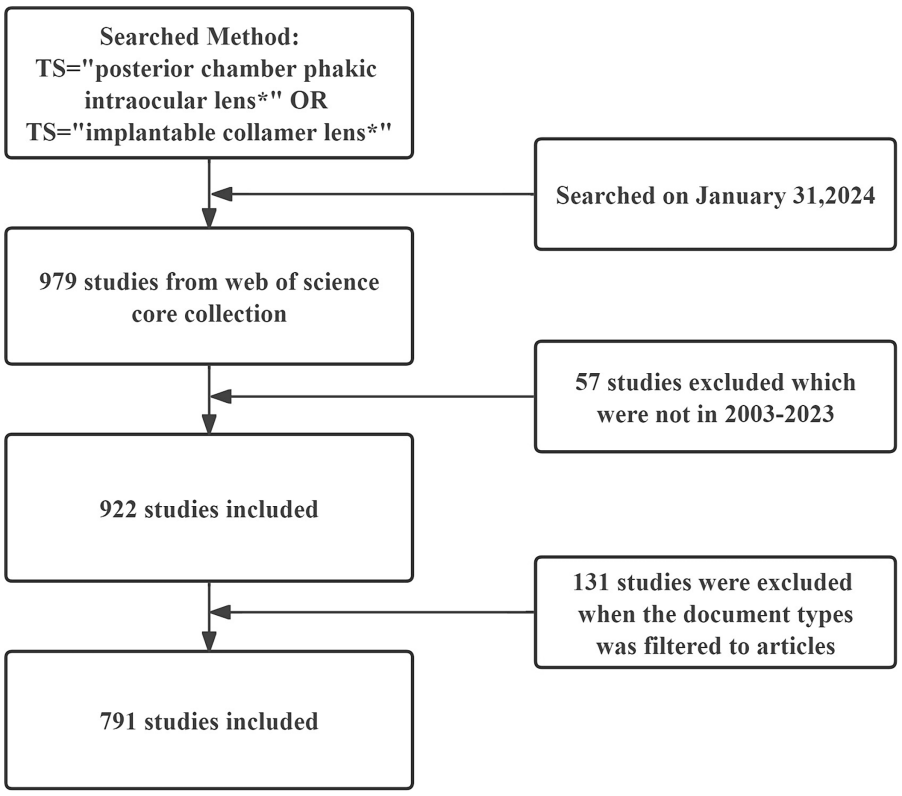

FIGURE 1
Data sources and search strategies.

3.3 Distribution and co-authorship of research organizations

The 791 articles identified using WoSCC were published across 822 institutions. The top 10 institutions involved in posterior chamber pIOL research contributed 386 articles, accounting for 48.8% of the total publications (Table 2). Regarding publication count, Fudan University had the highest number of publications (68 articles, 8.6%, China), followed by Kitasato University (52 articles, 36.6%, Japan) and the University of Valencia (44 articles, 5.6%, Spain). With respect to publication impact, Kitasato University's articles received the highest number of citations (1,657 citations, 13%, Japan), followed by the University of Valencia (1,138 citations, 8.9%, Spain) and the University of Oviedo (907 citations, 7.1%, Spain). Figure 5 shows the collaborative network of research institutions generated using coauthor analysis. The size of each node represents the number of articles published by the respective research institution, and the links between nodes indicate collaboration. The strength of these links reflects the intensity of cooperation.

3.4 Distribution and co-authorship of authors

According to the search results of WoSCC, 2,581 authors participated in posterior chamber pIOL research. Table 3 presents the top 10 authors with the highest productivity and influence in this field. Regarding productivity, Xingtao Zhou from China published the highest number of articles (61 articles), followed by Xiaoying Wang (52 articles, China) and Kamiya Kazutaka (50 articles, Japan). Regarding influence, Shimizu Kimiya from Japan has the highest number of citations (1,742 citations), followed by Kamiya Kazutaka (1,648 citations, Japan) and Igarashi Akihito (1,361 citations, Japan). Figure 6 shows the authors' collaboration network generated using the coauthor analysis. The size of each node represents the number of articles published by the respective research institutions, and the links between the nodes represent collaborations. The strength of the link indicates the intensity of cooperation.

3.5 Contribution and citation analysis of journals

The analysis of 791 articles using WoSCC revealed that they were published across 100 journals. Table 4 displays the Top 10 productive/influential journals in posterior chamber pIOL research. The top three journals in terms of productivity are 'Journal of Cataract & Refractory Surgery', 'Journal of Refractive Surgery', and 'BMC Ophthalmology', with 118, 98, and 55 articles, respectively. 'Journal of Cataract & Refractive Surgery' stands out with 2,701 citations, establishing it as the most influential journal in the field. Figure 7 illustrates the citation network of the journal through citation analysis. The size of each node corresponds to the number of articles published by the research

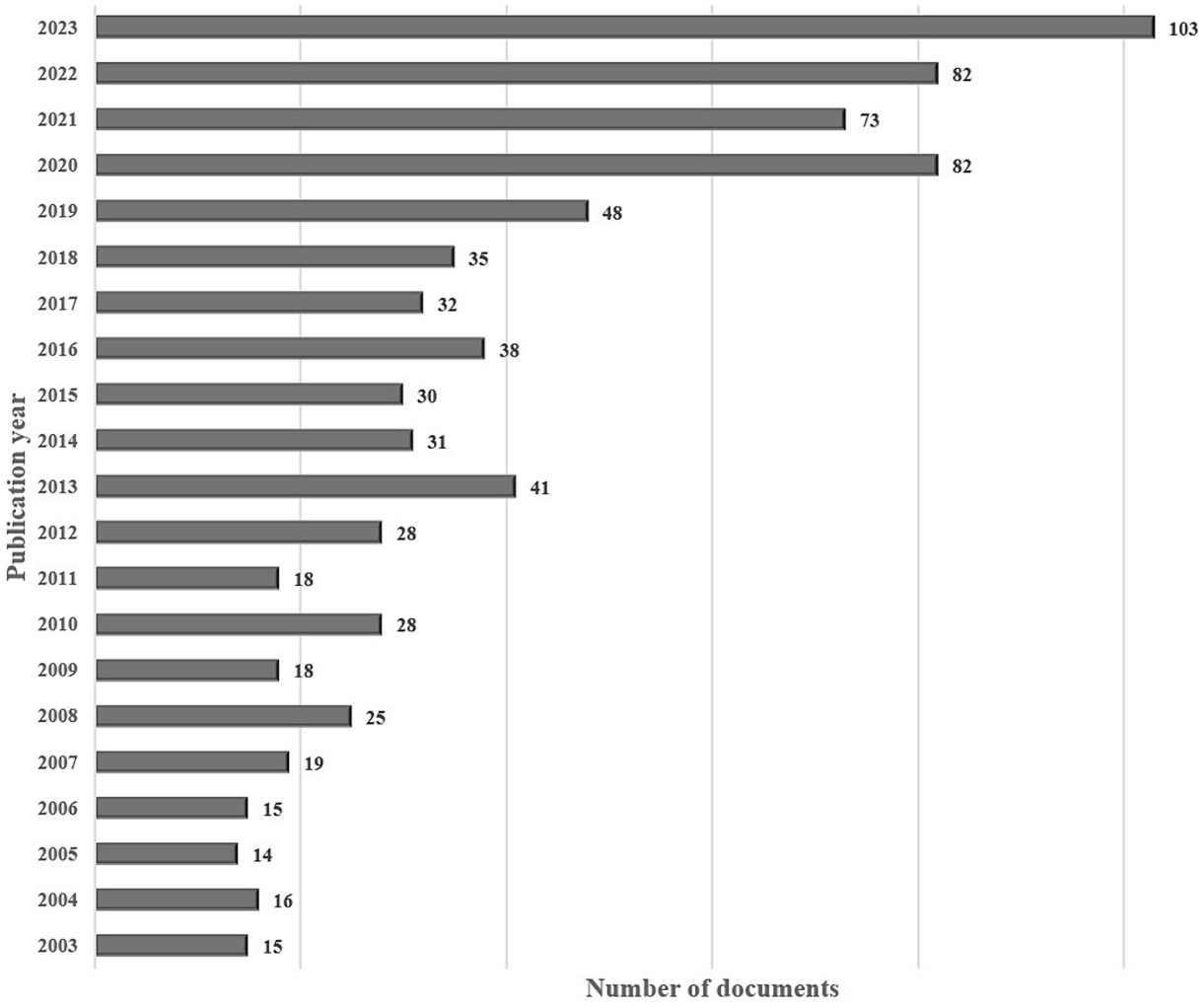

FIGURE 2
Annual number of publications in posterior chamber pIOL research between 2003 and 2023.

journals, while the links between nodes signify collaborations. The strength of the link reflects the level of cooperation.

3.6 Co-citation analysis of reference

In total, 8,119 references were cited in 791 publications. Notably, 166 documents met the threshold when the minimum number of citations for cited documents was set at 20. Table 5 lists the top 10 cited documents. The most cited reference is 'United States Food and Drug Administration clinical trial of the Implantable Collamer Lens (ICL) for moderate to high myopia: three-year follow-up' published in Ophthalmology in 2004.

3.7 Co-occurrence analysis of keywords and citation bursts

A high-frequency keyword co-occurrence analysis was conducted to identify the research topics in this field. A keyword co-occurrence network for studying posterior chamber pIOL was generated using VOSviewer. The minimum number of co-occurrences for a keyword was set at 10. Of the 1,591 extracted keywords associated with posterior chamber pIOL, 117 were grouped into four main clusters with red, green, blue, and yellow colors as indicators (Figure 8). Figure 9 shows the 25 keywords with the strongest citation bursts in this field between 2003 and 2023. After 2020, some of the popular keywords in the academic discourse were "management," "v4c," "safety," and "size."

4 Discussion

4.1 Global trends in research on posterior chamber pIOL

This study analyzed 791 original articles on posterior chamber pIOL published between 2003 and 2023. The findings indicate that there has been a consistent increase in the number of articles over the past two decades. This suggests that posterior chamber pIOLs are gaining acceptance and significant attention from the academic community. The number of publications in the past four years

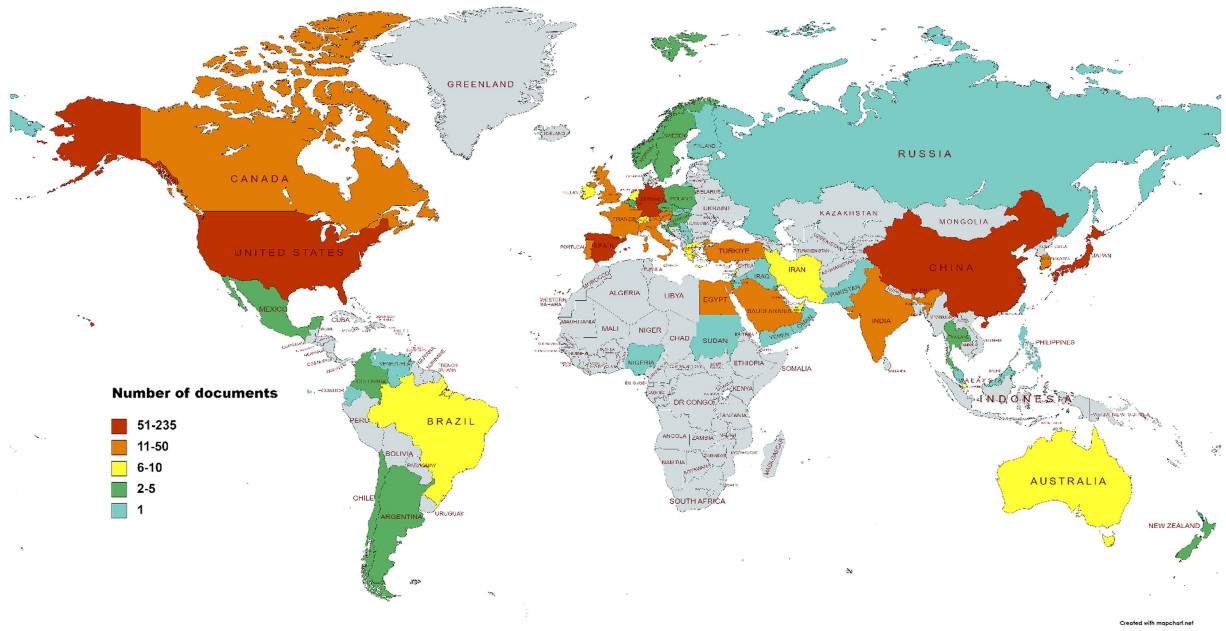

FIGURE 3
Distribution of main research countries/regions in posterior chamber pIOL research.

TABLE 1 Top 10 productive/influential countries/regions in posterior chamber pIOL research, 2003–2023.

Rank	Countries	Documents	Rank	Countries	Citations
1	China	235 (29.7%)	1	Japan	2,942 (23%)
2	Spain	123 (15.5%)	2	Spain	2,928 (22.9%)
3	USA	92 (11.6%)	3	USA	2,707 (21.2%)
4	Japan	81 (10.2%)	4	China	1,632 (12.8%)
5	Germany	60 (7.6%)	5	India	982 (7.7%)
6	South Korea	40 (5.1%)	6	France	915 (7.2%)
7	India	37 (4.7%)	7	South Korea	912 (7.1%)
8	Egypt	28 (3.5%)	8	Germany	686 (5.4%)
9	Portugal	24 (3.0%)	9	Brazil	637 (5%)
10	England	19 (2.4%)	10	Portugal	625 (4.9%)

doubled, accounting for 43% of the total documents published in the last 20 years. This increase may be attributed to the bursts of keywords such as "management," "v4c," "safety," and "size" in 2020. These findings indicate that the current research interests are centered on the perioperative management of posterior chamber pIOL and the safety and size selection of new generation v4c type ICL.

After publication location analysis, we discovered that research on this topic has been published in 62 countries and regions worldwide, indicating a global interest in posterior chamber pIOL. China, Spain, the United States, and Japan emerged as the top four contributors to productivity and influence among the 62 countries. In addition, our coauthor analysis revealed collaborations in this field across various countries, with the United States being central and exhibiting the highest total link strength. This suggests that the United States is a hub for international collaboration in posterior-chamber pIOLs.

It is possible to identify the most productive and influential organizations by examining the distribution of research institutions. Based on the findings presented in Table 2, the Kitasato University emerged as the top publisher and citation receiver, establishing itself as the most authoritative organization in this research field. The visualization diagram illustrates this further, with nodes representing the number of releases and links indicating collaboration. Figure 5 demonstrates that Fudan University (link = 9) and the Singapore National Eye Center (link = 9) have the highest number of connections, indicating strong collaborative ties with other institutions.

Building an author knowledge graph can provide valuable information to researchers seeking opportunities for collaboration. As shown in Table 3, Professor Shimizu Kimiya published 48 papers and was cited 1742 times, establishing him as a prominent figure in this research field. Figure 6 shows that the size of each node corresponds to the number of releases, and the strength of the links indicates the level of collaboration. We used coauthor analysis with the green and cyan groups to identify the four

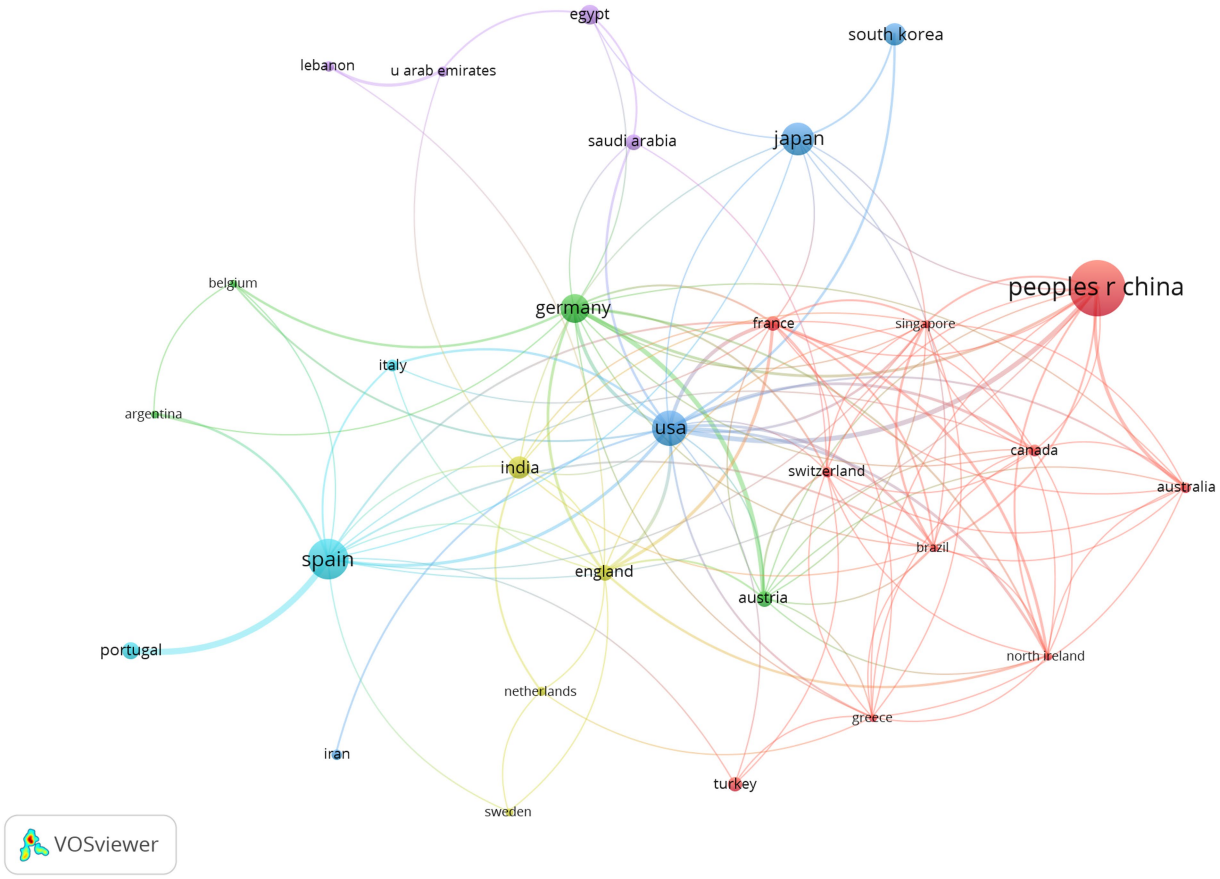

FIGURE 4
Co-authorship network of countries/regions in posterior chamber pIOL research (The minimum number of documents of a country/region was set as 5; 29 of the 62 countries involved in posterior chamber pIOL research met the threshold).

TABLE 2 Top 10 productive/influential organizations in posterior chamber pIOL research, 2003–2023.

Rank	Organization (Country)	Documents	Rank	Organization (Country)	Citations
1	Fudan University (China)	68 (8.6%)	1	Kitasato University (Japan)	1,657 (13%)
2	Kitasato University (Japan)	52 (6.6%)	2	University of Valencia (Spain)	1,138 (8.9%)
3	University of Valencia (Spain)	44 (5.6%)	3	University of Oviedo (Spain)	907 (7.1%)
4	Sanno Hospital (Japan)	29 (3.7%)	4	Sanno Hospital (Japan)	825 (6.5%)
5	University of Oviedo (Spain)	29 (3.7%)	5	Center for Clinical Research (USA)	724 (5.7%)
6	Nagoya Eye Clinic (Japan)	23 (2.9%)	6	Autonomous University of Barcelona (Spain)	688 (5.4%)
7	University of Minho (Spain)	20 (2.5%)	7	University of Arizona (USA)	629 (4.9%)
8	Zhejiang University (China)	20 (2.5%)	8	L. V. Prasad Eye Institute (India)	620 (4.9%)
9	Sun Yat-sen University (China)	19 (2.4%)	9	Singapore National Eye Centre (Singapore)	618 (4.8%)
10	Keio University (Japan)	17 (2.1%)	10	University of Minho (Spain)	617 (4.8%)

research groups that exhibited the highest global productivity in this field, indicating Prof. Xingtao Zhou (Fudan University, China) as the core.

The red group indicates Prof. Robert Montés-Micó (University of Valencia, Spain); the blue group indicates Prof. Kazutaka Kamiya (Kitasato University, Japan); and the yellow group

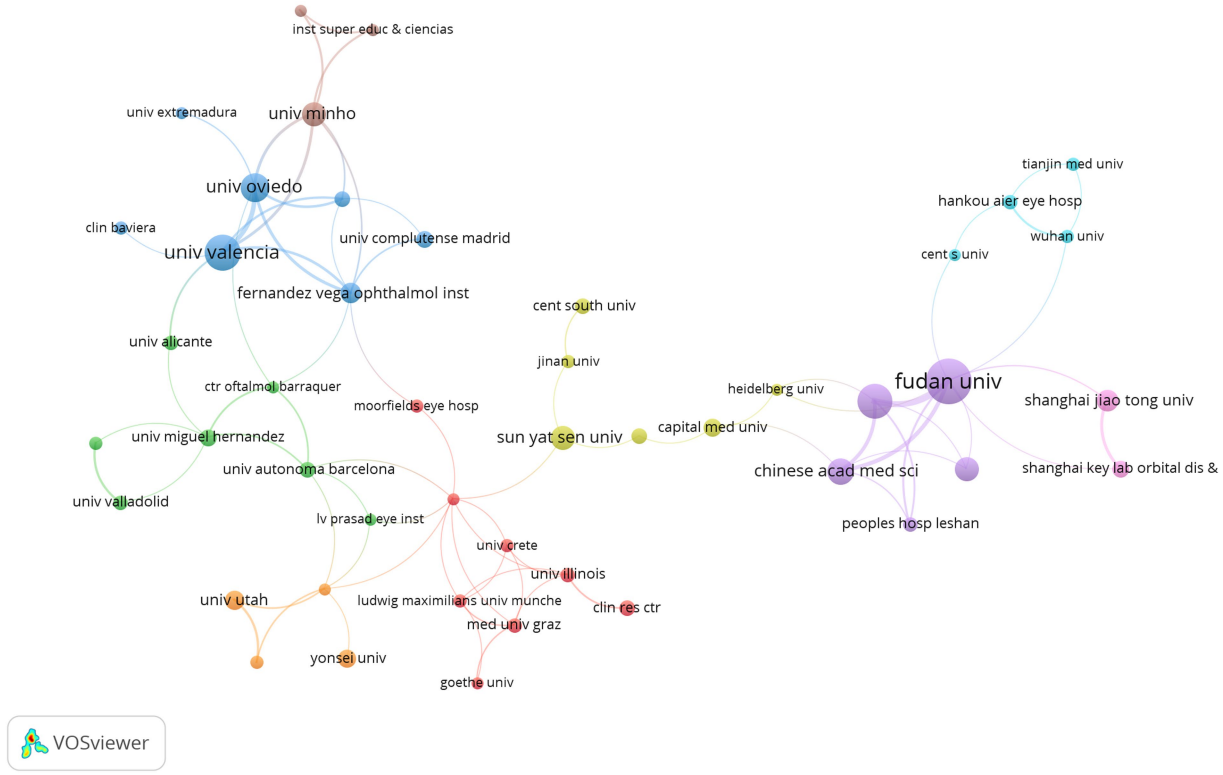

FIGURE 5
Co-authorship network institutions in posterior chamber pIOL research (The minimum number of an organization's documents was set as 5; 66 of the 822 organizations involved in posterior chamber pIOL research met the threshold).

TABLE 3 Top 10 productive/influential authors in posterior chamber pIOL research, 2003–2023.

Rank	Author(Countries)	Documents	Rank	Author(Countries)	Citations
1	Zhou XT (China)	61	1	Shimizu K (Japan)	1742
2	Wang XY (China)	52	2	Kamiya K (Japan)	1,648
3	Kamiya K (Japan)	50	3	Igarashi A (Japan)	1,361
4	Shimizu K (Japan)	48	4	Montes-Mico R (Spain)	950
5	Igarashi A (Japan)	35	5	Alfonso JF (Spain)	853
6	Montes-Mico R (Spain)	33	6	Nakamura T (Japan)	582
7	Alfonso JF (Spain)	27	7	Komatsu M (Japan)	581
8	Niu LL (China)	26	8	Zhou XT (China)	569
9	Chen X (China)	25	9	Ambrósio R (Brazil)	567
10	Nakamura T (Japan)	23	10	Belin MW (USA)	567

indicates Prof. Takashi Kojima (Keio University, Japan) as their respective cores.

4.2 Intellectual base

We comprehensively elucidated the intellectual foundation and research context surrounding posterior chamber pIOL using co-citation analysis of publication references. Table 4 shows how the three co-cited references primarily examined the safety, effectiveness, and predictability of ICL surgery in addressing moderate to high myopic refractive errors and its impact on anterior subcapsular cataracts development, which ranked first in citation frequency and total link strength, indicating their central position in the knowledge network.

4.3 Research frontiers

Keyword co-occurrence analysis is a widely employed research method in bibliometrics that helps to uncover the primary internal knowledge structure and hotspot classification of relevant documents.

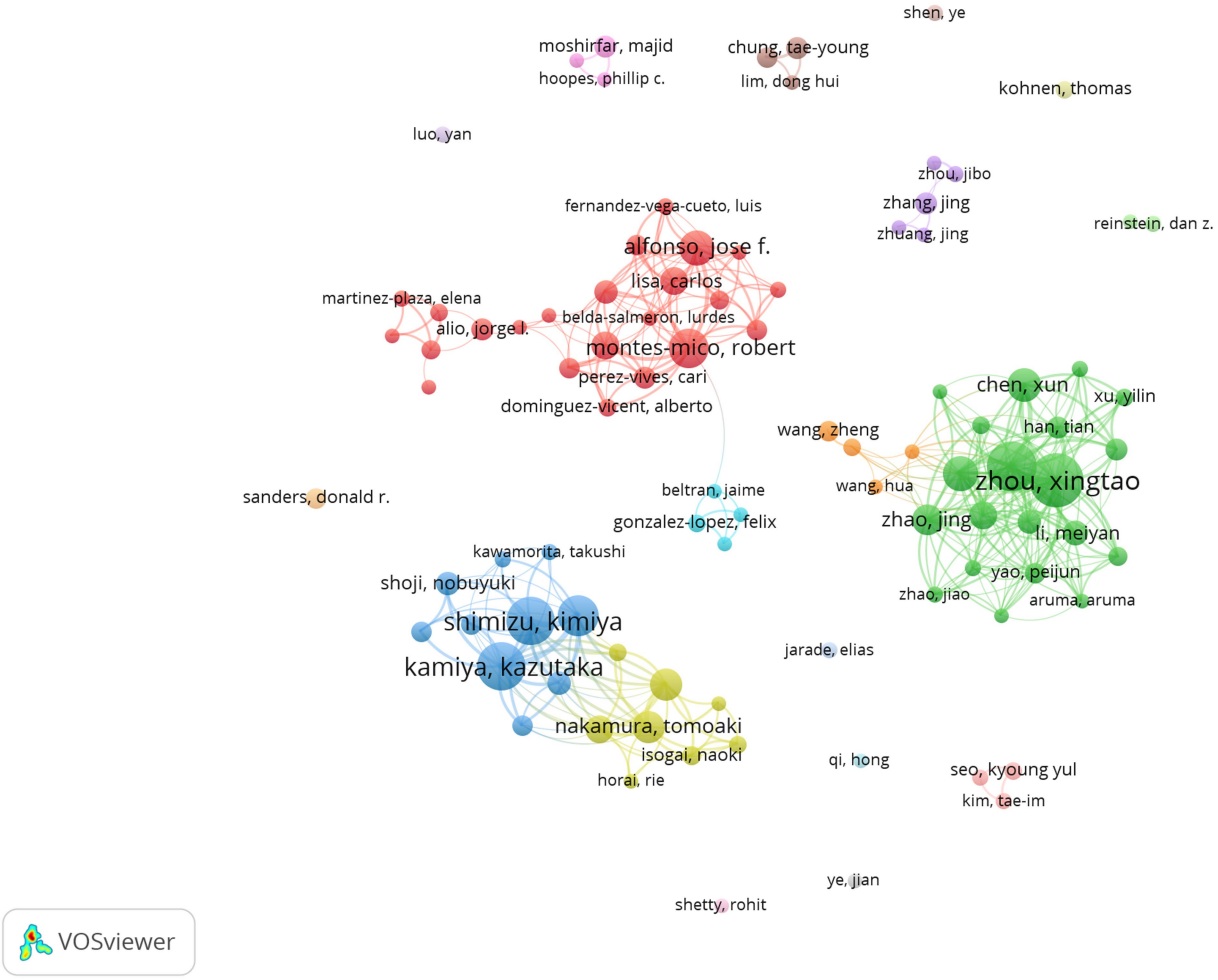

FIGURE 6
Co-authorship network of authors in posterior chamber pIOL research (The minimum number of documents of an author was set as 5; 93 of the 2,518 authors involved in posterior chamber pIOL research met the threshold).

TABLE 4 Top 10 productive/influential journals in posterior chamber pIOL research, 2003–2023.

Rank	Journal	Documents	Rank	Journal	Citations
1	Journal of Cataract & Refractive Surgery	118	1	Journal of Cataract & Refractive Surgery	2,701
2	Journal of Refractive Surgery	98	2	Journal of Refractive Surgery	1814
3	BMC Ophthalmology	55	3	Ophthalmology	1,419
4	American Journal of Ophthalmology	41	4	American Journal of Ophthalmology	1,375
5	Graefe's Archive for Clinical and Experimental Ophthalmology	28	5	Cornea	757
6	International Journal of Ophthalmology	26	6	Graefe's Archive for Clinical and Experimental Ophthalmology	478
7	International Ophthalmology	24	7	British Journal of Ophthalmology	425
8	European Journal of Ophthalmology	23	8	BMC Ophthalmology	401
9	Ophthalmology	22	9	Acta Ophthalmologica	251
10	Clinical Ophthalmology	21	10	PLOS One	218

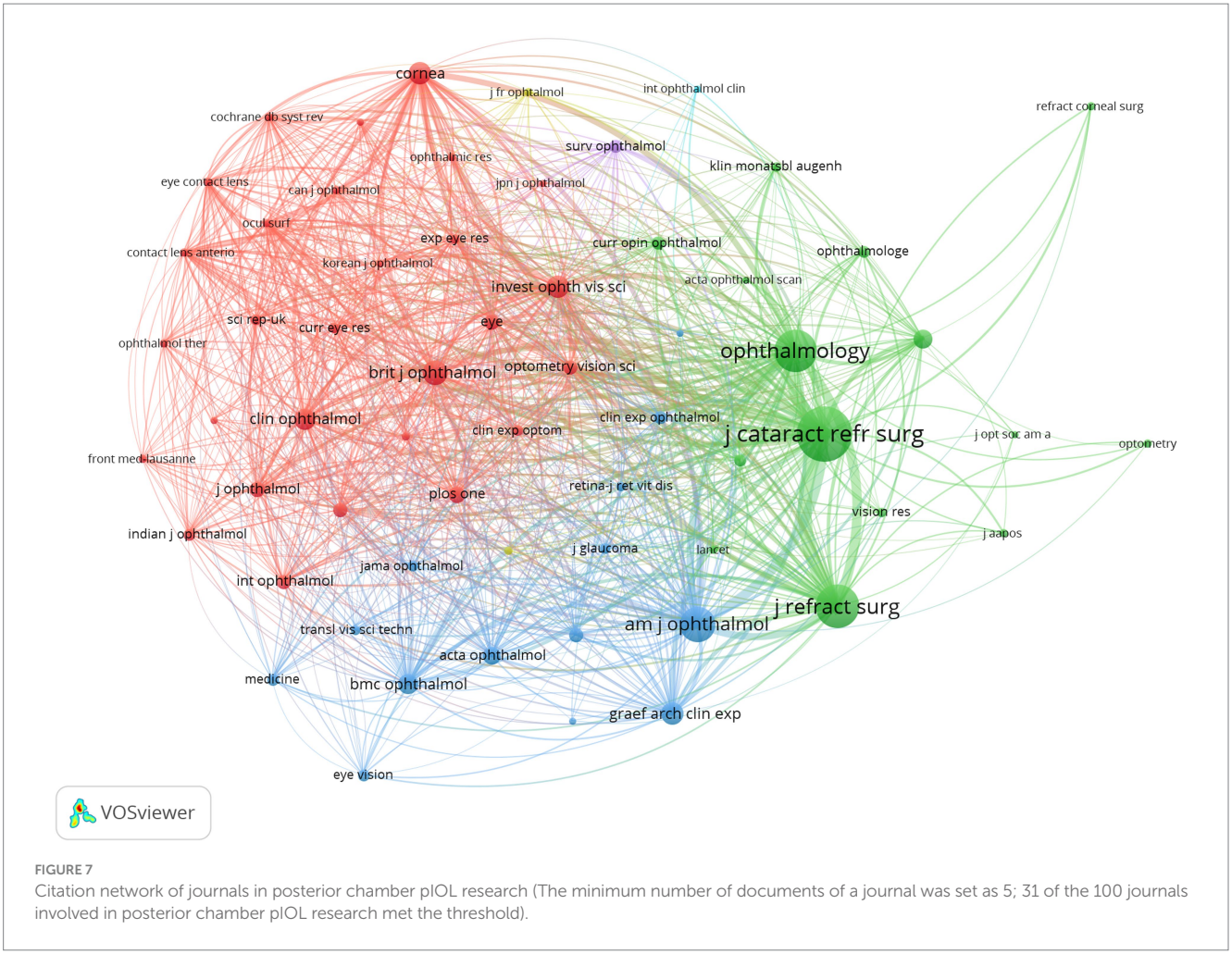

FIGURE 7
Citation network of journals in posterior chamber pIOL research (The minimum number of documents of a journal was set as 5; 31 of the 100 journals involved in posterior chamber pIOL research met the threshold).

Figure 8 illustrates that posterior chamber pIOL themes primarily form four clusters, with keywords in the same cluster sharing more similarities in research topics. Considering the characteristics and current state of posterior chamber pIOL research, we analyzed these four clusters.

Cluster#1 (red) focused on keywords associated with posterior chamber pIOL clinical outcomes for correcting myopic astigmatism. The frequently co-occurring keywords included myopia, outcomes, astigmatism, lasik, safety, central hole, keratoconus, stability, and penetrating keratoplasty. Studies have shown that ICL and toric ICL (TICL) are effective, safe, and predictable for myopia and myopic astigmatism correction (9–11). Multiple meta-analyses have demonstrated that ICL implantation can achieve comparable or superior effectiveness and safety in correcting moderate-to-high myopia compared with laser *in situ* keratomileusis (LASIK) and small incision lenticule extraction (SMILE) (5, 12–15). Notably, several clinical follow-up studies conducted over 5 years have consistently demonstrated the favorable stability of ICL and TICL (16–19). However, in super-high myopia cases with a diopter (D) < −12D, stability after ICL implantation may be slightly compromised, leading to continued myopia increase and axial growth (20, 21). Li et al. conducted a study in which ICL implantation was performed in the eyes of 60 patients with subclinical keratoconus. The findings revealed favorable postoperative efficacy, safety, and predictability, and the refractive outcomes remained stable throughout the 2-year follow-up period (22). Al-Amri et al. studied the clinical effects of TICL implantation in patients with stable keratoconus for >5 years (23). The results showed a significant improvement in the uncorrected visual acuity, changing from 20/248 preoperatively to 20/24 postoperatively. These findings suggest that TICL is a safe, effective, and stable treatment for vision enhancement. Alfonso-Bartolozzi et al. conducted a clinical observation of 15 eyes that underwent penetrating keratoplasty and received TICL for refractive error correction over 2 years (24). The results showed that 46.6 and 80% of the eyes achieved an uncorrected and corrected distance visual acuity (20/40), respectively. The safety index was 1.58, indicating TICL safety and effectiveness for residual myopia and astigmatism treatment after penetrating keratoplasty surgery. Currently, research on the use of posterior-chamber pIOL after corneal transplantation is limited. Further investigations are required to assess its predictability and safety.

Cluster #2 (green) focused on complications following posterior chamber IOL implantation. The frequently co-occurring keywords included high myopia, implantation, hyperopia, cataracts, complications, glaucoma, extraction, pupillary block, risk factors, and retinal detachment. Post-surgical cataract development is a frequent complication of posterior chamber pIOL. Cataract is primarily formed by placing the posterior chamber pIOL between the iris and lens,

TABLE 5 Top 10 cited references in posterior chamber pIOL research, 2003–2023.

Rank	Title	Citations	Year	Author
1	United States Food and Drug Administration clinical trial of the Implantable Collamer Lens (ICL) for moderate to high myopia: three-year follow-up (PMID: 15350323)	223	2004	Sanders DR
2	US food and drug administration clinical trial of the implantable contact lens for moderate to high myopia (PMID:12578765)	151	2003	Vukich JA
3	Implantable contact lens for moderate to high myopia: relationship of vaulting to cataract formation (PMID:12781276)	134	2003	Gonvers M
4	Implantable collamer posterior chamber intraocular lenses: a review of potential complications (PMID: 21710954)	121	2011	Fernandes P
5	Eight-year follow-up of posterior chamber phakic intraocular lens implantation for moderate to high myopia (PMID: 24239774)	119	2014	Igarashi A
6	Meta-analysis and review: effectiveness, safety, and central port design of the intraocular collamer lens (PMID: 27354760)	118	2016	Packer M
7	Safety of posterior chamber phakic intraocular lenses for the correction of high myopia: anterior segment changes after posterior chamber phakic intraocular lens implantation (PMID: 11150270)	106	2001	Jiménez-Alfaro I
8	Toric Implantable Collamer Lens for moderate to high myopic astigmatism (PMID: 17198849)	101	2007	Sanders DR
9	Posterior chamber collagen copolymer phakic intraocular lenses to correct myopia: five-year follow-up (PMID: 21511154)	95	2011	Alfonso JF
10	Four-year follow-up of posterior chamber phakic intraocular lens implantation for moderate to high myopia (PMID: 19597102)	94	2009	Kamiya K

disrupting the circulation of aqueous humor around the lens. According to Vargas et al., cataract formation was the primary reason for bilensectomy following posterior chamber pIOL implantation, accounting for 93.1% of cases (25). Similarly, Hayakawa et al. discovered that the most prevalent cause of posterior chamber pIOL extraction is the progression of cataract formation, which accounted for 63% of cases (26). Meta-analyses show that cataract occurrence after ICL implantation was 1.1–5.9% before central-hole ICLs were introduced (27). Old age (> 40 years), high myopia (< −12.0D), and low vault (< 230 μm) are risk factors for cataract progression (27). In long-term follow-up studies of patients with central-hole ICLs over 5 years, the incidence of anterior subcapsular cataracts was 0.53%, whereas that of nuclear cataracts was 0.08% (28). Notably, nuclear cataract occurrence is associated with age and not influenced by ICL implantation (18). A 0.36-mm central hole facilitates the normal flow of aqueous humor, essential for maintaining proper fluid dynamics in the eye. This also enhances aqueous humor circulation around the lens, reducing anterior subcapsular cataracts (29).

Ocular hypertension is a common complication. Senthil et al. studied 638 eyes of 359 patients who underwent V4b and V4c model ICL implantation for 8 months. They found that 4.85% of patients developed intraocular pressure (IOP), whereas 0.3% developed glaucoma (30). The most common cause of increased IOP was steroid use, followed by viscoelastic agent residue and pupillary block (30). Another study by Naripthaphan et al. found no statistical difference in postoperative IOP between traditional ICL with peripheral iridotomy and central-hole ICL without a preoperative prophylactic incision (31). Qian et al. discovered that, in patients with shallow anterior chambers who underwent V4c model ICL implantation, a high vault may lead to narrowing of the anterior chamber, resulting in a long-term IOP increase. Therefore, in eyes with shallow anterior chambers, a narrower safe vault range is recommended (32).

Posterior chamber pIOL and other forms of inner eye surgery may pose a potential risk for vitreoretinal complications and retinal detachment (33). In their retrospective cohort study, Arrevola-Velasco et al. demonstrated that retinal detachment prevalence in patients who underwent ICL implantation over 10 years was 1.71% (34). The study found no evidence of increased retinal detachment risk in these patients compared with similar patients who did not undergo surgery (34). Myopia is a significant risk factor for rhegmatogenous retinal detachment, and its incidence increases with myopia severity (35). A strict fundus examination should be conducted before and after posterior chamber IOL implantation. In addition, preventive retinal laser photocoagulation can effectively mitigate the risk of retinal detachment if deemed necessary.

Cluster#3 (blue) focused on keywords associated with ICL size selection and postoperative vault predictions. Frequently co-occurring keywords included vault, ultrasound biomicroscopy (UBM), optical coherence tomography (OCT), angle, white-to-white, anterior segment, ciliary sulcus diameter, biometry, 3-year follow-up, v4c, size, pentacam, and anterior chamber depth. Currently, v4c ICL is the most widely used posterior chamber pIOL. The lens is available in four sizes, with lengths of 12.1 mm, 12.6 mm, 13.2 mm, and 13.7 mm (36). The postoperative vault, which is the distance between the posterior surface of the pIOL and the anterior surface of the crystalline lens, influences the risk of postoperative complications. Current methods for measuring vault height include UBM, anterior segment OCT, and Scheimpflug tomography (Pentacam). Studies have demonstrated that the vault height measurement value obtained from anterior segment OCT is higher than that obtained from UBM and Pentacam, with Pentacam showing the lowest measurement value (37). According to research, the ICL optimal vault typically falls within 250–750 μm (38–40). If the vault is >750 μm, it can result in the ICL pushing the iris forward, leading to changes in the angle shape, pupillary block,

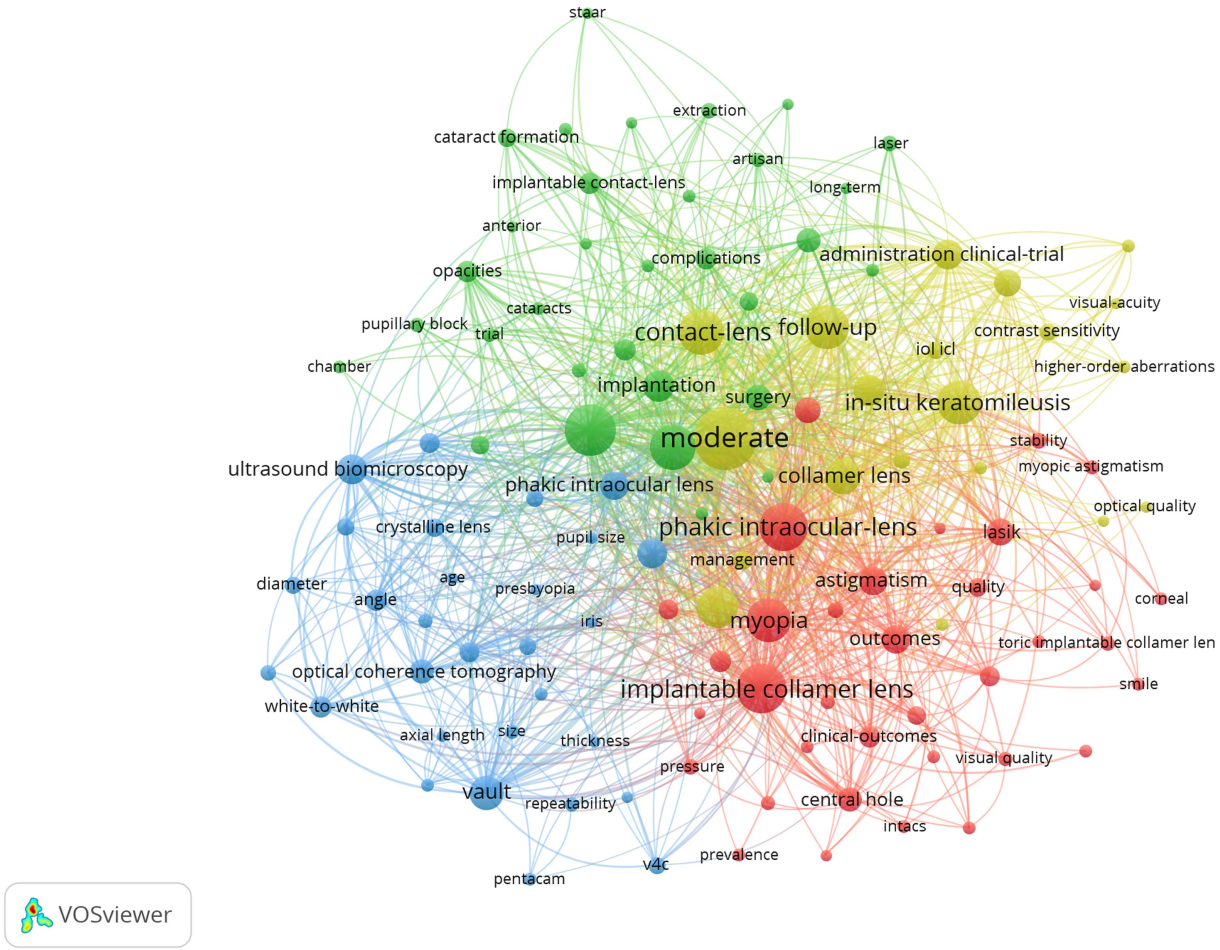

FIGURE 8
Co-occurrence network of keywords in posterior chamber pIOL research (The minimum number of occurrences of a keyword was set as 10; 117 of the 1,591 keywords involved in posterior chamber pIOL research met the threshold).

and an elevated risk of pigment dispersion glaucoma. Conversely, if the vault is too low (< 250 μm), cataract formation is more likely. ICL size selection is crucial in vault determination; therefore, optimizing the choice of ICL length is essential in reducing postoperative complications (41). According to the manufacturer's recommended nomogram, ICL size selection has traditionally been based on anterior chamber depth and white-to-white diameter measurements (17). A meta-study conducted on 2,263 eyes across 24 studies revealed that considering a normal distribution of vaults, approximately 16% of eyes had vaults ranging from 0–250 μm, whereas 0.4% had vaults >1,000 μm (42). The inadequate vault can be partly attributed to the weak correlation between the white-to-white and ciliary sulcus diameters where the ICL was placed (43). Ciliary sulcus diameter measurement using UBM is a contact examination that requires the examiner to possess specific experience and is susceptible to subjective interference. This limits its widespread use in ICL size selection. A meta-analysis indicated that ICL-sizing methods based on sulcus-to-sulcus and white-to-white measurements do not yield clinically meaningful or statistically significant differences in the vault (42). Anterior segment OCT is a reliable and non-invasive method for obtaining anterior segment parameters. Research has shown that ICL size selection using anterior segment OCT multiple regression models or machine learning yields comparable or even superior outcomes compared with traditional nomograms (44–46). A crystalline lens rise was identified as an additional independent factor contributing to postoperative vault differences. It can be used for preoperative ICL-sizing calculations (47).

Cluster#4 (yellow) focused on keywords associated with postoperative visual quality following the posterior chamber pIOL implantation for myopia and astigmatism of varying diopters correction. The frequently co-occurring keywords included moderate *in situ* keratomileusis, follow-up, refractive surgery, administration clinical trials, photorefractive keratectomy, management, contrast sensitivity, higher-order aberrations, and spherical aberration. Compared with spectacle correction, ICL implantation has decreased intraocular scattering and enhanced optical quality in individuals with high myopia (48, 49). A study conducted on 42 patients who underwent ICL implantation for 1 year revealed a significant improvement in contrast sensitivity at 6, 12, and 18 cycles per degree after the procedure (50). Similarly, Bai et al. utilized the binoptometer 4P to measure contrast sensitivity and observed a significant enhancement compared with preoperative measurements (51). Shin et al. discovered that ICL implantation resulted in lower levels of ocular and corneal higher-order aberrations (HOA) in patients with highly myopic eyes than in those with wavefront-guided laser epithelial keratomileusis (52). Notably,

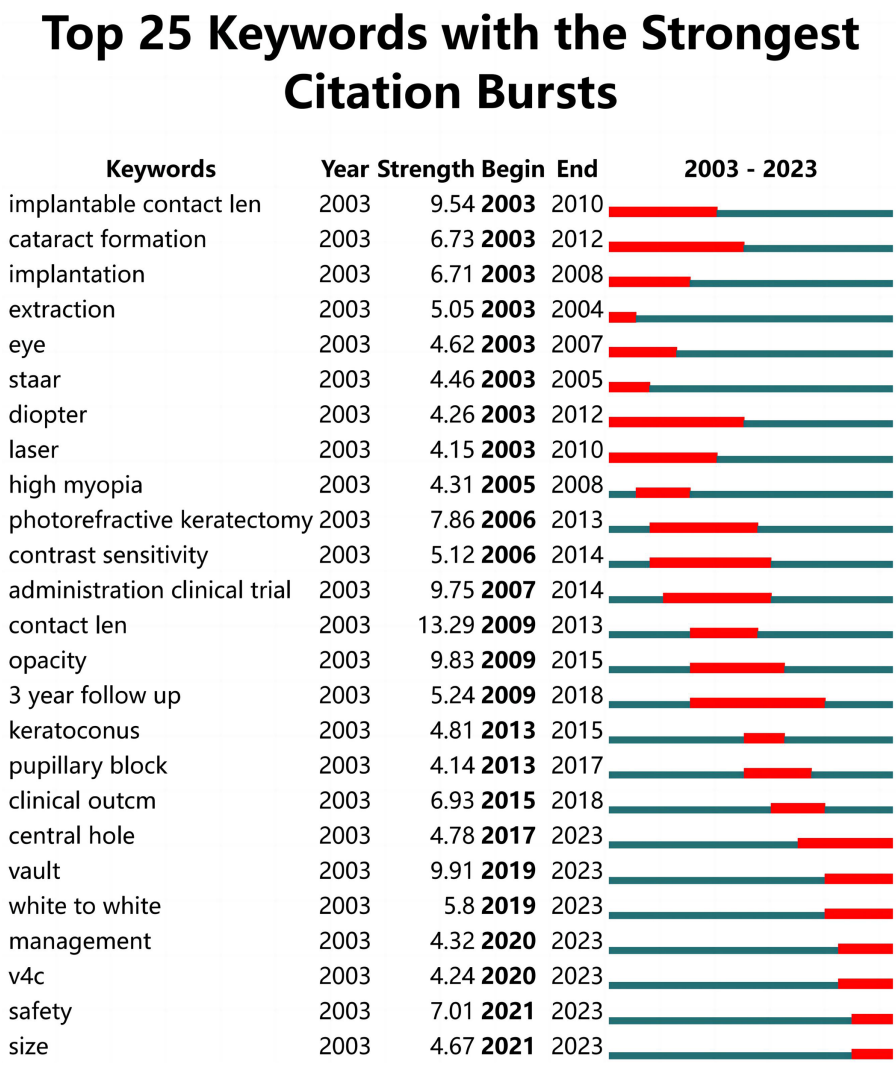

FIGURE 9
Top 25 keywords with the strongest citation bursts in posterior chamber pIOL research.

multiple systematic reviews and meta-analyses have consistently demonstrated that high myopia ICL treatment yields a lower HOA than LASIK and SMILE (4, 5, 14). According to a study conducted by Tian et al., V4 ICL and central hole V4c ICL had comparable post-implantation visual qualities. However, V4c ICL resulted in higher levels of high-order and spherical aberrations (53). According to previous reports, some individuals experience visual interference known as "ring-shaped dysphotopsia" after ICL implantation. This phenomenon is associated with the refraction of stray light between the inner wall of the hole and the ICL posterior surface (54). However, it has been observed that patients can adapt to this interference within 6 months postoperatively (55).

4.4 Limitations

This study has some limitations. First, the analysis was based on publications between 2003 and 2023, which may not encompass all relevant topics in pIOL research. Second, the quality of published articles was not considered, and articles with varying research qualities were assigned equal weights. Finally, this study relied solely on data from the WoSCC database, potentially resulting in incomplete coverage of publications. Future studies should consider combining data from multiple databases to ensure a more comprehensive assessment.

5 Conclusion

This study presents the first bibliometric analysis of research trends in posterior chamber pIOL over the past two decades. We investigated the current state and emerging trends in global collaboration and research focal points in this field by visually analyzing pIOL-related research to offer researchers fresh insights and guidance.

Author contributions

JN: Conceptualization, Methodology, Writing – original draft, Writing – review & editing. QZ: Conceptualization, Methodology, Writing – original draft, Writing – review & editing. WL: Data curation, Writing – original draft, Writing – review & editing. RZ: Visualization, Writing – original draft, Writing – review & editing. ZX: Software, Writing – original draft, Writing – review & editing. LJ: Validation, Writing – original draft, Writing – original draft. LZ: Writing – original draft, Writing – review & editing, Conceptualization.

Funding

The author(s) declare that financial support was received for the research, authorship, and/or publication of this article. This study was supported by National Natural Science Foundation of China (No. 82171032), Liaoning Provincial Applied basic research project (No. 2022JH2/101300036), Liaoning Provincial Natural Science Foundation of China (Nos. 201800209 and 2020-MS-339), Youth Science and Technology Star Project of Dalian (No. 2021RQO33), Health Commission Foundation of Dalian (No. 2111008), and Dalian Science and Technology Innovation Fund project (No. 2023JJ12034).

Conflict of interest

The authors declare that the research was conducted in the absence of any commercial or financial relationships that could be construed as a potential conflict of interest.

Publisher's note

References

1. Holden BA, Fricke TR, Wilson DA, Jong M, Naidoo KS, Sankaridurg P, et al. Global prevalence of myopia, high myopia and temporal trends from 2000 through 2050. *Ophthalmology*. (2016) 123:1036–42. doi: 10.1016/j.ophtha.2016.01.006

2. Sugar A, Hood CT, Mian SI. Patient-reported outcomes following LASIK quality of life in the PROWL studies. *JAMA*. (2017) 317:204–5. doi: 10.1001/jama.2016.19323

3. Jonker SMR, Berendschot TTJM, Saelens IEY, Bauer NJC, Nuijts RMMA. Phakic intraocular lenses: an overview. *Indian J Ophthalmol*. (2020) 68:2779–96. doi: 10.4103/ijo.IJO_2995_20

4. Chen D, Zhao X, Chou Y, Luo Y. Comparison of visual outcomes and optical quality of femtosecond laser–assisted SMILE and visian implantable collamer lens (ICL V4c) implantation for moderate to high myopia: a meta-analysis. *J Refract Surg*. (2022) 38:332–8. doi: 10.3928/1081597X-20220411-01

5. Cao K, Zhang J, Wang J, Yusufu M, Jin S, Chen S, et al. Implantable collamer lens versus small incision lenticule extraction for high myopia correction: a systematic review and meta-analysis. *BMC Ophthalmol*. (2021) 21:450. doi: 10.1186/s12886-021-02206-9

6. Pritchard A. Statistical bibliography or bibliometrics? *J Doc*. (1969) 25:348–9.

7. Van Raan AFJ. Sleeping beauties in science. *Scientometrics*. (2004) 59:467–72. doi: 10.1023/B:SCIE.0000018543.82441.f1

8. Van Eck NJ, Waltman L. Software survey: VOSviewer, a computer program for bibliometric mapping. *Scientometrics*. (2010) 84:523–38. doi: 10.1007/s11192-009-0146-3

9. Wei R, Li M, Niu L, Aruma A, Miao H, Shen Y, et al. Comparison of visual outcomes after non-toric and toric implantable collamer lens V4c for myopia and astigmatism. *Acta Ophthalmol*. (2021) 99:511–8. doi: 10.1111/aos.14652

10. Du J, Zhou W, Zhao T, Qian T, Lu Y, Li H, et al. Efficacy and safety of implantable collamer lens V4c implantation in 1, 834 myopic eyes for 1 year of follow-up. *J Refract Surg*. (2023) 39:694–704. doi: 10.3928/1081597X-20230908-02

11. Albo C, Nasser T, Szynkarski DT, Nguyen N, Mueller B, Libfraind L, et al. A comprehensive retrospective analysis of EVO/EVO+ implantable collamer lens: evaluating refractive outcomes in the largest single center study of ICL patients in the United States. *Clin Ophthalmol*. (2024) 18:69–78. doi: 10.2147/OPTH.S440578

12. Li HY, Ye Z, Li ZH. Postoperative efficacy, safety, predictability, and visual quality of implantable collamer lens implantation versus small incision lenticule extraction in myopic eyes: a metaanalysis. *Int J Ophthalmol*. (2023) 16:442–52. doi: 10.18240/ijo.2023.03.16

13. Di Y, Cui G, Li Y, Luo Y. A meta-analysis of visual outcomes and optical quality after small incision lenticule extraction versus implantable collamer lens for myopia. *Eur J Ophthalmol*. (2023) 33:136–44. doi: 10.1177/11206721221097249

14. Goes S, Delbeke H. Posterior chamber toric implantable collamer lenses vs LASIK for myopia and astigmatism: systematic review. *J Cataract Refract Surg*. (2022) 48:1204–10. doi: 10.1097/j.jcrs.0000000000001007

15. Chen H, Liu Y, Niu G, Ma J. Excimer laser versus phakic intraocular lenses for myopia and astigmatism: a meta-analysis of randomized controlled trials. *Eye Contact Lens*. (2018) 44:137–43. doi: 10.1097/ICL.0000000000000327

16. Chen X, Wang X, Xu Y, Cheng M, Han T, Wang X, et al. Long-term comparison of vault and complications of implantable collamer lens with and without a central hole for high myopia correction: 5 years. *Curr Eye Res*. (2022) 47:540–6. doi: 10.1080/02713683.2021.2012202

17. Kamiya K, Shimizu K, Takahashi M, Ando W, Hayakawa H, Shoji N. Eight-year outcomes of implantation of posterior chamber phakic intraocular lens with a central port for moderate to high ametropia. *Front Med*. (2021) 8:799078. doi: 10.3389/fmed.2021.799078

18. Papa-Vettorazzi MR, Güell JL, Cruz-Rodriguez JB, Moura-Coelho N, Elies D. Long-term efficacy and safety profiles after posterior chamber phakic intraocular lens implantation in eyes with more than 10 years of follow-up. *J Cataract Refract Surg*. (2022) 48:813–8. doi: 10.1097/j.jcrs.0000000000000848

19. Lwowski C, Van Keer K, Ruscher T, Van Keer L, Shajari M, Kohnen T. Five-year follow-up of a posterior chamber phakic intraocular lens with a central hole for correction of myopia. *Int Ophthalmol*. (2023) 43:4933–43. doi: 10.1007/s10792-023-02896-8

20. Chen X, Wang X, Xu Y, Cheng M, Han T, Niu LL, et al. Five-year outcomes of EVO implantable collamer lens implantation for the correction of high myopia and super high myopia. *Eye Vis*. (2021) 8:40. doi: 10.1186/s40662-021-00264-0

21. Chen X, Chen Z, Miao H, Wang X, Wang X, Zhou X. One-year analysis of the refractive stability, axial elongation and related factors in a high myopia population after implantable Collamer Lens implantation. *Int Ophthalmol*. (2022) 42:3295–302. doi: 10.1007/s10792-022-02328-z

22. Li K, Wang Z, Zhang D, Wang S, Song X, Li Y, et al. Visual outcomes and corneal biomechanics after V4c implantable collamer lens implantation in subclinical keratoconus. *J Cataract Refract Surg*. (2020) 46:1339–45. doi: 10.1097/j.jcrs.0000000000000262

23. Al-Amri AM, Al Jabbar IS, Bedywi RM, Alhadi WA, Alhashim NS, Fihrah RS, et al. Long-term outcomes and safety of the phakic visian toric implantable collamer lens in eyes with non-progressive keratoconus. *Bahrain Medical Bulletin*. (2023) 45:1432–5.

24. Alfonso JF, Lisa C, Abdelhamid A, Montés-Micó R, Poo-López A, Ferrer-Blasco T. Posterior chamber phakic intraocular lenses after penetrating keratoplasty. *J Cataract Refract Surg*. (2009) 35:1166–73. doi: 10.1016/j.jcrs.2009.02.027

25. Vargas V, Alió JL, Barraquer RI, D' Antin JC, García C, Duch F, et al. Safety and visual outcomes following posterior chamber phakic intraocular lens bilensectomy. *Eye Vis*. (2020) 7:34. doi: 10.1186/s40662-020-00200-8

26. Hayakawa H, Kamiya K, Ando W, Takahashi M, Shoji N. Etiology and outcomes of current posterior chamber phakic intraocular lens extraction. *Sci Rep*. (2020) 10:21686. doi: 10.1038/s41598-020-78661-z

27. Igarashi A, Kamiya K, Ichikawa K, Kitazawa Y, Kojima T, Nakamura T, et al. Multicenter clinical outcomes of hole implantable collamer lens implantation in middle-aged patients. *Sci Rep*. (2022) 12:4236. doi: 10.1038/s41598-022-08298-7

28. Wannapanich T, Kasetsuwan N, Reinprayoon U. Intraocular implantable collamer lens with a central hole implantation: safety, efficacy, and patient outcomes. *Clin Ophthalmol*. (2023) 17:969–80. doi: 10.2147/OPTH.S379856

29. Packer M. The implantable collamer lens with a central port: review of the literature. *Clin Ophthalmol*. (2018) 12:2427–38. doi: 10.2147/OPTH.S188785

30. Senthil S, Choudhari NS, Vaddavalli PK, Murthy S, Reddy J, Garudadri CS. Etiology and management of raised intraocular pressure following posterior chamber phakic intraocular lens implantation in myopic eyes. *PLoS One*. (2016) 11:e0165469. doi: 10.1371/journal.pone.0165469

31. Naripthaphan P, Pachimkul P, Chantra S. Efficacy and safety of hole implantable collamer lens in comparison with original implantable collamer lens in patients with moderate to high myopia. *J Med Assoc Thail*. (2017) 100:S48–55.

32. Qian T, Du J, Ren R, Zhou H, Li H, Zhang Z, et al. Vault-correlated efficacy and safety of implantable collamer lens v4c implantation for myopia in patients with shallow anterior chamber depth. *Ophthalmic Res*. (2023) 66:445–56. doi: 10.1159/000528616

33. Kohnen T, Kook D, Morral M, Güell JL. Phakic intraocular lenses: part 2: results and complications. *J Cataract Refract Surg*. (2010) 36:2168–94. doi: 10.1016/j.jcrs.2010.10.007

34. Arrevola-Velasco L, Beltrán J, Rumbo A, Nieto R, Druchkiv V, Martínez De La Casa JM, et al. Ten-year prevalence of rhegmatogenous retinal detachment in myopic eyes after posterior chamber phakic implantable collamer lens. *J Cataract Refract Surg*. (2023) 49:272–7. doi: 10.1097/j.jcrs.0000000000001099

35. Burton TC. The influence of refractive error and lattice degeneration on the incidence of retinal detachment. *Trans Am Ophthalmol Soc*. (1989) 87:143–55.

36. Lee H, Kang DSY, Ha BJ, Choi M, Kim EK, Seo KY, et al. Effect of accommodation on vaulting and movement of posterior chamber phakic lenses in eyes with implantable collamer lenses. *Am J Ophthalmol*. (2015) 160:710–6.e1. doi: 10.1016/j.ajo.2015.07.014

37. Yang Y, Wan T, Yin H, Yang Y, Wu F, Wu Z. Comparative study of anterior segment measurements using 3 different instruments in myopic patients after ICL implantation. *BMC Ophthalmol*. (2019) 19:182. doi: 10.1186/s12886-019-1194-y

38. Fernandes P, González-Méijome JM, Madrid-Costa D, Ferrer-Blasco T, Jorge J, Montés-Micó R. Implantable collamer posterior chamber intraocular lenses: a review of potential complications. *J Refract Surg*. (2011) 27:765–76. doi: 10.3928/1081597X-20110617-01

39. Alfonso JF, Fernández-Vega L, Lisa C, Fernandes P, González-Meijome J, Montés-Micó R. Long-term evaluation of the central vault after phakic Collamer® lens (ICL) implantation using OCT. *Graefes Arch Clin Exp Ophthalmol*. (2012) 250:1807–12. doi: 10.1007/s00417-012-1957-0

40. Kato S, Shimizu K, Igarashi A. Assessment of low-vault cases with an implantable collamer lens. *PLoS One*. (2020) 15:e0241814. doi: 10.1371/journal.pone.0241814

41. Kang EM, Ryu IH, Lee G, Kim JK, Lee IS, Jeon GH, et al. Development of a web-based ensemble machine learning application to select the optimal size of posterior chamber phakic intraocular lens. *Transl Vis Sci Technol*. (2021) 10:5. doi: 10.1167/tvst.10.6.5

42. Packer M. Meta-analysis and review: effectiveness, safety, and central port design of the intraocular collamer lens. *Clin Ophthalmol*. (2016) 10:1059–77. doi: 10.2147/OPTH.S111620

43. Reinstein DZ, Lovisolo CF, Archer TJ, Gobbe M. Comparison of postoperative vault height predictability using white-to-white or sulcus diameter-based sizing for the visian implantable collamer lens. *J Refract Surg*. (2013) 29:30–5. doi: 10.3928/1081597X-20121210-02

44. Di Y, Li Y, Luo Y. Prediction of implantable collamer lens vault based on preoperative biometric factors and lens parameters. *J Refract Surg*. (2023) 39:332–9. doi: 10.3928/1081597X-20230207-03

45. Kamiya K, Ryu IH, Yoo TK, Kim JS, Lee IS, Kim JK, et al. Prediction of phakic intraocular lens vault using machine learning of anterior segment optical coherence tomography metrics. *Am J Ophthalmol*. (2021) 226:90–9. doi: 10.1016/j.ajo.2021.02.006

46. Igarashi A, Shimizu K, Kato S. Assessment of the vault after implantable collamer lens implantation using the KS formula. *J Refract Surg*. (2021) 37:636–41. doi: 10.3928/1081597X-20210610-06

47. Gonzalez-Lopez F, Bilbao-Calabuig R, Mompean B, Luezas J, Ortega-Usobiaga J, Druchkiv V. Determining the potential role of crystalline lens rise in vaulting in posterior chamber phakic collamer lens surgery for correction of myopia. *J Refract Surg*. (2019) 35:177–83. doi: 10.3928/1081597X-20190204-01

48. He T, Zhu Y, Zhou J. Optical quality after posterior chamber phakic implantation of an intraocular lens with a central hole (V4c implantable collamer lens) under different lighting conditions. *BMC Ophthalmol*. (2020) 20:82. doi: 10.1186/s12886-020-01340-0

49. Yu Z, Li J, Song H. Short-time evaluation on intraocular scattering after implantable collamer lens implantation for correcting high myopia. *BMC Ophthalmol*. (2020) 20:235. doi: 10.1186/s12886-020-01482-1

50. Reinstein DZ, Vida RS, Archer TJ. Visual outcomes, footplate position and vault achieved with the visian implantable collamer lens for myopic astigmatism. *Clin Ophthalmol*. (2021) 15:4485–97. doi: 10.2147/OPTH.S330879

51. Meng D, Chang R, Zhu R. Analysis of nosocomial infection and risk factors in lung transplant patients: a case-control study. *Ann Transl Med*. (2022) 10:804. doi: 10.21037/atm-22-3023

52. Shin JY, Ahn H, Seo KY, Kim EK, Kim TI. Comparison of higher order aberrations after implantable collamer lens implantation and wavefront-guided LASEK in high myopia. *J Refract Surg*. (2012) 28:106–11. doi: 10.3928/1081597X-20111018-02

53. Tian Y, Jiang HB, Jiang J, Wen D, Xia XB, Song WT, et al. Comparison of implantable collamer lens visian ICL V4 and ICL V4c for high myopia: a cohort study. *Medicine (Baltimore)*. (2017) 96:e7294. doi: 10.1097/MD.0000000000007294

54. Eom Y, Kim DW, Ryu D, Kim JH, Yang SK, Song JS, et al. Ring-shaped dysphotopsia associated with posterior chamber phakic implantable collamer lenses with a central hole. *Acta Ophthalmol*. (2017) 95:e170–8. doi: 10.1111/aos.13248

55. Martínez-Plaza E, López-Miguel A, López-de la Rosa A, McAlinden C, Fernández I, Maldonado MJ. Effect of the EVO+ visian phakic implantable collamer lens on visual performance and quality of vision and life. *Am J Ophthalmol*. (2021) 226:117–25. doi: 10.1016/j.ajo.2021.02.005

frontiers | Frontiers in Medicine

TYPE Original Research
PUBLISHED 15 April 2024
DOI 10.3389/fmed.2024.1389201

OPEN ACCESS

EDITED BY
Georgios D. Panos,
Nottingham University Hospitals NHS Trust, United Kingdom

REVIEWED BY
Donny W. Suh,
University of California, Irvine, United States
Tao Shen,
Sun Yat-sen University, China
Emmanuel Bui Quoc,
Assistance Publique Hopitaux De Paris, France

*CORRESPONDENCE
Weidong Zheng
✉ wdzheng@fjmu.edu.cn

RECEIVED 21 February 2024
ACCEPTED 04 April 2024
PUBLISHED 15 April 2024

CITATION
Wang H and Zheng W (2024) Effect of the prism and Maddox rod test as the surgical target for type III acute acquired comitant esotropia.
Front. Med. 11:1389201.
doi: 10.3389/fmed.2024.1389201

Effect of the prism and Maddox rod test as the surgical target for type III acute acquired comitant esotropia

Huihang Wang[1,2] and Weidong Zheng[1,2]*

[1]Department of Ophthalmology, The First Affiliated Hospital, Fujian Medical University, Fuzhou, China, [2]Department of Ophthalmology, National Regional Medical Center, Binhai Campus of the First Affiliated Hospital, Fujian Medical University, Fuzhou, China

Introduction: This study aims to explore more accurate and efficient examination methods to provide precise target surgical measurements for patients with type III acute acquired comitant esotropia (AACE).

Methods: The study conducted a retrospective analysis of 108 patients diagnosed with AACE who received surgical treatment at the Department of Ophthalmology, the First Affiliated Hospital of Fujian Medical University, from January 2018 to September 2023. All patients underwent examinations of the deviation angle, including the Hirschberg test, prism and Maddox rod test (PMT), and prism and alternate cover test (PACT). For the PACT, the minimum value (PACTmin) and maximum value (PACTmax) were obtained based on differences in examination methods, as well as the deviation angle range (PACT range), which represents the difference between PACTmax and PACTmin. Postoperatively, these patients were followed up for at least 6 months to assess changes in eye position and whether diplopia symptoms recurred.

Results: In both near and distant examinations, the results of PACTmax were significantly greater than those of PACTmin ($p < 0.001$), while the deviation angles obtained from PACTmax and PMT showed no significant statistical difference [$p = 0.689$ (33 cm), $p = 0.436$ (5 m)]. There was a strong linear correlation between PACTmin and PMT at both near ($R = 0.8887$) and distant ($R = 0.8950$) distances, but each PACTmin corresponded to multiple PMT values. There was no significant difference between the results of PACT range at near and distant distances ($p = 0.531$). The deviation angles obtained by PMT and PACTmin significantly decreased postoperatively compared to preoperative values, and diplopia disappeared in all patients, with alternative cover test showing no movement or presenting as an esophoria state.

Conclusion: The PMT can provide precise target surgical measurements for type III AACE, making it a fast, effective, and cost-efficient examination method. It is worthy of being promoted and applied in clinical practice.

KEYWORDS

acute acquired concomitant esotropia, prism and Maddox rod test, examination method, prism and alternate cover test, deviation angle

1 Introduction

Acute acquired comitant esotropia (AACE) is a specific type of esotropia commonly seen in older children or adults with mature visual development, often accompanied by symptoms such as ipsilateral diplopia, headache, and eye fatigue (1–3). Traditionally, AACE is classified into three types (4): Type I, Swan type; Type II, Burian-Franceschetti type; and Type III, Bielschowsky type. In a retrospective study based on 48 children, that took place from 2000 to 2013, Buck et al. reclassified AACE into 7 types (5), however, this classification is not yet widely recognized. Therefore, this study still uses the traditional classification.

Swan type, first proposed by Swan in 1947 (4), is characterized by AACE that occurs following the interruption of binocular single vision, such as after treatment for amblyopia, occlusion after unilateral corneal injury or surgery, or resolution of eyelid swelling after ocular trauma. Burian-Franceschetti (4) type presents with sudden onset of large-angle esotropia without apparent triggers, no accommodative factors, and no significant refractive error or mild hyperopia. It often occurs in situations of physical or psychological stress. Bielschowsky type (4, 6), first reported by Bielschowsky in 1922, occurs in adults or older children with uncorrected myopia greater than −5.00D, but later studies have found that AACE type III also occurs in people with low and intermediate myopia (7, 8). It results from imbalanced convergence and divergence due to excessive near work, leading to accommodative esotropia. Early manifestations include esotropia with ipsilateral diplopia when looking at distance with fusion but without diplopia when looking at near. As the condition progresses, diplopia may gradually appear even at near. With the proliferation of electronic devices and the prolonged period of working and studying from home due to the COVID-19 pandemic, the incidence of AACE has increased (9, 10). In recent years, the majority of AACE patients presenting for treatment have been Type III (11, 12).

The primary treatment goals for AACE patients are to eliminate diplopia and correct esotropia. Currently, the main treatment methods for AACE include prism correction, botulinum toxin type A injection into the extraocular muscles, and surgical treatment. Prism correction and botulinum toxin injection are often used in the early stages of the disease when diplopia is not severe and the degree of esotropia is small or unstable. For most patients with stable esotropia, surgery is the main treatment method, but there is a risk of postoperative undercorrection, recurrence, and the need for multiple surgeries (13). Regarding the phenomenon of postoperative undercorrection or recurrence, some scholars believe it is due to the characteristic of AACE patients "eating up prisms," making it difficult to obtain accurate target surgical measurements during examinations (14). Therefore, some scholars suggest increasing the surgical increment for AACE patients to reduce the possibility of postoperative recurrence or undercorrection (15, 16). Additionally, some researchers have found that prism adaptation tests can reveal larger degrees of deviation in AACE patients (13), but these tests are time-consuming, expensive, and currently lack consensus in clinical practice. For AACE patients, we believe that determining precise target surgical measurements preoperatively is crucial for surgical success.

Currently, the commonly used clinical methods for assessing strabismus include the Hirschberg test, prism and alternative cover test (PACT), prism and Maddox rod test (PMT), and prism adaptation test (PAT) (14, 17–19). However, there are few published research papers that use the measurement results of PMT as the target surgical amount for type III AACE. Therefore, this study focuses on type III AACE, which is the most common type, using the measurement results of PMT as the target surgical measurements for surgical treatment, while observing postoperative efficacy. The study aims to explore suitable examination methods and treatment modalities for type III AACE.

2 Materials and methods

2.1 Subjects

This study retrospectively analyzed 108 cases of type III AACE patients who underwent surgical treatment at the Department of Ophthalmology, the First Affiliated Hospital of Fujian Medical University, from January 2018 to September 2023. The study adhered to the Helsinki Declaration and was approved by the Medical Ethics Committee of the First Affiliated Hospital of Fujian Medical University. Patients or their guardians were informed and consented, and signed informed consent forms. Type III AACE was defined as acute non-accommodative esotropia occurring in older children and adult patients. Early manifestations included diplopia at distance but not at near, with the degree of esotropia gradually increasing as the disease progressed, resulting in diplopia at both distance and near. The deviation angle was the same in all gaze directions, and there were no limitations in ocular motility.

2.2 Examination

This study retrospectively reviewed data from 108 cases of type III AACE patients, collecting information including patient gender, age, duration of illness, refractive error, and deviation angle measured using various methods. At the initial visit, all patients underwent cycloplegic refraction using 0.5% tropicamide eye drops to obtain refractive values. The refractive values were converted to spherical equivalent (SE), calculated as the algebraic sum of the sphere and half of the cylinder. Refractive correction was performed using the maximum positive diopter lens that provided the best-corrected visual acuity (BCVA) according to the Maximum Plus to Maximum Visual Acuity (MPMVA) principle, with BCVA recorded as LogMAR visual acuity. Ocular anterior segment examination using a slit lamp (Haag-Streit AG, BQ 900) was conducted to exclude organic lesions. Scanning laser ophthalmoscopy (SLO, Heidelberg Engineering, Heidelberg, Germany) was performed for fundus examination to rule out fundus diseases. All patients underwent orbital and cranial imaging examination, and were thoroughly questioned about common causes of type III AACE; patients with orbital diseases, head trauma, or central nervous system abnormalities were excluded from this study. Additionally, patients with residual or secondary esotropia after strabismus correction surgery, those with combined extraocular muscle dysfunction, A-V pattern strabismus, monocular suppression, or dissociated vertical deviation were also excluded from this study.

In this study, all patients underwent deviation angle examination based on refractive correction. We used three methods to assess the deviation angle: the HT, PACT and PMT. The HT was used to assess near deviation by placing a point light source in front of the patient at

a distance of 33 cm and determining the angle of ocular deviation based on the position of the corneal light reflex. For the PMT, a red Maddox rod was placed horizontally in front of the patient's eye, and a base-out prism was placed in front of the other eye. The patient was instructed to fixate on a distant target (5 m) and a near target (33 cm). The base-out prism was gradually increased until the vertical streak overlapped with the point light source, and the PMT values were recorded at 5 m and 33 cm. During the PACT, an accommodative target was set at both near (33 cm) and distant (5 m) distances. The patient was instructed to fixate on the target while alternating eye occlusion, and the base-out prism power was gradually increased. The prism power at which the eye movement disappeared after uncovering and returning to fixation was recorded as PACTmin. Then, the prism power was gradually increased until eye movement reappeared after uncovering and returning to fixation, and the prism power at this point was recorded as PACTmax. The examination process of PMT and PACT is shown in Figures 1, 2. This process was repeated to measure the PACT values when the patient fixated at 15° to the left, 15° to the right, 25° upward, and 25° downward. Preoperatively, HT, PMT, and PACT examinations were performed at three different time points. To expose the maximum deviation angle, the highest value obtained from three consecutive measurements was used for each examination method to eliminate the phenomenon of "prism adaptation" in type III AACE patients.

2.3 Surgery and follow-up assessment

All surgeries were performed by the same experienced ophthalmologist (WD. Zheng). We used the results of the PMT examination as the target surgical measurements for AACE patients undergoing surgery. Based on the magnitude of the deviation angle,

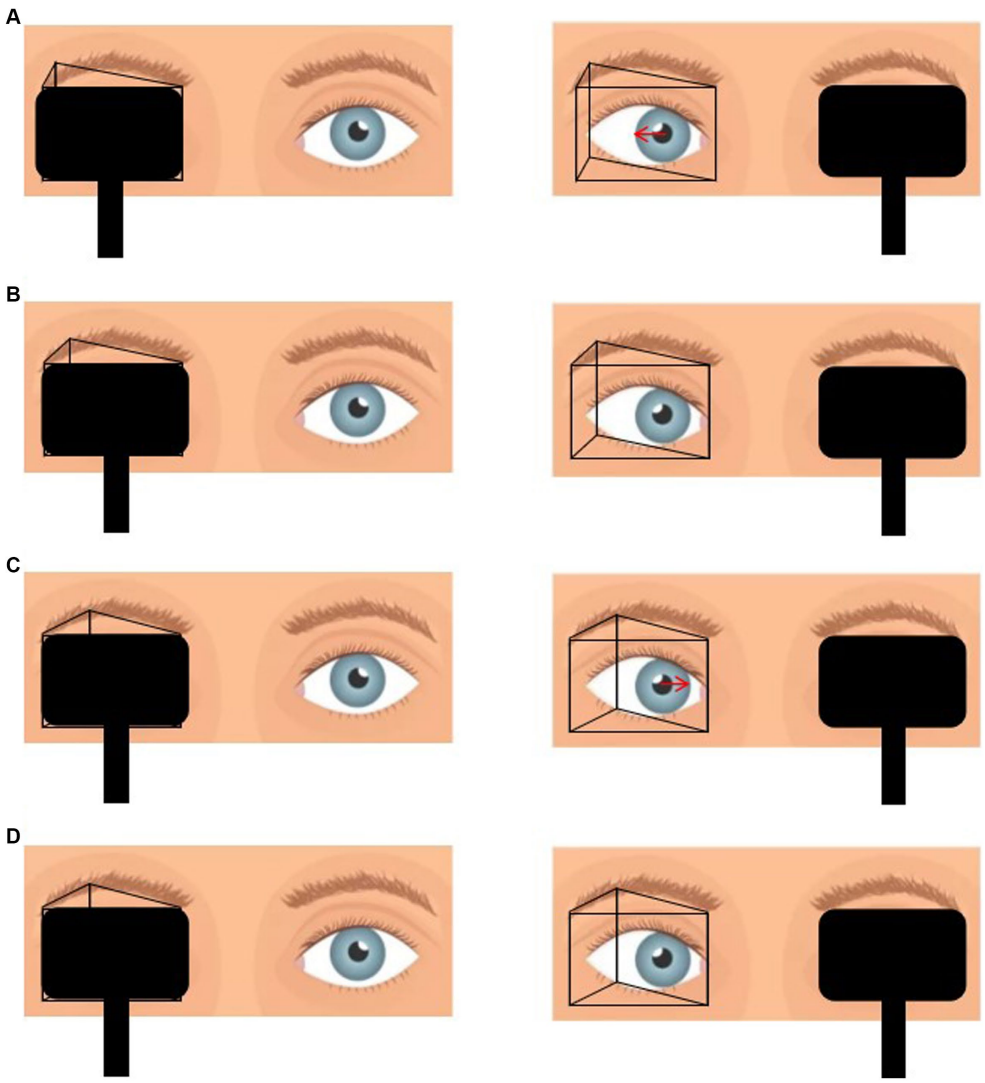

FIGURE 1
(A) Placement of prism in front of the one eye with alternate cover test reveals that the eye position is from inside to center, which suggests that the prismaticity is still insufficient. **(B)** Gradually increase the prismaticity until the eye position immobile during alternate cover test, at which point the prismaticity is recorded as PACTmin. **(C)** Continue to increase the prismaticity until the eye position is from outside to center. **(D)** Decrease the prismaticity until the eye position was immobile, at which point the prismaticity was recorded as PACTmax.

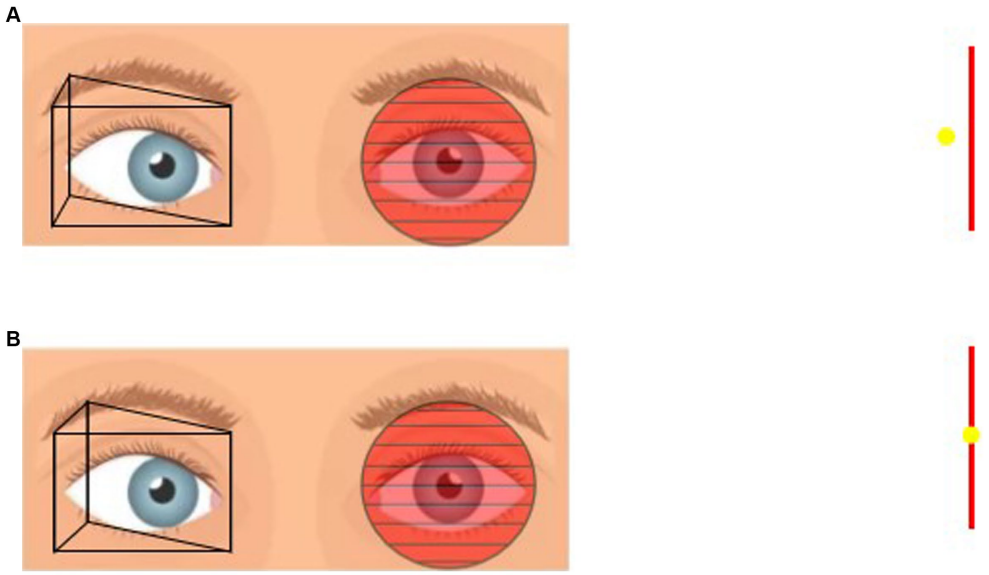

FIGURE 2
(A) Placement of prism in front of the one eye and Maddox rod in front of the other eye. If the patient sees the vertical line on the left and the point light on the right then the prismaticity is still insufficient. **(B)** Gradually increase the prismaticity until the vertical line and the point light fit together, at which point the prismaticity was recorded as PMT.

unilateral medial rectus recession (MRrec) of the non-dominant eye or combined MRrec and lateral rectus resection (LRres) of the non-dominant eye were performed. For patients with PMT results exceeding 80 prism diopters (PD), bilateral MRrec combined with non-dominant eye LRres was considered. The surgical dosage was determined according to the Parks scale. All patients in this study were able to cooperate with surgery under local anesthesia. During surgery, patients needed to wear refractive correction glasses and fixate on targets at 5 m and 33 cm to confirm the disappearance of diplopia. We reserved adjustable sutures and ligated them after observing that the patients had no diplopia in all directions and orthotropia in the distance position, orthotropia or slight exotropia in the near position. No adjustments were made in all patients in this study eventually. Follow-up examinations were conducted at 1 day, 1 week, 1 month, 3 months, and 6 months postoperatively, including evaluations of HT, PMT, and PACT. Patients with a follow-up period exceeding 6 months were also followed up via telephone. Surgical success was defined as the disappearance of diplopia postoperatively, and residual objective and subjective deviation angle were evaluated based on PACT min and the far and near horizontal deviation measured by PMT.

2.4 Statistics

The data were analyzed using descriptive statistics, reporting mean and standard deviation for normally distributed data, and counts and percentages for categorical data. In the study of deviation angle examination methods, paired-sample t-tests and two independent-sample t -test were used to analyze differences in near-distance disparity (NDD) measured by different examination methods. Correlation analysis was conducted using linear regression and Pearson correlation coefficient (r). All data analyzes were performed using SPSS (StatLab, SPSS version 25.0) and Prism (StarBio-LLC, Prism 9 version 9.4.1). A two-tailed test was used, with $p < 0.05$ considered statistically significant. The Pearson correlation coefficient (r) values were interpreted as follows: $0 \leq |r| < 0.3$ indicates weak linear correlation, $0.3 \leq |r| < 0.8$ indicates moderate linear correlation, and $0.8 \leq |r| \leq 1$ indicates strong linear correlation.

3 Results

3.1 Study population

This study included a total of 108 cases of type III AACE patients, all of whom were Chinese. The basic information and clinical characteristics of the patients are summarized in Table 1. The patients were all older children and adults, with an average age of 26.86 ± 11.59 years (ranging from 10 to 53 years), and the male proportion was 56.48%. The LogMAR BCVA of both eyes of all patients was less than 0.10, with no significant statistical difference in BCVA and SE between the eyes (p values were 0.654 and 0.597, respectively), and the proportion of eyes with refractive disparities was only 5.55%. For detailed information, please refer to Table 1.

3.2 Epidemiological characteristics

This study included patients who underwent treatment from January 2018 to September 2023. Statistical analysis revealed a gradual increase in the number of type III AACE patients treated each year since 2018 (Figure 3). Furthermore, we observed a sudden surge in the number of type III AACE patients after 2020, possibly due to the increased use of close-up activities such as remote work or online teaching resulting from the outbreak of the COVID-19 pandemic.

We categorized type III AACE patients into adult and pediatric groups and conducted epidemiological analyzes separately. We found that the number of pediatric patients gradually increased after the COVID-19 pandemic (Figure 3A), while the number of adult patients significantly increased one to two years after the outbreak (Figure 3B). To further explore the differences between the two groups, we statistically analyzed the duration of illness at the time of initial diagnosis and found that the duration of illness in the pediatric group was significantly shorter than that in the adult group, with a statistically significant difference ($p = 0.015$) (Figure 3C). The average spherical equivalent refractive error of both eyes of type III AACE patients was predominantly moderate myopia, followed by mild myopia, with high myopia, hyperopia, and emmetropia being rare. This is consistent with our previous research findings on independent risk factors for type III AACE (14).

TABLE 1 Epidemiology and clinical characteristics of the type III AACE patients.

Subjects ($N = 108$)	Values	Mean ± SD	p-value
Sex, male No. (%)	61 (56.48%)		
Sex, female No. (%)	47 (43.52%)		
Age (years)	10–53	27.03 ± 10.94	
Duration (months)	1–120	33.96 ± 30.12	
BCVA OD (logMAR)	−0.079–0.097	−0.0050 ± 0.044	0.654
BCVA OS (logMAR)	−0.079–0.097	−0.0068 ± 0.042	
SE OD (D)	−11.5–1.25	−4.23 ± 2.09	0.597
SE OS (D)	−11.25–2	−4.18 ± 2.29	
Dominant eye OD No. (%)	58 (53.70%)		
Dominant eye OS No. (%)	50 (46.30%)		
Anisometropia No. (%)	6 (5.55)		

BCVA, best-corrected visual acuity; OD, right eye; OS, left eye; logMAR, logarithm of the minimum angle of resolution; SE, spherical equivalent; D, diopter; No., number of patients; P, Paired samples t-test; N, number of cases.

3.3 Comparison of different examination methods

In this study, we employed various methods of deviation angle examination to measure the degree of ocular deviation in patients with type III AACE, including HT, PACT, and PMT. Among them, HT examined only the ocular deviation angle at near distance, while the other two methods provided measurements of ocular deviation angles at both near and far distances. These results help us better understand

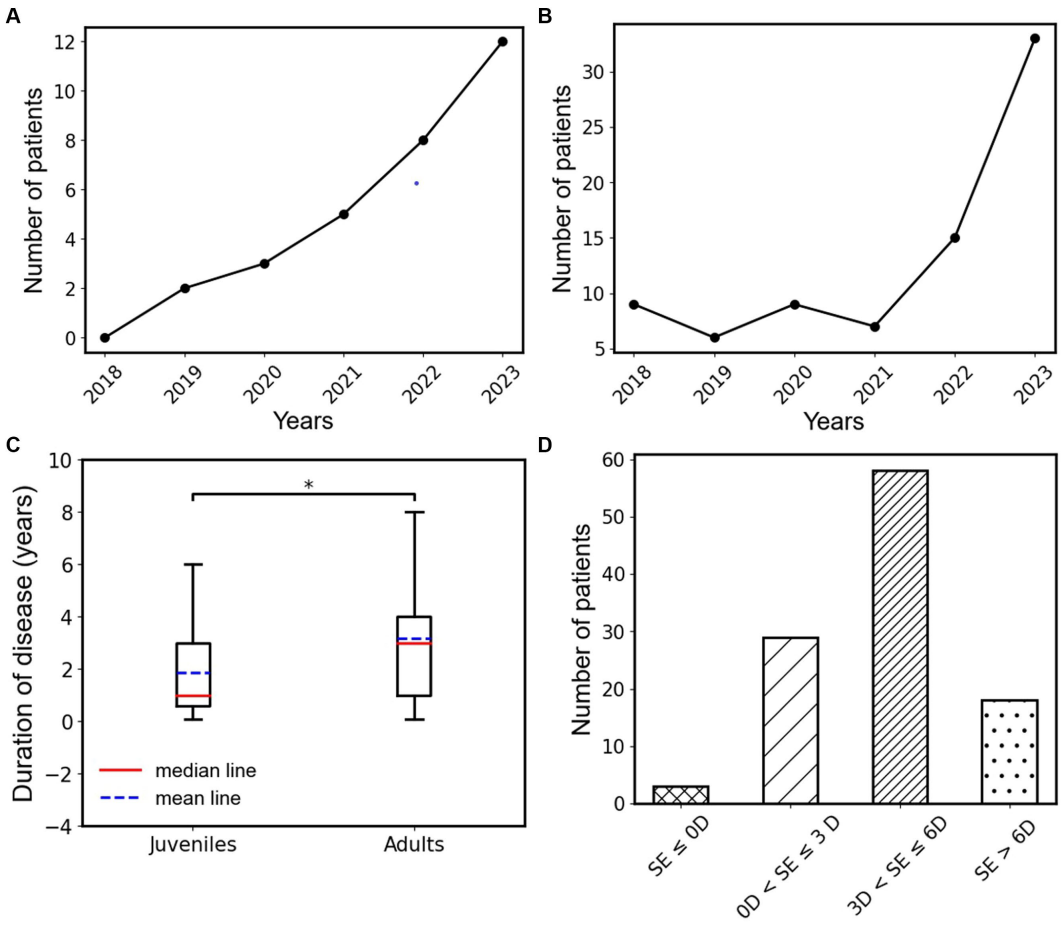

FIGURE 3
(A) Annual change trend in the number of type III AACE patients in the juvenile group from 2018 to 2023. **(B)** Annual change trend in the number of type III AACE patients in the adult group from 2018 to 2023. **(C)** The box plots of disease duration in juvenile and adult groups of type III AACE. **(D)** Binocular mean equivalent spherical distribution of type III AACE patients; *indicates the $p < 0.05$.

the characteristics of type III AACE and select appropriate surgical target amounts. Table 2 visually compares the mean ocular deviation angles at near and far distances obtained from PACT and PMT, along with standard deviations and numerical ranges. As shown in Table 2, there were no significant statistical differences ($p > 0.05$) in the ocular deviation angles measured at near and far distances by all examination methods, including PMT, PACTmin, and PACTmax, indicating that the ocular deviation angles of type III AACE patients are not correlated with distance.

To further observe the differences among various examination methods in patients with type III acute acquired comitant esotropia (AACE), we conducted additional statistical analyzes. As shown in Figure 4A, in the examination at near distance (33 cm), we performed paired t-tests on PMT, PACTmax, and PACTmin for each patient. The results showed that PACTmax was significantly greater than PACTmin, with extremely significant statistical differences ($p < 0.001$); PMT was also significantly greater than PACTmin, with extremely significant statistical differences ($p < 0.001$); however, there was no significant statistical difference between PMT and PACTmax ($p = 0.689$). Similar phenomena were observed in the examination at far distance (5 m), as shown in Figure 4B. PACTmax was significantly greater than PACTmin, with extremely significant statistical differences ($p < 0.001$); PMT was also significantly greater than PACTmin, with extremely significant statistical differences ($p < 0.001$); there was no significant statistical difference between PMT and PACTmax ($p = 0.436$). We further conducted linear regression analysis between PMT and PACTmin, as illustrated in Figure 5. Strong linear correlations were observed between PMT and PACTmin at both near and far distances. According to the linear regression results, at near distance, PMT = 1.226 × PACTmin +10.58, with R = 0.8887. At far distance, PMT = 1.211 × PACTmin +11.48, with R2 = 0.8950. The results indicate that larger PACTmin values correspond to larger PMT values, but there is not a one-to-one correspondence between PACTmin and PMT values. For different patients, although the PACTmin values are the same, they may correspond to different PMT values.

Due to the phenomenon of "eating up prisms" in patients with type III acute acquired comitant esotropia (AACE), there is a certain range between the minimum and maximum values of PACT, which we refer to as the deviation angle range (PACT range). It reflects the ability of patients with type III AACE to conceal ocular deviation within a certain range. According to the results in Table 2, the deviation angle range is approximately the same in both far distance (15.11 PD) and near distance (15.72 PD) examinations, with an average of 15.42 PD. To further explore the differences in PACT range between far and near distances, we represented the results of PACT range for far and near distances in the form of a violin plot for easier observation. As shown in Figure 6A, there was no significant statistical difference between the PACT range at far distance and that at near distance. We calculated the difference between the PACT range for each patient at far and near distances and plotted it using a histogram. And as shown in Figure 6B, the distributions of both were approximately centered around 0 PD, indicating a normal distribution, further illustrating that the numerical values of PACT range are roughly equal between far and near distances.

TABLE 2 The results of different inspection distances and methods.

Methods	Near deviation (33 cm, PD)	Distance deviation (5 m, PD)	t	*p*-value
PMT	45.69 ± 24.19 (10 to 115)	46.70 ± 24.13 (12 to 115)	−0.486	0.628
PACTmin	28.65 ± 17.54 (0 to 70)	29.08 ± 17.83 (4 to 75)	−0.282	0.778
PACTmax	44.37 ± 24.30 (8 to 105)	44.19 ± 23.11 (10 to 110)	0.085	0.932

PACT, prism and alternative cover test; PMT, prism and Maddox rod test; PD, prism diopter.

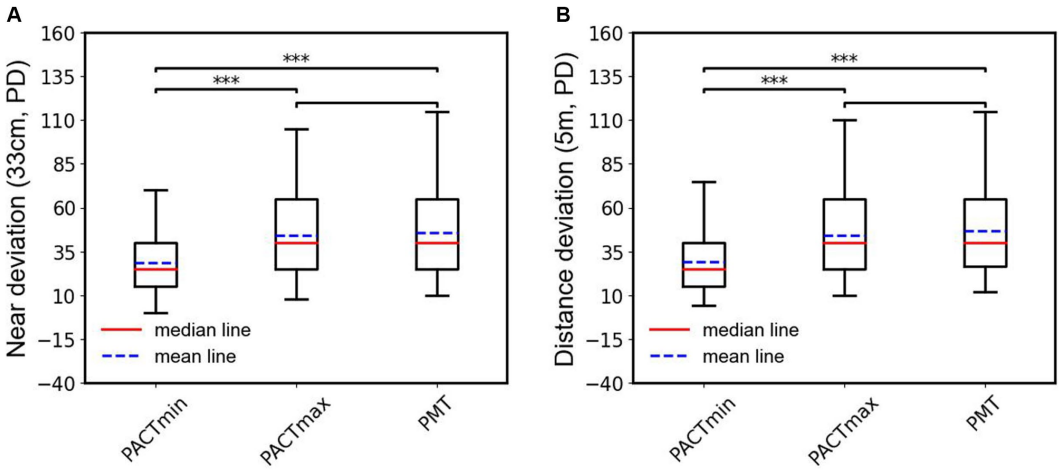

FIGURE 4
(A) Box plots and statistical analysis of the PACTmin, PACTmax and PMT in near range. **(B)** Box plots and statistical analysis of the PACTmin, PACTmax and PMT in distance range; ***indicates the $p < 0.001$.

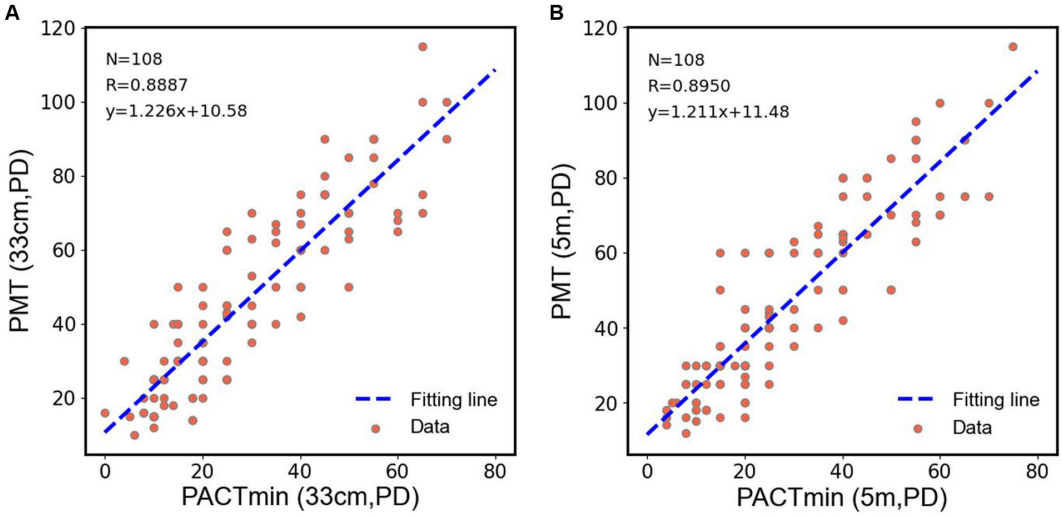

FIGURE 5
(A) Scatter plots were drawn by PACTmin and PMT of each patient in near range, and linear regression and correlation analysis were performed for the scatter plots. **(B)** Scatter plots were drawn by PACTmin and PMT of each patient in distance range, and linear regression and correlation analysis were performed for the scatter plots.

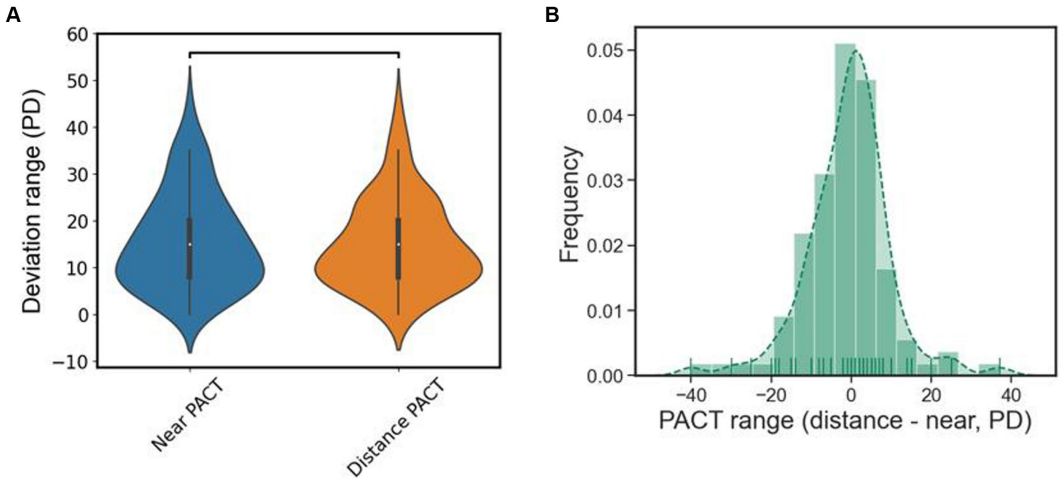

FIGURE 6
(A) The violin plot of the deviation range of PACT, there is no statistical difference in distance and near. **(B)** Subtract the results of the PACT deviation range at distance from the PACT deviation range at near and plot it as a histogram, it roughly normally distributed.

3.4 Postoperative effect and analysis

We further analyzed the postoperative outcomes of patients with type III acute acquired comitant esotropia (AACE). As shown in Figure 7, we conducted deviation angle examinations using both PMT and PACT methods before surgery and at postoperative intervals of 1 day, 1 week, 1 month, 3 months, and 6 months, and performed statistical analysis. We found that after surgical treatment, the magnitude and variability of esotropia significantly decreased in patients, with the alternating cover test showing no movement or esotropia at postoperative day 1. The esotropia values were lowest at postoperative day 1 and showed a gradual increase over time, with a similar pattern observed in both near and far distance examinations. However, none of the patients reported a recurrence of diplopia symptoms, indicating successful treatment outcomes for all type III patients without recurrence.

4 Discussion

In recent years, the prevalence of type III AACE has significantly increased, particularly with the growing duration of near-work activities in the population, especially excessive use of smartphones. Our previous research also identified that increased daily near-work time and uncorrected myopia during near-work are independent risk factor for the onset of type III AACE (20). In this study, we observed a similar pattern where, following the outbreak of the COVID-19 pandemic, there was an explosive growth in type III AACE cases,

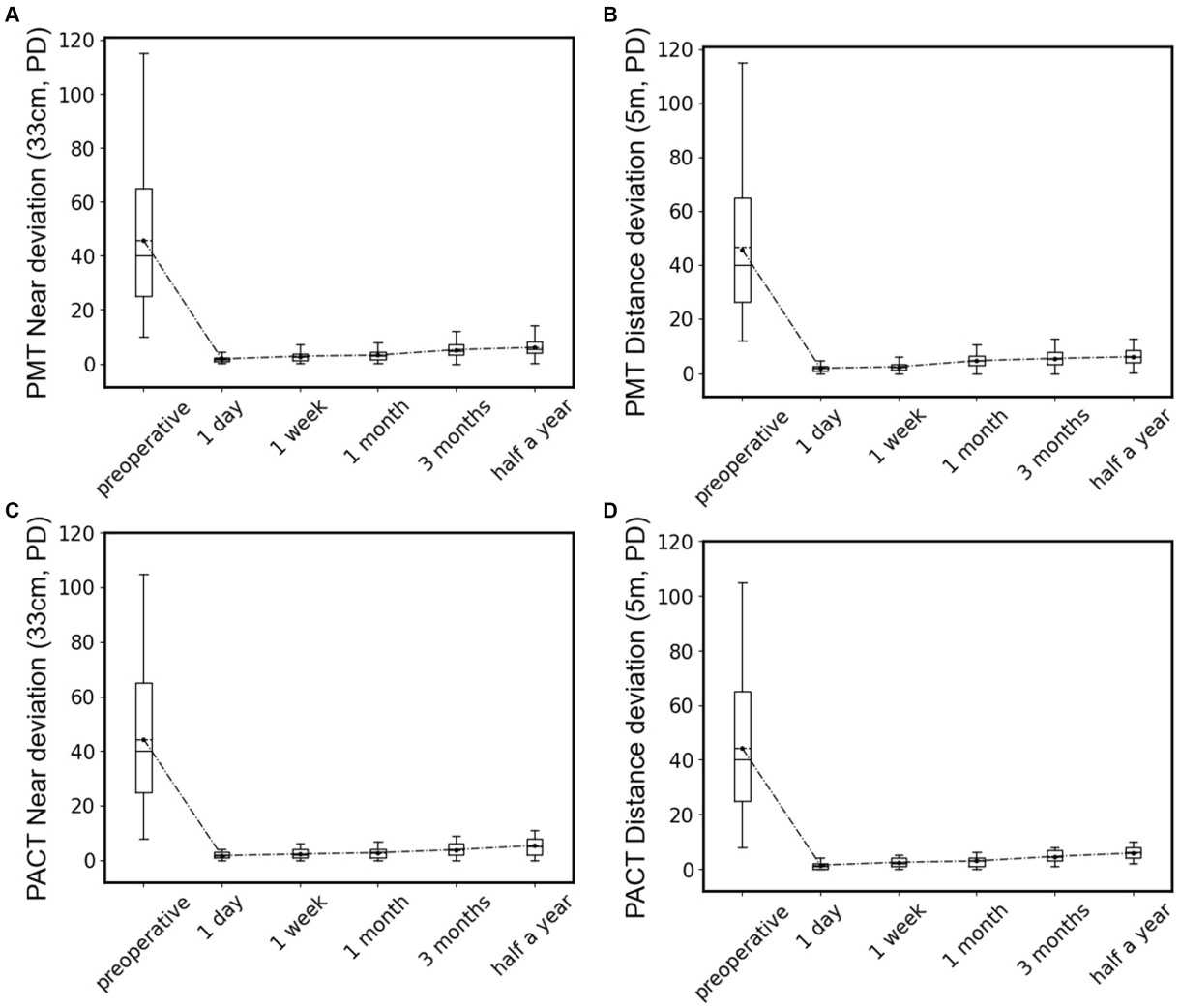

FIGURE 7
Statistical box plots of patients' deviation angle preoperative and 1 day, 1 week, 1 month, 3 months, and 6 months after surgery, test by PMT at near location **(A)** and distant location **(B)**, or by PACT at near location **(C)** and distant location **(D)**.

likely attributed to reduced outdoor activities and prolonged use of electronic devices. This increase may be associated with increased tension in the medial rectus muscles due to prolonged near work, convergence spasm induced by myopia, and compensatory esotropia (11, 12). We conducted a retrospective analysis of 108 cases of type III AACE, stratifying them into adult and pediatric groups for statistical observation. We found that the number of cases in the adult group surged 1–2 years later than in the pediatric group, and the duration of disease at the initial visit was significantly longer in the adult group compared to the pediatric group. We speculate that this difference may be due to adults having higher tolerance to abnormal accommodation and convergence compared to children, or it may be related to parents of pediatric patients being more concerned about the visual disturbances affecting their children's learning and daily life, prompting earlier medical consultations. However, the etiology of AACE is not yet fully understood, and further research is needed to explore its mechanisms in the future.

Regarding the treatment of type III AACE, surgery is currently widely employed as the primary therapeutic approach. Due to the notable phenomenon of "prism adaptation" in AACE patients, relying solely on traditional PACT for assessing the deviation angle and using the prism diopter at which the eye movement disappears upon uncovering (referred to as PACTmin) as the target surgical dosage often leads to postoperative under-correction or long-term recurrence (21). Therefore, the ability to expose the maximum deviation angle preoperatively in type III AACE patients becomes a crucial factor in determining the success of surgery. Zhou et al. (16) proposed a method in which the preoperative PACT results (referred to as PACTmin in this paper) are used as the target surgical dosage, and intraoperatively, the surgery is adjusted incrementally based on whether the patient's subjective diplopia symptoms disappear until diplopia is resolved. By retrospectively analyzing the surgical increments required by these AACE patients, they are used as a reference for the target surgical dosage in other AACE patients. However, we believe that the incremental data obtained from postoperative retrospective analysis of surgical dosage may not accurately reflect the true deviation angle in AACE patients, as we found that the same PACTmin may correspond to multiple

different PMT values, making it challenging to generalize and apply clinically. Dai et al. (22) used the recovery point from PACT (referred to as PACTmax in this paper) as the target surgical dosage design and achieved significant and stable improvements postoperatively, indicating that using PACTmax as the target surgical dosage design for AACE can yield significant results.

PMT examination is only suitable for patients with mature binocular vision, which is exactly the case for type III AACE patients who are typically older children or adults with some level of binocular vision. This study found that PMT, as a subjective method for measuring deviation angle, showed no significant difference compared to the objective PACTmax. Moreover, since PMT examination can completely disrupt fusion, it suggests that PMT can expose the maximum deviation angle in type III AACE. Our research found that there was no significant statistical difference between PMT and PACTmax, whether in distance or near examination. Therefore, we propose using PMT as the target surgical dosage for the surgical treatment of type III AACE.

In this study, we also investigated the performance of PACT range in both distance and near examinations. Our research revealed that there was no significant statistical difference in PACT range between distance and near examinations, indicating a substantial "buffer zone" in PACT examinations for type III AACE patients. This buffer zone is the main cause of the "eating prism" phenomenon. Due to insufficient understanding of type III AACE among many ophthalmologists, PACTmin is often used as the target surgical amount, leading to postoperative under-correction or recurrence. Because PACT recovery values and PAT can expose the maximum deviation angle of type III AACE patients, some scholars in previous studies have also used these two examination methods as target surgical amounts, achieving good results. If referring to the PAT examination used in previous studies, regular replacement of prisms is required, which may take weeks or even longer, and during this period, frequent replacement of prism lenses is needed, incurring significant diagnostic and treatment costs. Therefore, using PMT as the target surgical amount can not only achieve good therapeutic effects but also effectively reduce the number of patient visits and the associated costs, making it worth promoting as a method for determining the target surgical amount for type III AACE patients in clinical practice. This study was retrospective, with complete follow-up data collected up to 6 months postoperatively, but lacked a comprehensive assessment of binocular visual function. No control group was set up in this study, and further support from large-sample clinical observations and prospective studies is needed to validate the research conclusions.

In conclusion, preoperative exposure of the maximum deviation angle serves as a crucial factor for the success of surgery in type III AACE. We believe that preoperative PMT examination can expose the maximum deviation angle in type III AACE, offering a rapid, effective, and cost-effective method. Utilizing PMT examination results as the target surgical amount can lead to favorable outcomes for type III AACE patients, including the elimination of diplopia and correction of esotropia. Therefore, it is worthy of clinical promotion and application.

Data availability statement

The raw data supporting the conclusions of this article will be made available by the authors, without undue reservation.

Ethics statement

The studies involving humans were approved by Branch for Medical Research and Clinical Technology Application, Ethics Committee of First Affiliated Hospital of Fujian Medical University. The studies were conducted in accordance with the local legislation and institutional requirements. Written informed consent for participation in this study was provided by the participants' legal guardians/next of kin.

Author contributions

HW: Funding acquisition, Investigation, Software, Writing – original draft. WZ: Conceptualization, Data curation, Project administration, Resources, Supervision, Validation, Writing – review & editing.

Funding

The author(s) declare that no financial support was received for the research, authorship, and/or publication of this article.

Conflict of interest

The authors declare that the research was conducted in the absence of any commercial or financial relationships that could be construed as a potential conflict of interest.

Publisher's note

References

1. Kemmanu V, Seetharam R, Shetty BK, Hegde K. Varied aetiology of acute acquired comitant esotropia: a case series. *Oman J Ophthalmol.* (2012) 5:103–5. doi: 10.4103/0974-620X.99373

2. Sturm V, Menke MN, Knecht PB, Schöffler C. Long-term follow-up of children with acute acquired concomitant esotropia. *J AAPOS.* (2011) 15:317–20. doi: 10.1016/j.jaapos.2011.03.018

3. Lee JM, Kim SH, Lee JI, Ryou JY, Kim SY. Acute comitant esotropia in a child with a cerebellar tumor. *Korean J Ophthalmol.* (2009) 23:228–31. doi: 10.3341/kjo.2009.23.3.228

4. Burian HM, Miller JE. Comitant convergent strabismus with acute onset. *Am J Ophthalmol.* (1958) 45:55–64. doi: 10.1016/0002-9394(58)90223-X

5. Dragomir MS, Merticariu M, Merticariu CI. Management of acute acquired comitant esotropia in children. *Rom J Ophthalmol.* (2023) 67:87–91. doi: 10.22336/rjo.2023.16

6. Lee HS, Park SW, Heo H. Acute acquired comitant esotropia related to excessive smartphone use. *BMC Ophthalmol*. (2016) 16:37. doi: 10.1186/s12886-016-0213-5

7. Lekskul A, Chotkajornkiat N, Wuthisiri W, Tangtammaruk P. Acute acquired Comitant Esotropia: etiology, clinical course, and management. *Clin Ophthalmol*. (2021) 15:1567–72. doi: 10.2147/OPTH.S307951

8. Hoyt CS, Good WV. Acute onset concomitant esotropia: when is it a sign of serious neurological disease? *Br J Ophthalmol*. (1995) 79:498–501. doi: 10.1136/bjo.79.5.498

9. Neena R, Remya S, Anantharaman G. Acute acquired comitant esotropia precipitated by excessive near work during the COVID-19-induced home confinement. *Indian J Ophthalmol*. (2022) 70:1359–64. doi: 10.4103/ijo.IJO_2813_21

10. Nouraeinejad A. Neurological pathologies in acute acquired comitant esotropia. *Graefes Arch Clin Exp Ophthalmol*. (2023) 261:3347–54. doi: 10.1007/s00417-023-06092-3

11. Zheng K, Han T, Han Y, Qu X. Acquired distance esotropia associated with myopia in the young adult. *BMC Ophthalmol*. (2018) 18:51. doi: 10.1186/s12886-018-0717-2

12. Vagge A, Giannaccare G, Scarinci F, Cacciamani A, Pellegrini M, Bernabei F, et al. Acute acquired concomitant Esotropia from excessive application of near vision during the COVID-19 lockdown. *J Pediatr Ophthalmol Strabismus*. (2020) 57:e88–91. doi: 10.3928/01913913-20200828-01

13. Roda M, Pellegrini M, Rosti A, Fresina M, Schiavi C. Augmented bimedial rectus muscles recession in acute acquired concomitant esotropia associated with myopia. *Can J Ophthalmol*. (2020) 56:166–70. doi: 10.1016/j.jcjo.2020.10.006

14. Savino G, Colucci D, Rebecchi MT, Dickmann A. Acute onset concomitant esotropia: sensorial evaluation, prism adaptation test, and surgery planning. *J Pediatr Ophthalmol Strabismus*. (2005) 42:342–8. doi: 10.3928/01913913-20051101-02

15. Lee HJ, Kim SJ. Clinical characteristics and surgical outcomes of adults with acute acquired comitant esotropia. *Jpn J Ophthalmol*. (2019) 63:483–9. doi: 10.1007/s10384-019-00688-1

16. Zhou Y, Ling L, Wang X, Jiang C, Wen W, Zhao C. Augmented-dose unilateral recession-resection procedure in acute acquired Comitant Esotropia. *Ophthalmology*. (2023) 130:525–32. doi: 10.1016/j.ophtha.2022.12.019

17. Choi RY, Kushner BJ. The accuracy of experienced strabismologists using the Hirschberg and Krimsky tests. *Ophthalmology*. (1998) 105:1301–6. doi: 10.1016/S0161-6420(98)97037-3

18. Ela-Dalman N, Velez G, Thacker N, Britt MT, Velez FG. Maximum motor fusion combined with one-hour preoperative prism adaptation test in patients with acquired esotropia. *J AAPOS*. (2006) 10:561–4. doi: 10.1016/j.jaapos.2006.09.011

19. Newman-Toker DE, Rizzo JF 3rd. Subjectively quantified Maddox rod testing improves diagnostic yield over alternate cover testing alone in patients with diplopia. *J Clin Neurosci*. (2010) 17:727–30. doi: 10.1016/j.jocn.2009.10.002

20. Zhang J, Chen J, Lin H, Huang L, Ma S, Zheng W. Independent risk factors of type III acute acquired concomitant esotropia: a matched case-control study. *Indian J Ophthalmol*. (2022) 70:3382–7. doi: 10.4103/ijo.IJO_318_22

21. Parks MM, Mitchell PR, Wheeler MB. Concomitant Esodeviations In: WW Tasman and E Jaeger, editors. *Duane's ophthalmology*. Philadelphia: Lippincott Williams & Wilkins (2006)

22. Dai Z, Zheng F, Xu M, Zhou J, Wan M, Yu H, et al. Effect of the base-out recovery point as the surgical target for acute acquired comitant esotropia. *Graefes Arch Clin Exp Ophthalmol*. (2021) 259:3787–94. doi: 10.1007/s00417-021-05318-6

frontiers | Frontiers in Medicine

TYPE Brief Research Report
PUBLISHED 11 June 2024
DOI 10.3389/fmed.2024.1402853

OPEN ACCESS

EDITED BY
Horace Massa,
Hôpitaux Universitaires de Genève (HUG), Switzerland

REVIEWED BY
Katarzyna Krysik,
Wojewódzki Szpital Specjalistyczny nr 5 Sosnowiec, Poland
Ashok Sharma,
Dr Ashok Sharma's Cornea Centre, India

*CORRESPONDENCE
Jiewei Liu
✉ Jieweiliu1967@sina.com

RECEIVED 18 March 2024
ACCEPTED 28 May 2024
PUBLISHED 11 June 2024

CITATION
Liu W, Ma JX, Tan X, Chai F and Liu J (2024) A technique to treat Descemet's membrane detachment following cataract surgery. *Front. Med.* 11:1402853. doi: 10.3389/fmed.2024.1402853

A technique to treat Descemet's membrane detachment following cataract surgery

Wenjie Liu[1], Jack X. Ma[2], Xin Tan[1], Feiyan Chai[1] and Jiewei Liu[1]*

[1]Department of Cataract, Shanxi Eye Hospital, Taiyuan, Shanxi, China, [2]Department of Ophthalmology, Baylor College of Medicine, Houston, TX, United States

We describe a technique to reattach the detached Descemet's membrane, following cataract surgery. From the main clear corneal cataract incision, aqueous humor is ejected completely by apposition of the cornea to the iris for approximately 3 s. This ensures the fluid in the space between the stroma and Descemet's membrane is ejected and the detached Descemet's membrane returns to its original position. Sterile air is injected through a paracentesis 180 degrees away from the Descemet's membrane detachment, to maintain a complete air-filled chamber. Full air tamponade is maintained for 20 min, following which one-third of the air is ejected from the chamber to prevent an increase of postoperative intraocular pressure.

KEYWORDS

Descemet's membrane detachment, cataract surgery, reattachment of Descemet's membrane detachment, DMD, cataract

Introduction

Descemet's membrane is the basement membrane for the corneal endothelium. Descemet's membrane and corneal endothelium play a pivotal role in maintaining corneal clarity. Descemet's membrane detachment (DMD) is a well-recognized and potential vision-threatening complication following cataract surgery (1). Corneal edema appears over the area of DMD and bullous keratopathy may occur, if not managed appropriately. Prompt reattachment of Descemet's membrane may restore corneal clarity immediately and prevent wrinkling, scrolling, fibrosis, and scarring of Descemet's membrane (2).

Conservative management is used as an approach to treat mild and nonscrolled DMD (3–7). Spontaneous resolution of corneal edema and reattachment of DMD in early and late cases has been reported. However, early surgical treatment is now advocated for cases with severe, scrolled, extensive, and visually impairing DMDs (1–9).

Pneumodescemetopexy with intracameral injection of air or gases has become the preferred treatment for DMD. Due to the concerns of endothelial toxicity induced by gases (10), there is a trend toward using intracameral air alone in repairing DMD (9). In this report, we present a technique to manage DMD following cataract surgery.

Surgical technique

This technique has four steps. First, a paracentesis is made on the opposite side of the DMD. Second, the aqueous humor is ejected from the main clear corneal cataract incision. To ensure complete ejection of aqueous humor from the anterior chamber, the

cornea is apposed to the iris for a short time duration. This approach squeezes out the fluid in the space between the stroma and Descemet's membrane and ensures the detached Descemet's membrane returns to its original position. To prevent damage to the corneal endothelial cells, apposition of the cornea to the iris is limited to a short duration of 3 s. Third, from the paracentesis, sterile air is injected into the anterior chamber to maintain a complete air-filled chamber and sustained air tamponade. Finally, full-air tamponade is maintained for 20 min, and then approximately one-third of the air is ejected from the chamber to prevent an increase of intraocular pressure (IOP) after the procedure (Figure 1).

Results

Five cases with DMD and reattachment procedures are listed in Table 1. From among these five, two cases, one with air injection alone into the anterior chamber (case #1) and second with complete ejection of aqueous humor without air injection (case #3) failed to reattach the Descemet's membrane. Complete aqueous ejection followed by air injection increased IOP (cases #1 and #2). In cases 4 and 5, complete aqueous ejection, full air tamponade, and ejection of one-third of air successfully reattached the DMD (Figure 2).

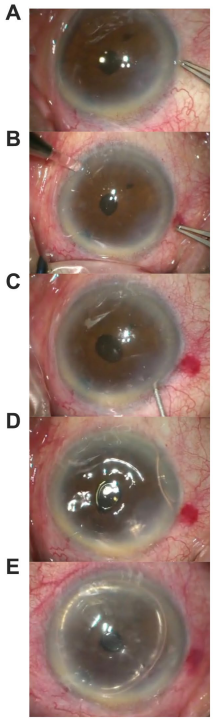

FIGURE 1
Images showing steps of surgical steps: **(A)** shows DMD; **(B)** shows a paracentesis is made at the opposite site of the DMD; **(C)** shows aqueous humor is ejected from the main clear corneal cataract incision, the cornea is briefly apposed to the iris; **(D)** shows sterile air is injected into the anterior chamber to maintain a complete air-filled chamber; **(E)** shows approximately one third of the air is ejected from the chamber after 20 min.

Discussion

Air injection into the anterior chamber is the most common procedure used to treat DMD. Unsuccessful pneumatic descemetopexy occurs when there is fluid entrapped in the supra-descemet's space, which prevents the apposition of Descemet's membrane to the stroma. In such cases, an alternate method of fluid drainage by corneal venting incision or external stab incision, with or without air tamponade, has been reported (10). Internal aspiration with a needle may also be used for drainage of the fluid in the supra-descemet's space, but these methods are complicated and prone to cause corneal damage.

Our procedure is easy to perform. By apposition of the cornea to the iris, the underlying principle of our technique is to: (1) squeeze out the fluid in the supra-descemet's space to ensure that the Descemet's membrane returns to its anatomical position, and (2) completely eject aqueous humor out of the anterior chamber so that the anterior chamber can be completely filled with air to ensure effective air tamponade. In case #1, sterile air was injected into the anterior chamber at the end of the surgery without complete ejection of the fluid in the anterior chamber anda complete air-fill was achieved in the anterior chamber. Detached Descemet's membrane was reattached to the cornea at the end of surgery, but detachment was noted again on the 5th Post-operative Day (POD 5). Air injection into the anterior chamber is another important step. In case #3, although we completely squeezed out aqueous humor and ensured the apposition of the cornea to the iris without air injection at the end of the procedure, Descemet's membrane detached again on POD 1. This indicates that it is important to maintain full-air tamponade for 20 min. In case #1 and case #2, both without air ejection after the surgery, the IOP increased on POD 1. To prevent this from happening, approximately one-third of the air is ejected from the chamber after full air tamponade is maintained for 20 min. In our last two cases, the IOP did not increase postoperatively.

Prolonged apposition of the iris to angle structures of the eye can cause permanent peripheral anterior synechiae and chronic angle-closure glaucoma. Corneal contact with vitreous humor or an IOL (Intraocular Lens implant) can result in endothelial cell loss and chronic corneal edema. With our technique, the cornea touches the iris for only a few seconds, which should not cause peripheral anterior synechiae or corneal endothelial cell damage. Due to diffuse corneal edema, the Corneal Endothelial Cell Count (CECC) before the DMD reattachment procedure could not be obtained in cases #1–3. In case #4, CECC decreased by 3.7% on day 1 and 5.5% on day 6 following the DMD reattachment procedure. In this case, the CECC before the cataract surgery was low, presumably caused by previous glaucoma surgery. In case #5, the CECC at 1 month after the DMD reattachment procedure was similar to the CECC before the cataract surgery. Long-term follow-up on CECC is needed in cases undergoing DMD reattachment procedures.

Kumar et al. (1) introduced an algorithm that classifies Descemet membrane detachment (DMD) based on anterior segment optical coherence tomography (AS-OCT) imaging parameters. The classification is made according to the height and length of the detachment, as well as the area affected and whether

TABLE 1 Cases with Descemet's membrane detachment (DMD) and reattachment procedures.

	Case #1	Case #2	Case #3	Case #4	Case #5
Sex	Female	Male	Male	Female	Female
Age	75	88	82	80	66
Eye	Left eye	Left eye	Right eye	Right eye	Right eye
DMD occurred	Intraoperative	POD 1	Intraoperative	POD 1	POD 1
Time of reattachment procedure	End of surgery	POD 1	End of surgery	POD 12	POD 1
Reattachment procedure	Air injection	Cornea and iris apposition + air injection	Cornea and iris apposition	Cornea and iris apposition + air injection +1/3 air ejection	Cornea and iris apposition + air injection +1/3 air ejection
Results	DMD reattached	DMD reattached, high IOP	DMD reattachment failed	DMD reattached	DMD reattached
Second DMD occurred	POD 5	no	POD 1	no	no
Reattachment procedure	Cornea and iris apposition + air injection		Cornea and iris apposition + air injection +1/3 air ejection		
Results	DMD reattached, high IOP		DMD reattached		
CECC before cataract surgery	-	-	-	1357.0/mm^2	2290.4/mm^2
CECC before DMD reattachment procedure	-	-	-	1239.9/mm^2	-
CECC after DMD reattachment procedure	-	-	-	1194.2/mm^2 on day 1, and 1171.9/mm^2 on day 6	2,139/mm^2 on day 1, and 2279.8/mm^2 at 1 month

POD, postoperative day; IOP, intraocular pressure; CECC, corneal endothelial cell count with the specular microscope SP-3000P (Topcon Medical Systems, Inc., Oakland, NJ); –, not available.

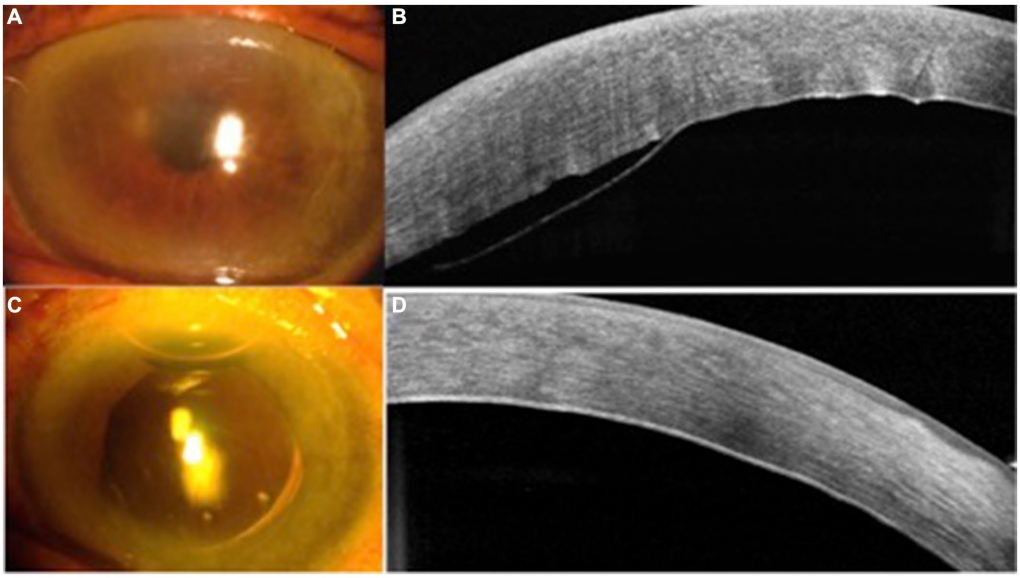

FIGURE 2
Case #5 slit lamp photos and anterior segment optical coherence tomography (OCT) maps. **(A)** corneal edema at 1 day after the cataract surgery; **(B)** Descemet's membrane detachment (DMD) seen on OCT map; **(C)** cornea clear at 1 day following the DMD reattachment procedure; and **(D)** DMD reattached.

it involves the pupil. Specifically, they categorized DMD into three groups based on height: under 100 micrometers, between 100 and 300 micrometers, and over 300 micrometers. The length was similarly divided into three categories: under 1 millimeter, between 1 and 2 millimeters, and over 2 millimeters. The extent and pupil involvement were divided into zones: zone 1 for the

central 5 mm, zone 2 for the paracentral 5-8 mm, and zone 3 for the periphery beyond 8 mm. The eyes were then allocated to medical or surgical treatment, with their outcomes assessed in terms of functionality and anatomy.

Mackool and Holtz (11) further refined the understanding of DMD after surgery. They distinguished between planar and non-planar DMD based on the degree of separation in the detached membrane. A planar DMD, with less than 1 mm of separation, typically reattaches on its own and has a more favorable prognosis compared to non-planar DMD, which has a separation greater than 1 mm and usually requires surgical management. Additionally, they identified a peripheral type of DMD located within the 3 mm range from the limbus, which can be monitored without immediate intervention and a combined central and peripheral DMD that necessitates treatment.

In managing DMD, it's crucial to emphasize that prevention measures are more effective than treatment post-facto. A preoperatively low endothelial cell count has been identified as a substantial risk indicator; thus, it is advisable to proceed with heightened vigilance in such instances (7). When performing the primary surgical incision and creating access ports, disposable sharp blades are recommended for their precision and to minimize trauma to surrounding tissue. Furthermore, special care must be taken when inserting cannulas for delivering viscoelastic material and hydrating the corneal incisions with a balanced salt solution (BSS).

Early intervention could be instrumental in preventing complications associated with prolonged DMD. Delaying treatment might result in an excessive loss of endothelial cells, potentially leading to bullous keratopathy. Our technology offers a safe and effective approach for treating early-stage DMD before it progresses to more advanced stages that might require complex procedures such as penetrating keratoplasty, Descemet's Stripping Endothelial Keratoplasty (DSEK), or Descemet Membrane (DM) endothelial keratoplasty.

Our technique is advocated for early cases of DMD. DMD following cataract surgery produces corneal edema. Early surgical treatment should be performed to prevent decreased vision. If the detached Descemet's membrane cannot be reattached with conservative management, the detached Descemet's membrane may become stiff or scrolled, and surgical management may become difficult. If extensive DMD is observed after the surgery, the reattachment procedure should be performed immediately.

In summary, our case samples demonstrate that this technique is a simple and effective approach to managing DMD following cataract surgery. Further study is needed to evaluate its long-term safety in a large number of cases.

Data availability statement

The original contributions presented in the study are included in the article/supplementary material, further inquiries can be directed to the corresponding author.

Ethics statement

The studies involving humans were approved by Ethics Committee of Shanxi Eye Hospital. The studies were conducted in accordance with the local legislation and institutional requirements. Written informed consent for participation was not required from the participants or the participants' legal guardians/next of kin in accordance with the national legislation and institutional requirements. Written informed consent was obtained from the minor(s)' legal guardian/next of kin for the publication of any potentially identifiable images or data included in this article.

Author contributions

WL: Writing – original draft. JM: Writing – review & editing. XT: Writing – review & editing. FC: Writing – review & editing. JL: Writing – review & editing.

Funding

The author(s) declare financial support was received for the research, authorship, and/or publication of this article. The study was supported by the Science Foundation of Shanxi Eye Hospital (C201804) and the Science Foundation of Health and Family Planning Commission of Shanxi Province (2021097).

Conflict of interest

The authors declare that the research was conducted in the absence of any commercial or financial relationships that could be construed as a potential conflict of interest.

Publisher's note

References

1. Kumar DA, Agarwal A, Sivanganam S, Chandrasekar R. Height-, extent-, length-, and pupil-based (HELP) algorithm to manage post-phacoemulsification Descemet membrane detachment. *J Cataract Refract Surg.* (2015) 41:1945–53. doi: 10.1016/j.jcrs.2015.01.020

2. Mahmood MA, Teichmann KD, Tomey KF, Al-Rashed D. Detachment of Descemet's membrane. *J Cataract Refract Surg.* (1998) 24:827–33. doi: 10.1016/S0886-3350(98)80139-9

3. Gatzioufas Z, Schirra F, Löw U, Walter S, Lang M, Seitz B. Spontaneous bilateral late-onset Descemet membrane detachment after successful cataract surgery. *J Cataract Refract Surg.* (2009) 35:778–81. doi: 10.1016/j.jcrs.2008.09.034

4. Couch SM, Baratz KH. Delayed, bilateral Descemet's membrane detachments with spontaneous resolution: implications for nonsurgical treatment. *Cornea.* (2009) 28:1160–3. doi: 10.1097/ICO.0b013e318197eef1

5. Chow VW, Agarwal T, Vajpayee RB, Jhanji V. Update on diagnosis and management of Descemet's membrane detachment. *Curr Opin Ophthalmol*. (2013) 24:356–61. doi: 10.1097/ICU.0b013e3283622873

6. Lee DA, Wilson MR, Yoshizumi MO, Hall M. The ocular effects of gases when injected into the anterior chamber of rabbit eyes. *Arch Ophthalmol*. (1991) 109:571–5. doi: 10.1001/archopht.1991.01080040139045

7. Ti SE, Chee SP, Tan DT, Yang YN, Shuang SL. Descemet membrane detachment after phacoemulsification surgery: risk factors and success of air bubble tamponade. *Cornea*. (2013) 32:454–9. doi: 10.1097/ICO.0b013e318254c045

8. Sharma A, Sharma R, Kulshreshta A, Nirankari VS. Double bubble pneumo-descemetopexy for the management of Descemet membrane detachment: an innovative technique. *Indian J Ophthalmol*. (2023) 71:2234–6. doi: 10.4103/ijo.IJO_1623_22

9. Sharma A, Sharma R, Kulshreshta A, Nirankari V. Manual schism and intracameral air injection for impacted Descemet's membrane detachment. *BMJ Case Rep*. (2023) 16:e253252. doi: 10.1136/bcr-2022-253252

10. Bhatia HK, Gupta R. Delayed-onset descemet membrane detachment after uneventful cataract surgery treated by corneal venting incision with air tamponade: a case report. *BMC Ophthalmol*. (2016) 4:35. doi: 10.1186/s12886-016-0212-6

11. Mackool RJ, Holtz SJ. Descemet membrane detachment. *Arch Ophthalmol*. (1977) 95:459–63. doi: 10.1001/archopht.1977.04450030101014

frontiers | Frontiers in Medicine

TYPE Original Research
PUBLISHED 30 July 2024
DOI 10.3389/fmed.2024.1429791

OPEN ACCESS

EDITED BY
Georgios D. Panos,
Aristotle University of Thessaloniki, Greece

REVIEWED BY
Kaijun Wang,
Zhejiang University, China
Sylvain Roy,
Swiss Federal Institute of Technology Lausanne, Switzerland
Yuanbo Liang,
Affiliated Eye Hospital of Wenzhou Medical University, China

*CORRESPONDENCE
Guoping Kuang
✉ kgp@163.com

RECEIVED 08 May 2024
ACCEPTED 10 July 2024
PUBLISHED 30 July 2024

CITATION
Li Z, Wang A, Zhu M, Zhou N, Liu L, Li Q and Kuang G (2024) CO_2 laser-assisted sclerectomy surgery for secondary open-angle glaucoma after vitrectomy. *Front. Med.* 11:1429791. doi: 10.3389/fmed.2024.1429791

CO_2 laser-assisted sclerectomy surgery for secondary open-angle glaucoma after vitrectomy

Zheng Li[1,2], Ao Wang[1,2], Mingqiong Zhu[1,2], Na Zhou[1,2], Li Liu[1,2], Qiaolian Li[1,2] and Guoping Kuang[3]*

[1]Department of Ophthalmology, The First People's Hospital of Chenzhou, Chenzhou, Hunan, China, [2]Department of Ophthalmology, The Affiliated Chenzhou Hospital, Hengyang Medical School, University of South China, Chenzhou, Hunan, China, [3]Shenzhen Aier Eye Hospital affiliated to Jinan University, Shenzhen, Guangdong, China

Purpose: To explore the efficiency and safety of carbon dioxide (CO_2) laser-assisted sclerectomy surgery (CLASS) in Chinese patients with glaucoma secondary to vitrectomy.

Methods: This retrospective study consisted of 16 eyes from 16 patients with glaucoma secondary to vitrectomy who underwent CLASS and were followed up for 12months. Main outcome measures included preoperative and postoperative intraocular pressure, best corrected visual acuity (BCVA), number of anti-glaucoma medications, and postoperative surgical success rate and complications.

Results: The postoperative IOP and number of anti-glaucoma medications used at all follow-up time point were significantly lower than those preoperatively. The difference in BCVA was not significant before and after surgery. The main complicatios were peripheral anterior synechiae (PAS) and scleral reservoir reduction, which were controlled after neodymium-doped yttrium aluminum garnet (Nd:YAG) laser, 2 (12.50%) patients underwent re-operation. The complete and total success rates at 12 months were 68.75% and 87.50%, respectively.

Conclusion: CLASS is a safe and effective procedure for Chinese patients with glaucoma secondary to vitrectomy. PAS and scleral reservoir reduction is a major contributor to postoperative IOP elevation, and trabecular minimally invasive perforation with the Nd:YAG laser is effective in lowering IOP and increasing scleral cistern volume.

KEYWORDS

secondary glaucoma, post-vitrectomy, CO2 laser, deep sclerectomy, PAS, Nd:YAG laser

1 Introduction

High intraocular pressure (IOP) following vitrectomy is a frequent occurrence in clinical settings, with reported incidence rates in the literature ranging from 25.7 to 56.0% (1, 2). The etiology and pathogenesis of high IOP exhibit complexity and diversity. The majority of high IOP cases occur in the early postoperative stage, primarily due to factors such as the injection of excessive or high-concentration expansive gas, over-injection of silicone oil, inflammation, hemorrhage, and glucocorticoid sensitivity (1). The incidence of late ocular hypertension following surgery is relatively lower compared to the early stage, yet it remains occult and can have a significant impact on visual function. The etiologies of middle and late stage open-angle

glaucoma primarily comprise silicone oil emulsification, elevated resistance of aqueous humor outflow resulting from glucocorticoids in the trabecular meshwork, and neovascular glaucoma during the open-angle phase. On the other hand, the etiologies of middle and late stage angle closure glaucoma encompass pupil block, peripheral anterior synechiae induced by chronic inflammation, and neovascular glaucoma in the angle closure phase.

The treatment of secondary glaucoma following vitrectomy is typically challenging (3). When medications prove ineffective in controlling IOP or are not well-tolerated due to long-term side effects, surgical intervention frequently becomes necessary. Nevertheless, traditional surgical approaches are plagued by a low success rate, numerous complications, and a poor prognosis, categorizing them as refractory glaucoma cases. During routine filtration surgery, the vitreous cavity following vitrectomy is filled with liquid, Penetrating the ocular wall may result in a sudden drop in IOP, collapse and deformation of the eyeball, and even pose risks such as explosive suprachoroidal hemorrhage and choroidal detachment. Furthermore, vitreoretinal surgery can disturb the conjunctiva and trigger a postoperative inflammatory reaction, thereby increasing the risk of long-term filtration bleb scarring, which may ultimately lead to the failure of the filtration surgery. Hence, non-filtering bleb-dependent and non-penetrating glaucoma surgery could be a viable approach for the management of refractory glaucoma post vitrectomy (4, 5). Hence, non-penetrating glaucoma surgery could be a viable approach for the treatment of refractory glaucoma post vitrectomy.

There has recently been renewed interest in non-penetrating deep sclerectomy (NPDS) for glaucoma. NPDS reduced many potential vision-threatening complications by preserving the integrity of the trabeculo-Descemet membrane (TDM) and stabilize the anterior chamber (AC), and improved the safety of conventional filtering procedures (6, 7). However, the NPDS procedure is technically difficult to perform manually, which has limited its popularity. CLASS is an improved version of NPDS that uses a CO2 laser, which is precise and easily strips the deep sclera, unroofs the Schlemm's canal (SC) and leaves the TDM thin enough for aqueous humor percolation. Perforations can be avoided by a CO2 laser because of its unique characteristics and effectiveness in ablating only dry tissues.

CLASS can increase drainning aqueous humor through trabecular meshwork, superior choroidal space, and other routes without bleb dependency, safely reduce IOP, and avoid the common complications associated with filtration surgery. Several studies have confirmed that CLASS is safe and effective for treating primary open angle glaucoma (POAG) with its unique advantages of CO_2 laser (8, 9), while only a few studies have reported the application of some special types of glaucoma such as primary congenital glaucoma, uveitic glaucoma, pseudoexfoliative glaucoma and a case of refractory chidhood glaucoma (6, 10–12). In this study, patients with secondary open-angle glaucoma after vitrectomy who met the inclusion criteria (whose IOP was not better controlled with medications) were treated with the CLASS surgical approach, and the postoperative outcomes were evaluated.

2 Materials and methods

2.1 Participants

This is a retrospective study. A total of 21 cases (21 eyes) that met the inclusion and exclusion criteria were collected between January 2021 and January 2022, of which 5 cases had incomplete data, so 16 eyes were included in this study. All procedures adhered to the tenets of the Declaration of Helsinki and were approved by the hospital's ethics committee (No. 2022024). Written informed consent was provided by all patients before joining the study.

All patients underwent vitrectomy and laser photocoagulation of the retina, and the original vitreous cavity filler was removed. Among them, the primary diseases were central retinal vein occlusion (3 eyes, 18.75%), proliferative diabetic retinopathy (10 eyes, 62.50%), and rhegmatogenous retinal detachment (3 eyes, 18.75%). Intraocular lens in 4 eyes, aphakia in 3 eyes. The vitreous cavity was filled with silicone oil in 7 eyes and with filtered air in 9 eyes. The silicone oil retrieval was performed at the longest time of 14 months and the shortest of 3 months from the time of this surgery, with an average months of 7.26 ± 1.05.

Inclusion criteria: (1) The vitreous cavity filling had been removed and the retina was flat, but the IOP was elevated, which remained at >21 mmHg with the application of maximum tolerable anti-glaucoma medication, glaucomatous optic nerve morphology, and progressive visual field (VF) loss; (2) Willing to undergo surgery and sign the informed consent. (3) Preoperative gonioscopy revealed an open angle and no obstructive lesions on the trabecular meshwork surface. (4) no active inflammation for at least 3 months before the CLASS surgery.

Exclusion criteria: (1) corneal opacity or opaque refractive media that may interfere with optic nerve evaluations. (2) A history of anti-glaucoma surgery. (3) Withdrew from the study or were lost to follow-up. (4) POAG, neovascular glaucoma, pigmentary glaucoma, exfoliation syndrome, and other types of glaucoma.(5) presence of eye trauma or inflammation. (6) severe systemic disease.

2.2 Methods

Superficial anesthesia and bulbar subconjunctival infiltration anesthesia were used. A conjunctival flap with the superior fornix as the base was made, and Tennon's capsule was removed. The scleral flap with size about 5 mm × 5 mm, scleral thickness of about ½, and extending 1 mm into the clear corneal zone was isolated anteriorly to fully expose the trabecular Descemetic window (TDW). After placing a 0.2–0.4 mg/mL mitomycin C (MMC) cotton sheet under the conjunctival and scleral flaps for 2–5 min (the specific time length was determined by the operating surgeon based on the patient's condition), they were rinsed with normal saline. The sclera is ablated by a CO2 laser to make the scleral cisterna. It is recommended that the area of the sclera pool should be at least 4.0 mm × 2.0 mm, with a supporting edge of at least 0.5 mm away from the edge of the sclera flap. The initial ablation power is recommended to be 21 W, and the rectangular laser is excited perpendicular to the sclera. Ablation to reveal the uveal pigment. MMC at a recommended concentration of 0.4 mg/mL is placed at the bottom of the deep sclera pool, and the duration of exposure depends on the patient's condition. It is recommended to remove the cotton piece after 30 s to 2 min and rinse it thoroughly. CO_2 laser ablation of corneoscleral rim site, TDW, arc ablation was selected with ablation size at least 4.0 mm × 1.0 mm, until the Schlemm's canal outer wall was opened and visible aqueous humor percolated, which absorbed the CO_2 laser, preventing deep ablation, leaving a thin corneoscleral trabeculae and uveal trabecular meshwork tissue,

followed by 10–0 polypropylene suture scleral flap and closed suture conjunctival flap.

If the intraoperative IOP was still >30 mmHg, a paracorneal incision puncture was performed intraoperatively before the ablation of Schlemm's canal, slowly lowering the IOP to <30 mmHg.

Postoperatively, prednisolone acetate eye drops were applied for 1 month, every 2 h for the first 3 days, later changed to 1 day four times, and then gradually tapered according to the resolution of the inflammatory reaction for 3 weeks, followed by 1% pilocarpine eye drops for four times 1 day for 3 months.

2.3 Outcome measures

Patients were followed up for 1 day, 1 week, 1 month, 3 months, 6 months, and 12 months after surgery for ocular conditions, including IOP (Goldmann applanation tonometry), fundus examination, BCVA (described in LogMAR form), inflammatory reactions in the anterior segment of the eye, the number of anti-glaucoma drugs, and complications. UBM examination was required at 1, 3, 6, and 12 months after surgery.

If the IOP was >21 mmHg postoperatively and the UBM showed significant narrowing of the scleral cistern, 0.2 mL of 5-fluorouracil (5-FU, 25 mg/mL) solution was administered subconjunctivally and episclerally. Laser goniopuncture (LGP) was performed if the effect was poor, considering insufficient filtration of the aqueous humor through the trabecular meshwork and TDW. If the IOP was still >21 mmHg and UBM demonstrated peripheral anterior synechiae (PAS) to TDM, a laser peripheral iridectomy was indicated.

2.4 Success criteria

Complete success: 5 mmHg < IOP < 18 mmHg, IOP drop ≥20%, and no need for IOP-lowering medication or re-operation postoperatively. Conditional success: 5 mmHg < IOP < 18 mmHg, IOP reduction ≥20%, and the need for IOP-lowering medication postoperatively.

2.5 Statistical analysis

Descriptive statistical results are presented as mean ± standard deviation (SD) or median and range. Gender was assessed with the chi-squared test. Data normality was tested using the Shapiro–Wilk test. Nonparametric tests were applied accordingly when the normal distribution is not satisfied. Quantitative variables were compared using the paired-samples *t*-test (if normally distributed) or the Wilcoxon signed-rank test (otherwise). A *p*-value <0.05 was considered statistically significant. Statistical analysis was performed using SPSS 21.0.

3 Results

3.1 Baseline characteristics and changes in visual acuity

A total of 16 patients (16 eyes) underwent the class procedure, including 10 males (62.50%) and 6 females (37.50%). The age of the cohort was 55. 94 ± 9.84 years (range 37–72 years); IOP ranged from 33.37 ± 4. 92 mmHg (range 26–42 mmHg) preoperatively, and 3.06 ± 0.77 number (range 2–4 number) of IOP-lowering agents were used.

The preoperative logMAR BCVA was 0.80 ± 0.52, and the 1-day, 1-week, 1-month, 3-month, 6-month, and 12-month postoperative logMAR BCVA were 0.80 ± 0.49, 0.76 ± 0.46, 0.75 ± 0.45, 0.78 ± 0.53, 0.77 ± 0.52, and 0.76 ± 0.52, respectively. No significant differences were detected in BCVA between before and after surgery ($H = 0.156$, $p = 1.000$).

3.2 Changes in IOP and medications

The baseline IOP was 33.37 ± 4. 92 mmHg, which decreased significantly to 15.25 ± 3.27 mmHg at 1 M after CLASS and gradually increased to 18.31 ± 4. 93 mmHg at 3 M, due to the occurrence of PAS (2 eye) and scleral cistern narrowing (2 eye). While timely Nd:YAG laser treatment, subconjunctival and scleral subvalvular injections of 5-FU solution can effectively lower and control IOP (Figure 1).

The number of medications was 3.06 ± 0.77 before surgery. Most patients did not require anti-glaucoma medication after surgery. After 12 months of follow-up, the mean anti-glaucoma medications were only 0.19 ± 0.40 ($p < 0.001$ compared to preoperative) (Figure 2).

3.3 Procedural success rate

The complete success rate was 68.75%, and the conditional success rate was 87.5% at 12 months after surgery.

3.4 Postoperative complications

The anterior chamber hemorrhage occurred in 1 eye (6.25%), which disappeared after 1 week. The IOP was >21 mmHg in 1 eye in the first month and 2 eyes in the third month postoperatively. UBM showed PAS to trabecular meshwork Descemet's layer (TDM), which disappeared after Nd: YAG laser treatment and IOP was lowered to the baseline value. At 3 months postoperatively, the IOP fluctuated from 20 to 22 mmHg in 2 eyes, and UBM showed scleral cistern narrowing, which improved after subconjunctival and scleral subvalvular injections of 0.2 mL 5-FU solution (25 mg/mL). During the follow-up period, the IOP was maintained 13-15 mmHg without any medication. At 6 months postoperatively, IOP was >21 mmHg in 3 eyes, UBM showed a significantly small scleral pool, the subconjunctival and scleral subvalvular injections of 5-FU were ineffective, and the IOP decreased to 16 mmHg after treatment with LGP. The scleral pool disappeared in 2 eyes at 12 months postoperatively, the IOP remained high at 35 mmHg after treatment with two types anti-glaucoma drugs, 1 eye underwent a CLASS procedure again, 1 eye underwent intraoperative perforation of the ablated area that required the conversion to trabeculectomy, and the IOP was controlled to normal levels. During the follow-up, no severe sight-threatening or irreversible complications, such as choroidal detachment, malignant glaucoma, and endophthalmitis, occurredin all patients.

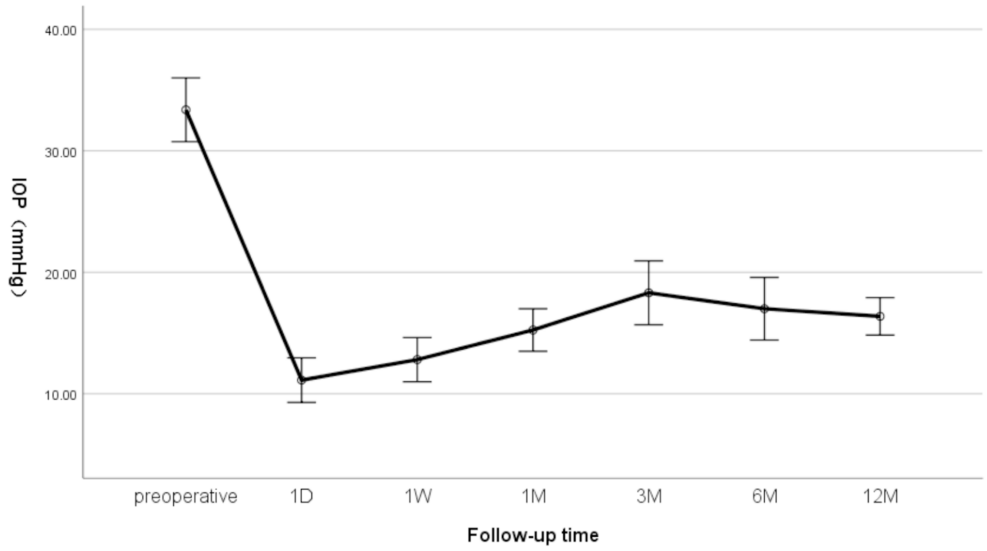

FIGURE 1
Changes in IOP at preoperative and 1 day (D), 1 week (W), and 1, 3, 6, and 12 months (M) after CLASS.

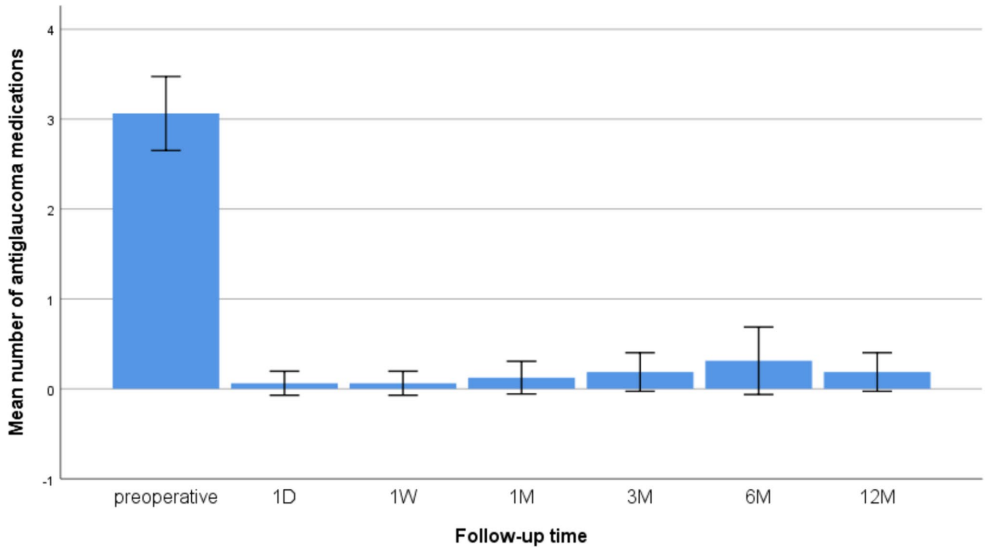

FIGURE 2
Changes in the mean number of anti-glaucoma medications at preoperative and 1 D, 1 W, and 1, 3, 6, and 12 M after CLASS.

By the end of follow-up, 6 individuals showed significantly smaller or disappearing scleral cisternae, including 3 eye need for 1–2 types anti-glaucoma medication, the IOP was maintained 14-16 mmHg, 2 eye underwent anti-glaucoma procedure again. The difference in age was statistically significant compared to patients without this complication ($t = 2.466$, $p = 0.027$) (Table 1).

4 Discussion

In this study, it is presumed that the increased IOP may be attributed to alterations in the trabecular meshwork and augmented resistance in aqueous humor outflow, which are induced by postoperative inflammation and glucocorticoid use. CLASS was applied to this specific type of refractory glaucoma secondary to open-angle glaucoma after vitrectomy (watery eye) and achieved good results, with the complete and success rates of 68.75 and 87.50%, respectively. Strikingly, no serious sight-threatening or irreversible complications, such as choroidal detachment, malignant glaucoma, and endophthalmitis, occurred throughout the procedure.

BCVA improved in 37.5% of the affected eyes at the last follow-up in our series, although the preoperative and postoperative visual acuity did not differ statistically significantly. Also, the number of anti-glaucoma drugs were significantly lower than before surgery.

TABLE 1 Comparison of patients with reduction of the scleral reservoir after CLASS.

	With the reduction of the scleral reservoir	Without reduction of the scleral reservoir	*p*-values
N	6	10	
Female/Male	1/5	3/7	0.551*
Age (years)	51.17 ± 10.16	62.00 ± 7.42	0.027†
Baseline IOP	34.00 ± 6.48	33.00 ± 4.08	0.708†

*Chi-squared test. †Independent sample *t*-test.

CLASS is an improved version of the difficult manual procedure of NPDS that uses the unique characteristic of CO2 laser to ablate only the dry scleral tissue in a precise and efficient manner. Once the outer wall of Schlemm's canal (SC) is opened, the CO2 laser becomes ineffective due to aqueous percolation; consequently, excessive tissue ablation is prevented and the inner wall of the SC is kept intact, avoiding penetration into the anterior chamber. This is due to the wavelength of the laser that interacts specifically with the molecules of water. CLASS with its unique aqueous humor drainage pathway, avoid the sudden drop of IOP after trabeculectomy surgery. Also, it is minimally invasive, easy to operate, has fewer complications, and has been gradually applied to some refractory glaucomas (13, 14).

The results of this study confirmed that the CLASS procedure is effective in favorably lowering surgical complications, reducing anti-glaucoma medications use and accelerating visual recovery, which is consistent with previous studies (4, 15, 16). However, details of the CLASS procedure and postoperative follow-up are essential. First, the Tennon's capsule needs to be removed to reduce the scarring possibility in the scleral cistern. Second, the extent, depth, and energy magnitude of laser ablation are major issues in addition to wide range and high energy, which causes secondary damage and coagulation of surrounding tissues. A deep ablation depth has the potential to open the Schlemm canal's inner wall, creating TDM microperforations, and requiring a trabeculectomy. None of the above complications occurred in this study, and our experience is that arcuate ablation opens the Schlemm canal's outer wall. In the event of aqueous humor leakage, the energy of ablation needs to be reduced or the aqueous humor leakage site avoided, and the ablation of the surrounding tissue continued until the Schlemm canal outer wall is fully opened. Despite such improvement, postoperative complications, such as PAS seemed to be inevitable after CLASS. Zhang et al. observed a 30.0% PAS incidence in the CLASS group (15). Compared to Caucasian patients (16, 17), relatively higher rates of PAS were detected in Chinese patients. In this study, the incidence of PAS was 18.75%, significantly lower than the above-mentioned studies. A total of 3 patients experienced different degrees of PAS at 1 and 3 M postoperatively, which was the main cause of IOP elevation at the early-and middle-stage after CLASS. We also found that the variation of PAS incidence was consistent with the fluctuation of success rate, indicating that follow-up after CLASS was critical work for postoperative management.

Studies have shown that CLASS is prone to PAS after surgery, with iris incarceration, scleral cistern narrowing, and increased aqueous humor resistance via trabecular meshwork or TDW (11, 18, 19). Therefore, some studies proposed to modify the CLASS procedure, and hence laser peripheral iridectomy (LPI) and argon laser peripheral iridoplasty (ALPI) were performed 24–72 h before the operation (10, 11). None were preoperatively pretreated in this study, considering the following: first, not all patients who were not laser prophylactic preoperatively developed a PAS or iris incarceration postoperatively. This was also confirmed in the present study, wherein the incidence of PAS was only 18.75%. Second, guaranteeing the consistency of the location of preoperative laser therapy with the area of intraoperative laser ablation is difficult. The pervious and present studies confirmed that PAS could occur at any time after CLASS (11, 20); hence, regular follow-up and personalized postoperative management are more crucial for these patients than prevention.

No iris incarceration occurred postoperatively in our cases. Analyzing the reasons for the occurrence of iris incarceration, we speculated that this patient developed microperforation during the surgery, and previous laser intervention might cause small tears in the TDW, which aggravated iris incarceration. Therefore, meticulous ablation and energy adjustment were critical to avoid perforation during the surgery. Moreover, IOP was maintained at <30 mmHg preoperatively, and intraoperative anterior chamber puncture was performed to slowly reduce IOP, and the scleral flap was sutured tightly to avoid early postoperative hyperfiltration. Miotics were used routinely for ≥3 months postoperatively, and the massage of the eyeballs was avoided. Second, the local inflammatory response may accelerate iris incarceration. This group of cases consisted of patients with glaucoma secondary to vitrectomy, pre-existing fundus disease, and putative inflammatory factors in the eye from the trauma of vitrectomy surgery (21). The thermal damage to the surrounding tissues by laser ablation in CLASS intraoperatively can aggravate the inflammatory response. Therefore, postoperative anti-inflammation is critical.

Three cases in our series developed PAS in patients <45 years, consistent with previous studies that concluded that younger age is more likely to have postoperative complications in CLASS (20). The current study also showed that younger patients had a higher chance of developing significant scleral pool narrowing or even disappearance after CLASS, and the mean age of the 6 patients was (51.17 ± 10.16) years, which was lower than the mean age of our cases. Asian glaucoma patients, including Chinese, are characterized by crowded anterior chamber structures, intractable ocular hypertension, and easy scarring after surgery, especially young patients in whom postoperative wound fibrous proliferation is active. Therefore, prophylactic LPI and argon ALPI may be considered before CLASS for patients with high-risk interatrial angle and young glaucoma (10), and postoperative enhanced anti-inflammatory and close follow-up will improve the success rate of the procedure.

Nevertheless, the present study had several limitations. First, the sample size was small and the follow-up period was limited. Therefore, a prospective randomized controlled study with longer follow-up is necessary. Second, the morphological classification of the filtration bleb and the quantitative analysis of the scleral pool remain unclear in their correlation with IOP after CLASS. Despite these limitations, we distinguished PAS from iris incarceration by UBM examination and provided personalized timely interventions that were found to be effective in controlling IOP clinically.

To conclude, CLASS is a safe and effective approach for Chinese patients with secondary glaucoma after vitrectomy. It not only controls the IOP and reduces the dependence on drugs, but also has obvious

advantages in the control of surgical complications and postoperative visual recovery. PAS and reduction of the scleral reservoir is a common cause of postoperative IOP elevation. A UBM-guided individualized Nd:YAG laser intervention resolves PAS at the early-middle stage after CLASS and achieves further IOP reduction as required, which helps in improving the long-term outcomes after CLASS.

Data availability statement

The original contributions presented in the study are included in the article/supplementary material, further inquiries can be directed to the corresponding author/s.

Ethics statement

The studies involving humans were approved by the Institutional Review Board/Ethics Committee of the First People's Hospital of Chenzhou. The studies were conducted in accordance with the local legislation and institutional requirements. The participants provided their written informed consent to participate in this study. Written informed consent was obtained from the individual(s) for the publication of any potentially identifiable images or data included in this article.

Author contributions

ZL: Data curation, Formal analysis, Funding acquisition, Methodology, Resources, Software, Validation, Writing – original draft. AW: Methodology, Writing – original draft, Supervision. MZ: Data curation, Formal analysis, Writing – original draft. NZ: Formal analysis, Writing – original draft. LL: Supervision, Writing – review & editing. QL: Writing – review & editing, Data curation, Formal analysis. GK: Conceptualization, Funding acquisition, Investigation, Project administration, Supervision, Writing – review & editing.

Funding

The author(s) declare that financial support was received for the research, authorship, and/or publication of this article. This research was supported by the Chenzhou First People's Hospital, China (No. 2020–23), and Hunan Natural Science Foundation，China (No. 2024JJ7033).

Acknowledgments

We would thank Xiaoxia Luo for performing and evaluating some of the image.

Conflict of interest

The authors declare that the research was conducted in the absence of any commercial or financial relationships that could be construed as a potential conflict of interest.

Publisher's note

References

1. Kornmann HL, Gedde SJ. Glaucoma management after vitreoretinal surgeries. *Curr Opin Ophthalmol*. (2016) 27:125–31. doi: 10.1097/icu.0000000000000238

2. Brasil MV, Rockwood EJ, Smith SD. Comparison of silicone and polypropylene ahmed glaucoma valve implants. *J Glaucoma*. (2007) 16:36–41. doi: 10.1097/01.ijg.0000243477.82779.31

3. Wangsupadilok B, Tansuebchueasai N. Pars planectomy: preliminary report of a new glaucoma filtering technique in vitrectomized eyes. *Clin Ophthalmol*. (2021) 15:791–8. doi: 10.2147/OPTH.S299347

4. Alagöz N, Taskoparan S, Altan AC, Solmaz B, Basgil Pasaoglu I, Basarır B, et al. Pressure restoration and visual recovery time in hypotony after trabeculectomy. *Int Ophthalmol*. (2021) 41:3183–90. doi: 10.1007/s10792-021-01883-1

5. Dada T, Bhartiya S, Vanathi M, Panda A. Pars plana ahmed glaucoma valve implantation with triamcinolone-assisted vitrectomy in refractory glaucomas. *Indian J Ophthalmol*. (2010) 58:440–2. doi: 10.4103/0301-4738.67068

6. Elhofi A, Helaly HA. Non-penetrating deep sclerectomy versus trabeculectomy in primary congenital glaucoma. *Clin Ophthalmol*. (2020) 14:1277–85. doi: 10.2147/OPTH.S253689

7. Xiao JY, Wang YL. Efficacy and safety of non-penetrating glaucoma surgery with phacoemulsification versus non-penetrating glaucoma surgery: a meta-analysis. *Int J Ophthalmol*. (2021) 14:1970–8. doi: 10.18240/ijo.2021.12.24

8. Zhang Y, Mao J, Zhou Q, Li L, Zhang S, Bian A, et al. Comparison of long-term effects after modified CO_2 laser-assisted deep sclerectomy and conventional trabeculectomy in chinese primary open-angle glaucoma. *Ophthalmol Ther*. (2022) 11:321–31. doi: 10.1007/s40123-021-00413-7

9. Yu X, Chen C, Sun M, Dong D, Zhang S, Liu P, et al. CO_2 laser-assisted deep sclerectomy combined with phacoemulsification in patients with primary open-angle glaucoma and cataract. *J Glaucoma*. (2018) 27:906–9. doi: 10.1097/IJG.0000000000001056

10. Xiao J, Zhao C, Zhang Y, Liang A, Qu Y, Cheng G, et al. Surgical outcomes of modified CO_2 laser-assisted sclerectomy for uveitic glaucoma. *Ocul Immunol Inflamm*. (2022) 30:1617–24. doi: 10.1080/09273948.2021.1924385

11. Zhang Y, Cheng G. Modified CO_2 laser-assisted sclerectomy surgery in chinese patients with primary open-angle glaucoma and pseudoexfoliative glaucoma: a 2-year follow-up study. *J Glaucoma*. (2020) 29:367–73. doi: 10.1097/IJG.0000000000001460

12. Zhang Y, Bian AL, Liang AY, Mo F, Cheng GW. A case of refractory childhood Glaucoma secondary to Weill-Marchesani syndrome: management with combined CO(2) laser-assisted Sclerectomy surgery and trabeculectomy. *Chin Med Sci J*. (2022) 37:159–63. doi: 10.24920/003956

13. Xiao J, Zhao C, Zhang Y, Qu Y, Liang A, Zhang M, et al. Results of modified CO_2 laser-assisted sclerectomy monotherapy versus trabeculectomy combination therapy in the eyes with uveitic glaucoma. *Lasers Med Sci*. (2022) 37:949–59. doi: 10.1007/s10103-021-03339-5

14. Yuan MZ, Chen H, Cao D, et al. CO_2 laser-assisted sclerectomy surgery and trabeculectomy combination therapy in peters' anomaly-related glaucoma: a case report. *Int J Ophthalmol*. (2022) 15:666–8. doi: 10.18240/ijo.2022.04.22

15. Zhang H, Tang Y, Yan X, Geng Y, Li F, Tang G, et al. CO_2 laser-assisted deep sclerectomy surgery compared with trabeculectomy in primary open-angle glaucoma: two-year results. *J Ophthalmol*. (2021) 2021:1–9. doi: 10.1155/2021/6639583

16. Jankowska-Szmul J, Dobrowolski D, Wylegala E. CO(2) laser-assisted sclerectomy surgery compared with trabeculectomy in primary open-angle glaucoma and exfoliative glaucoma. A 1-year follow-up. *Acta Ophthalmol*. (2018) 96:e582–91. doi: 10.1111/aos.13718

17. Cutolo CA, Bagnis A, Scotto R, Bonzano C, Traverso CE. Prospective evaluation of CO_2 laser-assisted sclerectomy surgery (class) with mitomycin c. *Graefes Arch Clin Exp Ophthalmol*. (2018) 256:181–6. doi: 10.1007/s00417-017-3844-1

18. Ho D, Perera SA, Hla MH, Ho CL. Evaluating CO_2 laser-assisted sclerectomy surgery with mitomycin c combined with or without phacoemulsification in adult asian glaucoma subjects. *Int Ophthalmol*. (2021) 41:1445–54. doi: 10.1007/s10792-021-01707-2

19. Geffen N, Mimouni M, Sherwood M, Assia EI. Mid-term clinical results of co2 laser-assisted sclerectomy surgery (class) for open-angle glaucoma treatment. *J Glaucoma*. (2016) 25:946–51. doi: 10.1097/IJG.0000000000000437

20. Chen M, Gu Y, Yang Y, Zhang Q, Liu X, Wang K. Management of intraocular pressure elevation after CO_2 laser-assisted sclerectomy surgery in patients with primary open-angle glaucoma. *Front Med*. (2021) 8:806734. doi: 10.3389/fmed.2021.806734

21. Liu Z, Fu G, Liu A. The relationship between inflammatory mediator expression in the aqueous humor and secondary glaucoma incidence after silicone oil tamponade. *Exp Ther Med*. (2017) 14:5833–6. doi: 10.3892/etm.2017.5269

frontiers | Frontiers in Medicine

TYPE Systematic Review
PUBLISHED 31 July 2024
DOI 10.3389/fmed.2024.1405261

OPEN ACCESS

EDITED BY
Georgios D. Panos,
Aristotle University of Thessaloniki, Greece

REVIEWED BY
Norlina Ramli,
University of Malaya, Malaysia
Pingting Zhong,
Guangdong Provincial People's Hospital, China

*CORRESPONDENCE
Yu He
✉ 306244843@qq.com

RECEIVED 22 March 2024
ACCEPTED 22 July 2024
PUBLISHED 31 July 2024

CITATION
He C-Z, Lu S-J, Zeng Z-J, Liu J-Q, Qiu Q, Xue F-L and He Y (2024) The efficacy and safety of anti-vascular endothelial growth factor combined with Ahmed glaucoma valve implantation in the treatment of neovascular glaucoma: a systematic review and meta-analysis.
Front. Med. 11:1405261.
doi: 10.3389/fmed.2024.1405261

The efficacy and safety of anti-vascular endothelial growth factor combined with Ahmed glaucoma valve implantation in the treatment of neovascular glaucoma: a systematic review and meta-analysis

Chang-Zhu He[1], Song-Jie Lu[1], Zhao-Jun Zeng[1], Jun-Qiao Liu[1], Qin Qiu[1], Fu-Li Xue[1] and Yu He[2]*

[1]Chengdu University of Traditional Chinese Medicine, Chengdu, Sichuan, China, [2]Department of Ophthalmology, Chengdu First People's Hospital/Chengdu Integrated TCM and Western Medicine Hospital, Chengdu, Sichuan, China

Background: The intraocular injections of anti-vascular endothelial growth factor (anti-VEGF) demonstrates significant efficacy in inhibiting the formation of ocular neovascularization in neovascular glaucoma (NVG). Ahmed glaucoma valve implantation (AGVI) is extensively employed for the management of diverse glaucoma types.

Objective: To further evaluate the efficacy and safety of anti-VEGF combined with AGVI in the treatment of neovascular glaucoma.

Methods: A thorough search for randomized controlled trials (RCTs) was conducted across eight databases: PubMed, EMBASE, the Cochrane Library, Web of Science, China National Knowledge Infrastructure, Wanfang, SinoMed, and VIP. The search period was set from the inception of each database until March 2, 2024, to identify RCTs investigating the effectiveness and safety of combining AGVI with anti-VEGF therapy for NVG. We used the Cochrane Risk of Bias Assessment Tool to evaluate the quality of the literature and performed statistical analysis using Stata 15.0 software.

Results: Fourteen RCTs were included in this study. Compared with AGVI alone, the combination of anti-VEGF drugs and AGVI can reduce postoperative intraocular pressure (IOP) at 1 week [WMD = −4.03, 95% CI (−5.73, −2.34), $p < 0.001$], 1 month [WMD = −5.39, 95% CI (−7.05, −3.74), $p < 0.001$], 3 months [WMD = −6.59, 95% CI (−7.85, −5.32), $p < 0.001$], 6 months [WMD = −4.99, 95% CI (−9.56, −0.43), $p = 0.032$], and more than 12 months [WMD = −3.86, 95% CI (−6.82, −0.90), $p = 0.011$], with a higher Effective rate [RR = 1.27, 95% CI (1.18, 1.37), $p < 0.001$], decreased incidence of postoperative hyphema [RR = 0.24, 95% CI (0.15, 0.39), $p < 0.001$], reduced use of postoperative antiglaucoma medications [WMD = −0.48, 95% CI (−0.61, −0.35), $p < 0.001$], and decreased aqueous humor VEGF levels [SMD = −2.84, 95% CI (−4.37, −1.31), $p < 0.001$].

Conclusion: In comparison to AGVI alone, the combination of AGVI with anti-VEGF therapy has better effects in reducing IOP at various time intervals, diminishing postoperative antiglaucoma medication requirements and reducing aqueous humor VEGF levels. Furthermore, it effectively minimizes the incidence

of postoperative hyphema. Nevertheless, due to the variability in the quality of the trials included, further high-quality experiments will be required in the future to substantiate this conclusion.

Systematic review registration: PROSPERO, identifier CRD42024519862, https://www.crd.york.ac.uk/prospero/display_record.php?ID=CRD42024519862.

KEYWORDS

Ahmed glaucoma valve implantation, anti-vascular endothelial growth factor, neovascular glaucoma, meta-analysis, systematic review

1 Introduction

Neovascular glaucoma (NVG) constitutes a form of secondary glaucoma characterized by the emergence of rubeosis iridis and elevated intraocular pressure (IOP), which poses a potential threat to vision impairment (1). Chronically red and painful eyes are the first visible clinical symptoms of NVG, however, in younger patients, these symptoms may be absent owing to insufficient endothelial functional reserve (2). More importantly, NVG typically represents an end-stage disease associated with the potential for blindness, persistent pain, and loss of the eyeball (3). The primary etiologies of NVG include diabetic retinopathy (DR), ischemic central retinal vein occlusion (CRVO), and ocular ischemic syndrome (OIS) (4). According to relevant reports, about 40 to 45% of eyes affected by ischemic retinal vein occlusion are predisposed to developing NVG, with 80% of these cases manifesting within a timeframe of 6 to 8 months (5). Retinal ischemia leads to the release of vascular endothelial growth factors (VEGF), which diffuse into the aqueous humor and anterior segment, triggering the formation of neovascularization in the iris and anterior chamber angle, this process impedes the outflow of aqueous humor, leading to elevated IOP (6). Studies reveal a significant increase in VEGF levels in the aqueous humor of NVG patients, suggesting that VEGF plays a crucial role in mediating active intraocular neovascularization in patients with ischemic retinal diseases (7). Based on data from the European Union, the prevalence of NVG in Europe ranges from 75,000 to 113,000 individuals, constituting 3.9% of the total glaucoma cases (8). In the United States, approximately 17,500 diabetic patients suffer from iris neovascularization, with the majority experiencing proliferative diabetic retinopathy, and the incidence of iris neovascularization is as high as 65% in these patients (9).

The Ahmed valve features a unidirectional pressure-sensitive control mechanism, limiting drainage device operation to IOP levels between 8 and 14 mmHg, thereby mitigating excessive postoperative aqueous humor drainage (10). Therefore, compared to traditional trabeculectomy, the Ahmed valve is more suitable for refractory glaucoma (11). Unfortunately, research reports indicate that AGVI is associated with a high rate of encapsulation and inadequate intraocular pressure reduction (IOPR), necessitating ongoing glaucoma medication postoperatively (12). Anti-VEGF drugs such as ranibizumab and bevacizumab have been demonstrated to efficiently reduce neovascularization progression and leakage in ocular neovascular disease (13). Relevant studies also indicate that supplementary anti-VEGF therapy could be advantageous for neovascular glaucoma, given its anti-angiogenic properties (14).

Among patients with NVG undergoing AGVI, there is still a lack of consensus on the necessity of intraocular injections of anti-VEGF. Several retrospective studies have found that combined AGVI with anti-VEGF drugs can lower postoperative IOP compared to AGVI alone, reduce the use of postoperative antiglaucoma medications, and decrease the occurrence of adverse events (15, 16). Nevertheless, comparative studies by Tang et al. (17) and Ma et al. (18) found that the use of anti-VEGF drugs did not affect the final outcome of AGVI. Currently, there have been several randomized controlled trials (RCTs) comparing the postoperative outcomes of AGVI alone versus AGVI combined with intraocular injections of anti-VEGF for NVG, however, few systematic reviews or meta-analyses have been performed to compare their clinical effects and safety and most of the relevant meta-analyses mainly focus on retrospective studies. Additionally, existing meta-analyses have not examined the different anti-VEGF drugs, nor have they addressed the long-term effects of combining anti-VEGF drugs with AGVI. This study separately discussed three common anti-VEGF drugs (ranibizumab, bevacizumab, and conbercept) and examined their effects when combined with AGVI at intervals of 1 week, 1 month, 3 months, 6 months, and beyond 12 months. Subgroup analysis was also performed on follow-up time to investigate the long-term efficacy of VEGF drugs combined with AGVI. To update the existing data and better evaluate the efficacy and safety of AGVI combined with intraocular injections of anti-VEGF for NVG, we conducted this systematic review to compare the postoperative IOP, effectiveness, number of postoperative anti-glaucoma medications used, the incidence of postoperative hyphema and aqueous humor VEGF levels between the two groups. The objective is to aid clinical ophthalmologists in choosing more appropriate treatment for patients with NVG.

2 Methods

The study was registered with PROSPERO (registration number: CRD42024519862) and followed the PRISMA (Preferred Reporting Items for Systematic Reviews and Meta-Analyses) guidelines, consistent with the recommendations of the Cochrane Collaboration (19, 20). Details of the PRISMA checklist can be found in Supplementary materials S1.

2.1 Search strategy

PubMed, EMBASE, the Cochrane Library, Web of Science, China National Knowledge Infrastructure, Wanfang Database, SinoMed, and

the VIP Database were systematically searched for eligible studies from their inception up to March 2, 2024, by two independent authors (CZH and SJL). The search was conducted without any restrictions based on race, age, or language. We employed medical subject headings (MeSH) along with free terms and a set of keywords to formulate search strategies. For example, when searching English databases, we selected the following five core components: (1) Glaucoma Drainage Implants (e.g., Aqueous Humor Shunt, Shunt, Aqueous Humor, Shunts, Aqueous Humor, Glaucoma Filtration Implant, Aqueous Shunt, Shunt, Aqueous Shunts, Aqueous, Aqueous Humor Shunts, Aqueous Shunts, Glaucoma Drainage Implant, Drainage Implant, Glaucoma, Drainage Implants, Glaucoma, Implant, Glaucoma Drainage, Implants, Glaucoma Drainage, Glaucoma Filtration Implants, Filtration Implant, Glaucoma, Filtration Implants, Glaucoma, Implant, Glaucoma Filtration, Implants, Glaucoma Filtration); (2) vascular endothelial growth factor (e.g., VEGFs); (3) Ranibizumab (e.g., Lucentis, RhuFab V2, V2, RhuFab); (4) Bevacizumab (e.g., Avastin); (5) Glaucoma, Neovascular (e.g., Glaucomas, Neovascular, Neovascular Glaucoma, and Neovascular Glaucomas). Additionally, relevant articles from initial search meta-analyses and grey literature were reviewed and included. Detailed retrieval procedures are outlined in Supplementary materials S2.

2.2 Inclusion criteria

1. *Type of study*: RCTs of intraocular injections of anti-VEGF combined with AGVI in the treatment of NVG.
2. *Type of participants*: Patients diagnosed as NVG according to any authoritative clinical guidelines, such as Neovascular glaucoma--etipathogeny and diagnosis (21) or Consensus of Chinese experts on the diagnosis and treatment of neovascular glaucoma (22).
3. *Type of interventions and controls*: All patients diagnosed with NVG underwent AGVI treatment. In the experimental group, NVG patients received both AGVI therapy and intraocular injections of anti-VEGF, including ranibizumab, bevacizumab, and conbercept. We did not impose restrictions on the timing of intraocular anti-VEGF injections, whether administered preoperatively or postoperatively, both injections met the inclusion criteria.
4. *Type of outcomes*: Included studies examined at least one of the following outcomes:

The primary outcome:

a. Intraocular pressure (IOP): The IOP measurements obtained with the Goldmann applanation tonometer (GAT), the non-contact tonometer (NCT), and the rebound tonometer (RBT) all met the inclusion criteria for this study (23). The study selected IOP data at 1 week, 1 month, 3 months, 6 months, and more than 12 months postoperatively for follow-up.

b. Incidence of postoperative hyphema: Hyphema, a potential postoperative complication of ophthalmic surgery, was defined as hemorrhage in the anterior chamber sufficient to form a layered clot, even if minimal. Eyes with only suspended red blood cells in the anterior chamber, without forming a layered clot, were not considered to have hyphema (24). The incidence of postoperative hyphema is primarily determined by the proportion of participants experiencing postoperative hyphema to the total number of participants in the experimental or control group.

c. Effective rate: The effective rate was determined by the proportion of participants with significantly improved or recovered symptoms relative to the total number in the test or control group.

The second outcome:

d. Postoperative antiglaucoma medication requirements: The primary outcome measure of this study revolves around quantifying the quantity of antiglaucoma medications required by NVG patients post-surgery.

e. Aqueous humor VEGF levels: VEGF stimulated the growth of retinal endothelial cells *in vitro*, as did vitreous fluid containing measurable VEGF (25).

2.3 Exclusion criteria

Exclusion criteria comprise the following criteria: (1) The animal experiments, review articles, case reports, meta-analysis, any non-RCTs were ruled out. (2) The NVG patients who did not use Ahmed glaucoma drainage devices and intraocular injection of anti-VEGF would be excluded. (3) RCTs without relevant outcomes or complete data were not available. (4) Patients with concurrent intraocular diseases that could impact surgical outcomes, including congenital vitreoretinopathies and traumatic retinal detachment.

2.4 Data extraction

The two authors (CZH and SJL) conducted initial screening by reviewing the titles and abstracts of the literature, adhering to predefined inclusion and exclusion criteria. Subsequently, the final appropriate literature were identified through comprehensive reading of the full texts. The author, year, region, sample, age of the patient, intervention and control, injection dose and outcomes were extracted independently by two authors (CZH and SJL). When consensus could not be solved by discussion, the third author (YH) were consulted. When part of the data was missing from the included literature, the first author or corresponding author was contacted to acquire the necessary information.

2.5 Assessment of risk of bias

Two authors (CZH and SJL) independently assessed the risk of bias of the included studies using the Cochrane Risk of Bias Version 2 (RoB 2) assessment tool (26). RoB 2 includes the following six assessment items: (1) the random sequence generation, (2) deviations from the intended interventions, (3) missing outcome data, (4) measurement of the outcome, (5) selection of the reported result, and (6) overall bias. Each section is assessed as "low risk," "some concern," or "high risk," based on the specific circumstances of the article.

2.6 Statistical analysis

The study employed Stata15.0 software for conducting a meta-analysis of the data. For continuous variables, we used the standard

mean difference (SMD) or weighted mean difference (WMD) and 95% confidence interval for analysis. For binary variables, we used the risk ratio (RR) and 95% confidence interval for analysis. Considering the great differences in research methodologies, basic characteristics of NVG patients, surgical proficiency of the surgeon in each study was inevitable, statistical heterogeneity was disregarded. As a result, a random-effects model was employed for analysis on all data, irrespective of whether I2 was less than 50%. Additionally, for further investigation, we also conducted subgroup analyses on different anti-VEGF drugs. For all statistical procedures, $p < 0.05$ was considered statistically significant.

2.7 Sensitivity analysis

To evaluate the robustness of our findings, we conducted a sensitivity analysis, systematically excluding individual studies in sequence. If the exclusion of an article influenced the outcome and reversed the conclusion, we meticulously scrutinized the complete text of the article to ascertain its role as a potential source of heterogeneity. Conversely, this suggested the stability of the study's findings.

2.8 Assessment of reporting bias

When the number of included studies is greater than or equal to 10, a funnel plot is employed. Initially, visual assessment is utilized to evaluate potential publication bias. Based on the generated funnel plot, the Begg' test or the Egger' test was both further utilized to examine publication bias.

3 Results

3.1 Study selection

Following the initial database search, 344 pieces of literature were retrieved, subsequently, after eliminating duplicate documents, the total has been reduced to 230 pieces. Through reviewing the titles and abstracts, 169 literature pieces were deemed ineligible for inclusion. These exclusions comprised 18 studies involving animal experiments, 23 conference or case reports, 53 non-RCTs, and 75 studies disqualified due to intervention measures not meeting the stipulated criteria. Finally, A total of 14 literature pieces (27–40) met the inclusion criteria. Among the 61 excluded pieces, 22 lacked pertinent outcome measures (including IOP, Incidence of postoperative hyphema, effective rate, postoperative antiglaucoma medication requirements, BCVA and aqueous humor VEGF levels), 13 did not adhere to randomized controlled trial protocols, 8 were retrospective studies and 4 were unable to furnish valid data. The specific literature screening process is shown in Figure 1.

3.2 Study characteristics

Among the 14 studies incorporated, one study (27) was from Egypt, one (28) from Iran, one (29) from Brazil, and the remaining studies were all from China. The sample sizes in these studies varied from 9 to 48, spanning the years 2013 to 2022. Moreover, all the studies incorporated were characterized as RCTs. The treatments assessed were as follows: 3 trials (27–29) assessed the effectiveness of AGVI in combination with bevacizumab, while 7 studies (30–36) primarily examined the therapeutic effects of AGVI combined with ranibizumab. Additionally, 3 studies (37–39) concentrated on conbercept, whereas the remaining one did not specify the type of anti-VEGF drug used in the experimental group. Two studies (28, 29) favored postoperative administration, the remaining studies uniformly adopted preoperative administration of anti-VEGF drugs. Three studies (27, 29, 38) explicitly stated that all patients underwent pan-retinal photocoagulation (PRP) therapy, while three others (30, 33, 34) indicated that only a subset of patients received PRP treatment. The remaining studies provided detailed accounts of the utilization of PRP. One study (29) documented three administrations of anti-VEGF drugs, another study (38) utilized them twice, whereas the remaining investigations employed these drugs once. 4 studies (27–29, 33) had a follow-up period of 12 months or more, with the longest extending to 24 months. 3 studies (32, 34, 36) had a 6-month follow-up period, while one study (31) did not report specific follow-up durations. The remaining studies had follow-up periods of 3 months or less, with the shortest being just 1 week. The characteristics of the included studies were detailed in Table 1.

3.3 Risk of bias

The risk of bias in the included RCTs is listed in Figure 2. In the 14 included studies, two (35, 38) utilized the random number table method, while the remaining did not provide specific descriptions of the random allocation method. Only one study (28) explicitly mentioned blinding, while the others were considered to potentially lack blinding, allowing participants and caregivers to know the allocated interventions. One study (28) had missing data, but the data in the other studies were complete, with the missing data falling within an acceptable range. None of the articles deviated from the expected interventions, nor did they selectively report results (Table 2).

3.4 Effects of interventions

3.4.1 IOP at 1 week postoperatively

Six RCTs (27, 28, 30, 31, 37, 39), comprising 368 eyes, investigated the effects of combined AGVI with anti-VEGF drugs versus AGVI alone on IOP at 1 week postoperatively. Pooled results showed that AGVI combined with anti-VEGF was more effective in lowering IOP in NVG patients 1 week after surgery compared to AGVI alone [WMD = −4.03, 95% CI (−5.73, −2.34), $p < 0.001$]. The results of subgroup analysis indicated that the ranibizumab group, bevacizumab group and conbercept group all demonstrated superior efficacy in reducing intraocular pressure at 1 week postoperatively compared to AGVI alone ([WMD = −6.24, 95% CI (−7.35, −5.13), $p < 0.001$], [WMD = −2.71, 95% CI (−4.55, −0.87), $p = 0.004$] and [WMD = −3.20, 95% CI (−5.07, −1.33), $p = 0.001$] respectively) (Figure 3A).

3.4.2 IOP at 1 month postoperatively

Six RCTs (27, 32, 33, 37, 38, 40), comprising 401 eyes, investigated the effects of combined AGVI with anti-VEGF drugs versus AGVI

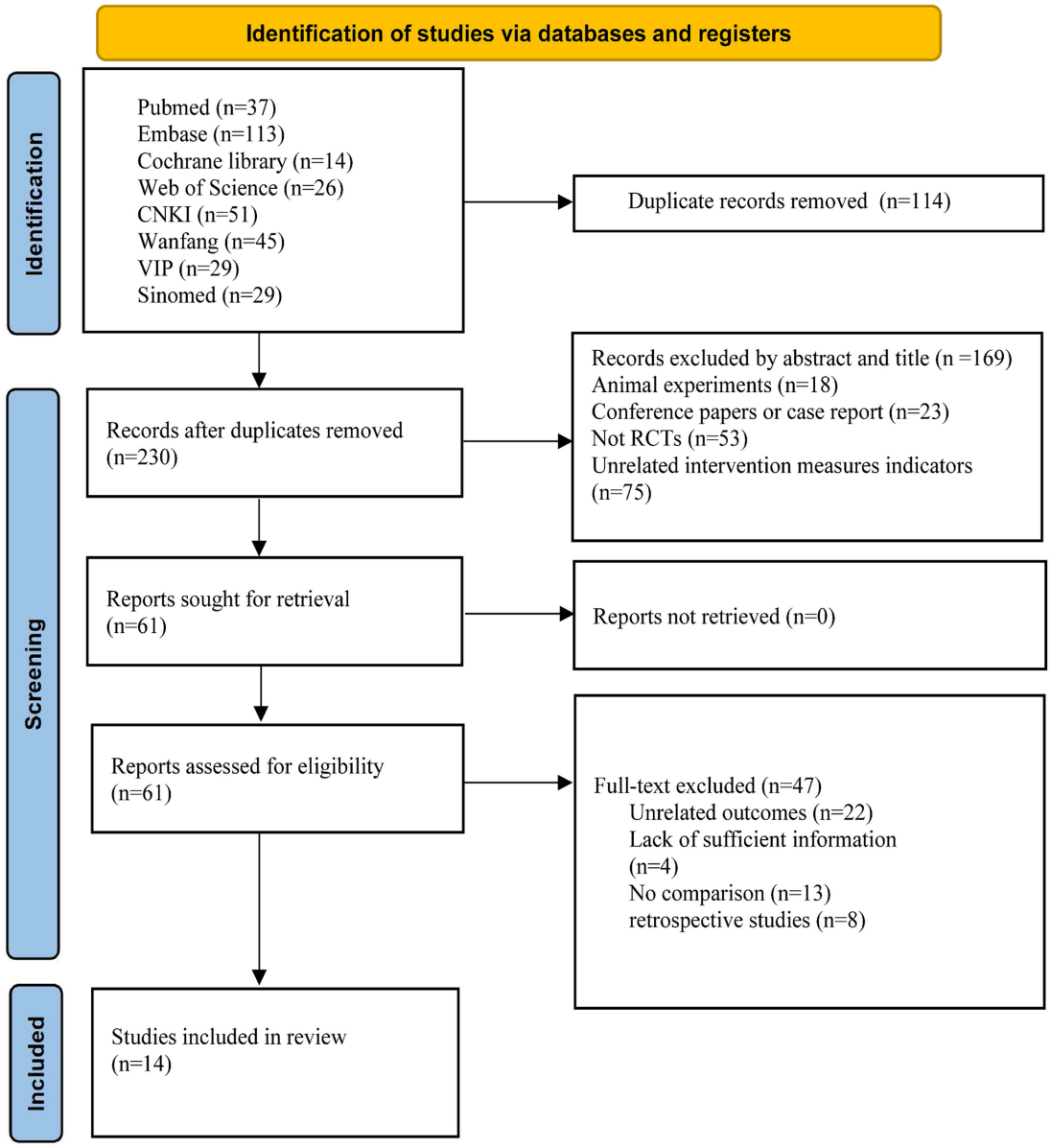

FIGURE 1
Flow chart of selection studies and specific reasons for exclusion.

alone on IOP at 1 month postoperatively. Pooled results showed that AGVI combined with anti-VEGF was more effective in lowering IOP in NVG patients 1 month after surgery compared to AGVI alone [WMD = −5.39, 95% CI (−7.05, −3.74), $p < 0.001$]. The results of subgroup analysis indicated that the ranibizumab group and conbercept group all demonstrated superior efficacy in reducing intraocular pressure at 1 month postoperatively compared to AGVI alone ([WMD = −5.84, 95% CI (−7.68, −4.01), $p < 0.001$] and [WMD = −4.14, 95% CI (−6.69, −1.59), $p = 0.001$] respectively) (Figure 3B).

3.4.3 IOP at 3 months postoperatively

Five RCTs (27, 28, 32, 35, 37), comprising 347 eyes, investigated the effects of combined AGVI with anti-VEGF drugs versus AGVI alone on IOP at 3 months postoperatively. Pooled results showed that AGVI combined with anti-VEGF was more effective in lowering IOP in NVG patients 3 months after surgery compared to AGVI alone [WMD = −6.59, 95% CI (−7.85, −5.32), $p < 0.001$]. The results of subgroup analysis indicated that the ranibizumab group and bevacizumab group all demonstrated superior efficacy in reducing intraocular pressure at 3 months postoperatively compared to AGVI alone ([WMD = −6.83, 95% CI (−8.06, −5.61), $p < 0.001$] and [WMD = −5.88, 95% CI (−10.38, −1.39), $p = 0.010$] respectively) (Figure 4A).

3.4.4 IOP at 6 months postoperatively

Five RCTs (27, 28, 32–34), comprising 301 eyes, investigated the effects of combined AGVI with anti-VEGF drugs versus AGVI alone on IOP at 6 months postoperatively. Pooled results showed that AGVI combined with anti-VEGF was more effective in lowering IOP in

TABLE 1 Basic characteristics of the included studies.

References	Year	Region	Study design	Sample(T/C)	Age		Intervention regimen		Number of anti-VEGF used		Combine PRP		Follow-up	Time of injection	Dosage of anti-VEGF	Outcome
					T	C	T	C	T	C	T	C				
Mahdy RA, et al	2013	Egypt	RCT	20/20	55 ± 1.3	56 ± 4.3	AGVI+B	AGVI	1	1	Yes	Yes	18 months	Pre-operation	1.25 mg/0.05 mL	IOP, Number of hyphaema, Total efficiency
Zarei R, et al	2021	Iran	RCT	30/30	56.7 ± 17.2	57.4 ± 16.4	AGVI+B	AGVI	1	1	NR	NR	12 months	Post-operation	1.25 mg/0.05 mL	IOP, Total efficiency
Arcieri ES	2015	Brazil	RCT	20/20	59.25 ± 8.05	62.40 ± 11.78	AGVI+B	AGVI	3	3	Yes	Yes	24 months	Post-operation	0.05 mL/1.25 mg	IOP, Number of hyphaema, Number of antiglaucoma medications
Xu JH, et al	2015	China	RCT	9/19	NR	NR	AGVI+R	AGVI	1	1	Partial acceptance		1 week	Pre-operation	0.5 mg	IOP, Number of hyphaema
Li YB, et al	2019	China	RCT	46/34	58.06 ± 7.33	57.49 ± 8.42	AGVI+R	AGVI	1	1	NR	NR	NR	Pre-operation	10 mg /ml	Number of hyphaema, Total efficiency
Zong LM, et al	2018	China	RCT	38/35	56.9 ± 8.3	55.2 ± 9.4	AGVI+R	AGVI	1	1	NR	NR	6 months	Pre-operation	1.25 mg/0.05 mL	IOP, Number of hyphaema
Xie Z, et al	2018	China	RCT	31/35	48.32 ± 11.63	52.77 ± 15.22	AGVI+R	AGVI	1	1	Partial acceptance		12 months	Pre-operation	NR	IOP, Number of antiglaucoma medications
Liu H, et al	2019	China	RCT	31/31	55.87 ± 9.84	55.09 ± 10.13	AGVI+R	AGVI	1	1	Partial acceptance		6 months	Pre-operation	1.25 mg/0.05 mL	IOP, Number of hyphaema, VEGF
Xu KK, et al	2022	China	RCT	46/48	36.28 ± 4.37	36.61 ± 3.56	AGVI+R	AGVI	1	1	NR	NR	3 months	Pre-operation	10 mg/mL	Number of hyphaema, Total efficiency, VEGF
Tian LJ, et al	2019	China	RCT	28/24	NR	NR	AGVI+R	AGVI	1	1	NR	NR	6 months	Pre-operation	1.25 mg/0.05 mL	Total efficiency
Liu XR, et al	2020	China	RCT	40/40	49.8 ± 5.7	42.7 ± 5.6	AGVI+C	AGVI	1	1	NR	NR	3 months	Pre-operation	10 mg/mL	IOP, Number of hyphaema, Number of antiglaucoma medications, Total efficiency

(Continued)

10.3389/fmed.2024.1405261

TABLE 1 (Continued)

References	Year	Region	Study design	Sample(T/C)	Age		Intervention regimen		Number of anti-VEGF used		Combine PRP		Follow-up	Time of injection	Dosage of anti-VEGF	Outcome
					T	C	T	C	T	C	T	C				
Li XY, et al	2022	China	RCT	45/45	50.11 ± 4.2	50.25 ± 4.68	AGVI+C	AGVI	2	2	Yes	Yes	1 months	Pre-operation	NR	IOP, Number of hyphaema, Total efficiency, VEGF
Zheng HF, et al	2021	China	RCT	40/40	52.12 ± 1.03	51.96 ± 1.01	AGVI+C	AGVI	1	1	NR	NR	1 week	Pre-operation	0.5 mg	IOP, VEGF, Total efficiency
Luo GE, et al	2018	China	RCT	28/24	58.8 ± 11.9	58.0 ± 13.3	AGVI+anti-VEGF	AGVI	1	1	NR	NR	1 months	Pre-operation	NR	IOP, Number of hyphaema, Total efficiency, Number of antiglaucoma medications

NR, not report; T, test group; C, control group; RCT, randomized Controlled Trial; AGVI, Ahmed glaucoma valve implantation; IOP, intraocular pressure; VEGF, vascular endothelial growth factor; mg, milligram; ml, milliliter.

NVG patients 6 months after surgery compared to AGVI alone [WMD = −4.99, 95% CI (−9.56, −0.43), $p = 0.032$]. The results of subgroup analysis indicated that the ranibizumab group demonstrated superior efficacy in reducing intraocular pressure at 6 months postoperatively compared to AGVI alone [WMD = −4.19, 95% CI (−5.77, −2.62), $p < 0.001$]. Nevertheless, it is important to mention that the outcomes of bevacizumab group did not reach statistical significance ($p = 0.260$) (Figure 4B).

3.4.5 IOP more than 12 months postoperatively

Four RCTs (27–29, 33), comprising 209 eyes, investigated the effects of combined AGVI with anti-VEGF drugs versus AGVI alone on IOP more than 12 months postoperatively. Pooled results showed that AGVI combined with anti-VEGF was more effective in lowering IOP in NVG patients more than 12 months after surgery compared to AGVI alone [WMD = −3.86, 95% CI (−6.82, −0.90), $p = 0.011$] (Supplementary materials S3).

3.4.6 Effective rate

Nine studies (27, 28, 31, 35–40), including 628 eyes, compared the overall efficacy of AGVI combined with anti-VEGF drugs versus AGVI alone in patients with NVG. The aggregated findings demonstrated a superior overall efficacy of AGVI combined with anti-VEGF drugs compared to AGVI alone [RR = 1.27, 95% CI (1.18, 1.37), $p < 0.001$]. The summarized findings indicated that both ranibizumab group and conbercept group all demonstrated a significant positive impact on enhancing effective rates. ([RR = 1.27, 95% CI (1.13, 1.42), $p < 0.001$] and [RR = 1.30, 95% CI (1.05, 1.62), $p = 0.017$] respectively). However, the outcomes of bevacizumab group did not reach statistical significance ($p = 0.149$) (Figure 5A). Subgroup analysis based on follow-up time revealed that the efficacy of anti-VEGF drugs combined with AGVI was superior to AGVI alone at 3 months and 6 months post-operation ([RR = 1.41, 95% CI (1.18, 1.69), $p < 0.001$] and [RR = 1.47, 95% CI (1.13, 1.91), $p = 0.004$] respectively). Nevertheless, there was no significant difference in efficacy between the two groups beyond 12 months post-operation [RR = 1.42, 95% CI (0.88, 2.28), $p = 0.149$] (Figure 5B).

3.4.7 Incidence of postoperative hyphema

Ten studies (27, 29–32, 34, 35, 37, 38, 40), including 641 eyes, compared the incidence of postoperative hyphema of AGVI combined with anti-VEGF drugs versus AGVI alone in patients with NVG. The pooled results showed that compared to AGVI alone, the combination of AGVI with anti-VEGF drugs effectively reduces the probability of postoperative hyphema [RR = 0.24, 95% CI (0.15, 0.39), $p < 0.001$]. The results of subgroup analysis indicated that the ranibizumab group and bevacizumab group all demonstrated superior efficacy in reducing the incidence of postoperative hyphema ([RR = 0.27, 95% CI (0.13, 0.57), $p = 0.001$] and [RR = 0.26, 95% CI (0.12, 0.56), $p = 0.001$]). Conversely, the outcomes of conbercept group did not reach statistical significance ($p = 0.186$) (Figure 6A).

3.4.8 Aqueous humor VEGF levels

Four RCTs (34, 35, 38, 39), comprising 326 eyes, investigated the effects of combined AGVI with anti-VEGF drugs versus AGVI alone on aqueous humor VEGF levels. Due to the different units for measuring aqueous humor VEGF levels in the included literature, we conducted the analysis using SMD. The pooled results showed that

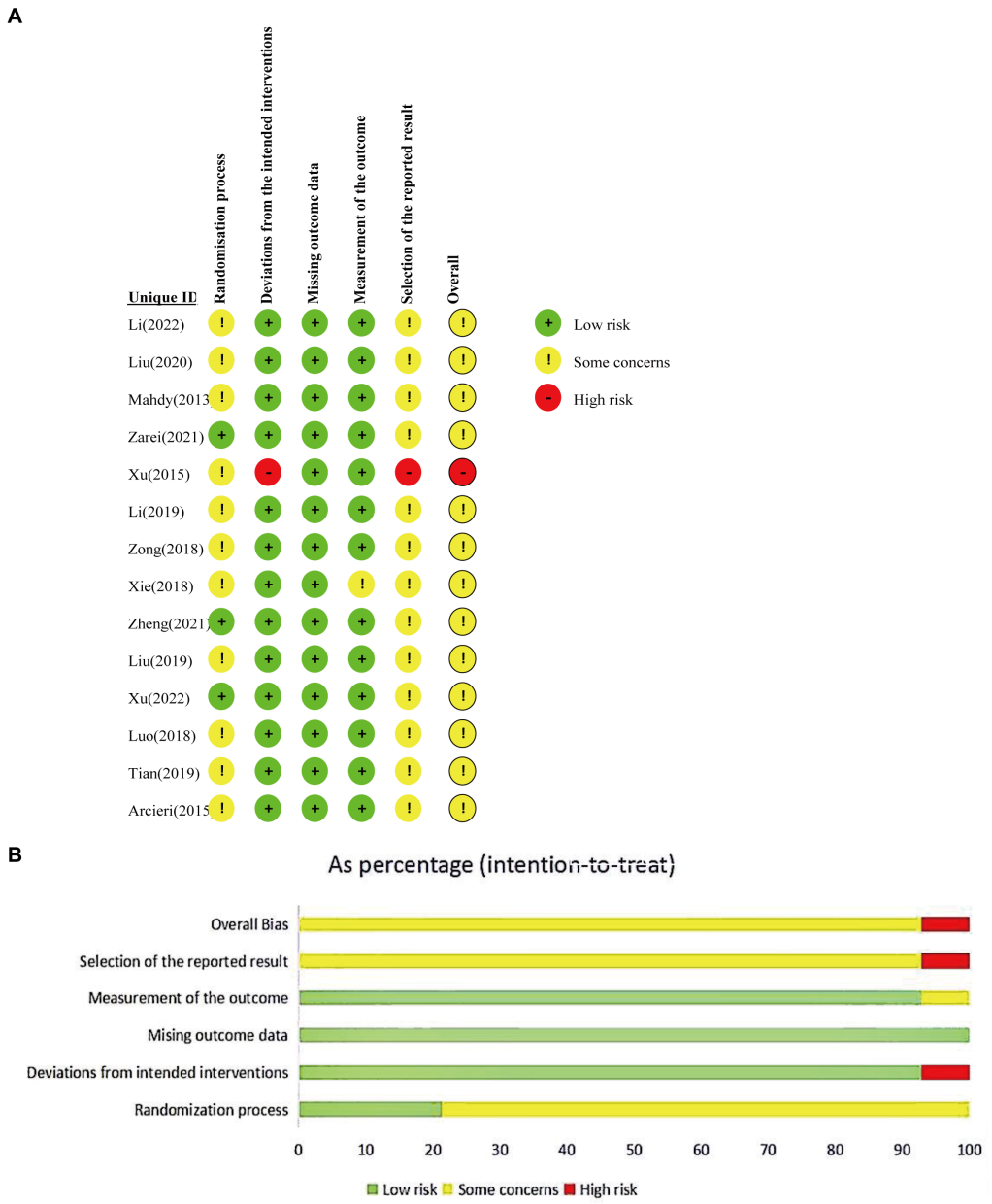

FIGURE 2
Risk of bias of RCTs. **(A)** Risk of bias graph; **(B)** Risk of bias summary.

compared to AGVI alone, the combination of AGVI with anti-VEGF drugs had a better effect on reducing aqueous humor VEGF levels [SMD = −2.84, 95% CI (−4.37, −1.31), $p < 0.001$] (Figure 6B).

3.4.9 Postoperative antiglaucoma medication requirements

Four studies (29, 33, 37, 40), involving 238 eyes, compared the impact of AGVI combined with anti-VEGF drugs versus AGVI alone on postoperative glaucoma medication use in NVG patients. The pooled results showed that compared to AGVI alone, AGVI combined with anti-VEGF drugs effectively reduced the postoperative use of antiglaucoma medications [WMD = −0.48, 95% CI (−0.61, −0.35), $p < 0.001$] (Figure 7). Subgroup analysis based on follow-up time revealed that the use of anti-glaucoma medications was significantly lower with the combination of anti-VEGF drugs and AGVI than with AGVI alone at both 1 month and 3 months post-operation ([WMD = −0.45, 95% CI (−0.67, −0.22), $p < 0.001$] and [WMD = −0.50, 95% CI (−0.66, −0.34), $p < 0.001$] respectively) (Figure 7).

3.5 Sensitivity analysis

We conducted a sensitivity analysis to assess the impact of individual studies on the overall results of comparing the treatment outcomes for NVG using anti-VEGF drugs combined with AGVI versus AGVI alone. The findings revealed that no single study

TABLE 2 The outcome of the meta-analysis.

Outcomes	Number	Sample size	WMD/RR/SMD	95%CI	Heterogeneity	*p*-value	F/R	Note
IOP at 1 week	6	368	WMD = −4.03	(−5.73, −2.34)	73.20%	$p < 0.001$	R	Overall
	2	108	WMD = −6.24	(−7.35, −5.13)	0%	$p < 0.001$	R	Ranibizumab group
	2	100	WMD = −2.71	(−4.55, −0.87)	10%	$p = 0.004$	R	Bevacizumab group
	2	160	WMD = −3.20	(−5.07, −1.33)	31.90%	$p = 0.001$	R	Conbercept group
IOP at 1 month	6	401	WMD = −5.39	(−7.05, −3.74)	80%	$p < 0.001$	R	Overall
	2	139	WMD = −5.84	(−7.68, −4.01)	0%	$p < 0.001$	R	Ranibizumab group
	2	170	WMD = −4.14	(−6.69, −1.59)	82.10%	$p = 0.001$	R	Conbercept group
IOP at 3 months	5	347	WMD = −6.59	(−7.85, −5.32)	61.80%	$p < 0.001$	R	Overall
	2	167	WMD = −6.83	(−8.06, −5.61)	0%	$p < 0.001$	R	Ranibizumab group
	2	100	WMD = −5.88	(−10.38, −1.39)	89.20%	$p = 0.010$	R	Bevacizumab group
IOP at 6 months	5	301	WMD = −4.99	(−9.56, −0.43)	95.60%	$p = 0.032$	R	Overall
	3	201	WMD = −4.19	(−5.77, −2.62)	15.80%	$p < 0.001$	R	Ranibizumab group
	2	100	WMD = −6.36	(−17.44, 4.71)	98.70%	$p = 0.260$	R	Bevacizumab group
IOP more than 12 months	4	209	WMD = −3.86	(−6.82, −0.90)	86%	$p = 0.011$	R	Overall
Effective rate	9	628	RR = 1.27	(1.18, 1.37)	1.80%	$p < 0.001$	R	Overall
	4	306	RR = 1.27	(1.13, 1.42)	0%	$p < 0.001$	R	Ranibizumab group
	2	170	RR = 1.30	(1.05, 1.62)	49.80%	$p = 0.017$	R	Conbercept group
	2	100	RR = 1.42	(0.88, 2.28)	75.20%	$p = 0.149$	R	Bevacizumab group
Incidence of postoperative hyphema	10	641	RR = 0.24	(0.15, 0.39)	0%	$p < 0.001$	R	Overall
	5	337	RR = 0.27	(0.13, 0.57)	0%	$p = 0.001$	R	Ranibizumab group
	2	100	RR = 0.26	(0.12, 0.56)	0%	$p = 0.001$	R	Bevacizumab group
	2	170	RR = 0.34	(0.07, 1.68)	0%	$p = 0.186$	R	Conbercept group
Aqueous humor VEGF levels	4	326	SMD = −2.84	(−4.37, −1.31)	95.80%	$p < 0.001$	R	Overall
Postoperative antiglaucoma medication requirements	4	238	WMD = −0.49	(−0.62, −0.37)	0%	$p < 0.001$	R	Overall

WMD, weighted mean difference; SMD, standard mean difference; RR, risk ratio; CI, confidence interval; *p*, *p* value represents clinical significance; T, test group; C, control group; F, fixed effects model; R, random effects model; IOP, intraocular pressure; VEGF, vascular endothelial growth factor.

10.3389/fmed.2024.1405261

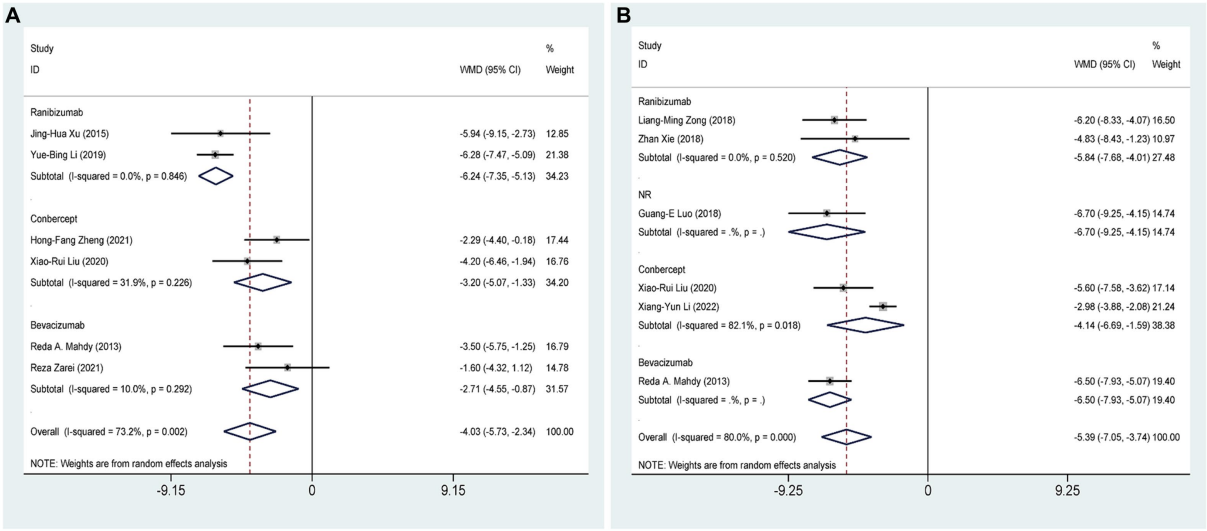

FIGURE 3
AGVI alone vs. AGVI combined with anti-VEGF drugs: **(A)** IOP at 1 week: subgroup analysis based on anti-VEGF drugs; **(B)** IOP at 1 month: subgroup analysis based on anti-VEGF drugs.

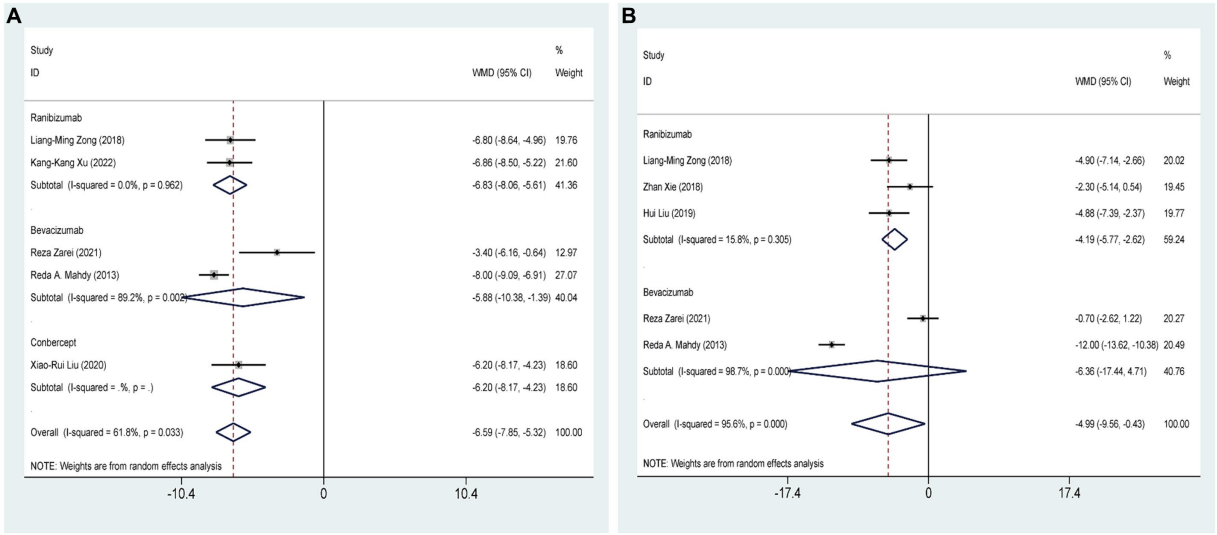

FIGURE 4
AGVI alone vs. AGVI combined with anti-VEGF drugs: **(A)** IOP at 3 months: subgroup analysis based on anti-VEGF drugs; **(B)** IOP at 6 months: subgroup analysis based on anti-VEGF drugs.

significantly impacted the final results, suggesting the robustness and stability of the study's findings (Figure 7).

3.6 Publication bias

For outcome metrics that include 10 or more studies, we visually inspected funnel plots to explore the potential for publication bias, the funnel plots appeared slightly asymmetrical. To go further with the exploration, we used Egger's test. Egger's test yielded a p value of 0.835, suggesting that publication bias is unlikely to have significantly influenced the results of this study (Figure 8).

4 Discussion

4.1 Summary of results

This study analyzed the effectiveness and safety of combined anti-VEGF drugs and AGVI treatment for NVG, examining bevacizumab, ranibizumab, and conbercept. Results from the study demonstrated that combining anti-VEGF medications with AGVI resulted in superior outcomes compared to AGVI alone, including reduced postoperative IOP, decreased incidence of postoperative hyphema, diminished use of postoperative anti-glaucoma medications, and decreased intraocular VEGF levels. In terms of

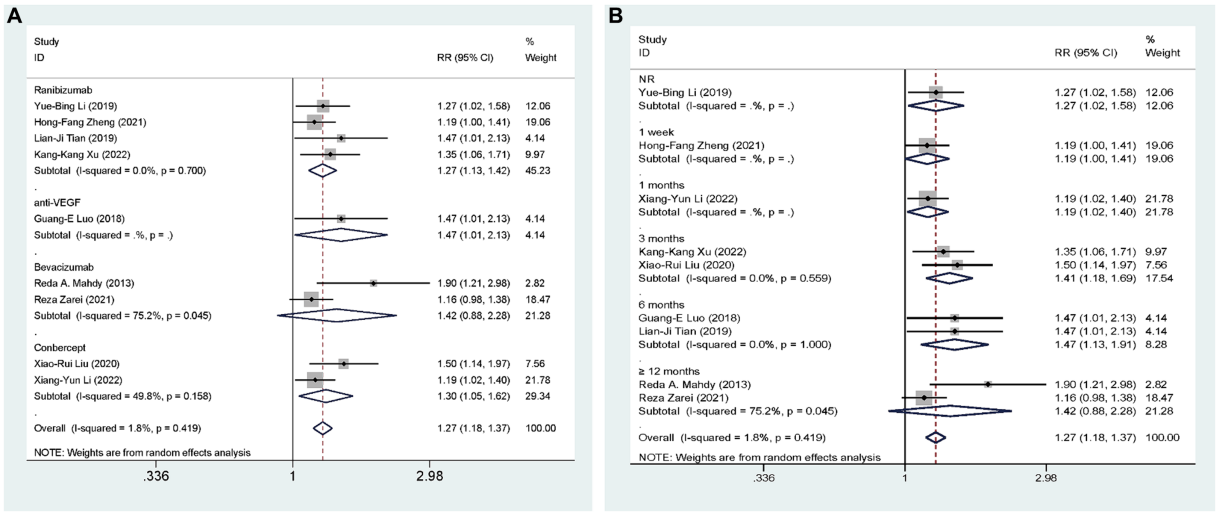

FIGURE 5
AGVI alone vs. AGVI combined with anti-VEGF drugs: **(A)** Effective rate: subgroup analysis based on anti-VEGF drugs; **(B)** Effective rate: subgroup analysis based on follow-up time.

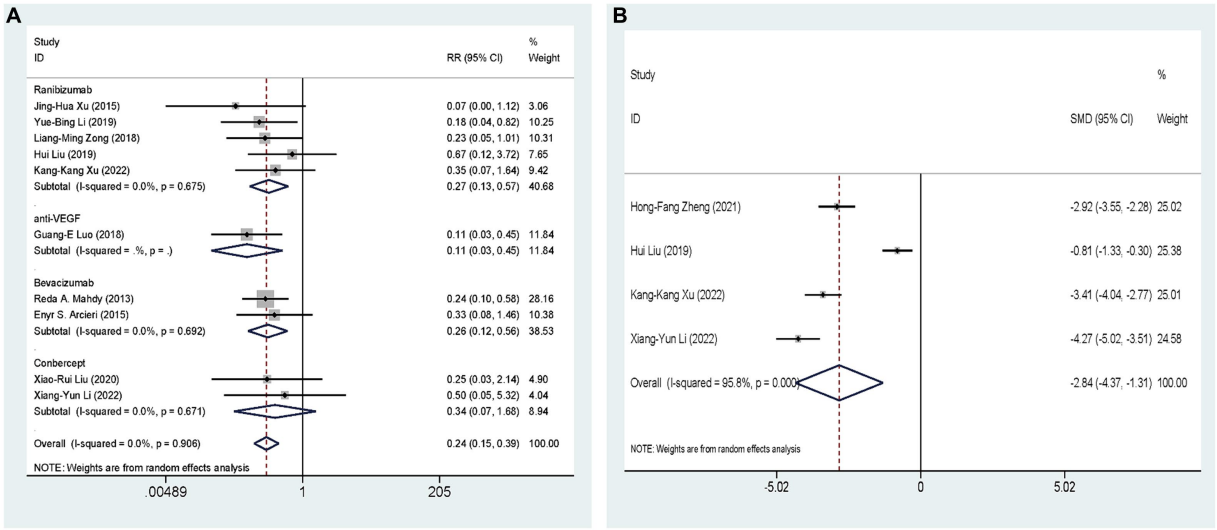

FIGURE 6
AGVI alone vs. AGVI combined with anti-VEGF drugs: **(A)** Incidence of postoperative hyphema: subgroup analysis based on anti-VEGF drugs; **(B)** Aqueous humor VEGF levels.

reducing intraocular pressure, both at 1 week and 1 month postoperatively, combined therapy achieved better results and could reduce postoperative medication use, consistent with the meta-analysis results by Lin et al. (41). Simultaneously, the combined therapy group exhibited a higher success rate and fewer postoperative adverse reactions, consistent with the meta-analysis findings by Chen and Mu (42) and Hwang and Lee (43). More importantly, through our research, we found that the combined therapy group had better long-term control of IOP postoperatively compared to AGVI alone. To this end, we analyzed IOP data from follow-up visits at 3 months, 6 months, and beyond 12 months postoperatively. Regarding safety, we found that the combination of anti-VEGF drugs with AGVI reduced the incidence of postoperative hyphema compared to AGVI alone. This finding is consistent with Zhou et al. (44) meta-analysis on the treatment of NVG with bevacizumab combined with AGVI.

To further explore the therapeutic effects of combining anti-VEGF drugs with AGVI on NVG, subgroup analyses were conducted on the anti-VEGF medications, including the ranibizumab, bevacizumab, and conbercept groups. Studies that did not specify the type of anti-VEGF medication used were excluded from the subgroup analyses. In the analysis of IOP results at 1 week postoperatively, all three subgroups exhibited statistically significant differences. Besides, ranibizumab group and conbercept group all demonstrated superior efficacy in reducing intraocular pressure at 1 month postoperatively compared to AGVI alone. At 3 months postoperatively, both the

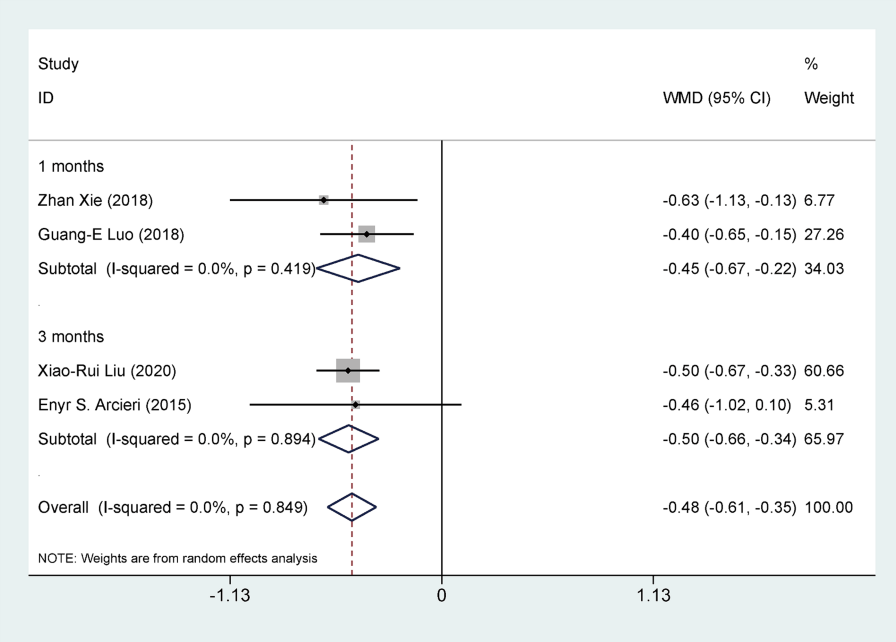

FIGURE 7
AGVI alone vs. AGVI combined with anti-VEGF drugs: postoperative antiglaucoma medication requirements.

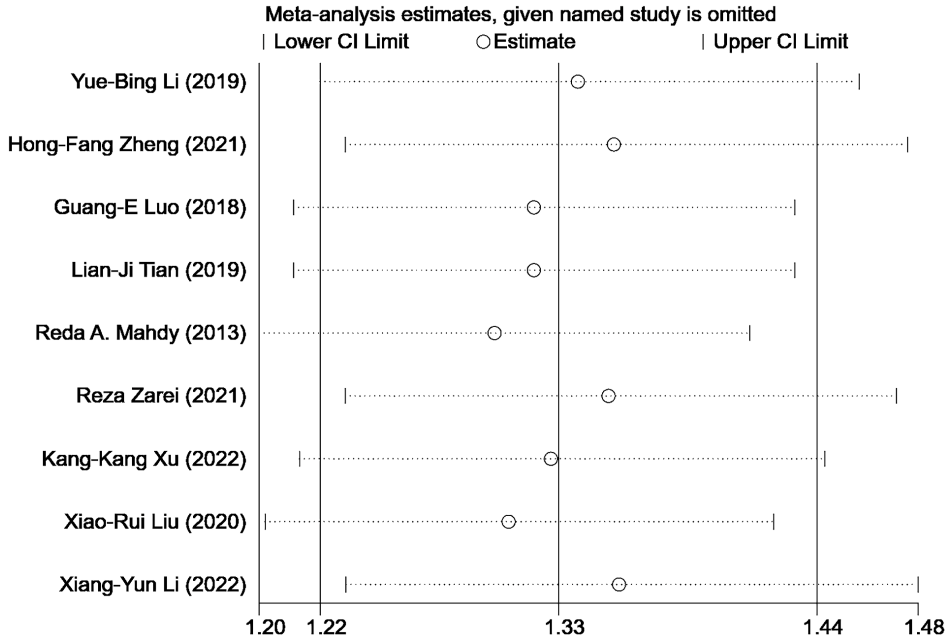

FIGURE 8
Sensitivity analysis: effective rate of AGVI alone vs. AGVI combined with anti-VEGF drugs.

bevacizumab and ranibizumab groups demonstrated significant differences compared to AGVI alone. Regarding the IOP results at 6 months postoperatively, the bevacizumab group did not exhibit statistically significant differences, while the ranibizumab group showed significant differences compared to AGVI alone. However, the conbercept group did not demonstrate significant differences in reducing postoperative hyphema. Subgroup analysis based on follow-up time revealed that the efficacy of anti-VEGF drugs combined with AGVI was superior to that of AGVI alone at 3 months and 6 months post-operation. However, there was no significant difference in efficacy between the two groups beyond 12 months post-operation. Additionally, the combination group significantly reduced the use of anti-glaucoma medications at 1 month and 3 months post-operation.

4.2 Discussion of anti-VEGF combined with AGVI vs. AGVI alone

NVG is a severe secondary glaucoma. Although endoscopic cyclophotocoagulation, cyclocryotherapy, simple trabeculectomy, and traditional filtering surgery have certain therapeutic effects, the postoperative conditions of intraocular hypertension, retinal detachment, loss of vision, and atrophy of the eyeball cannot be ignored (45). AVGI modulates the flow of aqueous humor by positioning a tube between the conjunctiva and sclera, theoretically, the incorporation of a restrictive valve-like mechanism within the AGVI confers substantial advantages in controlling early postoperative IOP and reducing the risk of hypotony in contrast to trabeculectomy (46). Drainage valve implantation is also considered the gold standard for treating NVG (47). A meta-analysis by Tan et al. (48) found that AGVI yielded similar outcomes to trabeculectomy, but with a significantly reduced incidence of postoperative complications. However, in a retrospective study, Netland (49) reported a success rate of 73.1% at 1 year, 61.9% at 2 years, and only 20.6% at 5 years, and considered NVG a high risk factor of AGV implantation failure.

Intraocular anti-VEGF drugs are increasingly utilized as adjunctive therapy for refractory NVG to enhance the outcomes of glaucoma surgery in high-risk patients (50). VEGF is a potent angiogenic stimulator, facilitating multiple stages of angiogenesis such as proliferation, migration, proteolytic activity, and capillary tube formation, it plays a crucial role in both normal and pathological angiogenesis (51). In patients with NVG, the concentration of VEGF is elevated in the aqueous humor, more importantly, an abundance of VEGF enters the anterior chamber of the eye from the posterior pole, initiating neovascularization (NV) primarily from the capillaries of the minor and major arterial rings of the iris before extending to the anterior chamber angle, it also leads to disruption of the blood-retinal barrier (52, 53). The currently available anti-VEGF inhibitors, including bevacizumab and ranibizumab, have proven to be effective suppressing anterior segment neovascularization and lowering IOP (4). In order to further investigate the effectiveness of anti-VEGF medications, this meta-analysis included a subgroup analysis of three distinct anti-VEGF drugs. According to the results of subgroup analysis, ranibizumab achieved favorable outcomes. Compared to AGVI alone, combination therapy with ranibizumab can lower IOP in both short-term and long-term postoperative periods, reduce postoperative medication usage, and decrease the incidence of hyphema. This may be attributed to ranibizumab's function as an antagonist of vascular endothelial growth factor-A (VEGF-A), allowing it to bind with high affinity to various VEGF-A isoforms (54). The binding of ranibizumab to VEGF-A inhibits the interaction between VEGF-A and its receptors (VEGFR1 and VEGFR2) on endothelial cell surfaces, thereby decreasing endothelial cell proliferation, vascular leakage, and angiogenesis (4). Ranibizumab is a monoclonal antibody fragment produced by the gram-negative bacterium *Escherichia coli*, with a molecular weight of 48 kD, the rationale for developing Ranibizumab as a fragment antigen-binding (Fab) is based on the hypothesis that its small size enables better tissue penetration through all retinal layers (55). Each molecule of ranibizumab possesses only one binding site for VEGF, allowing each VEGF dimer to be bound by two ranibizumab molecules (56). A study found that at clinically significant doses, bevacizumab (0.25 mg/mL) and ranibizumab (0.125 mg/mL) could completely neutralize vascular endothelial growth factor within 6 h, when diluted, bevacizumab lost its inhibitory effect at a concentration of 975 ng/mL, while ranibizumab neutralized vascular endothelial growth factor at a concentration of 120 ng/mL (57). Although the subgroup analysis results found that bevacizumab's performance in lowering IOP at 6 months postoperatively was suboptimal, it still reduced the occurrence of hyphema. Bevacizumab as a full-length humanized, can recombinant monoclonal IgG antibody that inactivates all VEGF isoforms (58). Ha et al. (59) found in a retrospective study that among 26 patients NVG who received intravitreal injections of bevacizumab, IOP significantly decreased 1 week later, but the effect was not significant at the one-year follow-up. Ghanem et al. (60) found that 1 week after intravitreal injection of bevacizumab, significant regression of iris neovascularization could be observed in eyes with NVG. The subgroup analysis of conbercept revealed that, when compared to AGVI alone, combination therapy with conbercept can effectively decrease IOP in both short-term and long-term postoperative periods, as well as reduce the need for postoperative medication. However, it appeared to have no effect on reducing the incidence of hyphema. Placental growth factor (PlGF) primarily functions as a pro-angiogenic growth factor, exhibiting upregulation specifically in pathological conditions and conbercept can bind to dual targets (VEGF and PIGF) for antiangiogenic therapy (61). Xu et al.'s study found that intravitreal injection of conbercept can reduce the levels of IL-4, IL-22, Ang-2, PlGF, and VEGF-A in the aqueous humor (62). Subgroup analysis based on follow-up time revealed that the combination of anti-VEGF drugs and AGVI did not improve efficacy beyond 12 months post-operation. Additionally, a study by Rittiphairoj et al. (63). found no evidence that VEGF drugs can maintain long-term efficacy as an adjunct therapy. This could be because after regression of neovascularization, the iridocorneal angle appears open on gonioscopy, however, ghost vessels, which are transparent and tend to form synechiae, can lead to subsequent angle closure, additionally, VEGF cannot work on the fibrovascular membrane that closes the iridocorneal angle (64). This also may be due to the regression of iris neovascularization, which can persist for 8–10 weeks after intraocular injection but typically returns to its previous condition within 6 months. Consequently, this treatment plays a limited and temporary role in managing NVG (24). More rigorous evidence is still needed to confirm that anti-VEGF drugs can serve as an effective long-term adjunct to AGVI. According to previous studies, PRP can effectively improve retinal ischemic conditions and reduce the release of VEGF, thus preventing the development of NVG, additionally, PRP facilitates the control of IOP and enhances the long-term outcomes of surgery (65). None of the studies included in this research explicitly mentioned not using PRP, therefore, we were unable to conduct a deeper analysis of the role of PRP through subgroup analysis or other methods.

During the course of this study, we found that the majority of cases were from the same region. For that, we explored the possible reasons for this phenomenon by searching relevant literature. In a meta-analysis by Tham et al. (66), it was found that due to the relatively large population of Asians, over half (53.4%) of global primary open-angle glaucoma (POAG) cases occurred in Asia, in addition, primary angle-closure glaucoma (PACG) is the predominant type of glaucoma in the Asian population (1.1%), with over three-quarters (76.7%) of global PACG cases occurring in Asia. According to Song et al.'s study (67), the number of patients with secondary glaucoma in China increased from 340,000 (95%CI = 0.23–0.53) to 760,000 (95%CI = 0.51–1.17) by 2015. A retrospective study from a

tertiary center in China revealed that patients with NVG constituted approximately 5.8% of all glaucoma patients in China (68). More importantly, the prevalence of glaucoma is positively correlated with advanced age, as China stands as the largest developing country, its population is rapidly aging, which results in a significant burden of glaucoma (69). Based on the aforementioned factors, this may explain why a large number of cases come from the same region.

4.3 Strength and limitations

This study has the following advantages: First, it includes an analysis of the current mainstream anti-VEGF drugs, which is more comprehensive and complete compared to analyzing a single anti-VEGF drug. Secondly, the paper conducts a subgroup analysis of three distinct anti-VEGF drug categories, aiming to aid clinicians in the selection of appropriate treatments. Thirdly, the outcome indicators included in this study are relatively comprehensive, covering both short-term and long-term postoperative IOP, BCVA, Incidence of postoperative hyphema, efficacy, Postoperative antiglaucoma medication requirements and aqueous humor VEGF levels. More importantly, compared to previous meta-analyses on the subject, this study exclusively included RCTs, excluding other types of research.

This study also presents certain limitations. Firstly, it is restricted to analyses of clinical practices and published studies; thus, it does not encompass research on anti-VEGF drugs currently under investigation or unpublished, including faricimab, nesvacumab, and squalamine. Secondly, the study did not exclude patients with NVG who may also suffer from other retinal conditions, such as diabetic retinopathy. Thirdly, despite the adoption of a multi-person collaborative assessment method, the bias risk assessment tool used in this systematic review still harbors unavoidable subjectivity, which may affect the final evaluation of the literature quality. Finally, as most of the included studies originate from the same region, their findings may have limited global applicability. Future research from diverse regions is necessary to validate the conclusions of this study.

5 Conclusion

In conclusion, compared to AGVI alone, the combination of AGVI with anti-VEGF drugs has a good effect in controlling postoperative intraocular pressure at different times, increasing the effective rate, reducing aqueous VEGF levels, decreasing the use of postoperative antiglaucoma drugs, and also reducing the occurrence of postoperative anterior chamber hemorrhage. Additionally, this study also found that the efficacy of ranibizumab appears to be more stable. In the future, it will be necessary to conduct multicenter, randomized, double-blind, large-sample, rigorously designed clinical trials with long-term follow-up to confirm the conclusions of this study.

Data availability statement

The original contributions presented in the study are included in the article/Supplementary material, further inquiries can be directed to the corresponding author.

Author contributions

C-ZH: Writing – original draft, Writing – review & editing. S-JL: Data curation, Methodology, Writing – review & editing. Z-JZ: Software, Writing – original draft. J-QL: Writing – review & editing. QQ: Writing – review & editing. F-LX: Writing – review & editing. YH: Writing – review & editing.

Funding

The author(s) declare that no financial support was received for the research, authorship, and/or publication of this article.

Acknowledgments

The contributions of each author in the process of literature collection, data extraction, and quality assessment are gratefully appreciated.

Conflict of interest

The authors declare that the research was conducted in the absence of any commercial or financial relationships that could be construed as a potential conflict of interest.

Publisher's note

Supplementary material

The Supplementary material for this article can be found online at: https://www.frontiersin.org/articles/10.3389/fmed.2024.1405261/full#supplementary-material

References

1. Senthil S, Dada T, Das T, Kaushik S, Puthuran GV, Philip R, et al. Neovascular glaucoma – A review. *Indian J Ophthalmol.* (2021) 69:525–34. doi: 10.4103/ijo.IJO_1591_20

2. Shazly TA, Latina MA. Neovascular glaucoma: etiology, diagnosis and prognosis. *Semin Ophthalmol.* (2009) 24:113–21. doi: 10.1080/08820530902800801

3. Zemba M, Dumitrescu OM, Vaida F, Dimirache EA, Pistolea I, Stamate AC, et al. Micropulse vs. continuous wave transscleral cyclophotocoagulation in neovascular glaucoma. *Exp Ther Med.* (2022) 23:278. doi: 10.3892/etm.2022.11207

4. Urbonavičiūtė D, Buteikienė D, Janulevičienė I. A review of neovascular glaucoma: Etiology, pathogenesis, diagnosis, and treatment. *Medicina (Kaunas).* (2022) 58:1870. doi: 10.3390/medicina58121870

5. Yang H, Yu X, Sun X. Neovascular glaucoma: handling in the future. *Taiwan J Ophthalmol*. (2018) 8:60–6. doi: 10.4103/tjo.tjo_39_18

6. Simha A, Aziz K, Braganza A, Abraham L, Samuel P, Lindsley KB. Anti-vascular endothelial growth factor for neovascular glaucoma. *Cochrane Database Syst Rev*. (2020) 2:Cd007920. doi: 10.1002/14651858.CD007920.pub3

7. Muth DR, Fasler KF, Kvanta A, Rejdak M, Blaser F, Zweifel SA. Real-world weekly efficacy analysis of Faricimab in patients with age-related macular degeneration. *Bioengineering (Basel)*. (2024) 11:478. doi: 10.3390/bioengineering11050478

8. Havens SJ, Gulati V. Neovascular Glaucoma. *Dev Ophthalmol*. (2016) 55:196–204. doi: 10.1159/000431196

9. Tang Y, Shi Y, Fan Z. The mechanism and therapeutic strategies for neovascular glaucoma secondary to diabetic retinopathy. *Front Endocrinol (Lausanne)*. (2023) 14:1102361. doi: 10.3389/fendo.2023.1102361

10. Xie Z, Liu H, Du M, Zhu M, Tighe S, Chen X, et al. Efficacy of Ahmed glaucoma valve implantation on neovascular glaucoma. *Int J Med Sci*. (2019) 16:1371–6. doi: 10.7150/ijms.35267

11. Elbaklish KH, Gomaa WA. A one-year follow-up of two Ahmed glaucoma valve models (S2 and FP7) for refractory glaucoma: a prospective randomized trial. *Clin Ophthalmol*. (2020) 14:693–705. doi: 10.2147/OPTH.S224653

12. Nouri-Mahdavi K, Caprioli J. Evaluation of the hypertensive phase after insertion of the Ahmed glaucoma valve. *Am J Ophthalmol*. (2003) 136:1001–8. doi: 10.1016/S0002-9394(03)00630-5

13. Zhou M, Wang J, Wang W, Huang W, Ding X, Zhang X. Placenta growth factor in eyes with neovascular glaucoma is decreased after intravitreal ranibizumab injection. *PLoS One*. (2016) 11:e0146993. doi: 10.1371/journal.pone.0146993

14. Beutel J, Peters S, Lüke M, Aisenbrey S, Szurman P, Spitzer MS, et al. Bevacizumab as adjuvant for neovascular glaucoma. *Acta Ophthalmol*. (2010) 88:103–9. doi: 10.1111/j.1755-3768.2008.01355.x

15. Sevim MS, Buttanri IB, Kugu S, Serin D, Sevim S. Effect of intravitreal bevacizumab injection before Ahmed glaucoma valve implantation in neovascular glaucoma. *Ophthalmologica*. (2013) 229:94–100. doi: 10.1159/000345490

16. Wang Q, Zhao XX, Wu J, Li HQ, Qin XP. Effect of intravitreal injection of bevacizumab combined with Ahmed glaucoma valve implantation on neovascular glaucoma and its influence on aqueous humor VEGF and IL-6 levels. *Hebei Med*. (2021) 27:789–94.

17. Tang M, Fu Y, Wang Y, Zheng Z, Fan Y, Sun X, et al. Efficacy of intravitreal ranibizumab combined with Ahmed glaucoma valve implantation for the treatment of neovascular glaucoma. *BMC Ophthalmol*. (2016) 16:7. doi: 10.1186/s12886-016-0183-7

18. Ma KT, Yang JY, Kim JH, Kim NR, Hong S, Lee ES, et al. Surgical results of Ahmed valve implantation with intraoperative bevacizumab injection in patients with neovascular glaucoma. *J Glaucoma*. (2012) 21:331–6. doi: 10.1097/IJG.0b013e31820e2fd0

19. Moher D, Liberati A, Tetzlaff J, Altman DG. Preferred reporting items for systematic reviews and meta-analyses: the PRISMA statement. *PLoS Med*. (2009) 6:e1000097. doi: 10.1371/journal.pmed.1000097

20. Cumpston M, Li T, Page MJ, Chandler J, Welch VA, Higgins JP, et al. Updated guidance for trusted systematic reviews: a new edition of the Cochrane handbook for systematic reviews of interventions. *Cochrane Database Syst Rev*. (2019) 10:ED000142. doi: 10.1002/14651858.ED000142

21. Călugăru D, Călugăru M. Neovascular glaucoma--etipathogeny and diagnosis. *Oftalmologia*. (2012) 56:3–14.

22. Chinese Medical Association Ophthalmology Branch Glaucoma Group. Expert consensus on diagnosis and treatment of neovascular glaucoma in China. *Chin J Ophthalmol*. (2019) 55:814–7.

23. Porwal AC, Shrishrimal M, Punamia RP, Mathew BC. Assessment of intraocular pressure measurement between Goldman applanation tonometer, rebound tonometer, non-contact tonometer, and its correlation with central corneal thickness. *Indian J Ophthalmol*. (2023) 71:1927–31. doi: 10.4103/ijo.IJO_1982_22

24. Nakatake S, Yoshida S, Nakao S, Arita R, Yasuda M, Kita T, et al. Hyphema is a risk factor for failure of trabeculectomy in neovascular glaucoma: a retrospective analysis. *BMC Ophthalmol*. (2014) 14:55. doi: 10.1186/1471-2415-14-55

25. Frank RN. Vascular endothelial growth factor--its role in retinal vascular proliferation. *N Engl J Med*. (1994) 331:1519–20. doi: 10.1056/NEJM199412013312212

26. Sterne JAC, Savović J, Page MJ, Elbers RG, Blencowe NS, Boutron I, et al. RoB 2: a revised tool for assessing risk of bias in randomised trials. *BMJ*. (2019) 366:l4898. doi: 10.1136/bmj.l4898

27. Mahdy RA, Nada WM, Fawzy KM, Alnashar HY, Almosalamy SM. Efficacy of intravitreal bevacizumab with panretinal photocoagulation followed by Ahmed valve implantation in neovascular glaucoma. *J Glaucoma*. (2013) 22:768–72. doi: 10.1097/IJG.0b013e318259aec4

28. Zarei R, Ghasempour M, Fakhraie G, Eslami Y, Mohammadi M, Hamzeh N, et al. Ahmed glaucoma valve implantation with and without subconjunctival bevacizumab in refractory glaucoma. *Int Ophthalmol*. (2021) 41:1593–603. doi: 10.1007/s10792-021-01691-7

29. Arcieri ES, Paula JS, Jorge R, Barella KA, Arcieri RS, Secches DJ, et al. Efficacy and safety of intravitreal bevacizumab in eyes with neovascular glaucoma undergoing Ahmed glaucoma valve implantation: 2-year follow-up. *Acta Ophthalmol*. (2015) 93:e1–6. doi: 10.1111/aos.12493

30. Xu JH, Wang YL, Lin L, Shi LX, Zuo J. Efficacy of intravitreal injection of ranibizumab combined with Ahmed drainage valve implantation in the treatment of neovascular glaucoma. *Jiangsu Med*. (2015) 41:2550–2.

31. Li YB, Luo X, Liu TX, Hu XY. Efficacy of Ahmed glaucoma valve implantation surgery and ranibizumab therapy in the treatment of neovascular glaucoma. *Int J Ophthalmol*. (2019) 19:1853–6.

32. Zong LM, Cao EB. Efficacy observation of intravitreal injection of ranibizumab combined with FP-7 Ahmed glaucoma valve implantation in the treatment of neovascular glaucoma. *Zhejiang Med*. (2018) 40:1347–50.

33. Xie Z, Sun H, Chen X, Du ML. Long-term efficacy observation of anti-VEGF treatment combined with Ahmed drainage valve implantation in the treatment of neovascular glaucoma. *J Clin Ophthalmol*. (2018) 26:530–3.

34. Liu H, Sun JC. Intravitreal injection of ranibizumab combined with Ahmed glaucoma valve implantation for the treatment of neovascular glaucoma. *Chin J Clin Res*. (2019) 32:1059–62.

35. Xu KK, Han B, Han X, Shi BJ, Zhang WB, Li W. Effects of ranibizumab combined with Ahmed glaucoma valve implantation on ocular hemodynamics and serum VEGF, PDGF in patients with neovascular glaucoma. *Mod Adv Biomed*. (2022) 22:2250–4.

36. Tian LJ, Cui J, Lu D, Lu Y, Cui RZ. Efficacy observation of intravitreal injection of ranibizumab combined with drainage valve implantation in the treatment of 28 cases of neovascular glaucoma. *J Yanbian Univ Med Coll*. (2019) 42:273–5.

37. Liu XR. Effect of anti-VEGF drugs combined with glaucoma drainage valve implantation in the treatment of neovascular glaucoma. *Chin J Occup Eye Vis Inj*. (2020) 42:611–6.

38. Li XY, Mei Y, Xa . Efficacy and complications analysis of anti-VEGF drugs combined with Ahmed glaucoma drainage valve implantation in the treatment of neovascular glaucoma. *Chin Sci Technol Period Database Med Health*. (2022) 9:0008–0011.

39. Zheng HF, Yang JH, Zhao X. Efficacy and safety of anti-VEGF drugs combined with Ahmed glaucoma valve in the treatment of neovascular glaucoma. *Clin Med*. (2021) 41:70–2.

40. Luo GE. Analysis of the Efficacy of Anti-VEGF Combined with Ahmed Valve in the Treatment of Neovascular Glaucoma. Yanbian University (2019).

41. Lin B, Chen LL, Li DK. Meta-analysis of the efficacy of Ahmed glaucoma valve combined with anti-VEGF drugs in the treatment of neovascular glaucoma. *Int J Ophthalmol*. (2022) 22:2022–7.

42. Chen SZ, Mu YL. Meta-analysis of bevacizumab combined with Ahmed glaucoma valve implantation in the treatment of neovascular glaucoma. *Int J Ophthalmol*. (2020) 20:1931–6.

43. Hwang HB, Lee NY. Effect of anti-vascular endothelial growth factor on the surgical outcome of neovascular glaucoma: an overview and meta-analysis. *Medicine (Baltimore)*. (2021) 100:e27326. doi: 10.1097/MD.0000000000027326

44. Zhou M, Xu X, Zhang X, Sun X. Clinical outcomes of Ahmed glaucoma valve implantation with or without intravitreal bevacizumab Pretreatment for neovascular glaucoma: a systematic review and meta-analysis. *J Glaucoma*. (2016) 25:551–7. doi: 10.1097/IJG.0000000000000241

45. He Y, Tian Y, Song W, Su T, Jiang H, Xia X. Clinical efficacy analysis of Ahmed glaucoma valve implantation in neovascular glaucoma and influencing factors: a STROBE-compliant article. *Medicine (Baltimore)*. (2017) 96:e8350. doi: 10.1097/MD.0000000000008350

46. Hill R, Ohanesian R, Voskanyan L, Malayan A. The Armenian eye care project: surgical outcomes of complicated paediatric glaucoma. *Br J Ophthalmol*. (2003) 87:673–6. doi: 10.1136/bjo.87.6.673

47. Zhou X, Chen J, Luo W, Du Y. Short-term outcomes of trabeculectomy with or without anti-VEGF in patients with neovascular glaucoma: a systematic review and meta-analysis. *Transl Vis Sci Technol*. (2023) 12:12. doi: 10.1167/tvst.12.9.12

48. Hai Bo T, Xin K, Shi Heng L, Lin L. Comparison of Ahmed glaucoma valve implantation and trabeculectomy for glaucoma: a systematic review and meta-analysis. *PLoS One*. (2015) 10:e0118142. doi: 10.1371/journal.pone.0118142

49. Netland PA. The Ahmed glaucoma valve in neovascular glaucoma (an AOS thesis). *Trans Am Ophthalmol Soc*. (2009) 107:325–42.

50. Nilforushan N, Es'haghi A, Miraftabi A, Abolfathzadeh N, Banifatemi M. Trabeculectomy in patients with diabetes: subconjunctival mitomycin C with or without intravitreal bevacizumab. *Br J Ophthalmol*. (2022) 106:648–54. doi: 10.1136/bjophthalmol-2020-317324

51. Azimi-Nezhad M, Stathopoulou MG, Bonnefond A, Rancier M, Saleh A, Lamont J, et al. Associations of vascular endothelial growth factor (VEGF) with adhesion and inflammation molecules in a healthy population. *Cytokine*. (2013) 61:602–7. doi: 10.1016/j.cyto.2012.10.024

52. Zhou M, Chen S, Wang W, Huang W, Cheng B, Ding X, et al. Levels of erythropoietin and vascular endothelial growth factor in surgery-required advanced

neovascular glaucoma eyes before and after intravitreal injection of bevacizumab. *Invest Ophthalmol Vis Sci*. (2013) 54:3874–9. doi: 10.1167/iovs.12-11507

53. Chalam KV, Brar VS, Murthy RK. Human ciliary epithelium as a source of synthesis and secretion of vascular endothelial growth factor in neovascular glaucoma. *JAMA Ophthalmol*. (2014) 132:1350–4. doi: 10.1001/jamaophthalmol.2014.2356

54. Ferrara N, Damico L, Shams N, Lowman H, Kim R. Development of ranibizumab, an anti-vascular endothelial growth factor antigen binding fragment, as therapy for neovascular age-related macular degeneration. *Retina*. (2006) 26:859–70. doi: 10.1097/01.iae.0000242842.14624.e7

55. Chatzimichail E, Pfau K, Gatzioufas Z, Panos GD. Ranibizumab biosimilars in treating retinal disorders: a cost-effective revolution? *Drug Des Devel Ther*. (2024) 18:365–74. doi: 10.2147/DDDT.S457303

56. Papadopoulos N, Martin J, Ruan Q, Rafique A, Rosconi MP, Shi E, et al. Binding and neutralization of vascular endothelial growth factor (VEGF) and related ligands by VEGF trap, ranibizumab and bevacizumab. *Angiogenesis*. (2012) 15:171–85. doi: 10.1007/s10456-011-9249-6

57. Klettner A, Roider J. Comparison of bevacizumab, ranibizumab, and pegaptanib in vitro: efficiency and possible additional pathways. *Invest Ophthalmol Vis Sci*. (2008) 49:4523–7. doi: 10.1167/iovs.08-2055

58. Yilmaz T, Cordero-Coma M, Gallagher MJ, Teasley LA. Systematic review of intravitreal bevacizumab injection for treatment of primary diabetic macular oedema. *Acta Ophthalmol*. (2011) 89:709–17. doi: 10.1111/j.1755-3768.2010.01918.x

59. Ha JY, Lee TH, Sung MS, Park SW. Efficacy and safety of intracameral bevacizumab for treatment of neovascular glaucoma. *Korean J Ophthalmol*. (2017) 31:538–47. doi: 10.3341/kjo.2017.0017

60. Ghanem AA, El-Kannishy AM, El-Wehidy AS, El-Agamy AF. Intravitreal bevacizumab (avastin) as an adjuvant treatment in cases of neovascular glaucoma. *Middle East Afr J Ophthalmol*. (2009) 16:75–9. doi: 10.4103/0974-9233.53865

61. Zuo L, Zhu S, Gu S, Xu X. Anti-scarring effects of conbercept on human Tenon's fibroblasts: comparisons with bevacizumab. *BMC Ophthalmol*. (2023) 23:183. doi: 10.1186/s12886-023-02914-4

62. Xu Q, Gong C, Qiao L, Feng R, Liu H, Liu Y, et al. Downregulation of angiogenic factors in aqueous humor associated with less intraoperative bleeding in PDR patients with NVG receiving conbercept: a randomized controlled trial. *BMC Ophthalmol*. (2022) 22:224. doi: 10.1186/s12886-022-02451-6

63. Rittiphairoj T, Roberti G, Michelessi M. Anti-vascular endothelial growth factor for neovascular glaucoma. *Cochrane Database Syst Rev*. (2023) 4:Cd007920. doi: 10.1002/14651858.CD007920.pub4

64. Dumbrăveanu L, Cușnir V, Bobescu D. A review of neovascular glaucoma. Etiopathogenesis and treatment. *Rom J Ophthalmol*. (2021) 65:315–29. doi: 10.22336/rjo.2021.66

65. Sato Y, Kojimahara N, Kitano S, Kato S, Ando N, Yamaguchi N, et al. Multicenter randomized clinical trial of retinal photocoagulation for preproliferative diabetic retinopathy. *Jpn J Ophthalmol*. (2012) 56:52–9. doi: 10.1007/s10384-011-0095-2

66. Tham YC, Li X, Wong TY, Quigley HA, Aung T, Cheng CY. Global prevalence of glaucoma and projections of glaucoma burden through 2040: a systematic review and meta-analysis. *Ophthalmology*. (2014) 121:2081–90. doi: 10.1016/j.ophtha.2014.05.013

67. Song P, Wang J, Bucan K, Theodoratou E, Rudan I, Chan KY. National and subnational prevalence and burden of glaucoma in China: a systematic analysis. *J Glob Health*. (2017) 7:020705. doi: 10.7189/jogh.07.020705

68. Liao N, Li C, Jiang H, Fang A, Zhou S, Wang Q. Neovascular glaucoma: a retrospective review from a tertiary center in China. *BMC Ophthalmol*. (2016) 16:14. doi: 10.1186/s12886-016-0190-8

69. Foster PJ, Johnson GJ. Glaucoma in China: how big is the problem? *Br J Ophthalmol*. (2001) 85:1277–82. doi: 10.1136/bjo.85.11.1277

frontiers | Frontiers in Medicine

TYPE Original Research
PUBLISHED 16 September 2024
DOI 10.3389/fmed.2024.1441196

OPEN ACCESS

EDITED BY
Horace Massa,
Hôpitaux universitaires de Genève (HUG), Switzerland

REVIEWED BY
Dhanunjay Mukhi,
University of Pennsylvania, United States
Mallika Somayajulu,
Wayne State University, United States

*CORRESPONDENCE
Xin-Yu Li
✉ xinyu@tjh.tjmu.edu.cn

RECEIVED 30 May 2024
ACCEPTED 23 August 2024
PUBLISHED 16 September 2024

CITATION
Guo X-X, Chang X-J, Pu Q, Li A-L, Li J and Li X-Y (2024) Urolithin A alleviates cell senescence by inhibiting ferroptosis and enhances corneal epithelial wound healing. *Front. Med.* 11:1441196.
doi: 10.3389/fmed.2024.1441196

Urolithin A alleviates cell senescence by inhibiting ferroptosis and enhances corneal epithelial wound healing

Xiao-Xiao Guo, Xue-Jiao Chang, Qi Pu, Ao-Ling Li, Jing Li and Xin-Yu Li*

Department of Ophthalmology, Tongji Hospital, Tongji Medical College, Huazhong University of Science and Technology, Wuhan, China

Purpose: To analyze the therapeutic effect and mechanism of Urolithin A (UA) on delayed corneal epithelial wound healing.

Methods: The C57BL/6 mice were continuously exposed to hyperosmotic stress (HS) for 7 days followed by the removal of central corneal epithelium to establish a delayed corneal epithelial wound healing model *in vivo*. *In vitro*, the human corneal epithelial cell line (HCE-T) was also incubated under HS. UA was administered *in vivo* and *in vitro* to study its effects on corneal epithelial cells. Senescence-associated β-galactosidase (SA-β-gal) staining was performed to detect the level of cell senescence. Transcriptome sequencing (RNA-seq) was conducted to elucidate the molecular mechanism underlying the effect of UA on corneal epithelial repair. Additionally, the expression of senescence-related and ferroptosis-related genes and the levels of lipid peroxides (LPO) and malondialdehyde (MDA) were measured.

Results: Hyperosmotic stress (HS) significantly increased the proportion of SA-β-gal staining positive cells in corneal epithelial cells and upregulated the expression of p16 and p21 ($p < 0.0001$). Topical application of UA decreased the accumulation of senescent cells in corneal epithelial wounds and promoted epithelial wound healing. The results of RNA-seq of HS-induced corneal epithelial cells showed that the ferroptosis pathway was significantly dysregulated. Further investigation revealed that UA decreased the level of oxidative stress in HCE-T cells, including the levels of LPO and MDA ($p < 0.05$). Inhibition of ferroptosis significantly prevented cellular senescence in HS-induced HCE-T cells.

Conclusion: In this study, UA promoted HS-induced delayed epithelial wound healing by reducing the senescence of corneal epithelial cells through the inhibition of ferroptosis.

KEYWORDS

Urolithin A, wound healing, corneal epithelial cell, cell senescence, ferroptosis

1 Introduction

The corneal epithelium acts as a physical barrier and prevents the entry of external substances into the eye. The integrity and health of the corneal epithelium largely depend on the normal healing of the corneal epithelium after injury (1, 2). Lesions can damage the corneal epithelium and disrupt its barrier function. Although the corneal epithelium usually heals

quickly, some pathological conditions impair or delay the healing of the corneal epithelium. Studies have shown that sustained hyperosmotic stress (HS) can induce cell cycle arrest, apoptosis, and DNA damage (3, 4). For example, corneal epithelial cells in patients with severe dry eye and diabetes remain in the HS state for a long time, resulting in corneal epithelial cell damage and a decrease in its healing ability; moreover, complications such as recurrent epithelial defects or persistent corneal erosion may occur (5, 6).

Cell senescence is induced by various stimuli and stress, including oxidative stress, DNA damage, metabolic damage, and activation of oncogenes (7–9). Studies have found that high accumulation of senescent cells may drive delayed wound healing (10, 11). Alleviating hyperglycemia-induced cell senescence can accelerate diabetic wound healing (12), and the removal of senescent cells can promote wound healing and delay age-related diseases (13–15). Therefore, targeting cellular senescence is a novel approach to treating chronic poor wound healing.

Urolithin A (UA) is a metabolite produced by gut microbes acting on ellagic acid and ellagitannin, which are found in pomegranates, berries, and nuts (16). UA has anti-inflammatory, antioxidant, anti-tumor, and anti-aging effects (17–19). Some studies have shown that UA can alleviate oxidative stress-induced senescence of nucleus pulposus cells and ultraviolet radiation A-induced senescence of human dermal fibroblasts (20–22). As UA also prevents auditory cell senescence, it is a promising agent for treating age-related hearing loss (23). However, the effect of UA on corneal epithelial cell senescence is unclear. Therefore, we investigated whether UA can alleviate corneal epithelial cell senescence in chronic wound healing and elucidated its mechanism of action.

2 Materials and methods

2.1 Animal model

In total, male C57BL/6 mice ($n = 83$; 6–8 weeks old) were purchased from Bernd Laboratory Animal Technology Co., Ltd. (Hubei, China). The mice were divided into the control, HS, and HS + UA groups. Corneas of HS group and HS + UA group were treated with 500 mOsm/L NaCl solution by eye drops 10 times a day for 7 days. After the last intervention, the corneal epithelium was scraped. Mice in the control group were administered physiological saline. Mice in the HS + UA group were administered subconjunctival injection of UA (5 μL, 10 mmol/L) every other day for five consecutive times since the beginning of the experiment. The mice in the HS group and the control group were injected with an equal volume of physiological saline. AlgerBrush II rust remover (Alger, Lago Vista, TX, United States) was used to remove the epithelium within 2.5 mm of the central cornea under anesthesia. The mouse cornea was harvested for subsequent experimental analysis at predetermined time points.

2.2 Evaluating the damage to the ocular surface

The healing time of the corneal epithelium in the C57BL/6 mice was recorded after de-epithelialization, and the corneal epithelial defect area was compared 0, 18, 24, 40, 48, and 64 h after surgery. The cornea was stained with 0.1% sodium fluorescein, and the degree of healing of the corneal epithelium was observed and photographed using a hand-held slit lamp. The area of corneal epithelial defect was quantified by the ImageJ software (National Institutes of Health, United States).

2.3 Hematoxylin and eosin staining

At the 18th hour after the epithelium was removed, eyeballs of mice from different groups were harvested, fixed, dehydrated with 70–99% ethanol, and then, embedded in paraffin. The sections (5 μm thick) were stained with hematoxylin and eosin (H&E) to assess the degree of pathological alteration.

2.4 Immunofluorescence staining

For immunofluorescence staining, corneal tissue sections or cells were blocked with a 10% donkey serum solution (Boster Biological Technology, United States) for 30 min. Then, the samples were incubated with primary antibodies overnight at 4°C. After incubation, the samples were washed twice with PBS, incubated with the corresponding source of secondary antibodies for 45 min, and washed twice with PBS again. The nuclei were stained with 10 μg/mL DAPI and analyzed. Images were captured under a fluorescence microscopy (Olympus, Japan). The quantitation was performed using the ImageJ software.

2.5 Immunohistochemical staining

Paraffin sections underwent immunohistochemical (IHC) staining following standard protocols. Antigen unmasking was required for paraffin sections and was performed using Tris-EDTA buffer (pH 9.0). The tissue endogenous peroxide activity was quenched using a blocking solution (3% hydrogen peroxide). The slides were incubated with 10% goat serum for 45 min. After incubation, excess serum was removed from the slides, and the primary antibodies against p16 (#bs-0740R, Bioss, China, 1:300), p21 (#28248-1-AP, Proteintech, China, 1:200), and p53 (#10442-1-AP, Proteintech, China, 1:300) were added and incubated at 4°C overnight. After washing with 1 × PBS buffer, the secondary antibodies were added and incubated with DAB and a substrate color development system. Then, the sections were observed and examined under an optical microscope.

2.6 Cell culture and treatments

The human corneal epithelial (HCE-T) cells were purchased from MeisenCTCC (Zhejiang, China). The HCE-T cells were cultured in plates in a humidified atmosphere containing 5% carbon dioxide at 37°C. Dulbecco's modified Eagle's medium/F12 containing 5 μg/mL insulin, 10 ng/mL human epidermal growth factor, 10% fetal bovine serum, and 1% penicillin/streptomycin were used as the culture medium. The hypertonic state was achieved by adding NaCl to the

medium. The HCE-T cells were cultured under different hypertonic conditions (400 mOsm/L, 450 mOsm/L, and 500 mOsm/L) for 120 h.

2.7 Cell viability and LDH assay

Cell viability was determined by the Cell Counting Kit 8 assay (CCK-8, #C0037, Beyotime, China), following the manufacturer's guidelines. The HCE-T cells were inoculated in 96-well plates at a density of 5,000 cells/well and cultured in the cell incubator at 37°C with 5% CO_2. After the cells were attached to the wall, different concentrations of UA were added, followed by treatment for 24 h and 48 h. The cells were further treated with 10 μL of CCK-8 solution for 1–4 h, and the optical density was measured at 450 nm by enzyme-labeler to obtain the OD values.

Cytotoxicity was measured by the lactate dehydrogenase (LDH) release assay. Extracellular LDH release was determined by the LDH cytotoxicity detection kit (#C0016, Beyotime, China), following the manufacturer's instructions.

2.8 Cell scratch test

The HCE-T cells were inoculated in six-well plates and incubated overnight at 37°C. When the cell fusion reached about 90%, the medium was discarded and a 200 μL pipette tip was used to scratch the bottom of the plate. The scattered cells were washed thrice with PBS. According to the group, the corresponding medium and drugs were added for intervention, and incubation was continued at 37°C for 24 h. The cells that migrated to the labeled reference area to repair the wound were photographed, and the images were quantified using the ImageJ software. Wound healing was assessed by calculating the ratio of the difference between the original and remaining wound areas at 24 h.

2.9 Senescence-associated β-galactosidase activity assay

The senescence-associated β-galactosidase (SA-β-gal) staining kit (Beyotime, China) was used to stain the corneal patch or HCE-T cells *in situ*, following the manufacturer's instructions, to detect the senescence status of the cells. Briefly, mouse corneas or cells were washed thrice with PBS. Then, β-galactosidase fixing solution was added to fix the cells at room temperature for 15 min, followed by washing with PBS three times. Subsequently, 1 mL of β-galactosidase staining solution was added and incubated overnight in a biochemical incubator at 37°C. Next, the dye working solution was discarded. SA-β-gal-positive cells appeared blue, and the number of positive-stained cells per 200 cells in a randomly selected field of view was calculated under an optical microscope.

2.10 RNA sequencing

To sequence cellular RNA, a high-throughput sequencing service (Dancheng Biotechnology, Shanghai, China) was used. The total RNA of HCE-T cells was extracted using Trizol, according to the instructions, and the mRNA was enriched by magnetic beads and Oligo (dT). The RNA concentration was determined using the Nanodrop 2000 spectrophotometer (Thermo Fisher Scientific). RNA was sequenced using the HiSeq 2000 system (Illumina, San Diego, CA, United States). Subsequently, $p < 0.05$ and fold change >2 generated by DESeq2 were analyzed for the enrichment of biological terms with the Database for Annotation, Visualization, and Integrated Discovery (DAVID) bioinformatics platform. The gene expression patterns were analyzed using volcano plots. The Kyoto Encyclopedia of Genes and Genomes (KEGG) pathway enrichment analysis of the differentially expressed transcripts was performed using R based on the hypergeometric distribution.

2.11 Measurement of intracellular iron and lipid peroxidation

Labile intracellular iron was measured using the calcein acetoxymethyl (AM) ester quenching method (#C2012-0.1 mL, Beyotime). The HCE-T cells were washed with 1× PBS, treated with calcein AM (1 μM), and incubated at 37°C for 30 min. The culture medium was replaced with a fresh medium and incubated for 30 min to ensure that calcein AM was fully hydrolyzed by lactase to generate calcein with green fluorescence. Finally, the cells were washed thrice with PBS and observed under a fluorescence microscope (Olympus, Japan).

Lipid peroxidation (LPO) in HCE-T cells was detected by the BODIPY 581/591 C11 (BODIPY C11) probe (#D3861, Thermo Fisher Scientific, United States). The HCE-T cells on the slide were incubated with BODIPY-C11 (2 μM) in the dark for 30 min. After incubation, the working solution was discarded, and the cells were washed with 1 x PBS buffer twice for 5 min each time. Imaging was performed using a fluorescence microscope (Olympus, Japan).

2.12 Measurement of malondialdehyde and glutathione

The malondialdehyde (MDA) content in HCE-T cells was determined using the MDA assay kit (#E-BC-K028-M, Elabscience, China), following the manufacturer's instructions. The oxidized glutathione (GSSG) and reduced glutathione (GSH) levels were estimated using a Total GSH/GSSG Colorimetric Assay Kit (#E-BC-K097-M, Elabscience, China).

2.13 Reverse transcription and quantitative real-time polymerase chain reaction

Total RNA was extracted from HCE-T cells with the RNeasy Mini Kit (Qiagen, Valencia, CA, United States), following the manufacturer's instructions. In total, 1–2 μg of total RNA was reverse-transcribed to cDNA using the cDNA Transcription Kit (Vazyme, United States). Reverse transcription and quantitative real-time polymerase chain reaction (RT-qPCR) were performed in a 20 μL solution containing cDNA, TaqMan Gene Expression Assay Mix, and a universal PCR Master Mix (Vazyme, United States). The expression of the target gene was normalized to that of Gapdh. The cDNA was amplified using the following primers: p16, forward, 5′-GGGTTTTCGTGGTTCACATC-3′, reverse, 5′-CTAGACGCTGGCTCCTCAGTA-3′; p21, forward, 5′-CGA TGGAACTTCGACTTTGTCA-3′, reverse, 5′-GCACAAGGGTACA

AGACAGTG-3′; p53, forward, 5′-TGAAGCTCCCAGAATGCCAG-3′, reverse, 5′-CAGTCAGAGCCAACCTCAGG-3′; Acyl-CoA synthetase long chain family member 4 (ACSL4), forward, 5′-CATCC CTGGAGCAGATACTCT-3′, reverse, 5′-TCACTTAGGATTTCCCTG GTCC-3′; ferritin heavy chain 1 (FTH1), forward, 5′-CCCCCATTTGT GTGACTTCAT-3′, reverse, 5′-GCCCGAGGCTTAGCTTTCATT-3′; glutathione peroxidase 4 (GPX4), forward, 5′-GAGGCAAGACCGAA GTAAACTAC-3′, reverse, 5′-CCGAACTGGTTACACGGGAA-3′. The expression of the target gene was calculated using the $2^{-\Delta\Delta Ct}$ method and expressed as a fold change over that of the control.

2.14 Western blotting analysis

After the samples were washed in ice-cold PBS, proteins were extracted using ice-cold RIPA lysis buffer. The protein content in the supernatant was determined by conducting a BCA assay. The samples were subjected to denaturing 10% SDS-PAGE and then transferred to polyvinylidene difluoride membranes. The membrane was sealed at room temperature for 1 h with a sealing solution (5% skim milk in TBST), followed by incubation with primary antibodies, including anti-human p16 (#10883-1-AP, Proteintech, China, 1:2,000), anti-human p21 (#28248-1-AP, Proteintech, China, 1:1,000), anti-human p53 (#10442-1-AP, Proteintech, China, 1:2,000), anti-human ACSL4 (#22401-1-AP, Proteintech, China, 1:2,000), anti-human FTH1 (#ET1610-78, HUABIO, China, 1:2,000), and anti-human GPX4 (#ab231174, Abcam, United States, 1:2,000) overnight at 4°C. The blots were washed and incubated with horseradish peroxidase (HRP)-conjugated goat anti-rabbit secondary IgG antibodies (Abcam, 1:20,000) for 1 h at 37°C. Then, they were developed with an ECL detection system (Santa Cruz Biotechnology, CA, United States). GAPDH was used as a loading control. Densitometry was performed using the ImageJ software.

2.15 Statistical analysis

All statistical analyses were performed using GraphPad Prism 8.0 (GraphPad Software, La Jolla, CA, United States) and ImageJ. The values are expressed as the mean ± standard deviation. The normality and homogeneity of variance of the data were evaluated by the Shapiro–Wilk test. The differences in parameters between groups were determined by independent samples *t*-test. The differences in parameters among multiple groups were determined by one-way ANOVA or chi-square test. The least significant difference method was used for post-hoc multiple comparisons. All differences among and between groups were considered to be statistically significant at $p < 0.05$.

3 Results

3.1 Hyperosmotic stress induced cellular senescence in corneal epithelial cells and delayed wound healing

To determine the effects of HS on corneal epithelial cells, the cornea and corneal epithelial cells were treated with a hyperosmolar solution *in vivo* and *in vitro*, respectively. The healing of the corneal epithelium after injury is illustrated in Figures 1A,B. The corneal epithelium of the control group healed completely within 48 h, while defects in the epithelium were detected even 64 h after the injury was induced in the HS group. A photograph of the anterior segment showed that the corneal epithelium was defective in both groups, and the difference in corneal transparency between the groups was not significant 18 h after corneal injury. The H&E-stained sections showed that the inflammatory response was more severe in the HS group, accompanied by the infiltration of a large number of inflammatory cells (Figure 1C). The immunofluorescence results of senescence markers (p21, p16, and p53) showed that the number of p16/p21-positive corneal epithelial cells in the HS group was more than that in the control group. However, the difference in the number of p53-positive cells between the groups was not significant (Figure 1D).

In vitro, the HCE-T cells were exposed to isotonic (312 mOsm/L) or hypertonic (400 mOsm/L, 450 mOsm/L, and 500 mOsm/L) conditions for 120 h. The percentage of SA-β-gal-stained senescent cells was significantly higher in the 450 mOsm/L group compared to that in the control group (Figures 1E,F, $p < 0.0001$). Many cells died in the 500 mOsm/L group. Therefore, 450 mOsm/L was selected as the condition for inducing hyperosmolarity in subsequent studies. We also detected the expression of p16, p21, and p53 and the DNA damage marker γ-H2AX in HCE-T cells. Similar to the results of *in vivo* experiments, the expression of p16 and p21 in the HS group was significantly higher than that in the control group, but the difference in the expression of p53 was not significant. Moreover, the expression of γ-H2AX was also significantly higher than that in the control group (Figures 1G,H, $p < 0.0001$). These results suggested that HS can induce senescence in corneal epithelial cells.

3.2 UA treatment alleviated HS-induced cellular senescence *in vitro*

We conducted relevant experiments to determine whether UA can rescue HCE-T cells under hyperosmotic conditions (Figure 2A). First, we treated HCE-T cells with 0.001, 0.01, 0.1, 1, and 10 μM UA for 24 h and 48 h, respectively. When the concentration was higher than 0.1 μM, the cell viability decreased significantly (Figure 2B, $p < 0.01$). Therefore, 0.1 μM UA was used in subsequent studies. There was no significant difference in SA-β-gal staining results between the cells treated with UA alone and the control group (Supplementary Figure S1). HCE-T cells were treated with UA for 24 h and then exposed to high-osmolarity conditions for 120 h. The percentage of SA-β-gal-stained cells increased significantly after hypertonic stimulation compared to that in the control group. Moreover, UA treatment decreased the percentage of SA-β-gal-stained cells (Figures 2C,D, $p < 0.0001$).

We also assessed mRNA and protein levels of cell senescence-relevant markers. The results showed that the level of expression of the p16, p21, and p53 mRNAs in HCE-T cells was significantly upregulated under hypertonic conditions compared to that in the control group, and this upregulation was reversed after UA treatment (Figure 2E). The results of western blotting assays showed that the expression of p16 and p21 was consistent with RT-qPCR, but no significant difference was found in p53 protein levels (Figure 2F). These findings indicated that UA can alleviate the senescence of HCE-T cells caused by HS.

We further assessed cell migration capacity. The result showed that the migration ability of HCE-T cells decreased significantly under

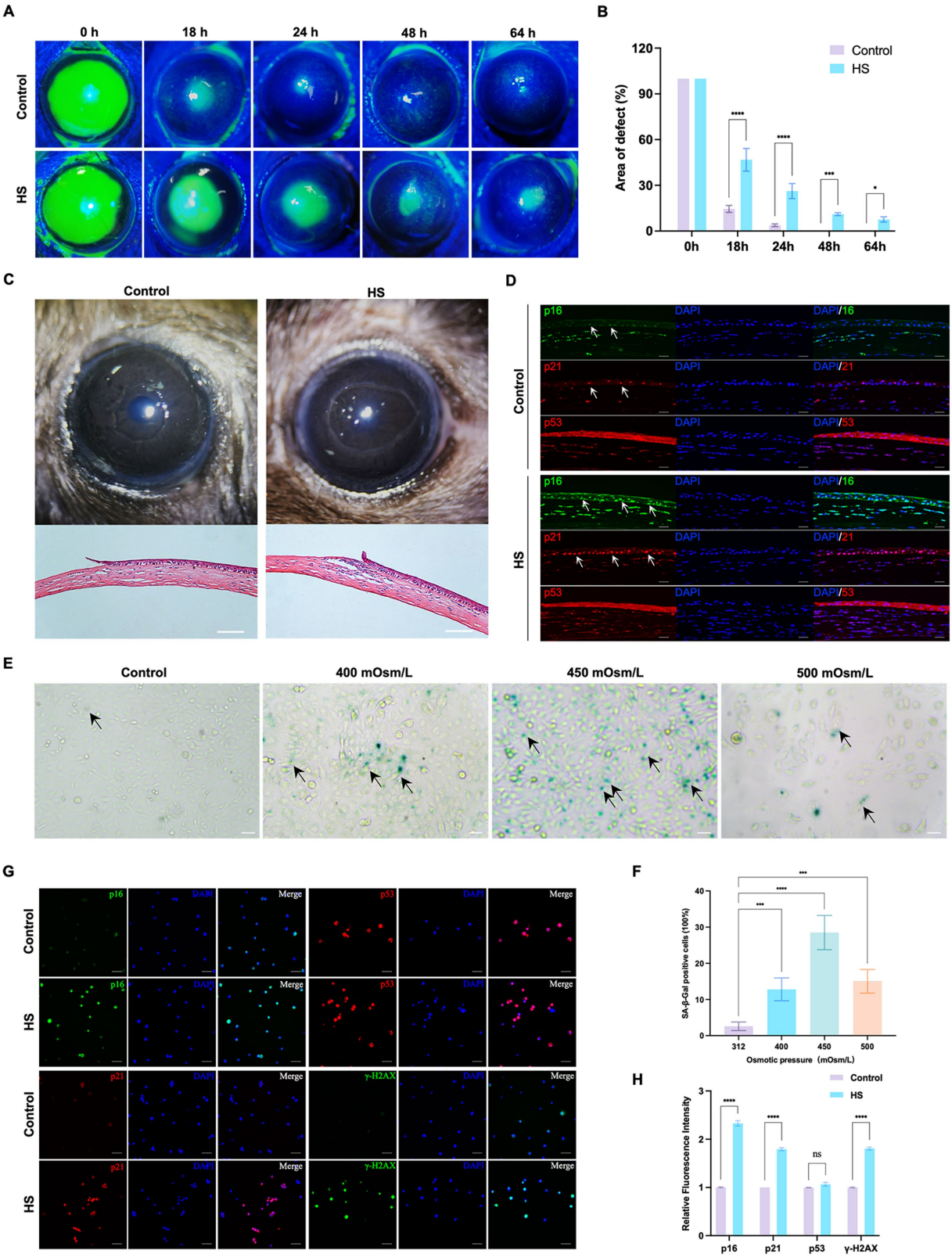

FIGURE 1
HS induced cellular senescence in cornea epithelial cells and delayed wound healing. **(A)** Representative images of corneal fluorescein staining. **(B)** Quantitative corneal epithelial defect area analysis at different times; $n = 5$. **(C)** Photos of corneal wound healing and HE staining results from 18 h after epithelial removal; scale = 100 μm. **(D)** Immunofluorescence staining of corneal epithelial senescence markers p16, p21, and p53; $n = 5$, scale = 50 μm. **(E)** SA-β-gal staining of HCE-T cells under different osmotic pressure conditions. Black arrows indicated staining positive cells; scale = 50 μm. **(F)** Quantitative analysis of SA-β-gal staining cells; $n = 3$. **(G)** Immunofluorescence staining of HCE-T cells for p16, p21, p53, and γ-H2AX; scale = 50 μm. **(H)** Quantitative analysis of immunofluorescence staining; $n = 3$. $^{*}p < 0.05$, $^{***}p < 0.001$, and $^{****}p < 0.0001$.

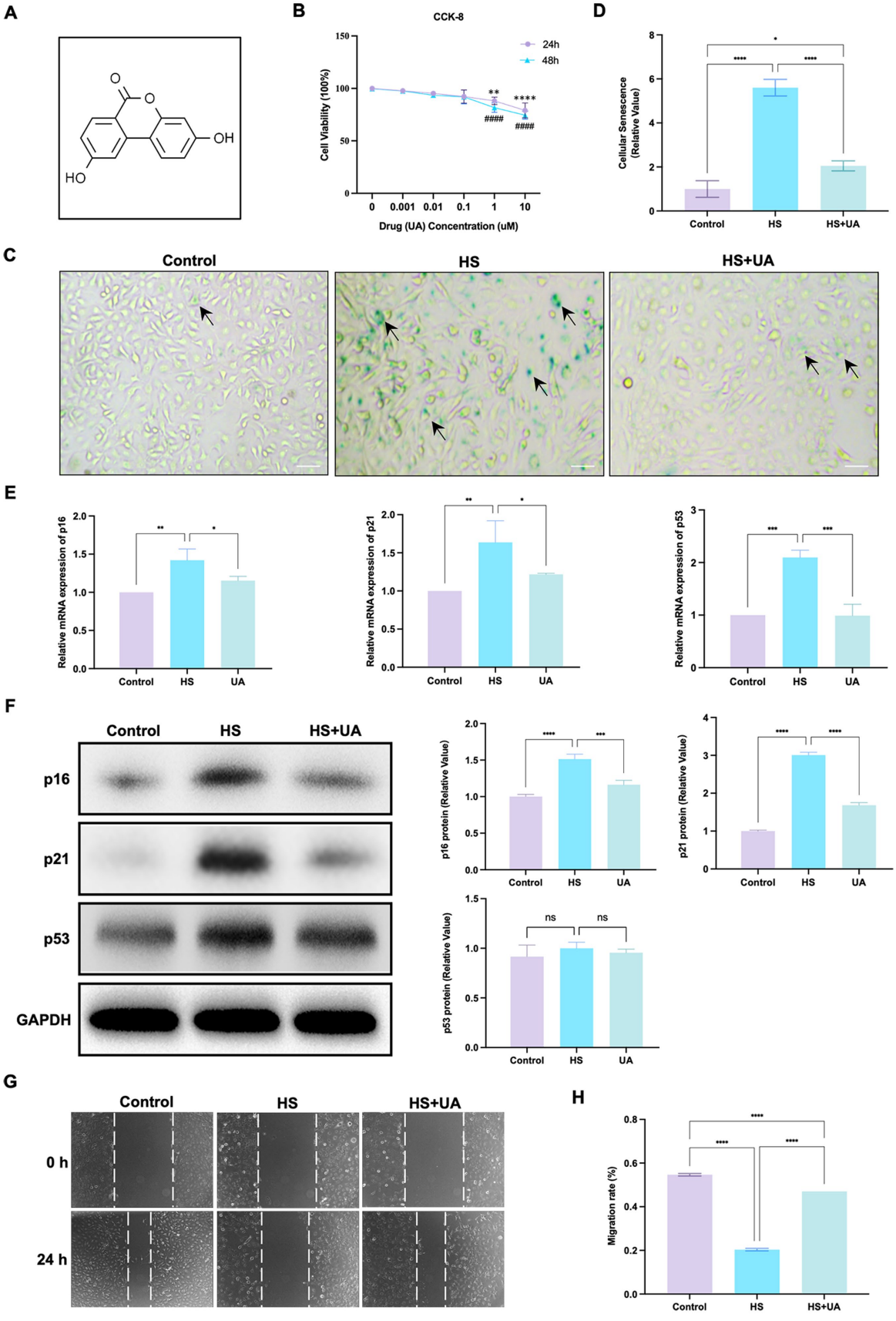

FIGURE 2
UA treatment alleviated HS-induced cellular senescence. **(A)** Molecular formula of UA. **(B)** Cell viability was tested by CCK-8 assay. **(C)** SA-β-gal staining of HCE-T cells. Black arrows indicated staining positive cells; scale = 50 μm. **(D)** Quantitative analysis of SA-β-gal staining results. **(E)** Relative mRNA expression of p16, p21, and p53. **(F)** Representative western blot images and quantitative analysis of brand intensity. **(G)** The scratch test and **(H)** quantitative analysis. $n = 3$, $^{*}p < 0.05$, $^{**}p < 0.01$, $^{***}p < 0.001$, and $^{****}p < 0.0001$.

HS conditions ($p < 0.0001$). After UA treatment, cell migration ability improved considerably (Figures 2G,H), which suggested that the accumulation of senescent cells caused by HS can inhibit the migration of cells, and UA treatment can reverse the delay in cell migration.

3.3 UA treatment can alleviate delayed corneal epithelial wound healing under hyperosmotic conditions

As the application of cell lines in simulating the physiological characteristics of corneal epithelial cells has some limitations, we established an animal model of corneal epithelial cell senescence by continuous eye intervention with hypertonic saline and further investigated the anti-senescence effects of UA *in vivo*. The corneal epithelium was carefully removed after intervention with the hypertonic solution, and the healing of corneal epithelium was observed at 0, 18, 24, 40, 48, and 64 h, respectively (Figure 3A). In the control and UA groups, the corneal epithelium healed completely within 48 h. However, the corneal epithelium of the HS group neither healed completely at 48 h nor at 64 h.

We also quantified the area of corneal epithelial defect in the three groups at different times. The results showed that the average defect area of the HS group was 55.37% 18 h after surgery and that of the UA intervention group was 27.55%, which was significantly smaller than that of the HS group ($p < 0.0001$). At 48 h after surgery, the defect area of the HS group was 14.18%. In contrast, the epithelium was fully healed in the UA group, similar to that in the control group (Figure 3B). Therefore, HS can delay the healing of corneal epithelium in mice, and the wound healing time is significantly shortened after UA treatment. These findings suggested that UA can relieve the symptoms of poor corneal epithelial wound healing caused by HS.

We also found that continuous hypertonic stimulation resulted in the accumulation of many SA-β-gal-stained positive cells around the central corneal epithelial wound, whereas, the number of senescent cells significantly decreased in the UA group (Figures 3C,D, $p < 0.0001$). We also examined the expression and distribution of senescence markers in the cornea. The results of immunohistochemical assays showed that the level of expression of p16 and p21 in the epithelium increased considerably in the HS group, and their levels recovered significantly after UA treatment (Figures 3E,F). Similarly, the level of expression of the p16 and p21 proteins in the HS group was significantly upregulated, and UA treatment decreased their expression (Figure 3G). Thus, a decrease in the expression of p16 and p21 and a decrease in the positive rate of SA-β-gal staining indicated that UA can inhibit HS-induced senescence of corneal epithelial cells. Thus, the effect of UA on the poor healing of corneal epithelial wounds might be related to its anti-senescence effect.

3.4 Ferroptosis was involved in cell senescence caused by hyperosmolarity

To further investigate the mechanisms underlying HS-induced cell senescence, we conducted transcriptome sequencing analysis on cells from the HS and control groups. The results revealed that the genes differentially expressed between the groups were primarily enriched in signaling pathways related to ferroptosis, amino acid metabolism, and phospholipid metabolism (Figures 4A,B). Ferroptosis is closely related to cell metabolism and cell fate, and we further examined the involvement of ferroptosis in cell senescence caused by HS. The results of calcein AM staining showed that the intracellular labile iron content in the HS group was significantly higher than that in the control group (Figures 4C,D). Ferroptosis is closely related to an increase in oxidative stress, especially lipid peroxidation. Our results indicated that the level of LPO in HCE-T cells was significantly higher in the HS group than in the control group (Figures 4E,F), manifesting as a significant increase in the fluorescence intensity of oxidized BODIPY-C11 and a relative decrease in the fluorescence intensity of non-oxidized BODIPY-C11. These results indicated that HS treatment can induce ferroptosis in HCE-T cells.

To further elucidate the role of ferroptosis in the senescence of HCE-T cells, we conducted an intervention experiment with the ferroptosis inducer ferric ammonium citrate (FAC) and the ferroptosis inhibitor Ferrostatin-1 (Fer-1). We designated the condition of treating HCE-T cells with 500 μmol/L FAC for 48 h as a positive control for inducing ferroptosis (Supplementary Figures S2A,B). The highest number of SA-β-gal positive cells was recorded in the FAC + UA group, while compared to the HS group, the number of SA-β-gal positive cells in the UA and Fer-1 groups decreased significantly (Figures 4G,H). Additionally, the level of expression of the mRNAs and proteins of p16 and p21 in the UA and Fer-1 groups were lower than their respective levels in the HS group (Figures 4I,J). This implied that FAC-induced ferroptosis can reverse the anti-senescence effects of UA, and conversely, inhibiting ferroptosis can alleviate the senescence of HCE-T cells. Our results also showed that there were no significant differences in p53 levels among all groups, similar to our previous findings, indicating that HS-induced senescence and ferroptosis may be independent of p53.

3.5 UA intervention inhibited ferroptosis induced by hyperosmolarity *in vitro*

As ferroptosis was involved in cell senescence caused by hyperosmolarity, we investigated whether UA alleviated cell senescence through ferroptosis and determined its exact regulatory mechanisms. First, the results of the CCK-8 assay showed that UA treatment strongly inhibited the HS-induced decrease in the viability of HCE-T cells (Figure 5A). These results were similar to those of the LDH release assay, which showed that HS exposure significantly increased the cell toxicity of HCE-T compared to the control group, while UA treatment effectively rescued HCE-T (Figure 5B). The fluorescence intensity of oxidized BODIPY-C11 significantly increased in the HS group compared to the fluorescence intensity recorded in the control group (Figure 5C). After UA treatment, the fluorescence intensity of non-oxidized BODIPY-C11 increased, which indicated that UA can significantly decrease the level of expression of LPO. However, when co-treated with FAC, the level of LPO increased significantly and reversed the effects of UA.

We also measured the levels of MDA and GSH related to oxidative stress. We found that HS stimulated the production of MDA in HCE-T cells relative to MDA production in the control group. In contrast, UA decreased intracellular MDA levels ($p < 0.0001$, Figure 5D). GSH metabolism strongly influences redox metabolism and ferroptosis. It serves as an electron donor of GPX4, and a decrease

10.3389/fmed.2024.1441196

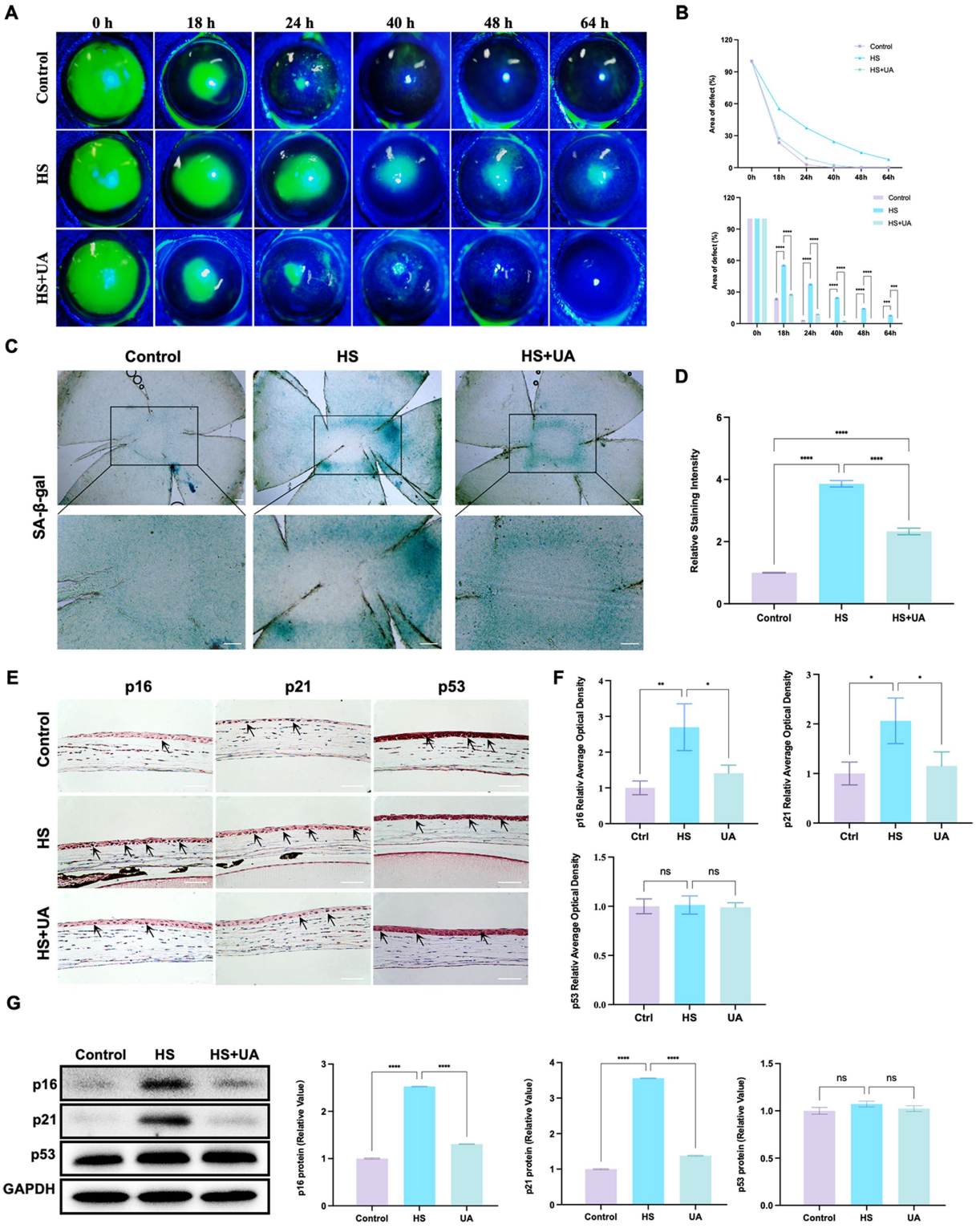

FIGURE 3
UA improved the symptoms of delayed healing of corneal epithelial wounds induced by HS in mice. **(A)** Representative images of corneal fluorescein sodium staining. **(B)** The trend of corneal epithelial defect areas at different follow-up times. **(C)** SA-β-gal staining of flat-mounted corneas; scale = 200 μm. **(D)** Quantitative analysis of SA-β-gal staining results. **(E)** Immunohistochemical staining results of p16, p21, and p53 in mouse corneal epithelium; scale = 100 μm. **(F)** Quantitative analysis of immunohistochemical results. **(G)** Representative western blot images and quantitative analysis of brand intensity. $n = 3$, $^{*}p < 0.05$, $^{**}p < 0.01$, $^{***}p < 0.001$, and $^{****}p < 0.0001$.

in GSH levels can influence the antioxidant capacity and lipid metabolism of cells. Our results showed that the total GSH level (GSH + GSSG) of HCE-T cells exposed to HS decreased. Among them, the GSSG level increased significantly, while the GSH/GSSG and GSH levels were considerably lower than those in the control group ($p < 0.0001$). After UA treatment, the GSSG level in HCE-T cells

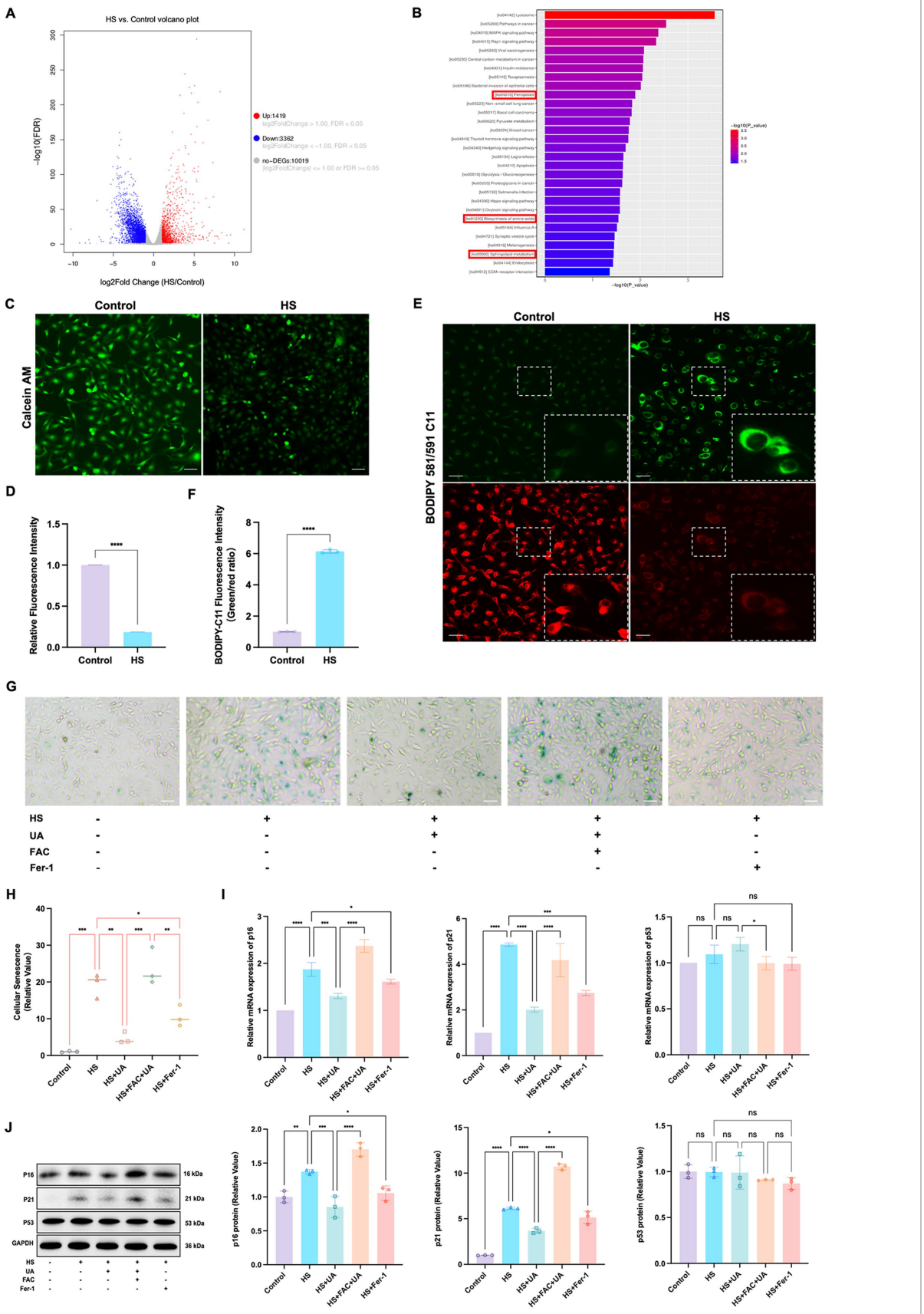

FIGURE 4
Ferroptosis was involved in cell senescence caused by hyperosmolarity. **(A)** Volcano plot shows significant genes that altered in the HS group and control group. **(B)** KEGG pathway enrichment bar chart of significantly different genes in the HS group and control group. **(C)** Representative images of

(Continued)

FIGURE 4 (Continued)
intracellular labile iron indicated by calcein-AM assay; scale = 50 μm. **(D)** Quantitative analysis of calcein fluorescence density. **(E)** Representative images of LPO indicated by BODIPY-C11 probe; scale = 50 μm. **(F)** Quantitative analysis of the fluorescence intensity of oxidized and non-oxidized BODIPY-C11. **(G)** SA-β-gal staining of HCE-T cells; scale = 50 μm. **(H)** Quantitative analysis of SA-β-gal staining cells. **(I)** Relative mRNA expression of p16, p21, and p53. **(J)** Representative western blot images and quantitative analysis of brand intensity. $n = 3$, $^{*}p < 0.05$, $^{**}p < 0.01$, $^{***}p < 0.001$, and $^{****}p < 0.0001$.

decreased, and the GSH/GSSG and GSH levels were significantly restored ($p < 0.0001$, Figure 5E). Moreover, additional treatment of FAC caused the levels of GSH/GSSG and GSH to decrease again, eliminating the inhibitory effect of UA on ferroptosis. Therefore, the inhibition of HS-induced ferroptosis in HCE-T cells by UA is associated with a decrease in oxidative stress levels.

Ferroptosis involves multiple molecules, among which FTH1 and GPX4 are negatively correlated with the occurrence of ferroptosis, while ACSL4 is positively correlated with ferroptosis. To determine the molecular mechanism of action of these molecules, we conducted RT-qPCR and western blotting assays on the aforementioned key molecules. The results of RT-qPCR assays showed that HS exposure upregulated the expression of ACSL4 in HCE-T cells but downregulated the expression of FTH1 and GPX4. In the UA group, the results were the opposite. The level of expression of ACSL4 was downregulated, while the expression of FTH1 and GPX4 mRNAs was significantly upregulated (Figure 5F). The results of western blotting assays matched those of the RT-qPCR assays (Figure 5G). These results indicated that UA inhibits HS-induced ferroptosis in cells by upregulating GPX4 and FTH1 and suppressing ACSL4.

4 Discussion

In this study, we analyzed the role of cell senescence in damage caused by HS to the corneal epithelium and determined the role of UA in HS-related cell senescence. We found that continuous hypertonic stimulation can cause the senescence of corneal epithelial cells and significantly delay wound healing. UA treatment can decrease the proportion of SA-β-gal staining positive cells, downregulate the expression of p16 and p21, and promote cell migration. We also found that the senescence of HCE-T cells is regulated by ferroptosis, and inhibiting ferroptosis can alleviate the senescence of HCE-T cells (Figure 6).

It is worth noting that the expression of p21 and p16 in corneal epithelial cells after HS treatment was significantly up-regulated, while p53 had no significant effect. When cells are stimulated by external stress, DNA-damage response leads to the activation of p53/p21 and p16 pathways, blocking the cell cycle and entering the cell senescence process. p21 is a downstream gene of p53 and its expression is regulated by p53. However, p21 has been found to induce premature senescence in p53-deficient H1299 cells (24). In senescent embryonic cells, p21 is regulated by TGF-β/SMAD and PI3K/ FOXO signaling pathways, but not by p53 (25). Englund et al. (26) found that p21 alone was sufficient to drive the cellular senescence process, leading to aging and functional decline of skeletal muscle cells. In addition, although the silencing of p53 gene can reduce the expression of p21, the expression of p21 can be significantly upregulated in cells that simultaneously knocked down the histone methyltransferase SETD8, indicating that the change of p21 is completely independent of p53 (27). Therefore, we speculate that HS may promote corneal epithelial cell senescence in a non-p53-dependent pathway.

Cellular senescence strongly influences wound healing (28). Senescent lung fibroblasts induce cell cycle arrest in the G2/M phase in alveolar epithelial cells, leading to abnormal wound repair and re-epithelialization (29). Samdavid Thanapaul et al. (11) found that in an irradiation-induced skin aging model, skin fibroblast aging delayed wound healing. Chia et al. (30) found that the level of expression of p21 increased significantly during wound healing in the elderly, and abnormal aging indicators explained the abnormal skin repair ability. Additionally, removing senescent cells can alleviate poor wound healing and delay age-related diseases. By inhibiting high glucose-induced cellular senescence, collagen deposition and the expression of α-SMA can be accelerated to promote the healing of diabetic wounds (12). Saul et al. (31) found that the intermittent administration of the senescent cell-eliminating drug dasatinib combined with quercetin decreased the senescence markers in the fracture callus of adult mice, significantly reduced the fracture healing time, and promoted tissue repair. We found that continuously exposing the corneal epithelium of mice to hypertonic conditions resulted in a significant delay in wound healing, and many senescent cells were observed at the edge of the corneal epithelial wound. After UA treatment, the level of expression of p16 and p21 in HCE-T cells and mouse corneal epithelial cells were significantly downregulated, and the proportion of SA-β-gal-stained cells decreased, which confirmed that corneal epithelial healing and damage repair could be promoted by alleviating cell senescence.

The RNA-seq results also indicated that ferroptosis was significantly dysregulated. Ferroptosis is immunogenic and causes cell damage along with a cascade of amplified inflammatory reactions, aggravating the damage in surrounding tissues (32). Some studies have shown that ferroptosis and cellular senescence are correlated (33–36). Several studies have reported abnormalities in iron metabolism in cells in many organisms (e.g., fruit flies, rodents, humans, etc.), especially in the brain, where excess iron can lead to neurodegenerative diseases, such as Alzheimer's and Parkinson's disease (37–39). Sun et al. (40) found that erastin, a ferroptosis inducer, increased the percentage of SA-β-gal positive cells by depleting GSH, which indicated that GSH depletion can induce ferroptosis in retinal pigment epithelial cells while also leading to cell growth arrest and premature cell senescence. In this study, HCE-T treated with FAC showed the highest number of SA-β-gal positive cells. However, compared to the HS group, the number of SA-β-gal positive cells in the UA and Fer-1 groups decreased significantly. Moreover, the expression of p16 and p21 in the UA and Fer-1 groups was lower than that in the HS group, which implied that FAC-induced ferroptosis reversed the

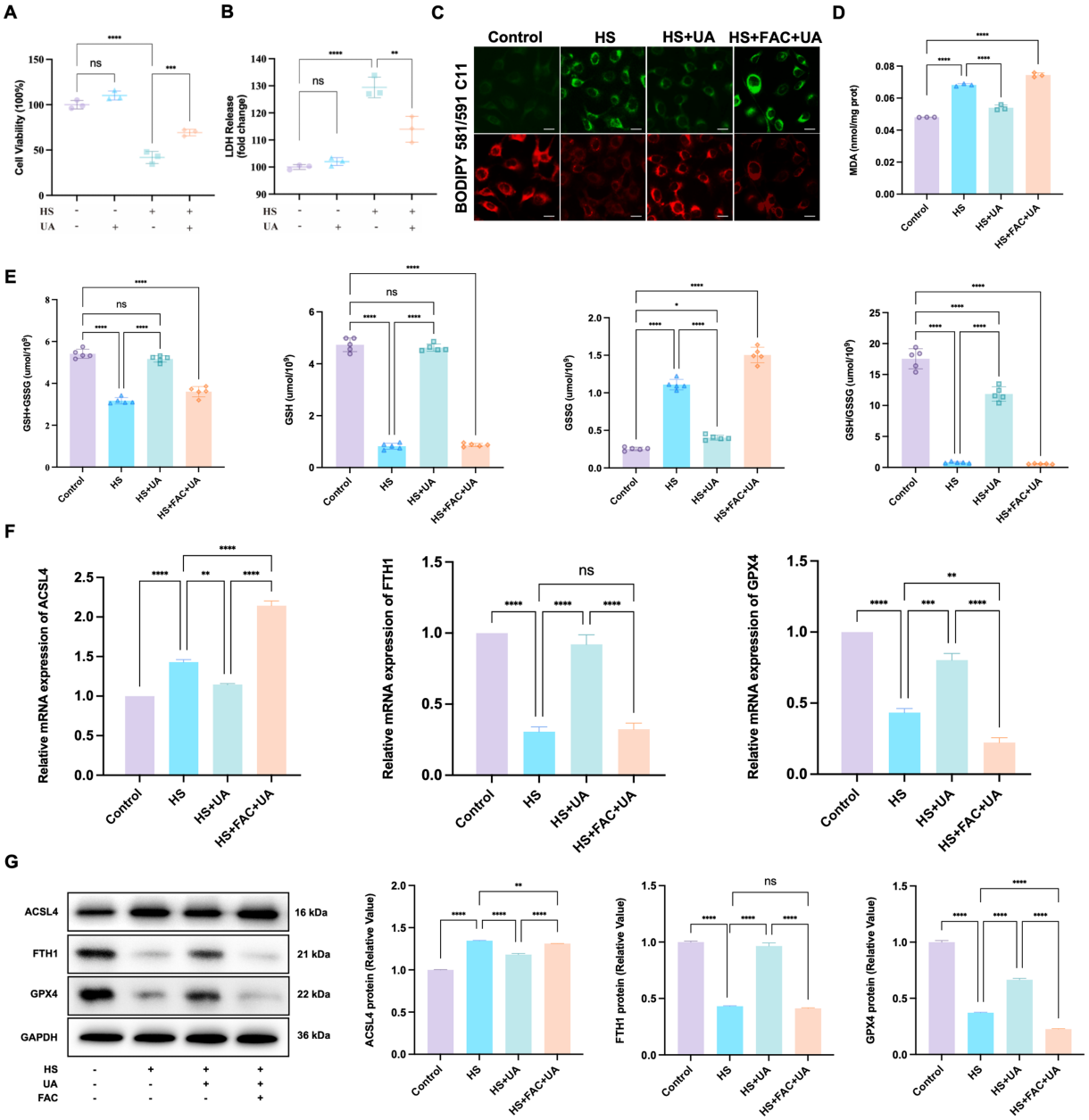

FIGURE 5
UA intervention inhibited the ferroptosis process induced by hyperosmolarity. **(A)** Cell viability was tested by CCK-8 assay. **(B)** Cytotoxicity was tested by LDH assay. **(C)** Representative images of LPO indicated by BODIPY-C11 probe; scale = 20 μm. **(D)** MDA levels in HCE-T cells. **(E)** The levels of GSH + GSSG, GSH, GSSG, and GSH/GSSG in HCE-T cells. **(F)** Relative mRNA expression of ACSL4, FTH1, and GPX4. **(G)** Representative western blot images and quantitative analysis of brand intensity. $n = 3$, $^{*}p < 0.05$, $^{**}p < 0.01$, $^{***}p < 0.001$, and $^{****}p < 0.0001$.

anti-senescence effects of UA, whereas, inhibiting ferroptosis alleviated the senescence of HCE-T cells.

Ferroptosis is closely related to an increase in oxidation levels, especially lipid peroxidation levels (41). Lou et al. (42) showed that UA can reduce the lung dry weight-to-wet weight ratio *in vivo*, decrease the production of ROS and MDA and the depletion of GSH, and thus, effectively alleviate LPS-induced ferroptosis and acute lung injury in mice. By estimating the levels of LPO, MDA, and GSH related to oxidative stress, we found that UA significantly reduced the susceptibility of HCE-T cells to the induction of HS and the levels of LPO, MDA, and GSSG. It also significantly recovered GSH, which showed a cytoprotective effect. These findings were also similar to those reported by Xu et al. (43), who showed that $1,25(OH)_2D_3$ can downregulate senescence-related genes, MDA, and 4-hydroxynonenal and upregulate GSH by inhibiting D-gal-induced ferroptosis, thus delaying osteoblast senescence and preventing osteoporosis. Therefore, UA treatment reduced the level of oxidative stress in HCE-T cells and inhibited ferroptosis. It also reversed the HS-induced upregulation of ACSL4 and downregulation of FTH1 and GPX4. This finding further supported the speculation that UA can delay HCE-T cell senescence by inhibiting ferroptosis.

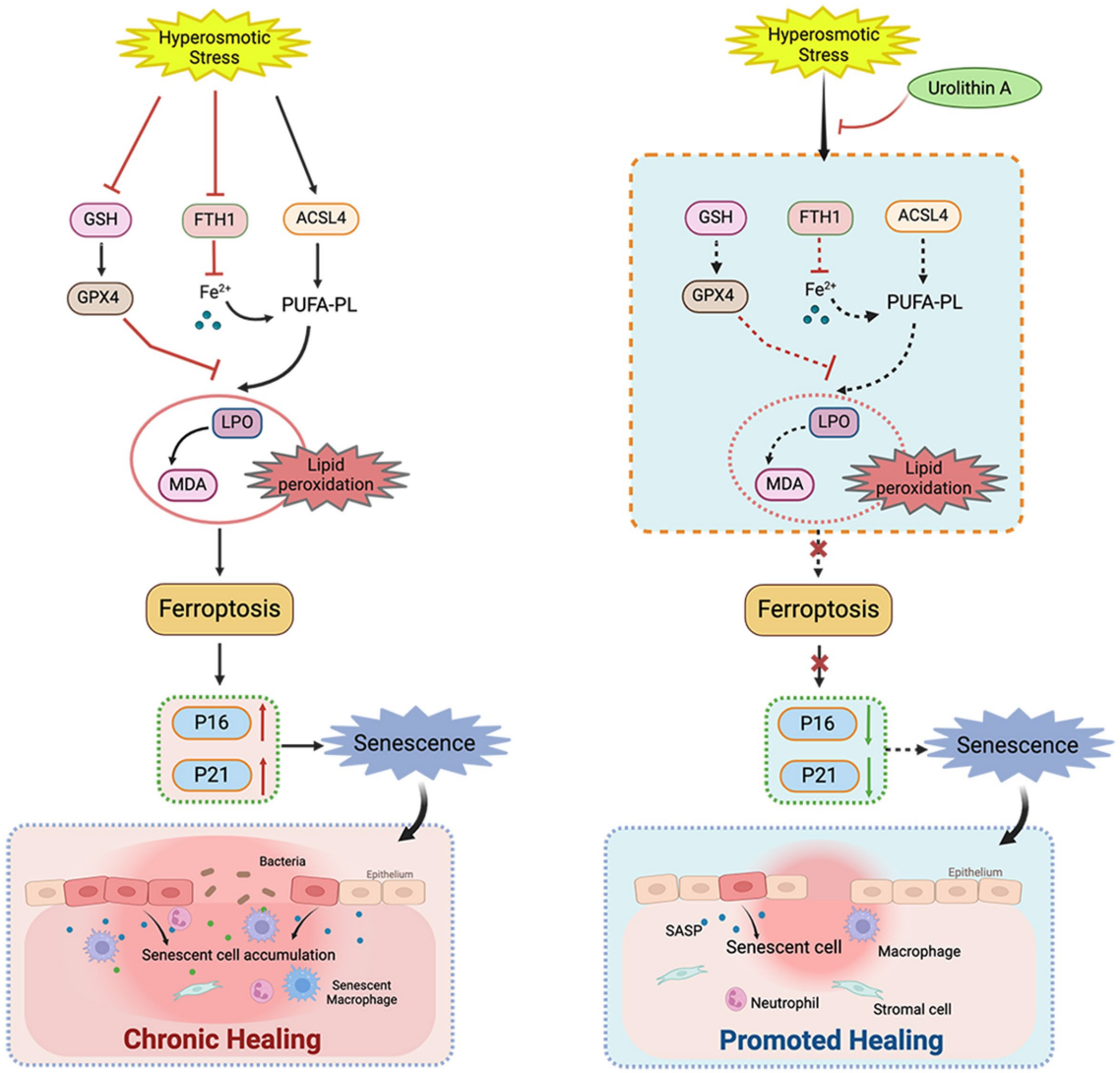

FIGURE 6
Schematic diagram of the mechanism of UA on corneal epithelial cells. UA alleviated HS-induced corneal epithelial cell senescence by inhibiting ferroptosis and thus promoted corneal epithelial healing.

However, this study had many limitations. First, the studies on the mechanism of action were mainly *in vitro*, and whether ferroptosis inhibition can inhibit cell senescence *in vivo* needs to be confirmed. Second, studies on macroscopic ferroptosis were preliminary. Thus, the role of specific molecules in this process needs to be investigated through gene editing. Finally, several causative agents account for cell senescence, and whether the conclusion of this study is consistent with the cell senescence caused by hypoxia, high sugar levels, and other stimuli needs to be confirmed by constructing larger and more robust models.

5 Conclusion

To summarize, our study suggested that cell senescence plays a crucial role in the healing of the corneal epithelium. As UA can alleviate the senescence of HCE-T cells by inhibiting ferroptosis, it can be used to develop effective strategies for treating poor corneal wound healing.

Data availability statement

The data presented in the study are deposited in the NCBI repository at https://www.ncbi.nlm.nih.gov/bioproject/1154417, accession number PRJNA1154417. Further inquiries can be directed to the corresponding author.

Ethics statement

The animal study was approved by Tongji Medical College, Huazhong University of Science and Technology. The study was conducted in accordance with the local legislation and institutional requirements.

Author contributions

X-XG: Data curation, Formal analysis, Methodology, Writing – original draft. X-JC: Formal analysis, Investigation, Writing – original draft. QP: Methodology, Project administration, Supervision, Writing – review & editing. A-LL: Software, Validation, Writing – review &

editing. JL: Resources, Visualization, Writing – review & editing. X-YL: Conceptualization, Project administration, Supervision, Writing – review & editing.

Funding

The author(s) declare that no financial support was received for the research, authorship, and/or publication of this article.

Conflict of interest

The authors declare that the research was conducted in the absence of any commercial or financial relationships that could be construed as a potential conflict of interest.

Publisher's note

Supplementary material

The Supplementary material for this article can be found online at: https://www.frontiersin.org/articles/10.3389/fmed.2024.1441196/full#supplementary-material

References

1. Lavker RM, Kaplan N, Wang J, Peng H. Corneal epithelial biology: lessons stemming from old to new. *Exp Eye Res*. (2020) 198:108094. doi: 10.1016/j.exer.2020.108094

2. Eghrari AO, Riazuddin SA, Gottsch JD. Overview of the cornea: structure, function, and development. *Prog Mol Biol Transl Sci*. (2015) 134:7–23. doi: 10.1016/bs.pmbts.2015.04.001

3. Dmitrieva NI, Burg MB. High NaCl promotes cellular senescence. *Cell Cycle*. (2007) 6:3108–13. doi: 10.4161/cc.6.24.5084

4. Yang L, Zhang S, Duan H, Dong M, Hu X, Zhang Z, et al. Different effects of pro-inflammatory factors and hyperosmotic stress on corneal epithelial stem/progenitor cells and wound healing in mice. *Stem Cells Transl Med*. (2019) 8:46–57. doi: 10.1002/sctm.18-0005

5. Sun CC, Lee SY, Chen LH, Lai CH, Shen ZQ, Chen NN, et al. Targeting Ca^{2+}-dependent pathways to promote corneal epithelial wound healing induced by CISD2 deficiency. *Cell Signal*. (2023) 109:110755. doi: 10.1016/j.cellsig.2023.110755

6. Chen WL, Lin CT, Ko PS, Yeh PT, Kuan YH, Hu FR, et al. *In vivo* confocal microscopic findings of corneal wound healing after corneal epithelial debridement in diabetic vitrectomy. *Ophthalmology*. (2009) 116:1038–47. doi: 10.1016/j.ophtha.2009.01.002

7. Di Micco R, Krizhanovsky V, Baker D, d'Adda di Fagagna F. Cellular senescence in ageing: from mechanisms to therapeutic opportunities. *Nat Rev Mol Cell Biol*. (2021) 22:75–95. doi: 10.1038/s41580-020-00314-w

8. d'Adda di Fagagna F. Living on a break: cellular senescence as a DNA-damage response. *Nat Rev Cancer*. (2008) 8:512–22. doi: 10.1038/nrc2440

9. Hubackova S, Krejcikova K, Bartek J, Hodny Z. IL1- and TGFβ-Nox4 signaling, oxidative stress and DNA damage response are shared features of replicative, oncogene-induced, and drug-induced paracrine 'bystander senescence'. *Aging*. (2012) 4:932–51. doi: 10.18632/aging.100520

10. Liu J, Zhang J, Lin X, Boyce BF, Zhang H, Xing L. Age-associated callus senescent cells produce TGF-β1 that inhibits fracture healing in aged mice. *J Clin Invest*. (2022) 132:e148073. doi: 10.1172/JCI148073

11. Samdavid Thanapaul RJR, Shvedova M, Shin GH, Crouch J, Roh DS. Elevated skin senescence in young mice causes delayed wound healing. *Geroscience*. (2022) 44:1871–8. doi: 10.1007/s11357-022-00551-1

12. Shu F, Gao H, Wu W, Yu S, Zhang L, Liu H, et al. Amniotic epithelial cells accelerate diabetic wound healing by protecting keratinocytes and fibroblasts from high-glucose-induced senescence. *Cell Biol Int*. (2022) 46:755–70. doi: 10.1002/cbin.11771

13. Baker DJ, Wijshake T, Tchkonia T, LeBrasseur NK, Childs BG, van de Sluis B, et al. Clearance of p16Ink4a-positive senescent cells delays ageing-associated disorders. *Nature*. (2011) 479:232–6. doi: 10.1038/nature10600

14. Chang J, Wang Y, Shao L, Laberge RM, Demaria M, Campisi J, et al. Clearance of senescent cells by ABT263 rejuvenates aged hematopoietic stem cells in mice. *Nat Med*. (2016) 22:78–83. doi: 10.1038/nm.4010

15. Baar MP, Brandt RMC, Putavet DA, Klein JDD, Derks KWJ, Bourgeois BRM, et al. Targeted apoptosis of senescent cells restores tissue homeostasis in response to chemotoxicity and aging. *Cell*. (2017) 169:132–47.e16. doi: 10.1016/j.cell.2017.02.031

16. D'Amico D, Andreux PA, Valdés P, Singh A, Rinsch C, Auwerx J. Impact of the natural compound Urolithin A on health, disease, and aging. *Trends Mol Med*. (2021) 27:687–99. doi: 10.1016/j.molmed.2021.04.009

17. Qiu J, Chen Y, Zhuo J, Zhang L, Liu J, Wang B, et al. Urolithin A promotes mitophagy and suppresses NLRP3 inflammasome activation in lipopolysaccharide-induced BV2 microglial cells and MPTP-induced Parkinson's disease model. *Neuropharmacology*. (2022) 207:108963. doi: 10.1016/j.neuropharm.2022.108963

18. Norden E, Heiss EH. Urolithin A gains in antiproliferative capacity by reducing the glycolytic potential via the p53/TIGAR axis in colon cancer cells. *Carcinogenesis*. (2019) 40:93–101. doi: 10.1093/carcin/bgy158

19. Ryu D, Mouchiroud L, Andreux PA, Katsyuba E, Moullan N, Nicolet-Dit-Félix AA, et al. Urolithin A induces mitophagy and prolongs lifespan in *C. elegans* and increases muscle function in rodents. *Nat Med*. (2016) 22:879–88. doi: 10.1038/nm.4132

20. Liu H, Kang H, Song C, Lei Z, Li L, Guo J, et al. Urolithin A inhibits the catabolic effect of TNFα on nucleus pulposus cell and alleviates intervertebral disc degeneration *in vivo*. *Front Pharmacol*. (2018) 9:1043. doi: 10.3389/fphar.2018.01043

21. Shi PZ, Wang JW, Wang PC, Han B, Lu XH, Ren YX, et al. Urolithin A alleviates oxidative stress-induced senescence in nucleus pulposus-derived mesenchymal stem cells through SIRT1/PGC-1α pathway. *World J Stem Cells*. (2021) 13:1928–46. doi: 10.4252/wjsc.v13.i12.1928

22. Liu W, Yan F, Xu Z, Chen Q, Ren J, Wang Q, et al. Urolithin A protects human dermal fibroblasts from UVA-induced photoaging through NRF2 activation and mitophagy. *J Photochem Photobiol B*. (2022) 232:112462. doi: 10.1016/j.jphotobiol.2022.112462

23. Cho SI, Jo ER, Song H. Urolithin A attenuates auditory cell senescence by activating mitophagy. *Sci Rep*. (2022) 12:7704. doi: 10.1038/s41598-022-11894-2

24. Wang Y, Blandino G, Givol D. Induced p21waf expression in H1299 cell line promotes cell senescence and protects against cytotoxic effect of radiation and doxorubicin. *Oncogene*. (1999) 18:2643–9. doi: 10.1038/sj.onc.1202632

25. Muñoz-Espín D, Cañamero M, Maraver A, Gómez-López G, Contreras J, Murillo-Cuesta S, et al. Programmed cell senescence during mammalian embryonic development. *Cell*. (2013) 155:1104–18. doi: 10.1016/j.cell.2013.10.019

26. Englund DA, Jolliffe A, Aversa Z, Zhang X, Sturmlechner I, Sakamoto AE, et al. p21 induces a senescence program and skeletal muscle dysfunction. *Mol Metab*. (2023) 67:101652. doi: 10.1016/j.molmet.2022.101652

27. Shih CT, Chang YF, Chen YT, Ma CP, Chen HW, Yang CC, et al. The PPARγ-SETD8 axis constitutes an epigenetic, p53-independent checkpoint on p21-mediated cellular senescence. *Aging Cell*. (2017) 16:797–813. doi: 10.1111/acel.12607

28. Prašnikar E, Borišek J, Perdih A. Senescent cells as promising targets to tackle age-related diseases. *Ageing Res Rev*. (2021) 66:101251. doi: 10.1016/j.arr.2020.101251

29. Blokland KEC, Waters DW, Schuliga M, Read J, Pouwels SD, Grainge CL, et al. Senescence of IPF lung fibroblasts disrupt alveolar epithelial cell proliferation and promote migration in wound healing. *Pharmaceutics*. (2020) 12:389. doi: 10.3390/pharmaceutics12040389

30. Chia CW, Sherman-Baust CA, Larson SA, Pandey R, Withers R, Karikkineth AC, et al. Age-associated expression of p21and p53 during human wound healing. *Aging Cell*. (2021) 20:e13354. doi: 10.1111/acel.13354

31. Saul D, Monroe DG, Rowsey JL, Kosinsky RL, Vos SJ, Doolittle ML, et al. Modulation of fracture healing by the transient accumulation of senescent cells. *eLife*. (2021):e69958:10. doi: 10.7554/eLife.69958

32. Dixon SJ, Lemberg KM, Lamprecht MR, Skouta R, Zaitsev EM, Gleason CE, et al. Ferroptosis: an iron-dependent form of nonapoptotic cell death. *Cell*. (2012) 149:1060–72. doi: 10.1016/j.cell.2012.03.042

33. Li S, Wang M, Wang Y, Guo Y, Tao X, Wang X, et al. p53-mediated ferroptosis is required for 1-methyl-4-phenylpyridinium-induced senescence of PC12 cells. *Toxicol In Vitro*. (2021) 73:105146. doi: 10.1016/j.tiv.2021.105146

34. Zhao T, Guo X, Sun Y. Iron accumulation and lipid peroxidation in the aging retina: implication of ferroptosis in age-related macular degeneration. *Aging Dis*. (2021) 12:529–51. doi: 10.14336/AD.2020.0912

35. James SA, Hare DJ, Jenkins NL, de Jonge MD, Bush AI, McColl G. φXANES: *in vivo* imaging of metal-protein coordination environments. *Sci Rep*. (2016) 6:20350. doi: 10.1038/srep20350

36. James SA, Roberts BR, Hare DJ, de Jonge MD, Birchall IE, Jenkins NL, et al. Direct *in vivo* imaging of ferrous iron dyshomeostasis in ageing *Caenorhabditis elegans*. *Chem Sci*. (2015) 6:2952–62. doi: 10.1039/C5SC00233H

37. Massie HR, Aiello VR, Banziger V. Iron accumulation and lipid peroxidation in aging C57BL/6J mice. *Exp Gerontol*. (1983) 18:277–85. doi: 10.1016/0531-5565(83)90038-4

38. Massie HR, Aiello VR, Williams TR. Iron accumulation during development and ageing of *Drosophila*. *Mech Ageing Dev*. (1985) 29:215–20. doi: 10.1016/0047-6374(85)90020-x

39. Ward RJ, Zucca FA, Duyn JH, Crichton RR, Zecca L. The role of iron in brain ageing and neurodegenerative disorders. *Lancet Neurol*. (2014) 13:1045–60. doi: 10.1016/S1474-4422(14)70117-6

40. Sun Y, Zheng Y, Wang C, Liu Y. Glutathione depletion induces ferroptosis, autophagy, and premature cell senescence in retinal pigment epithelial cells. *Cell Death Dis*. (2018) 9:753. doi: 10.1038/s41419-018-0794-4

41. Wang K, Jiang L, Zhong Y, Zhang Y, Yin Q, Li S, et al. Ferrostatin-1-loaded liposome for treatment of corneal alkali burn via targeting ferroptosis. *Bioeng Transl Med*. (2022) 7:e10276. doi: 10.1002/btm2.10276

42. Lou L, Wang M, He J, Yang S, Meng F, Wang S, et al. Urolithin A (UA) attenuates ferroptosis in LPS-induced acute lung injury in mice by upregulating Keap1-Nrf2/HO-1 signaling pathway. *Front Pharmacol*. (2023) 14:1067402. doi: 10.3389/fphar.2023.1067402

43. Xu P, Lin B, Deng X, Huang K, Zhang Y, Wang N. VDR activation attenuates osteoblastic ferroptosis and senescence by stimulating the Nrf2/GPX4 pathway in age-related osteoporosis. *Free Radic Biol Med*. (2022) 193:720–35. doi: 10.1016/j.freeradbiomed.2022.11.013

Frontiers in Medicine

Translating medical research and innovation into improved patient care

A multidisciplinary journal which advances our medical knowledge. It supports the translation of scientific advances into new therapies and diagnostic tools that will improve patient care.

Discover the latest Research Topics

See more →

Frontiers

Avenue du Tribunal-Fédéral 34
1005 Lausanne, Switzerland
frontiersin.org

Contact us

+41 (0)21 510 17 00
frontiersin.org/about/contact